THE UNIVERSITY
of EDINBURGH

The epigenetic regulation of heterochromatin structure and tumour progression

Peter Christopher Bruton

THE UNIVERSITY
of EDINBURGH

Thesis presented for the degree of Doctor of Philosophy

The University of Edinburgh

2018

Declaration

I declare that this thesis if of original work almost entirely undertaken by the author. Where collaborative contributions are included, they have been explicitly stated and acknowledged. All external sources have been specifically referenced where required. This body of work has not been submitted in any part to support any other degree or qualification.

Peter Bruton

March 2018

Acknowledgements

Ask any doctorate to describe what it's like to do a PhD, and you are inevitably informed that it is only comprehensible by those who have been there and done it. The unerring accuracy of 'PHDComics' is often quoted as a reference to those naïve enough to consider it. And yet here we are.

Researching and writing this thesis has frankly often felt like a car crash. From a so-called rabbit in the headlights, to the insomniac that may finally venture outside again, it has been a transformative process. That I live to tell the tale speaks only to the limits that 'doing a PhD' may take from someone. Despite my future calling lying away from academia, taking on this thesis – my Everest – will never be a regret.

"*People are like dirt. They can either nourish you and help you grow as a person or they can stunt your growth and make you wilt and die*."
- Anon (falsely attributed to Plato)

This body of work has required an endless supply of support, from too many sources to mention in full. Firstly, I would like to thank the MRC for funding my research, and Professor Nick Gilbert for taking on my project when I was already figuratively in intensive care. The scientific rigour and discussions within his lab dragged my project off the tarmac and to the finish line today.

I would also like to thank my supporting supervisors in Neil Carragher and Alexander 'Sasha' Kaganksy. Neil's insightful commentary and advice on the broader implications of my research, helped frame my thoughts. I would also like to thank Sasha for his stupendous positivity and enthusiasm, which reminded me that exploring life's unanswered questions should remain a fun and inspiring process.

Covadonga Huidobro-Fernandez provided much needed technical and emotional support to which I am hugely indebted. Her passion, smile, Polaroid camera, and endless organisational abilities kept me on the straight and narrow. Without her I would still be rummaging around the back of the wrong freezer looking for 'that reagent' I had managed to misplace.

The exceptional colleagues within the Gilbert lab created a supportive environment of great benefit to this project and myself. From the perfect role model in Ryu-ske to Jim's notable wisdom; Lora, Adam, Catherine, Sam, Hannah, Kate, and Maria have all generously supported this work and put up with my questionable music tastes in the lab.

I would be remised not to mention all the support provided by those outside the lab, from the Genome Regulation section and the wider IGMM. I have greatly benefitted from Matt Pearsons advice and training in microscopy, Lizzy Freyer for FACS support, Bernie Ramsahoye for mononucleotide analyses, and Technical Services for freedom from resource acquisition and stock solution preparations.

The greatest thanks, however, goes to my friends and family for feigning interest in my work, putting up with my enthusiastic and informing scientific monologues, and generally avoiding the question 'How's the PhD going?' I would finally like to say thank you to the unwavering constant that is my mum and dad. The lifetime of scientific discussions/arguments, mountainous amounts of proofreading, and unconditional support have made me the man I am today.

Lay Summary

DNA is packaged into 'on' and 'off' states, which are loosely more open and accessible and more compact and inaccessible respectively. How the compact heterochromatic 'off' state is regulated and its role in disease is poorly understood.

The 'off' heterochromatic state has defined characteristics of increased DNA methylation and Histone 3 trimethylation (H3K9me3). DNA methylation loss does not change the compact nature of heterochromatin. Loss of H3K9me3 results in an increase in cancer in mice; however visually compact DNA is still present.

Broadly I aimed to identify components that regulate the heterochromatic 'off' state, and investigate their role in the development of colon cancer drug resistance. I found that the loss of a component that turns 'on' genes appeared to regulate silent genes. This corresponded to a decrease in HP1 that is normally associated with maintaining the heterochromatic 'off' associated. This suggests that the activator is required to produce the components to maintain the compact 'off' state.

Additionally I aimed to address whether H3K9me3 effects the compaction of the heterochromatic 'off' state. I found that loss of H3K9me3 affected the level of compaction globally as well as at compact 'off' regions of the DNA. This correlated with an increase the amount of RNA bound to DNA. Re-establishing H3K9me3 ablated these effects. Further research is required to establish how H3K9me3 affects DNA bound RNA.

Abstract

Since the discovery of DNA packaging into chromatin, and McClintock's (1951) work on position-effect variegation providing evidence of non-mendelian inheritance, the principal of a genome maintaining 'on' and 'off' states has been widely adopted. However, the underlying mechanisms that regulate these dynamic chromatin states and their effect on disease are still poorly understood.

DNA methylation and histone trimethylation at H3K9 and H4K20 are the core hallmarks of the heterochromatic constitutively 'off' state. Constitutive heterochromatin is predominantly comprised of repetitive satellite containing pericentromeric regions and telomeres and in mouse heterochromatin clusters into large chromocenters. These regions are cytologically more compact and generally transcriptionally silent across embryonic and differentiated mouse cell types. However, in addition to increased genomic instability, mouse tumour cells sustain increased satellite expression suggesting constitutive heterochromatin is disrupted. Therefore how constitutive heterochromatin is maintained has important implications for genome regulation and disease, and remains poorly understood.

While satellite DNA sequences are not evolutionarily conserved, pericentromeric and telomeric heterochromatin occurs across species. Heterochromatin formation is therefore independent of the underlying DNA sequence, supporting the hypothesis that epigenetic components can regulate chromatin structure. DNA methylation is generally thought to be associated with transcriptional silencing and chromatin compaction.

However, Gilbert et al (2007) showed that the complete loss of DNA methylation did not affect the compaction at heterochromatin or global genome compaction.

The role of H3K9me3 in regulating heterochromatin has also been an area of keen interest. H3K9me3 patterns are established by suppressor of variegation 3-9 homologues and provide the binding site for heterochromatic protein 1 [HP1] which can in turn recruit Suv39h1. This Suv3-9h-HP1-H3K9 axis enables its propagation throughout heterochromatin. Peters et al (2001) demonstrated that in mice loss of suv39 homologues 1 and 2 caused a loss of H3K9me3 at constitutive heterochromatic domains. These Suv39h null mice demonstrated decreased genome stability, and an increased prevalence of oncogenesis. However cytological chromocenters are still present in the absence of H3K9me3. Therefore the function of H3K9me3 as a causative agent in heterochromatin formation is still debated.

Broadly the aim was to investigate the phenotypic role of heterochromatic epigenetic components in cancer progression, and address whether H3K9me3 effects large scale chromatin structure. To identify heterochromatic gene silencing components, an inhibitor screen was performed in an artificial silenced reporter system. The reporter fluorophore was silenced by the presence of centromeric arrays from yeast/bacterial artificial chromosomes and human alpha satellite repeats enriched for H3K9me3. To address the function of the de-silencing components identified in cancer, the fitness of colon cancer cells [HCT116] was investigated before and after the development of resistance to the MEK inhibitor trametinib. The most intriguing result was that BET protein inhibition resulted in de-repression of the reporter construct and trametinib resistant HCT116 cells

were more sensitive to BET inhibitors, while subsequent investigation showed HP1 protein levels were altered. Analysis of publically available datasets of tumour drug resistance, showed elevated BET protein binding at HP1 promoters in resistant cell lines suggesting an indirect role in gene silencing.

To investigate the consequence of H3K9me3 loss on chromatin structure, mouse embryonic stem cells that lacked both Suv39 homologues were used. Microccocal nuclease digestion and sucrose sedimentation demonstrated a global decompaction of large-scale chromatin fibres whilst re-expression of suv39h1 rescued H3K9me3 at chromocenters and global chromatin decompaction. Loss of Suv39h also increased chromatin associated RNA levels that were also rescued by Suv39h1 re-expression. This suggests that H3K9me3 has a role chromatin fibre compaction globally as well as at constitutive heterochromatin, potentially mediated by chromatin associated RNA.

To conclude, multiple components were identified that are involved in transcriptional silencing. Evaluating their function in tumour progression demonstrated a possible role of BET proteins in the development of MEKi resistance that may be mediated through HP1 proteins. H3K9me3 and its binding partner HP1 affect global chromatin compaction. The global decompaction after Suv39h loss correlates with an increase in chromatin associated RNA, suggesting a possible mechanism for changes in chromatin compaction beyond H3K9me3.

Table of contents

List of figures

List of tables

Abbreviations

3C:	one vs one chromosome conformation capture
BET:	Bromo extra-terminal domain
bp:	base pairs
BrdU:	5-bromo-2-deoxy-uridine
BSA:	bovine serum albumin
cDNA:	complementary DNA
CdLS:	cornelia de lange syndrome
CHD:	chromo helicase domain
ChIP:	chromatin immunoprecipitation
Coumarin-azide:	3-azido-7-hydroxycoumarin
DAPI:	4′,6-diamino-2-phenylindole
DMSO:	dimethyl sulfoxide
DNA	deoxyribonucleic acid
DnaseI:	deoxyribonucleic acid nuclease 1
dH_2O:	distilled water
dNTP:	deoxyribonucleotide triphosphate
DTT:	dithiothreitol
eGFP:	enhanced green fluorescence protein
EDTA:	ethylene-diamine-tetraacetic acid
EdC:	5-ethynyl-2′deoxy-cytidine
EdU:	5-ethynyl-2′deoxy-uridine
EGTA:	ethylene glycol tetraacetic acid

EMT:	epithelial mesenchymal transition
ENC:	evolutionary new centromere
eRNA:	enhancer RNA
EU:	5-ethynyl-2'uridine
FA:	formaldehyde
FACS:	fluorescence-activated cell sorting
FCS:	fetal calf serum
FISH:	fluorescence in situ hybridization
H1:	linker histone 1
HAC:	human artificial chromosome
HATs:	histone acetyltransferases
HDACs:	histone deacetylases
Hi-C:	all vs all chromosome conformation capture
HMTs:	histone methyltransferases
HKMTs:	Lysine methyltransferases
HJQ1R:	JQ1 resistant HCT116 cells
hnRNPs:	heterogeneous nuclear ribonucleoproteins
HP1:	heterochromatic protein 1
HPLC:	high performance liquid chromatography
HR:	homologous repair
HRP:	horseradish peroxidase
HSA:	highest single agent model
IC50:	inhibitory concentration 50
IRES:	internal ribosome entry site

kb:	kilobase
LAD:	lamina associated domain
LCR:	locus control region
lncRNA:	long non-coding RNA
M:	molar
me1/me2/me3:	monomethylation/dimethylation/trimethylation
MEF:	mouse embryonic fibroblasts
MEKi:	MEK inhibitors
MEL:	murine erythroleukeamia
mESCs:	mouse embryonic stem cells
MET:	mesenchymal endothelial transition
ml:	millilitre
mM:	milliMolar
MNase:	micrococcal nuclease
NAD:	nucleolar associated domain
ncRNA:	non-coding RNA
NHEJ:	non-homologous end joining
nM:	nanoMolar
nm:	nanometer
O.N:	overnight
p212:	MEL cells with constitutively active eGFP transgene
PARP:	poly(ADP-ribose) polymerase
PBS:	phosphate buffer saline
PCR	polymerase chain reaction

PEV:	Position-effect variegation
PFA	paraformaldehyde
PcG:	polycomb complexes
PI:	propidium iodide
PIC:	preinitiation complex
polII:	RNA polymerase II
PRC1:	polycomb repressor complex 1
PRC2:	polycomb repressor complex 2
PMSF:	phenylmethylsulfonyl fluoride
PTM:	post-translational modification
PVDF:	polyvinylidene fluoride
RFI:	relative fluorescence intensity
RFP:	red fluorescent protein
RTKs:	receptor tyrosine kinases
RL5:	endogenous MEL cells
RNA:	ribonucleic acid
RNase:	ribonucleic nuclease
ROI:	region of interest
rpm:	revolutions per minute
RT:	room temperature
SDS:	sodium dodecyl sulphate
SET:	su(var)3-9, enhancer-of-zeste and trithorax
SEM:	standard error of the mean
SMC:	structural maintenance of chromosome

Su(var):	suppressor of variegation
Suv39h1/2:	suppressor of variegation 3-9 homologue 1 or 2
SUMOs:	small ubiquitin-like modifiers
TADs:	topological associating domains
telRNA:	telomeric RNA
TF:	transcription factor
THPTA:	tris(3-hydroxypropyltriazolylmethyl)amine
TJQ1R:	JQ1 and trametinib resistant HCT116 cells
Top1:	type 1 topoisomerases
Top2:	type 2 topoisomerases
TRAMR:	trametinib resistant
Tris:	tris(hydroxymethyl)aminomethane
TSA:	trichostatin A
UV:	ultraviolet
v/v:	volume:volume
w/v:	weight:volume
YAC:	S. cerevisae artificial chromosomes
α-MEL:	MEL cells with alpha satellite eGFP transgene
μM:	micromolar

Chapter 1: Introduction

Since Friedrich Miescher discovered DNA in 1869 (Hoppe-Seyler, 1871) the structure and regulation of a cell's genetic material has remained a fundamental research question. For Watson and Crick's DNA structure to fit inside the nucleus of a eukaryotic cell the DNA requires multiple levels of packaging. DNA is initially wrapped around and bound to positively charged proteins forming fibres, which undergo further levels of folding.

The tight packaging of these fibres enables regulation of underlying DNA processes in addition to overcoming the spatial constraints of the nucleosome. This regulatory ability of fibre structure has been linked to gene expression, genome regulation, and repair pathways. Mechanisms to modulate the topology of chromatin fibres are loosely termed epigenetic, derived from the Greek term epi- meaning "on top of" genetics. These processes enable cells to differentiate into different sub types despite the same underlying genetic sequence.

The structure and regulation of condensed chromatin fibres is implicated in many biological processes, from faithful sister chromatid separation after replication to preventing gene expression at specific loci or in large Mb domains. For oncogenesis to occur tumour suppressor mechanisms must be disrupted, allowing uncontrolled oncogenic proliferation. DNA mutations, gene silencing, and gene activation mediate this process. Epigenetic pathways were first implicated in cancer when tumours were found to exhibit DNA hypomethylation (Feinberg and Vogelstein, 1983). With the addition of whole-genome sequencing, epigenetic components have been

demonstrated as the most frequently mutated in cancer (Forbes *et al.,* 2011). Metastatic tumour progression after initial treatment is often resistant to treatment and lacks common new mutations like initial oncogenesis. This has led to the proposal of epigenetic mechanisms in metastasis formation.

Studying epigenetic components that regulate a condensed fibre state provides insight into fundamental genome organisation in addition to its phenotypic relevance.

1.1 Chromatin constituents

Multiple levels of organisation can define the complexity of chromatin structure. Primarily 147 base pairs of the DNA helix are wrapped 1.7 times around an octamer of histone proteins forming a core particle. In chromatin this structure is stabilised by histone H1 that binds close to the dyad, the point at which DNA enters and exits the nucleosome. Nucleosomes are positioned regularly along the DNA and when unfolded appear as a 10-nm 'beads on a string' like structure (Alberts, Bray and Lewis, 1994). Under physiological conditions nucleosome arrays are further packaged into 30-nm diameter fibres. Additional levels of folding have been argued in the order of 40-60 nm and 117 nm (Pope *et al.*, 2005). Ultimately chromatin fibres are also folded by a looping model (Gibcus *et al.*, 2018), which during mitosis results in the chromosome cytological bodies first seen by Walter Flemming (1878).

1.1.1 Core histones

The base unit of chromatin, the nucleosome comprises eight core histones and a linker histone. Linker histones bind to the DNA and associate with neighbouring nucleosomes through the long c-terminal tail (Allan *et al.*, 1986). Core and linker histones, have many post-translational modifications [PTMs], including acetylation, methylation, phosphorylation, ubiquitination, and less well studied more "exotic" modifications. These modifications correlate with transcriptional states and it has been suggested they could influence chromatin fibre function. Along with PTMs, core histones of the nucleosome can be evicted and replaced with variants to regulate chromatin structure in a site-specific manner.

The histone octamer that forms a nucleosome when bound to DNA comprises of histones H2A, H2B, H3, H4, or their individual variants. H3 and H4 form a heterotetramer that binds to two H2A/H2B dimers. The histone octamer proteins are enriched with lysine and arginine residues resulting in a net positive charge whilst the antipodal negative charge of the DNA phosphate backbone results in a general propensity for DNA histone interactions.

DNA and histones interactions are confined by proximal electrostatic and Van de Waal forces on the surface of the histone globular domain, which results in the DNA wrapping around the histone octamer. These interaction forces also differ depending on the underlying nucleic acid sequence revealing a bias for nucleosome positioning (Gonzalez *et al.*, 2016).

Neighbouring nucleosomes are individually distinct due to linker DNA being enriched with GC, GG, CG, and CC dinucleotide sequences. The DNA length of these linker regions fluctuates from 10-90 bp throughout the genome, by cell type, and species (Van Holdebo, 1989). Linker histones H1 and its variant H5 also contain polar and charged surface amino acid residues, which allow binding to linker DNA. The linker histone H1 is composed of a globular domain with C-terminal and N-terminal unstructured tails. The globular domain of H1 associates with the dyad of the nucleosome, while the disordered tails interact with the naked linker DNA and nearby nucleosomes. H1 binding stabilises nucleosomes by reducing the free energy of the supramolecule. This increases the tolerance for nucleosome stacking and compaction to a 30 nm fibre state (Allan *et al.*, 1980).

1.1.2 Histone variants

Canonical histone genes cluster in the genome and their transcription activity is tightly regulated by the cell cycle. Histone variants, by contrast, are typically dispersed throughout the genome, and are constitutively expressed. Histone variant chromatin incorporation occurs at the expense of their canonical counterparts and is normally regulated by histone chaperones. Chaperones associated with additional complexes with preferential binding affinities to particular post-translational modifications, allows for histone variant deposition to be tightly regulated (Luk *et al.*, 2007; Obri *et al.*, 2014). Histone variants maintain a large percentage of sequence similarity; yet have multiple effects including altering the structural dynamics of chromatin (Talbert and Henikoff, 2017). This enables variants to have diverse functions in DNA repair, transcriptional, and replication processes.

H2A, H2B, H3 and H1 have known histone variants. Centromeric CENP-A, one of eight H3 variants, has greater than 60% similarity but unique N-terminal tails. Deposited by histone chaperone HJURP, CENP-A incorporated nucleosomes *in vitro* are more stable and form more compact fibres than canonical H3 (Panchenko *et al.*, 2011). *In vivo*, however, CENP-A nucleosomes are interspersed, except at structurally similar inactive centromeres. CENP-A is thought, therefore, to stabilise the fibre structure allowing for correct kinetochore formation (Blower, Sullivan and Karpen, 2002).

Other H3 variants of note include structurally similar H3.1/2 and H.3.3. Differing via a single amino acid H3.1 and H3.2 have yet to have distinguished functions, and are together described as canonical H3. Canonical H3 incorporation is mediated by CAF-1 in a replication dependent manner, representing the majority of H3 in chromatin. H3.3 DNA sequence diverges from H3.1 by five base pairs in humans, resulting in less stable nucleosomes, suggesting an altered chromatin incorporation and effect on chromatin structure (Tagami *et al.*, 2004; Chen *et al.*, 2013).

H3.3 is deposited independently of the cell cycle by chaperone HIRA, or the chromatin re-modellers CHD1, and DAXX (Konev *et al.*, 2007; Drané *et al.*, 2010). H3.3 is enriched at enhancer and transcribed loci, suggesting it might be frequently turned over, although it is also enriched at telomeric and pericentromeric regions (Wirbelauer and Bell, 2005). H3.3 enrichment at active and inactive regions is dependent on HIRA or DAXX mediated incorporation respectively (Goldberg *et al.*, 2010).

H2A variants have a diverse range of functions. H2A.Z is deposited at actively transcribed genes and is often found at the same loci as H3.3. Incorporation of H2A.Z destabilises nucleosomes synergistically with H3.3 resulting in nucleosome depleted regions thought to promote transcription factor binding (Suto *et al.*, 2000; Jin *et al.*, 2011; Chen *et al.*, 2013). The local chromatin environment also regulates the DNA damage response, through the replacement of H2A by H2A.X. Distributed throughout the genome, this variant has an alternate C-terminal, which upon DNA damage is phosphorylated at ser139 marking the loci for repair (Rogakou *et al.*, 1998). The most divergent variant is macro-H2A, which is nearly three times larger than canonical H2A.

Macro-H2A has 64% similarity to H2A, but also contains a linker to a large ancillary C-terminal domain that is located outside the core nucleosome particle (Pehrson and Fried, 1992). Found at the inactive X chromosome, macro-H2A is correlated to chromatin compaction and transcriptional repression, possibly through an association with HDAC1 (Chakravarthy *et al.*, 2005).

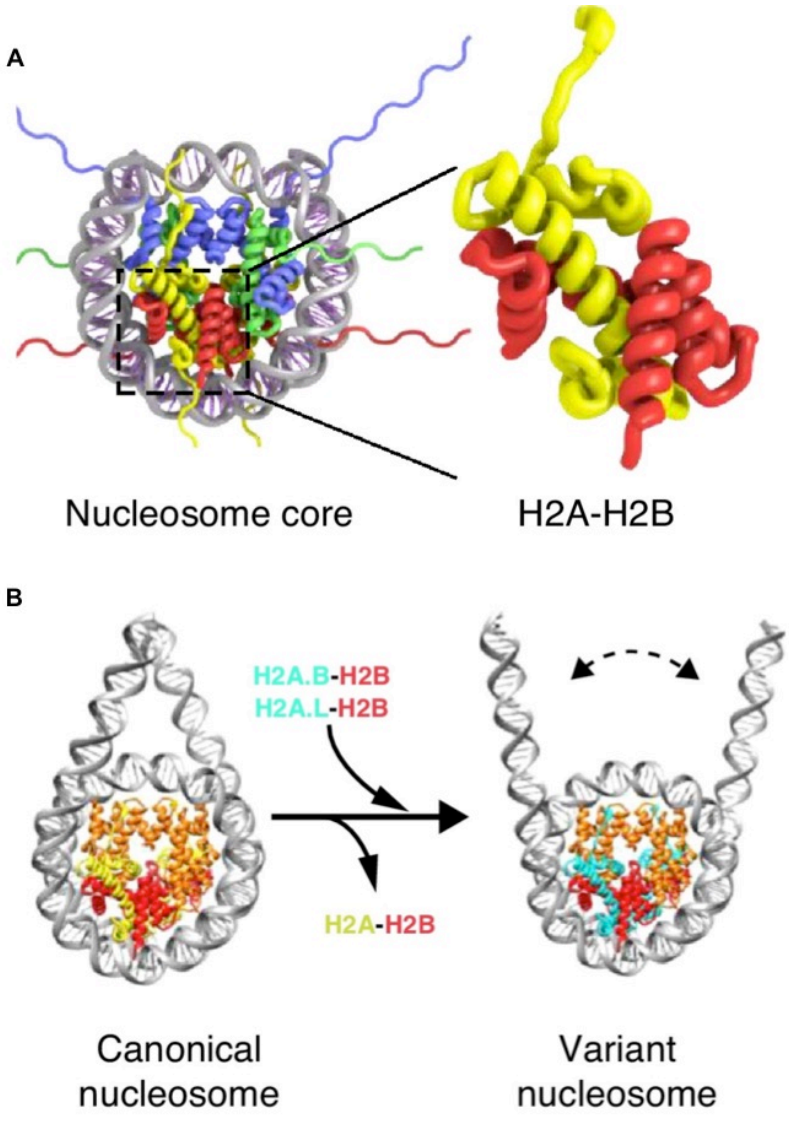

Figure 1.1 Nucleosome structure and the affect of histone variants. (A) Histone octomer containing two copies of H2A-H2B and H3-H4 heterodimers, with their disordered tails protruding from the core particle. (**B)** Depiction of the core nucleosome particle with certain histone variants that disrupt the DNA dyad resulting in a more open nucleosomal structure. Adapted from Shaytan, Landsman and Panchenko, (2015)

1.1.3 Histone modifications

While the replacement of histones with variants is the most extensive nucleosome modification, histone post-translational modifications [PTMs] are associated with regulating the local chromatin environment. The majority of known post-translations occur on the N-terminal histone tails that protrude from the nucleosome core. Many types of histone modification have been identified on lysine, arginine, glutamine, serine, and threonine residues. The function of these modifications including methylation, acetylation, phosphorylation, and ubiquitination is still not fully understood.

Lysine acetylation on H3 and H4 N-terminal tails correlates with euchromatin and actively transcribed regions. The positive lysine charge is lost upon acetylation, weakening inter-nucleosomal histone and DNA interactions. This mechanism is proposed to directly result in an open chromatin fibre structure. However *in vitro* studies of repetitive DNA on reconstituted nucleosome arrays showed no significant change to fibre structure due to pan acetylation (Neumann *et al.*, 2009), although globular domain acetylation at the interface of H3/H4 tetramer and H2A/H2B dimer, has been shown to destabilise the histone octamer resulting in more accessible chromatin fibres (Ye *et al.*, 2005).

Histone acetylation occurs at multiple lysines on H3 and H4 including H3 –K9, -K14, -K18, -K56 and H4 –K5, -K8, -K12, -K16, -K91, and is required for their correct assembly. This modification is transferred to histones via histone acetyltransferase enzymes (HATs) and removed by histone deacetylases (HDACs). Bromodomains, a left-handed highly charged pocket formed from four α-helices, recognise histone acetylation and occur

commonly in transcriptional activators and chromatin re-modellers (Filippakopoulos *et al.*, 2012). Maintaining acetylation profiles has an important role in gene regulation and genome stability, where HDAC loss results in aneuploidy. (Hebbes, Thorne and Crane-Robinson, 1988; Dovey *et al.*, 2013).

Methylation also occurs on histone lysines in direct competition with lysine acetylation, in addition to arginine residues. Arginines can be methylated twice while lysines can take three methylation groups and unlike acetylation, methylation does not alter the amino acids charge. Methylation is added to histones in a site-specific manner by different methyltransferases (HMTs); lysine histone methyltransferases (HKMTs) contain the Su(var)3-9, enhancer-of-zeste and trithorax (SET) domain while PRMTs are the class of methyltransferases specific to arginine residues.

Removal of mono-, di-, and tri- methyl groups is tightly regulated. Lysine-specific demethylase 1 (LSD1), uses oxidative demethylation to remove mono- and di- methyl groups (Shi *et al.*, 2004). LSD1 specificity is achieved from the addition of different protein complexes to regulate its binding (Lee *et al.*, 2005). All methylation states including trimethylated lysine residues are demethylated by the large class of jumonji domain containing proteins via Fe(II) and α-ketoglutarate mediated oxidation (Yamane *et al.*, 2006).

Unlike acetylation, histone methylation has been associated with both active and repressive chromatin states. Constitutively inactive chromatin, such as telomeres and pericentric regions are marked with H3K9me3 which in turn recruits heterochromatin protein 1 (HP1) and its own methyl transferase; Suppressor of variegation 3-9 homologue 1 or 2 (Suv39h1/2). This positive

feedback loop maintains the repressed chromatin state throughout the cell cycle (Haldar *et al.*, 2011). In contrast, H3K4me3 is associated with actively transcribed regions along with H3K36 and H3K79 methylation (Martin and Zhang, 2005).

The role of these methylation modifications on gene regulation does not appear to be universal. Confusingly, additional studies have found H3K9me3 at actively transcribed genes and H3K36me2 supressing intragenic transcription initiation (Carrozza *et al.*, 2005; Vakoc *et al.*, 2005). Despite the intricate functions of histone methylation, subsequent loss directly influences genome integrity. Double knockout of the Suv39h isoforms 1/2, responsible for H3K9me3 modification, results in increased rates of polyploidy, meiotic abnormalities, and chromosomal mis-segregation (Peters *et al.*, 2001). These murine models also showed increased incidence of tumour formation and decreased viability, demonstrating the importance of methylation for genome integrity.

Histone methylation is also known to play roles in cellular responses, such as DNA damage, where H3K79me is deposited. DOT1, the HKMT responsible for H3K79me, recruits 53BP1 to double strand break sites via its tudor domain which in turn binds to methylated lysines. This process is required for correct repair pathways to proceed. However whether double strand breaks directly affect the local chromatin structure, making it accessible to 53BP1 and DOT1, or if this signalling causes an increase in chromatin accessibility remains unclear (Huyen *et al.*, 2004).

Protein phosphorylation occurs frequently across protein classes and functions, and histone phosphorylation is important for cell cycle regulation.

Histone phosphorylation has been found at serine, threonine and tyrosine residues, for example, H3S10 adjacent to the H3K9 methylation site is phosphorylated by Aurora B as cells begin mitosis (Wei *et al.*, 1999). Phosphorylation at H3S10 causes HP1 proteins, that would normally bind to H3K9me3, to dissociate from the chromatin fibre (Hirota *et al.*, 2005). Without phosphorylation and subsequent loss of HP1 proteins, the loading of condensin is perturbed adversely affecting mitotic condensation and genome integrity (Adams *et al.*, 2001; Giet and Glover, 2001).

Histone modifications can also occur on histone variants such as the phosphorylation of H2A.X at ser139; this happens rapidly after DNA damage and requires the ATM, ATR, and DNA-PK kinases. This phosphorylation of the chromatin fibre occurs in megabase arrays around the double strand break site, where 53BP1 and BRCA1 are subsequently recruited (Soutoglou and Misteli, 2010). After DNA damage has been repaired, H2A.X is dephosphorylated by PP2A and PP4 (Chowdhury *et al.*, 2005) or removed from the chromatin fibre by the FACT complex (Heo *et al.*, 2008). H2A.X knockouts have shown increased genomic instability and cancer prevalence not recoverable in H2A.X rescue experiments with ser139 point mutations (Celeste *et al.*, 2003). While many histone modifications correlate with chromatin fibre states, the changes in fibre compaction after DNA damage provided a tractable system to test the consequences of various histone modifications. DNA damage marks such as phosphorylation of H2AX, H3, and H2B in addition to H2A ubiquitination were not causative however to the compaction state alterations in the chromatin fibre (Fernandez-capetillo, Allis and Nussenzweig, 2004; Kruhlak *et al.*, 2006; Lee *et al.*, 2015; Ui, Nagaura and Yasui, 2015).

In addition to histone modifications functioning in the DNA damage response pathway, recent studies have found that they can also predispose a region to chromosome instability. For instance, the frequency of double strand breaks and translocations is associated with H3K9me3 depletion whereas active marks H3K27ac and H3K4me1 were enriched irrespective of underlying transcription levels (Burman *et al.*, 2015). In this study causality was demonstrated by tethering histone modifiers to a lac operon, altering the density of H3K9me3, H3K27ac, and H3K4me1, which affected break frequency. Despite transcription levels not being affected, H3K9me3 decreased endonuclease accessibility suggesting that a more open chromatin environment is prone to greater instability than more compact H3K9me3 containing regions.

Given the plethora of histone modifications and their enzymatic regulators, histone modifications are often transient. The retention of histone modifications after DNA replication and nucleosome turnover was assessed by capturing nascent chromatin strands (Alabert *et al.*, 2014). In HeLa cells, expelled histones were recycled in the subsequent two nascent DNA strands resulting in a hemi-modified state. Full recovery of histone modifications then occurs within the next cell cycle, except for heterochromatic marks H3K9me3 and H3K27me3 which develop more slowly over multiple cycles. How more rapidly dividing cells, such as embryonic stem cells, maintain heterochromatic domains is an unanswered question.

1.1.4 Bromodomains

As described above, lysine acetylation has been identified as prevalent regulatory post-translation modification that removes the residues positive charge (Kim *et al.*, 2006; Choudhary *et al.*, 2009). Acetyl- ChIP-seq studies have demonstrated a correlation of histone acetylation with actively transcribed genes, with aberrant acetylation and gene expression associated with tumorigenesis (Zhao *et al.*, 2014).

Bromodomains are a highly conserved motif, first identified in the *brahma* gene, that forms and highly charged molecular pocket facilitating protein-protein interactions on acetylated lysines (Haynes *et al.*, 1992). This domain is present in 42 proteins in the human genome with some containing multiple bromodomains or other histone interacting domains (Filippakopoulos, 2012). These proteins display a wide range of functions regulating gene expression. These range from scaffolding roles of large transcriptional complexes and individual catalytic functions including: methyltransferases, HATs, and helicases to function in chromatin organisation (Haynes, 1992; Yamane, 2006; Alsarraj *et al.*, 2013; Bao and Shen, 2014).

The additional domains within bromodomain containing proteins can also affect the binding affinity of the bromodomain pocket. For instance, a single bromodomain typically binds to the histone peptide with the N-terminus at the back of the pocket between the ZA-BC α-helices. This positions the lysine residue at the exit vector on the ZA helix (Filippakopoulos, 2012). An adjacent PHD domain however, as found in TIF1α, engages the N-terminus on H3K4 forcing the bromodomain to bind further down the peptide at

H3K23ac (Tsai *et al.*, 2010). By contrast, the adjacent PHD domain in the BPTF transcription factor differs by having its orientation reversed. When the PHD domain engages with methylated H3K4, the bromodomain orientation is therefore inverted limiting interactions with lysine residues on the same histone tail, and encourages *trans* H4K16 interactions within the same nucleosome (Ruthenburg *et al.*, 2011; Xi *et al.*, 2011).

While bromodomains are highly conserved across the 42 proteins within the human genome and across species, there is a sub family of bromodomain extra terminal [BET] proteins. These contain a C-terminal extra terminal region that allows for selective targeting of these bromodomains from the bromodomain family (Filippakopoulos *et al.*, 2010). The BET protein sub family is comprised of four proteins, Brd2, Brd3, Brd4, and BrdT. Each of these proteins contain two adjacent bromodomains allowing them to bind two acetylated lysine residues such as H4K5 and H4K8 by BrdT (Rousseaux *et al.*, 2009). Whether these adjacent domains bind to lysine residues in *cis* or *trans* histone tails *in vivo* remains an area of discussion within the field.

More recent reports have demonstrated that BET proteins can also recognise non-acetyl lysine modifications including: propionylation, butyrylation, and crontonylation (Tan *et al.*, 2011; Sabari *et al.*, 2015; Goudarzi *et al.*, 2016). The functional role of such non-canonical lysine binding and its effect on BET acetylation interactions has yet to be fully elucidated however.

BET proteins are known to have key regulatory functions. Brd2 and Brd4 are both embryonic lethal in mice, and are known to function in cell cycle progression by regulating transcription of c-myc and other master growth regulatory genes (Houzelstein *et al.*, 2002; Shang *et al.*, 2009; Coudé *et al.*, 2015). Brd3 is known to interact with transcription factor GATA-1 to regulate erythroid specific differentiation genes, whilst BrdT is a testis specific transcription factor with similar functions to Brd4. Loss of BrdT results in aberrant testis development resulting in sterile mice (Shang *et al.*, 2007; Lamonica *et al.*, 2011).

The canonical transcriptional regulatory mechanism of BET proteins revolves around the recruitment of the p-TEFb complex (CDK9 and cyclin T) to transcriptional start sites, facilitating paused RNA polII phosphorylation and transcriptional elongation (Kyoo Jang *et al.*, 2005; Yang *et al.*, 2005; Itzen *et al.*, 2014). Given the fundamental functions of these proteins for efficient transcription and faithful cell cycle progression, their binding profiles vary significantly between cell types. The regulatory mechanism behind these different binding profiles has yet to be fully understood and is currently an area of significant interest.

Additionally bromodomain protein mutations commonly occur in cancer, likely due to their key role in transcription and proliferation. In Paediatric cancers, for instance, 21 of the 42 bromodomain containing proteins have increased mutation frequencies. How these mutations effect cellular phenotypes have yet to be fully explored however. Bromodomain proteins are also common sites of translocations and gene fusions in cancer. NUT midline carcinoma, for example, is caused by the fusion of Brd3 or Brd4 to nuclear protein in the testis (NUTM1). NUT proteins normally function to recruit HAT enzymes including CREBBP and P300, acetylating the surrounding histones. When fused to a BET protein that in turn recognises histone acetylation, this results in unregulated expanding regions of hyperacetylation only limited by TAD boundaries resulting in this disease (Haack *et al.*, 2009; Alekseyenko *et al.*, 2015). Understanding the function and regulation of BET proteins therefore is a key question in both developmental and therapeutic fields.

1.1.5 Chromatin remodelling complexes

A diverse range of proteins aside from histones bind chromatin *in vivo*. Chromatin re-modellers alter nucleosome frequency or composition where they act at a local level causing small scale disruptions to the chromatin fibre and changing the accessibility of the underlying DNA. With such a fundamental role chromatin re-modellers are found in many chromatin dependent processes, such as replication, cell cycle progression, DNA damage repair and transcription. The ATP dependent active domains of these re-modellers are split into four classes: SWI/SNF, ISWI, INO80, and CHD.

SWI/SNF re-modellers are found in large complexes with other polypeptides in two different classes: BAF (BRG1 associated factors) and PBAF (Polybromo associated factor). In humans, BAF complexes contain both ATPase subunits, BRM and BRG1. PBAF by contrast only contains BRG1, but sharing many other bromo associated core factors with BAF complexes (Mohrmann and Verrijzer, 2005). SWI/SNF specificity is regulated by varying the DNA binding domain and bromodomain composition of subunits, allowing loci and tissue specificity via nucleotide sequence and the nucleosome acetylation state (Shen *et al.*, 2007; Dechassa *et al.*, 2012). SWI/SNF function is important for genome regulation, and components have an increased mutation rate in cancer. PBAF component BAF180 is recruited to DNA damage sites resulting in silencing of the surrounding region (Kakarougkas *et al.*, 2014). SWI/SNF complexes also have important functions in sister chromatin cohesion and decatenation. Specifically, loss of SWI/SNF components results in an increase in cytological chromosome breaks and lagging chromosomes in mitosis respectively (Dykhuizen *et al.*, 2013; Brownlee *et al.*, 2014).

The ISWI class of re-modellers incorporate SNF2H or SNF2L ATPase's. They are associated with a diverse range of functions, both repressing and activating target loci. The ISWI complex NURF is recruited to promoters by the GAGA transcription factor, where it alters nucleosome spacing to facilitate transcription (Mizuguchi *et al.*, 1997; Xiao *et al.*, 2001). Studies investigating the distribution of core ISWI catalytic subunits in *Drosophila* found that ISWI rarely correlated with RNA polymerase II distribution on polytene chromosomes, suggesting it has a more general role at transcriptionally inactive genomic regions (Deuring *et al.*, 2000). Furthermore in yeast, ISWI homologues reposition nucleosomes at promoters, making them nuclease-inaccessible and repressing gene expression (Goldmark *et al.*, 2000). ISWI also functions in the DNA damage response pathway. The ACF and CHRAC complex subunit ACF-1 interacts with HP1 proteins and binds to DNA double strand breaks similarly to phosphorylated H2A.X facilitating NHEJ break repair (Eskeland, Eberharter and Imhof, 2007; Luijsterburg *et al.*, 2009).

INO80 chromatin re-modellers are characterised by having a split ATPase domain across two subunits. This ATPase module associates with RuvB-like helicase proteins, known to bind replication forks and holiday junctions *in vitro.* (Iwasaki and Takahagi, 1991; Shen *et al.*, 2000). These complexes were shown to regulate H2A.Z and phospho-H2A.X histone exchange throughout the genome and at DNA damage sites (Papamichos-chronakis *et al.*, 2012; Bao and Shen, 2014). Loss of INO80 and redistribution of H2A.Z causes fork collapse slowing S-phase progression (Hur *et al.*, 2010) whilst loss of INO80 at DNA damage foci disrupts the 5′-3′ resection of the DNA strands during homologous recombination (Gospodinov *et al.*, 2011). Histone acetyltransferase TIP60, a component of the INO80 complex, is required to open chromatin for DNA repair and to subsequently remove phospho-H2A.X to restore the basal chromatin state (Kusch *et al.*, 2004).

In addition to acetyl recruiting poly bromodomain re-modellers such as BAF180 (Porter and Dykhuizen, 2017), chromo helicase domain (CHD) complexes are characterised by their ability to bind methylated histones. The nucleosome remodelling and deacetylase complex NuRD is the only CHD complex currently thought to be recruited via transcriptional regulators. The active subunit CHD3/4 with HDAC1/2 promotes transcriptional repression of the Hox locus through its interaction with hunchback in *Drosophila* (Kehle *et al.*, 1998; Zhang *et al.*, 1998). NuRD's interaction with the ELKF transcription factors is mediated by the addition of small ubiquitin-like modifiers (SUMOs), resulting in KAP-1 target transcriptional repression (Siatecka, Xue and Bieker, 2007). In addition to gene regulation, CHD3 – NuRD complexes are released from heterochromatin after DNA damage resulting in chromatin fibre disruptions (Goodarzi, Kurka and Jeggo, 2011). CHD recruitment specificity via its chromodomain to methylated histones,

however, remains controversial and chromodomain deletions of CHD1 in *Drosophila* do not affect its distribution and can bind H3K4 peptides independently of the methylation state (Morettini *et al.*, 2011).

Chromatin re-modellers play an important role in facilitating the dynamic changes in chromatin fibre structure required throughout the cell cycle, kinase signalling responses and gene regulation. Understanding their mechanical properties in manipulating the chromatin fibre is an area of interest within the field; new cryo-electron microscopy approaches are providing significant new insight (Aramayo *et al.*, 2018). However, our limited knowledge of chromatin fibre structure still limits our understanding of how fibres are manipulated by remodelling complexes.

1.1.6 Topoisomerases

In addition to manipulating nucleosomes to alter chromatin fibre structure, abnormal DNA topology and catenation can affect the overlying chromatin structure. The topoisomerase family exhibit the capability to resolve these exotic DNA tertiary structures by inducing single or double stranded breaks (Charvin, Bensimon and Croquette, 2003). Type 1 topoisomerases (Top1) introduce single strand breaks and are subdivided into A/B depending on whether they bind to the 5′ or 3′ strand respectively. Top1A enzymes allow one DNA strand to pass, bridged by the enzyme, relaxing negative supercoiled DNA (Dekker *et al.*, 2002). Top1B in contrast allows the DNA strands to rotate independently of each other in a torsion dependent manner, releasing either positive or negative supercoils (Koster *et al.*, 2005; Taneja *et al.*, 2007). Type 2 topoisomerases (Top2) are also subdivided into A/B on their molecular structure but have similar mechanisms of action. Top2 releases topological stress by inducing double stranded DNA breaks facilitated by ATP-dependent reverse gyrase activity (Roca and Wang, 1992; Berger *et al.*, 1996).

Many biological processes induce mechanical stress on chromatin topology including, transcription, replication, and anaphase. During transcription RNA polymerase over-winds DNA downstream inducing positive supercoils, whilst negative supercoils are formed upstream (Liu and Wang, 1987; Giaever and Wang, 1988). This produces a positive or negative extra turn in the DNA molecule every 10 bp of transcription, making topoisomerase activity essential for the transcription of long genes, and prevents exotic DNA structures such as plectonenes and cruciforms (Cook *et al.*, 1992). Mutations in Top1 in autistic patients appear to preferentially affect transcripts >200 kb, indicating the important function of topoisomerases (King *et al.*, 2013). Transcription-dependent supercoiling from has been shown to stall replication forks, but normal Top1 activity functions to resolve these conflicts, facilitating replication of active genomic regions (Tuduri *et al.*, 2009).

Top2 enzymes are proposed to resolve the positive or negative supercoils across replication regions. Converging replication forks can amplify this topological stress slowing replication in the absence of Top2 (Baxter and Diffley, 2008). In addition to this function, Top2 has been implicated in chromatin condensation (Adachi, Luke and Laemmli, 1991). In metaphase Top2 forms a structural axis the length of the chromosome required for chromatid core separation (Giménez-Abián *et al.*, 1995), whilst Top2 loss reduces intra-chromatid fidelity resulting in entangled chromosome arms (Uemura *et al.*, 1987; Spence *et al.*, 2007). The consequences of a loss of chromatid fidelity results in multiple aberrant mitotic phenotypes, prevents cell cycle progression and induces cell death (Carpenter and Porter, 2004). The exact role of Top2 at mitotic chromosomes remains unclear, along with their role within high order chromatin structures.

1.1.7 Cohesin and Condensin

Structural maintenance of chromosome (SMC) proteins, are found in the highly conserved condensin and cohesin complexes. These complexes function in the modulation of chromosome structure and are required for transcription, mitotic condensation, and chromatid separation. SMC proteins have large coiled arms of alpha helices spanning 65 nm, with globular heads at either end. One of these domains interacts with its SMC partner forming a molecular hinge to the complex (Haering *et al.*, 2002). The diametrically free head domains of this SMC heterodimer interact with a kleisin-type component, in order to close the molecular loop in an ATP-dependent manner (Hu *et al.*, 2011). Due to this large ring like structure SMC complexes are thought to associate with chromatin topologically rather than a DNA sequence mediated interaction (Murayama and Uhlmann, 2014).

Cohesin complexes contain an SMC1/SMC3 heterodimer closed by RAD21, with chromosome loading facilitated by STAG (Tóth *et al.*, 1999; Hu *et al.*, 2011). Mammalian condensin has a SMC2/SMC4 heterodimer, and two separate groups of subunits. Condensin I is closed by CAP-H with CAP-D2 and CAP-G (Hirano, Kobayashi and Hirano, 1997; Schmiesing *et al.*, 2000). Condensin II contains CAP-H2, CAP-D2 and CAP-G comparatively (Ono *et al.*, 2003; Yeong *et al.*, 2003).

Despite their striking structural similarities, the molecular functions of cohesin and condensin are distinct. Cohesin maintains sister chromatid cohesion after replication to allow faithful separation upon its cleavage during anaphase (Uhlmann, Lottspeich and Nasmyth, 1999). Cohesin is initially loaded onto chromatin in an ATP-dependent manner during G1 by SMC loader NIPBL (Ciosk *et al.*, 2000). Throughout G1 cohesin levels equilibrate via its constant unloading via WAPL and PDS5 (Tedeschi *et al.*, 2013). During replication, the cohesin ring structure is stabilised by SMC3 acetylation mediated by Sororin which prevents WAPL-cohesin removal (Hou and Zou, 2005; Nishiyama *et al.*, 2010). In conditional WAPL knock out cells, cohesin unloading is also prevented resulting in vermicelli like chromatin condensation in G1 and abnormal chromosome segregation during mitosis (Tedeschi *et al.*, 2013). Regulation of cohesin loading and stabilisation therefore has a fundamental architectural role in chromatin organisation throughout the cell cycle.

In mitosis, for WAPL to access cohesin complexes and allow sister chromatid separation, Aurora B or CDK1 phosphorylates Sororin expelling it from cohesin complex, (Dreier, Bekier and Taylor, 2011). This initially occurs along the chromosome arms during prophase as the centromere is protected from phosphorylation by Shugoshin recruited phosphatases (Meppelink *et al.*, 2015). During anaphase, cleavage of centromeric cohesin occurs by separase (Uhlmann, Lottspeich and Nasmyth, 1999). In order for cohesin complexes to be reloaded in the following cell cycle, HDAC8 is required to deacetylate SMC3 (Xiong, Lu and Gerton, 2010; Deardorff *et al.*, 2012).

Cohesin has also been implicated in modulating large-scale chromatin structure. Cohesin chromatin loading correlates with CTCF sites at structural chromatin boundaries (Parelho *et al.*, 2008). This has led to the proposal of cohesin loops linking chromatin fibres in the same manner as sister chromatids but in *trans* across a chromosome. Recent Hi-C studies in cohesin knock out cells results in the loss of all loop domains (Rao *et al.*, 2017). Despite such stark changes in large-scale chromatin organisation, transcriptional regulation is only modestly affected. This suggests that while cohesin complexes help organise chromatin throughout the nucleus they do not inherently regulate the accessibility of the underlying genes (Schwarzer *et al.*, 2017).

It is maybe not surprising then that mutations in cohesin subunits are not lethal, albeit with severe pathology. Patients with cohesin mutations, such as Cornelia de Lange Syndrome (CdLS), exhibit cognitive impairment, limb defects, and delayed development. However rather than mitotic defects, CdLS cellular defects appear to be transcriptional, suggesting that the minor regulatory role of cohesin on transcription is an essential function in development outside of mitotic division (Liu *et al.*, 2009). Indeed the loss of a single boundary element can result in aberrant enhancer activity and transcription in nearby genes (Lupiáñez *et al.*, 2015).

Condensin's primary role is to compact chromosomes in the early stages of mitosis and resolve sister chromatid cohesion in cooperation with Top2 (Coelho, Queiroz-Machado and Sunkel, 2003; Hirota *et al.*, 2004). However, condensins also have regulatory roles within interphase. Hi-C data indicates that condensin complexes co-localise with transcription factor IIIC complexes (TFIIIC) to form strong TAD boundaries during interphase that support constitutively active gene cluster transcription (Yuen, Slaughter and Gerton, 2017).

During mitotic compaction condensin I facilitates lateral chromosome compaction, while condensin II is required for longitudinal compaction across the length of the chromosome (Green *et al.*, 2012).

Polymer modelling of Capture-C experiments first suggested the formation of consecutive chromatin loops 80-120 kb in mitotic chromatin fibres (Naumova *et al.*, 2013). This has led to the proposal that condensin modulates these large chromatin looping domains (Skoko *et al.*, 2006; Alipour and Marko, 2012). Once formed, these loops then undergo axial compression mediated by Top2 (Coelho, Queiroz-Machado and Sunkel, 2003). Condensin's role in chromatin condensation is however still questioned, as chromatin compaction is not completely abrogated in condensin or Top2 absence (Hudson *et al.*, 2003; Carpenter and Porter, 2004; Houlard *et al.*, 2015). This has led to the contrasting view that condensins regulate higher order chromosome architecture rather than the underlying chromatin fibre compaction state (Vagnarelli *et al.*, 2006).

Although Condensin I and II have contrasting roles, they function cooperatively for correct mitotic cytological compaction. Detailed experiments in *Xenopus* extracts demonstrated that altered ratios of condensin I and II resulted in longer and thinner chromosomes (Shintomi and Hirano, 2011). Primary condensin II mediated cytological condensation is thought to be essential for correct mitotic chromosome formation as condensin I is cytoplasmic until the breakdown of the nuclear envelope (Gerlich *et al.*, 2006).

Similar to cohesin loading, condensin II loading is stabilised during S-phase. After replication, condensin II stabilisation mediates the formation of sister axes functioning in faithful resolution of sister chromatids (Ono, Yamashita and Hirano, 2013). Once the nuclear envelope is dissolved, condensin I then associates along the chromosome in an alternating distribution with condensin II (Ono *et al.*, 2004). Recent seminal studies have demonstrated the spiral loading dynamics of condensin II complexes to form the axial core of metaphase chromosomes (Gibcus *et al.*, 2018). This spiral core supports the formation of condensin I mediated nested loops resulting in the characteristic late prometaphase chromosomes.

Recent studies have also suggested that condensin II interacts with holiday junction recognition protein (HJURP) and is required for correct centromeric deposition of CENP-A and centromere function (Barnhart-Dailey *et al.*, 2017). In conjunction with Gibcus's, (2018) work suggesting condensin II loading only occurring at the chromosome core, this would provide a mechanism for kinetochore attachment to each chromosome's for proper segregation.

1.2 Chromatin Structure

Chromatin structure is both dynamic and diverse making studying its structure a challenging goal. In nuclei, human interphase chromatin is not discernible by traditional microscopy techniques. Recent work has coupled DNA staining with polymerisation of diaminobenzidine (DAB) for electron microscopy to study chromatin in structure inside nuclei (Ou *et al.*, 2017). The validity of such techniques to broadly study chromatin structure is still debated however, as there may be a bias in the dye (DRAQ5) DNA binding distribution. DRAQ5 may preferentially bind to more open euchromatic regions or be unable to come into contact with DAB molecule when bound to heterochromatic DNA.

Unlike humans, mouse chromatin has distinct chromatin structures observable by traditional microscopy methods. Observable heterochromatic chromocenters form in many species including mice, although the underlying structure is still unresolvable. *In vitro* studies of chromatin via electron microscopy while revealing characteristics of fibre structure are limited in their applicability to the complexity of *in vivo* chromatin. For instance understanding how current fixation methods might affect fibre structure, in electron microscopy methodology remains an important question.

1.2.1 Nucleosome arrays and the 30-nM fibre

The base unit of eukaryotic chromatin contains, a nucleosome core particle of a H3:H4 tetramer with two H2A:H2B dimers bound to it. Wrapped twice in 147 base pairs of DNA, these nucleosome core particles are stabilised by histone H1 binding on the dyad and connected by 10-100 bp "linker" DNA (Holde, 1989). The exact position of H1 is still debated, with one model claiming the globular domain lies on top of the dyad interacting with both DNA linker strands (Allan *et al.*, 1980; Hussain *et al.*, 2010). Alternatively the globular domain is removed from the dyad and interacts with only one linker DNA strand (Pruss *et al.*, 1996; Brown, Izard and Misteli, 2006). More recent studies have shown that linker histone isoforms H1 and H5 differ in their binding positions due to altered DNA-contacting residues in *Drosophila* and chicken respectively (Zhou *et al.*, 2016). Off dyad binding has also been demonstrated in the human linker isoform H1.4 (Song *et al.*, 2014). Additionally canonical H1 has recently been shown to bind at the dyad but primarily associating with a single DNA linker, suggesting an asymmetrical nature to the nucleosome (Bednar *et al.*, 2017).

While our knowledge of nucleosome composition is well defined, how multiple nucleosomes are folded into a fibre with a width of 30-nm is still hotly debated. Multiple models have been advocated; the solenoid model with a helical array, the zig-zag model of alternating nucleosome stacking, and an irregular model with varying nucleosome spacing and organisation. Recent advances in super resolution microscopy in addition to electron microscopy techniques and small angle x-ray diffraction have been used over the past 50 years to discern fibre structure (Gall, 1966; Sperling and Tardieu, 1976; Ricci *et al.*, 2015). While investigating *in vitro* reconstituted chromatin has been possible, the structure of chromatin fibres within nuclei has remained elusive, only defined as a dense mass.

Despite such debate, chromatin within a living cell is required to be dynamic and malleable, unlikely to result from a homogenous 30-nm fibre structure. More likely is a heteromorphic fibre of multiple models, with more compact or disrupted loci dependent on the genomic region (Grigoryev *et al.*, 2009). This is likely due to the underlying transcriptional state with constitutively inactive regions having regular nucleosomes and forming a more uniform 30-nm fibre structure, whereas, global conformation is less regular and interspersed with many disruptions (Gilbert and Allan, 2001). Chromatin re-modellers alter nucleosome positioning allowing transcription factor binding, DNA replication, and repair to occur. Therefore one can see how in the dynamic nature of a living, dividing cell responding to environmental stimuli, fibre disruptions may occur resulting in a heteromorphic fibre structure. These disruptions to nucleosome occupancy can be investigated through the accessibility of the DNA to nuclease digestion (Allan *et al.*, 2012).

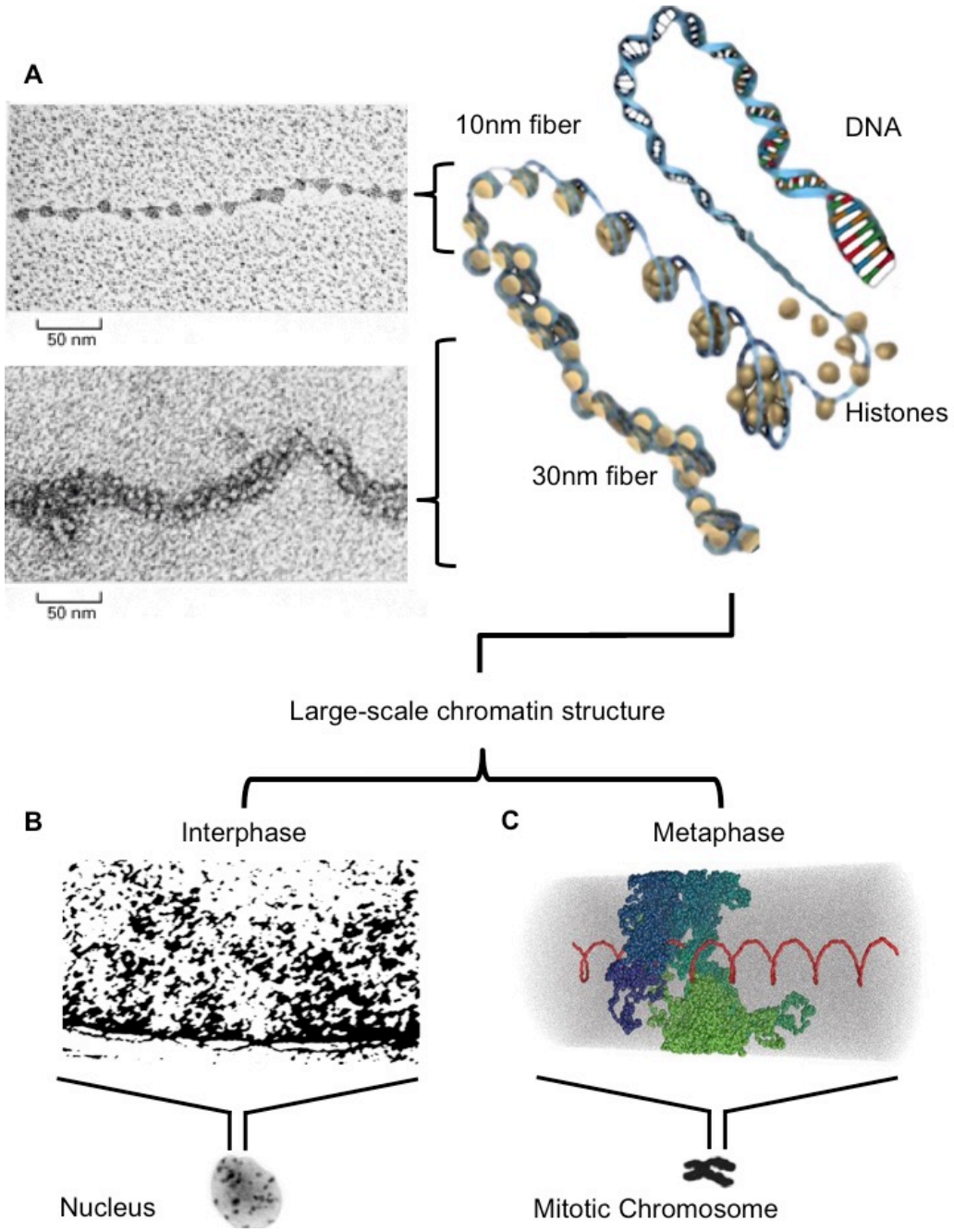

Figure 1.2 Overview of the different orders of chromatin organisation. (A) 147 bp of the helical DNA structure is wrapped around an octomer of histone proteins to form a nucleosome. Sequential histone deposition results in a 'beads on a string' like 10 nm fibre, while inter-nucleosome interactions generates a chromatin fibre in the order of 30 nm. The compaction mechanisms above 30 nm have not been fully resolved, however chromatin forms distinct large-scale structures in interphase that are then further compacted into metaphase chromosomes. (**B)** DRAQ5 staining in interphase demonstrates the accumulation of chromatin at the nuclear periphery (**C)** Hi-C modelling throughout mitosis suggests large-scale loop structures emanating from a spiral axial core on condensin molecules (red). Resources collated from Alberts, (1994); Ou, (2017); and Gibcus, (2018)

1.2.2 Large-scale chromatin structure

Beyond the 30-nm fibre, chromatin fibres are organised into large-scale chromatin structures. Methods to investigate large-scale structures are currently limited, and detailed understanding is lacking, outside the probable formation of chromatin loops. Domains thought to correspond to 'accessible' and 'compact' regions can be differentiated by their AT:GC nucleotide ratio, histone modification profiles and subsequent bound proteins. Historically this has been segmented into gene rich euchromatin, and gene poor heterochromatin, based on the intensity of intercalating dyes in interphase. Interphase euchromatin has a lower intensity of intercalating dyes than heterochromatin and therefore is perceived as more open, although this could be attributed to DAPI sequence bias. During metaphase however chromatin is uniformly dense suggesting that de-compaction post mitosis must be targeted.

Recent genome wide studies of transcription and modification states has provided greater stratification into five different classifications: 1- constitutively active regions, 2- tissue specific active loci, 3- silenced developmental and differentiation loci, 4- repressed gene rich regions, and 5- constitutive silenced satellite and repetitive elements (Steensel, 2011). Regions 1 and 2 contain the actively transcribed regions of the genome characterized by their enrichment in histone acetylation. Due to transcriptional activity within these loci, they are expected to contain more disruptions to the chromatin fibre, resulting in a more flexible open structure to facilitate transcription. Transcriptionally repressed genes and repetitive elements in the other classes by contrast will have a more ordered compact higher order structure.

Living cells do however maintain a functional need to access these more compact regions for biological processes such as replication and DNA damage repair mediated by chromatin re-modellers. The inherent property of the compact higher order structure does however reduce the accessibility of the underlying DNA when compared to a disrupted fibre. This is discernible by these regions being late replicating and responding more slowly to DNA damage (Keohane *et al.,* 1996; Sadoni *et al.,* 1999).

1.2.3 Higher order structure methods and TADs

Chromosome conformation capture (3C) and fluorescence *in situ* hybridization (FISH) based methods are the two most widely adopted techniques to study chromatin higher order structure (Bickmore and Van Steensel, 2013). FISH involves the hybridization of fluorescent probes with specificity to individual loci up to entire chromosomes. Chromosome conformation capture by contrast scores the frequency of a DNA fragment contacting with another that can be multiplexed by next-generation sequencing across the entire genome. This relies on "fixing" the chromatin structure with formaldehyde, fragmenting and ligating proximal DNA fragments, before the PCR or sequencing output. These techniques have complimentary technical methodologies. FISH benefits as a single cell technique but with resolution limited by microscopy methods, while 3C methods have base pair resolution, but is limited as it is population average data and has the potential bias input by the fixation technique.

The prevalence of 3C-based experiments has led to adoption of the topological associating domains (TADs) concept. This suggests that the human genome is divided into almost ten thousand loops/TADs on average 185 kbp in size (Rao *et al.*, 2014). These TADs prevent external chromatin interactions, correlating with histone modification profiles and replication timing (Pope *et al.*, 2014; Huang *et al.*, 2015). The functional relevance of TADs to genome regulation is nonetheless still under debate, as TAD profiles are not affected by cell type. However translocation frequency in B cells correlates with 3C interaction frequencies, demonstrating a functional role to interaction frequency (Y. Zhang *et al.*, 2012).

Validation of 3C results using FISH has however had varied success. The confinement of intra-TAD chromatin interactions and organisation identified by 3C methods was confirmed by intra-TAD FISH probes having a physically closer association within the nucleus when compared to similar probe genomic distances between TADs (Nora *et al.*, 2012). By contrast a comprehensive study at the HoxD locus demonstrated varying success of cross validation in different developmental stages (Williamson *et al.*, 2014), suggesting that the two techniques might report on different levels of organisation.

However, these techniques have facilitated a large step in our understanding of higher order chromatin structure, despite their limitations. The advancement of these methodologies currently in process hopes to resolve the current conflicting experimental data. 3C techniques have been combined with sequence capture methods to allow deeper sequencing of defined genomic regions increasing the techniques resolution. Additionally, the Mistelli lab has addressed the throughput limitations of FISH experiments (Shachar *et al.*, 2015). Subsequent studies comparing Hi-C datasets to high throughput FISH has demonstrated a common independent allele in addition to population heterogeneity that was not detected by Hi-C (Finn *et al.*, 2017). This suggests that cell population based techniques have limited scope to investigate chromatin structure.

The static nature of our current understanding of genomic interactions will soon be addressed by the adaption of the CRISPR-Cas9 system. A recent study demonstrated the use of modified guide RNAs to achieve live cell imaging of non-repetitive loci, demonstrating a significant advantage to aid our understanding of chromatin fibre dynamics (Qin *et al.*, 2017).

1.3 Nuclear environment

Chromatin *in vivo* is found within the nucleus of a eukaryotic cell, determining the spatial environment for chromatin organisation. The nuclear position of a locus has a functional role in chromatin organisation, affecting chromatin structure, transcriptional state, and replication timing. The nuclear spatial orientation of a locus is unfixed and dynamic. Throughout differentiation many loci alter their nuclear position changing their functional properties (Peric-hupkes *et al.*, 2010).

Nuclear positioning however is not tightly defined and varies between cells, although intra-chromosomal long range interactions are tightly regulated (Chambeyron and Bickmore, 2004). Despite undefined specific 3D spatial orientations, loci's radial 2D distribution appears to be conserved throughout the genome. In mammalian cells the nuclear periphery generally contains gene poor regions and heterochromatic elements, while active genes usually have a more central position. In contrast, centromeres are generally located at the nuclear periphery, while telomeres are equally distributed throughout the nucleus in differentiated cells (Gilchrist *et al.*, 2004; Wiblin *et al.*, 2005).

The nuclear membrane, which separates the nucleus from the cytoplasm, is composed of a lipid bilayer with nuclear pore complexes facilitating shuttling. Lamin proteins are transported into the nucleus where they accumulate around the inner nuclear membrane forming the nuclear periphery once they are phosphorylated and post-translationally mature (Henekes *et al*, 1993; Kilic et al, 1999). Genomic regions at the nuclear periphery form lamina associated domains (LADs) between 100 kbp and 10

Mbp in size. Nuclear membrane components; the lamin B receptor, emerin, BAF, LAP2α/β, and SUN proteins facilitate this association. Constitutive and facultative LADs are found within the genome. Facultative LADs tend to be the silenced developmental and differentiated genomic regions that differ between cell types, whereas constitutive LADs are universal. Signalling pathways and chromatin modifiers interact with nuclear lamina proteins to regulate nuclear periphery heterochromatin histone acetylation, H3K9me3, and subsequent HP1α/β association (Oca, Andreassen and Wilson, 2011; Solovei *et al.*, 2011). Importantly, Solovei (2011) showed that the lamin B receptor alone is required to tether heterochromatin to the nuclear periphery and is required for Lamin A and Lamin C mediated tethering.

Heterochromatic domains are also recruited to the periphery of the nucleolus in a mechanism requiring nuclear lamins. Absence of Lamin B1 leads to dissolution of nucleoli (Martin *et al.*, 2009). LADs and nucleolar associated domains (NADs) are often flanked by insulators such as CTCF which tether the ends of the domains to the nuclear periphery in a lamin A dependent manner (Ottaviani *et al.*, 2009).

Premature lamin A that has not undergone the required farnesylation, directly binds to HP1α in addition to lamina bridging proteins LAP2α and BAF causing their accumulation at the nuclear periphery (Mattioli *et al.*, 2007). The interaction with HP1α is lost when prelamin A is farnesylated. HP1α disassociation from prelamin A-LAP2α complex, is thought to be a key regulator of chromatin conformation and transcription in myoblast differentiation (Lattanzi *et al.*, 2007; Capanni *et al.*, 2008). LAP2α lamin-chromatin interaction loci are regulated by nucleosomal HMGN5 regulating the level of heterochromatin condensation and mobility (Zhang *et al.*, 2013).

A series of mutations have been identified in lamin proteins associated with a wide range of phenotypes including muscular dystrophies, neuropathies, metabolic disorders, and premature ageing, together classed as laminopathies (Peters, John *et al.*, 1998; Bonne *et al.*, 1999). Lamin knockout models only show defects postnatally continuing the idea that the nuclear periphery functions in terminal differentiation. The rare and fatal Hutchinson-Gilford progeria syndrome (HGPS) laminopathy presents a premature ageing phenotype at 12 months and has received the most attention. HGPS patients have an LMNA mutation, disrupting the nuclear periphery organisation, and altered histone modification distributions. In more common laminopathies such as skeletal muscular dystrophy only rare patient samples found any evidence of abnormal nuclear envelope and heterochromatin structure and this effect was heterogeneous throughout the tissue sample (Sabatelli *et al.*, 2001; Sewry *et al.*, 2001). This less severe disruption to the nuclear periphery likely leads to the less severe phenotype and increased survival.

1.3.1 Chromosome territories

Chromosomes are de-compacted from mitosis to interphase, and occupy distinct 3D spatial volumes. This was first demonstrated by hybridising large numbers of specific probes across a specific chromosome, in fluorescence *in situ* hybridisation (FISH), to visualise a whole chromosome within the nucleus (Cremer *et al.*, 1988). The radial distribution of a chromosome is determined by its gene density, with gene poor chromosomes more likely to be associated with the nuclear periphery (Boyle *et al.*, 2001). Comparison of chromosomes 18 and 19, which have similar genomic sizes, maintain significantly different nuclear volumes and position. Gene rich chromosome 19 is found more centrally and has a larger nuclear volume than gene poor chromosome 18 in lymphoblastoid and fibroblast cell types (Croft *et al.*, 1999). Chromosome territories are not fixed, however, and differ in a tissue specific manner, with more closely related cells maintaining more similar nuclear territories in mice (Parada, Mcqueen and Misteli, 2004). Unlike mice where every chromosome is acrocentric, humans have 5 acrocentric chromosomes containing the tandem repeats of the ribosomal genes on their short arms. These acrocentric chromosomes cluster around the nucleolus to allow processing of the ribosomal RNA.

The intra-chromosomal radial distribution within a nuclear territory is also affected by gene density. Again gene rich regions are more central than gene deserts that are more situated nearer the periphery (Boyle, Rodesch and Bickmore, 2011). This nuclear organisation allows transcriptionally silent chromatin to be packaged more densely at the periphery while the less dense central volume is occupied by transcriptionally active loci. This less crowded central volume increases the accessibility of complexes, and metabolic factors

required to facilitate transcription allowing for some tissue specific required expression (Moen and Johnson, 2003). Given our limited understanding of chromatin fibre structure, the more discriminating components behind chromatin territories currently remains unascertained.

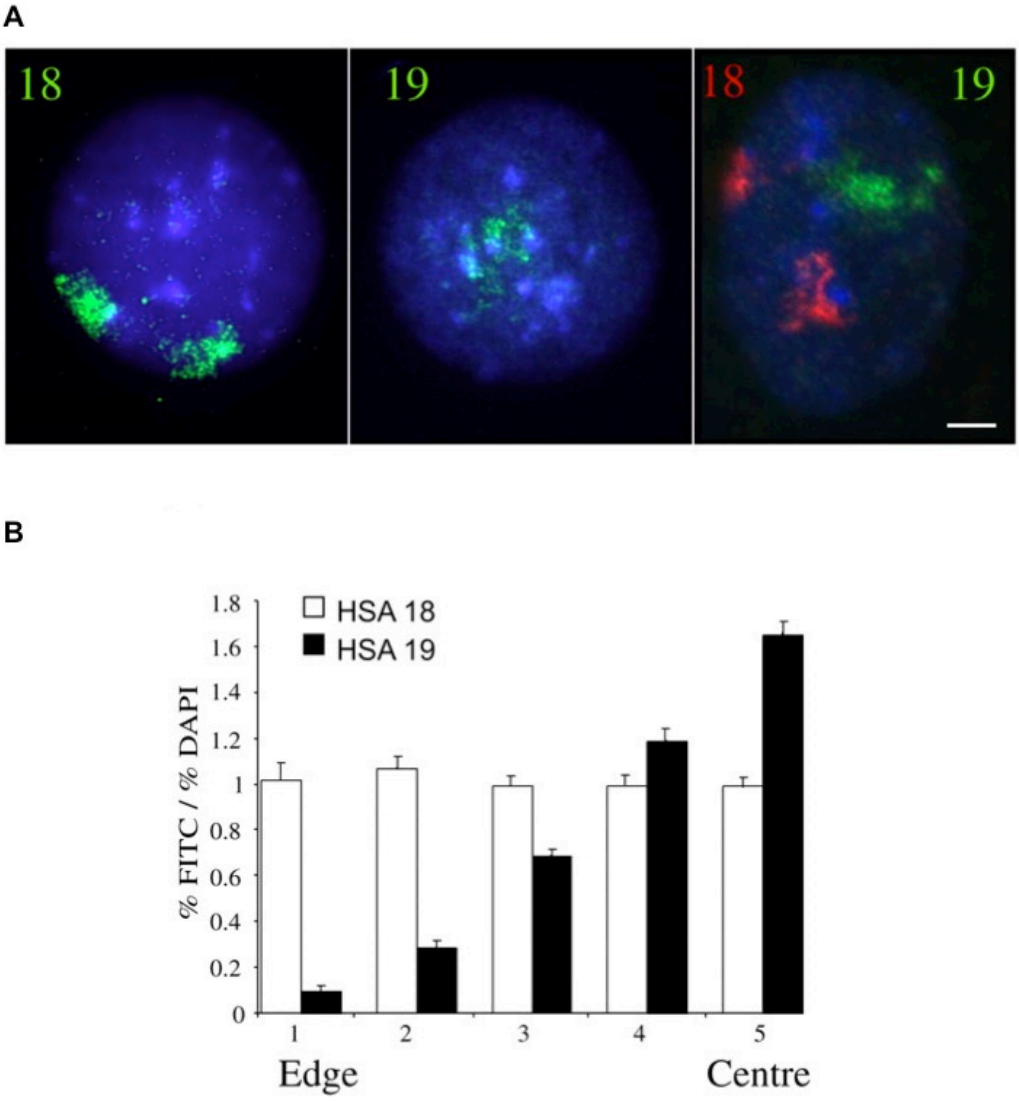

Figure 1.3 Nuclear radial distribution of HSA18 and HSA19 chromosomes in hESC's (A) hES cells DAPI stained nuclei, with hybridised HSA18 and HSA19 chromosome paints. Scale bar is 5 μm. (**B)** The radial distribution of HSA18 or HSA19 chromosome paints from de-convolved 2D images, binned into pentiles. N=50. Adapted from Wiblin, (2005)

1.3.2 Nuclear Scaffolds

Whether chromatin is suspended within the nucleus or attached to a nuclear matrix has been widely debated since the 1980s. Electron microscopy experiments demonstrated the presence of irregular fibres connected to the lamina at the nuclear periphery (Nickerson *et al.*, 1997) . This scaffold is lost after RNase but not DNase digestion suggesting an RNA component to its structure or regulation. However these structures have never been observed in live cells. (Craig *et al.*, 1997) demonstrated that the genomic regions associated with the scaffold were enriched for satellite repeats associated with cytological gene poor G bands. The nuclear matrix proteome was investigated by 2D electrophoresis after removing soluble proteins, lipids, cytoskeleton components, and chromatin from samples consecutively (Fey, Wan and Penman, 1984). Over 300 proteins have subsequently been identified as associating with this scaffold (Mika and Rost, 2005). The main classes of proteins identified were lamins, nuclear mitotic apparatus protein, and heterogeneous nuclear ribonucleoproteins (hnRNPs). The hnRNP A1 and B1 were proposed to regulate the nuclear matrix. This remained controversial due to their scarce abundance on the nuclear matrix filaments and inconsistent evidence, leading to the adoption of more dynamic models for nuclear organisation. Despite this concept of adoption remaining peripheral, recent studies have championed non-coding RNAs as pertaining nuclear scaffold functions.

The most defined role for a ncRNA on chromatin structure is XIST. Found on the X chromosome, this 15-17 kb long non coding RNA is required of X chromosome compaction and silencing (Penny *et al.*, 1996). Recent super resolution experiments suggest that XIST localises to around 200 foci on average 1 Mb apart along the X chromosome (Smeets *et al.*, 2014; Sunwoo, Wu and Lee, 2015). The interaction of XIST to the inactive X remains even in conditions that strip histones from the chromatin, suggesting a tight association with the underlying DNA (Clemson *et al.*, 1996). This tight association has made identifying protein interactors difficult, however an elegant study coupled RNA antisense purification with SILAC to identify functional interactions with SHARP, SAF-A, and LBR (McHugh *et al.*, 2015). SHARP, a subunit of the SMRT co-repressor, recruits HDAC3 and is required for the deposition of H3K27me3 by PRC2 along the X chromosome (You *et al.*, 2013). The XIST interaction with the lamin B receptor (LBR) has recently been supported by studies demonstrating a causative role for XIST RNA in X chromosome tethering to the nuclear lamina (Chen *et al.*, 2016).

More recent studies identified highly abundant interspersed repetitive elements, such as LINE-1 and CoT-1 associating with less dense euchromatic regions and fractionate with the nuclear scaffold components. Loss of these repetitive elements also causes chromatin condensation (Hall, Lisa *et al.*, 2014). Additionally long non-coding RNA HOTAIR interacts with polycomb component PRC2, targeting H3K27me3 mediated gene silencing at certain loci (Rinn, John *et al.*, 2007). These examples demonstrate that the interplay between non-coding RNA and their binding partners is likely crucial in their function in regulation of chromatin structure and transcription.

Recent papers have begun to contest the direct tethering of chromatin repressors by RNA, however. *In vitro* biochemical analysis by Wang *et al.*, (2017) suggested that PRC2 has robust DNA binding affinity towards methylated GC rich linker DNA, and that RNA acts as a competitive inhibitor to this DNA binding sequestering PRC2 away from the chromatin. This confirms the *in vivo* studies demonstrating PRC2 binding to nascent RNAs (Kaneko *et al.*, 2013). The nucleosome-depleted regions at active promoters would therefore enhance PRC2 binding, suggesting that RNA mediated sequestering of PRC2 from actively transcribed genes as a fundamental process of constitutive gene expression (Yuan *et al.*, 2005; Schones *et al.*, 2008; Helbo *et al.*, 2017). Additionally, the direct tethering of PRC2 by HOTAIR has recently been questioned. Portoso *et al.*, (2017) demonstrated that HOTAIR recruitment alone was required for gene silencing, and that PRC2 recruitment is a consequence of the loss of nascent RNA after transcriptional repression.

An example of RNA binding proteins regulating chromatin structure was recently demonstrated by the hnRNP protein, SAF-A. This protein was identified as being associated with the nuclear matrix (Romig *et al.*, 1992). The function of SAF-A remains unclear but has identified roles in DNA repair, kinetochore assembly and gene splicing (Ma *et al.*, 2011; Xiao *et al.*, 2012; Britton *et al.*, 2014). A recent comprehensive study demonstrated that SAF-A formed transcriptionally dependent large oligomers that maintain euchromatic chromatin structure. Additionally SAF-A loss resulted in the accumulation of phospho-H2AX, implicating SAF-A in genome stability (Nozawa *et al.*, 2017).

1.4 Chromatin structure and gene regulation

The first evidence for chromatin de-condensation upon gene activation was the accessibility of nucleases to digest active and inactive genes (Gottesfeld, Murphy and Bonner, 1975; Bloom and Anderson, 1979). This was first observed directly when transcriptional activators were tethered to regions labelled with GFP *in vivo* (Tumbar, Sudlow and Belmont, 1999; Tsukamoto *et al.*, 2000). Although this was a synthetic setting, FISH experiments also demonstrated chromatin de-condensation at the endogenous Hoxb cluster (Chambeyron and Bickmore, 2004) after activation. In addition to cytological de-condensation, gene activation is now associated with hyperacetylation, hypomethylation, DNaseI sensitivity, and loss of linker histones, indicative of generating more accessible chromatin fibres.

The basal state and level of de-compaction is dependent of the genomic loci. A heterochromatic transgene spanning 90 Mbs de-condensed 30 fold, while a 375 kb region of the major histocompatibility complex de-condensed less than 2 fold from a more open basal state (Tumbar, Sudlow and Belmont, 1999; Müller *et al.*, 2004). The highest level of cytological de-condensation has been observed at highly active genes such as 75S RNA and ribosomal RNA genes theoretically de-condensing to the level of the 10 nm fibre (Daneholt *et al.*, 1982; González-Melendi *et al.*, 2001). Experiments using sucrose sedimentation techniques demonstrated that chicken erythrocyte β-globin gene had a more disrupted chromatin fibre upon activation (Kimura *et al.*, 1983). This was later shown to be due to the loss of a nucleosome at a DNaseI

hypersensitive site, creating a disruption, thus fibre de-condensation upon gene activation has yet to be directly demonstrated (Caplan *et al.*, 1987). However the presence of a polymerase molecule on a chromatin fibre is associated with a temporary de-compaction from the 30 nm chromatin fibre state (Andersson, Bjorkroth and Daneholt, 1984). Additionally induced gene activation on plasmids in yeast sediment more slowly, indicative of a more disrupted chromatin fibre (Kim and Clark, 2002). Furthermore, the Bickmore lab later demonstrated that gene rich regions correlate with more disrupted chromatin fibres. Although this relationship is not directly indicative of transcription, it suggests that the de-condensed chromatin state is permissive for transcription (Gilbert *et al.*, 2004).

Active genes also maintain lower levels of linker histone H1 (Tazi and Bird, 1990) which is thought to influence folding of the 30nm fibre, and suggests that linker histones can be a repressor of gene transcription (Thomas, 1984). Loss of linker histones results in global changes in chromatin structure and mitotic defects (Fan *et al.*, 2005; Maresca, Freedman and Heald, 2005). Detailed studies demonstrated that the effect of linker histones on transcription was gene specific, mediated by the occlusion of transcription factors (Laybourn and Kadonaga, 1991; Shen and Gorovsky, 1996; Crane-Robinson, 1999). While triple knockouts in mice are embryo lethal, individual knockouts do not effect growth suggesting that these gene specific H1 functions are not essential or that there is significant compensation mechanisms (Takami and Nakayama, 1997; Hashimoto *et al.*, 2010).

The expression levels of genes are also inversely correlated with DNA methylation. Many highly expressed genes involved in cellular homeostasis contain un-methylated 5′ CpG islands (Mikkelsen *et al.*, 2007). These ubiquitously transcribed promoters also exhibit decreased linker histone levels (Kamakaka and Thomas, 1990). Recent work demonstrated that promoters with CpG islands resulted in a nucleosome depleted region independent of transcription levels (Valouev *et al.*, 2011; Fenouil *et al.*, 2012). The functional role of CpG islands and these depleted regions is a current area of debate. It's generally accepted that the nucleosome depletion increases accessibility to DNA binding transcription factors. Unpublished work from the Gilbert lab also suggests that these 5′ CpG islands have a structural function in facilitating transcription mediated supercoiling. Furthermore, the Balasubramanian lab has proposed the existence of the exotic DNA structure the G-quadruplex at promoters (Huppert and Balasubramanian, 2007) whilst further experiments have demonstrated that the stability of G-quadruplexes within promoters positively correlates with transcription (Renčiuk *et al.*, 2017).

Recently RNA has been associated with chromatin de-condensation upon gene activation. As mentioned earlier, interspersed repetitive elements, Line-1 and CoT-1 transcripts function within the nuclear scaffold, maintain the euchromatic de-condensed state (Hall, Lisa *et al.*, 2014). Complimentarily long non-coding RNA transcripts (lncRNA) from enhancers (eRNA) throughout the human genome have been implicated in gene activation (Andersson *et al.*, 2014; Pefanis *et al.*, 2015). These >200 bp transcripts are transcribed by RNA polymerase II (polII), lack open reading frames, and can be post-translationally modified (Kung, Colognori and Lee, 2013). However unlike other lncRNAs, eRNAs are rarely spliced and are rapidly degraded by the exosome. This results in most eRNA transcripts fractionating with chromatin bound proteins (de Santa *et al.*, 2010). Recent studies have demonstrated that exosome mediated termination of PolII enables nascent eRNAs to recruit transcription factors to the local environment (Lemay *et al.*, 2014; Sigova, 2015). Correspondingly, eRNAs are proposed to promote site specific chromatin disruptions to facilitate gene activation (Mousavi *et al.*, 2013). Furthermore, seminal experiments from Nozawa *et al.*, (2017) demonstrated that RNA in conjunction with SAF-A is required for transcriptional de-condensation of the chromatin fibre.

1.4.1 Facultative gene silencing

The basal chromatin state is broadly considered to be repressive. However, promoting this condensation further may be necessary to prevent aberrant transcription. As touched upon earlier, ncRNAs have been associated with classical X-inactivation, and recruitment of polycomb complexes (PcG). First identified in *Drosophila*, antipodal PcG and thrithorax complexes transiently modulate developmental gene expression in a tissue specific manner (Ingham, 1983). PcG proteins form PRC1 or PRC2 complexes depending on the presence of subunit RING1A/B or EZH1/2 respectively. PRC2 functions as a H3K27 histone methyltransferase (Kuzmichev *et al.*, 2002) but regulation of PRC2 targeting remains to be fully elucidated. Along with lncRNA HOTAIR, JARID2 and PHF19 have been implicated in directing PRC2 recruitment (Pasini *et al.*, 2010; Walker *et al.*, 2010). JARID2 functions with PRC2 component AEBP2 to facilitate *de novo* H3K27 methylation, although mechanistically this is not precisely defined (Son *et al.*, 2013). PRC2 subunit PHF19 via its tudor domain binds to the active histone mark H3K36me3 allowing repression of currently active genes in mESCs (Brien *et al.*, 2012; Cai *et al.*, 2013).

PRC1 core catalytic subunits, RING1A/B are E3 ubiquitinases targeting histone H2A lysine 119 (Wang *et al.*, 2004). Canonical targeting of PRC1 acts via subunits with CBX domains, which recognise the PRC2 modification H3K27me3 (Levine *et al.*, 2002; Fischle *et al.*, 2003). Non-canonical PRC1 complexes contain RYBP proteins instead of CBX proteins allowing PRC1 targeting independent of H3K27me3 (Tavares *et al.*, 2012; Gao *et al.*, 2013). Recent studies have now implicated non-canonical PRC1 complexes in

recruitment of PRC2 (Blackledge *et al.*, 2014). The complex regulation PcG demonstrates the need for tight regulation of gene repression for correct development and disease prevention.

Polycomb dependent compaction was demonstrated cytologically by FISH (Eskeland *et al.*, 2010), but this was independent of RING1B catalytic activity. Binding of PRC1 prevents transcription factor binding resulting in the inability to form a preinitiation complex (PIC) required for transcription (McCall and Bender, 1996; Lehmann *et al.*, 2012). Polycomb binding also precludes SWI/SNF nucleosome remodelling maintaining a condensed repressive state (Shao *et al.*, 1999). Maintaining this condensed state requires an evolutionarily conserved highly charged domain on PRC1 thought to function in its recruitment (Grau *et al.*, 2011). Meticulous super resolution microscopy from Boettiger *et al.*, (2016) demonstrated that PRC1 mediated large scale chromatin compaction occurs beyond transcriptional inactivation and across subdomains, showing it has a potentially larger role in genome organisation.

Polycomb mediated condensed chromatin fibres, as previously mentioned, are enriched for linker histones. Recent work has focused on the role of linker histone subtypes in maintaining this repressed chromatin structure. Unlike total linker histone, which is distributed genome-wide; linker histone variants form distinct topological domains. Linkers H1.2-H1.5 associate with HP1 domains at the nuclear periphery and are depleted from transcriptionally active regions. H1.1 by contrast is found at PcG domains, and weakly enriched at transcribed regions (Izzo *et al.*, 2013). This suggests that linker histone H1.1 functions complementary to polycomb in transient gene repression.

1.5 Constitutive heterochromatin

Position-effect variegation (PEV) was first defined by changes in the colour pattern in *Drosophila* eyes (Muller, H, 1930). This change in colouration is caused by the translocation of an eye pigment gene to the heterochromatic regions surrounding the centromere. The propagation of heterochromatic chromatin structure across the pigment gene occurs heterogeneously correlating with the patchy pigment distribution across the eye. Molecular studies show this clear phenotype directly relates to transcriptional repression, and chromatin compaction, over the translocated 'white' pigment gene. This enabled genetic screening to identify factors that supress or enhance the variegation of gene expression across the eye. Suppressors of variegation; Su(var)3-7, Su(var)2-5 (also named HP1), and Suv(var)3-9 all demonstrated a dose dependent effect on PEV demonstrating their key function in heterochromatin propagation (Reuter *et al.*, 1990; Eissenberg *et al.*, 1992; Tschiersch *et al.*, 1994). Additionally translocation screens identified multiple other loci across the chromosome that exhibited position-effect variegation including telomeres (Doheny, Mottus and Grigliatti, 2008; Riddle *et al.*, 2008). The heritable state of surrounding chromatin has since been demonstrated across multiple eukaryotes (Ottaviani, Gilson and Magdinier, 2008). However, as PEV sites are defined by the underlying chromatin structure, they were demonstrated to diverge between cell types (Hofmann, Brünner and Korge, 2009). This body of work was the foundation of our current understanding that chromatin structure is a major mechanisms for gene activation and repression.

The relationship between chromatin structure, nuclear organisation and transcription has led to much debate as to the causative agent behind genome regulation. This has been muddied by correlations with histone modifications and replication timing. Heterochromatin is strongly associated with the nuclear periphery and the idea of nuclear organisation associating with chromatin regulation was first put forward by Carl Rabl, (1885) observing peripheral centromere clustering in salamander nuclei.

A causative function of nuclear organisation was first put forward in *drosophila* (Dernburg *et al.*, 1996). Heterochromatic repeats were inserted near to the brown eye colour gene and using FISH they demonstrated that its nuclear distribution was not altered in embryonic cells. However, upon reaching the larval stage, the brown gene is tethered with other heterochromatic regions to the periphery supressing its expression (Dernburg *et al.*, 1996). Mammalian studies in primary B-lymphocytes have also shown inactive genes localising to the periphery in cycling but not quiescent cells. In these phenotypically similar cells without nuclear peripheral localisation, the heterochromatin foci were not heritable suggesting that nuclear organisation is required to maintain chromatin structure and transcriptional profiles (Brown *et al.*, 1999).

More recent studies furthered this work by showing that the early B cell factor (EBF1) locus relocates from the periphery to a more central position at the same stage of differentiation as its expression (Lin *et al.*, 2012). This effect can occur at single genes or at regions with multiple genes (Peric-hupkes *et al.*, 2010). An eloquent study recently showed that forcing a loop between the β-globin locus and its long-range control region without canonical transcription factor GATA-1 was sufficient to induce transcription (Deng *et al.*, 2012). Additionally, forcing this loop to γ-globin resulted in its up regulation at the expense of β-globin, demonstrating a clear link between genome organisation and transcription (Deng *et al.*, 2014).

Adversely, the Bickmore lab recently demonstrated that de-condensation of peripheral chromatin without transcription was enough to drive gene relocation away from the nuclear periphery. This did not, however, affect replication timing unless transcription was induced (Therizols *et al.*, 2014).
Lack of coupling between nuclear organisation and replication, however conflicts with other studies demonstrating TAD establishment in early G1 correlated with replication timing determination (Dileep *et al.*, 2015). The Misteli lab identifying multiple replication components affecting nuclear positioning supported this theory (Shachar *et al.*, 2015). They also demonstrated knockdown of chromatin structure and SWI/SNF remodelling components caused highly expressed genes to be relocated to the periphery while maintaining high expression levels (Shachar *et al.*, 2015). Thus the causative nature of silencing at the nuclear periphery is not universal, and remains poorly understood.

Heterochromatic histone modifications are also proposed to regulate the chromatin fibre. Heterochromatin is acetylated in yeast and *Drosophila* at H4K12 (Turner, Birley and Lavender, 1992; Braunstein *et al.*, 1996). However, acetylation in humans is excluded from the heterochromatic inactive X chromosome (Jeppesen and Turner, 1993). This hypoacetylated state, was demonstrated to regulate chromatin compaction and gene silencing by the Belmont lab. Targeting a VP16-lac repressor to a genomic region with an array of lac operator sequences, caused localised hyperacetylation, transcription, and chromatin unfolding (Tumbar, Sudlow and Belmont, 1999). Correspondingly, artificial recruitment of suppressor of variegation 3-9 homologue 1 (Suv39h1) or polycomb protein EZH2 was sufficient to reposition subTAD domains to polycomb bodies or pericentric heterochromatin respectively. With the recruitment of Suv39h1 repositioning occurred from an active and inactive domain. However Suv39h1 mediated repositioning requires the chromodomain not the methyltransferase activity of the enzyme and appears independent of transcriptional state (Wijchers *et al.*, 2016).

Intriguingly, dense heterochromatin is not continually refractory to gene transcription and contains multiple unique gene transcripts in *Drosophila* (Coulthard *et al.*, 2010). The requirement of constitutive heterochromatic domains for correct transcription of these genes was eloquently demonstrated by translocation studies from the Hilliker lab (Eberl, Daniel, Duyf, Brenda and Hilliker, Arthur, 1993). Key regulators of PEV, Su(var)3-7 and HP1, have subsequently been linked to correct expression of heterochromatic genes and piRNAs respectively (Lu *et al.*, 2000; Basquin *et al.*, 2014).

The interplay between nuclear positioning, chromatin structure, histone modifications, and replication has been extensively studied in relation to gene regulation. The complexity of this system is demonstrated the amount of conflicting studies in different systems. Pioneering work by Larson *et al.*, (2017) recently demonstrated that the formation of heterochromatin via suppressor HP1α occurs in phase separated droplets. Loss of this phase separation environment results in a decrease in HP1α foci size a frequency in cells. This suggests that the liquid environment around chromatin may itself contribute to chromatin structure regulation, demonstrating the unknown complexities that have yet to be fully elucidated.

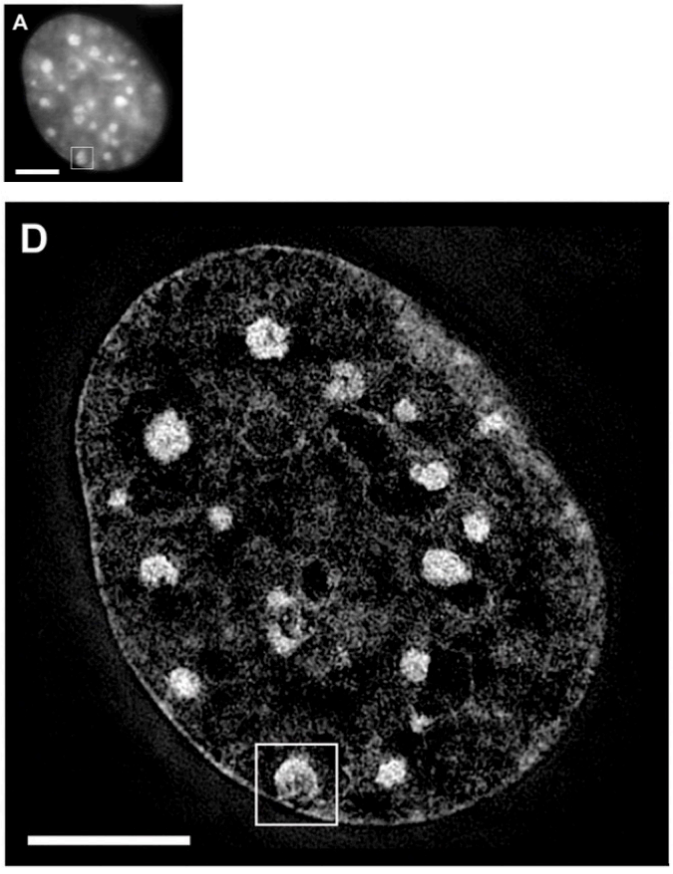

Figure 1.4 Subdiffraction resolution imaging with SIM. (A) Cross section of mouse muscle myoblast C2C12 cell nucleus stained with DAPI and imaged by conventional epifluorescence microscopy. (**D)** The same cross-section imaged by 3D SIM reconstruction. Bright aggregates are constitutive heterochromatic chromocenters. Increase in DAPI intensity at the nuclear periphery is indicative of the heterochromatinisation of the adjacent chromatin. Scale bars are 5 μm. Adapted from Schermelleh *et al.*, (2008)

1.5.1 Centromeres

The principal cytological constriction of human metaphase chromosomes, the centromere, was first observed by Walther Flemming (1882). However, due to stark heterogeneity across species, Cyril Darlington (1936) argued a centromere must be defined by its function. Centromeres function as loading platforms for spindle microtubules, in order to control chromosome movement throughout mitosis. Although most eukaryotes contain a monocentric restriction, some species have diffuse centromeres along whole chromosomes termed holocentricity (Guerra *et al.*, 2010).

The location of monocentric centromeres is characterized by the deposition of histone variant CENP-A or its homologue, in most eukaryotes (Earnshaw and Rothfield, 1985). Artificial targeting of CENP-A is sufficient for kinetochore assembly, indicating its role to nucleate centromere formation (Mendiburoa *et al.*, 2011). This allows centromere location to be independent of underlying DNA sequences and can heterogeneously drift between cells (Yao *et al.*, 2013; Purgato *et al.*, 2015). The amount of CENP-A required for centromere formation is also variable, with a single CENP-A required in some budding yeasts to kilobase regions of CENP-A deposition (Pluta *et al.*, 1995; Furuyama and Biggins, 2007; Bodor *et al.*, 2014). Regional centromeres are composed of a central core where CENP-A is deposited, and an outer heterochromatic domain defined as the pericentromere.

The underlying centromeric DNA sequences also demonstrate evolutionary variability, thought to be a by-product of meiotic drive in female meiosis (Malik and Henikoff, 2009). Most centromeres form over complex arrays of highly reiterative DNA sequences. These repetitive arrays are AT-rich domains interspersed with retrotransposon clusters, while the central core typically has homogenous ordered repeats, the pericentromere is less ordered and often has multiple repeat sequences (Fishel *et al.*, 1988; Schueler *et al.*, 2001).

These repetitive elements have increased frequency of meiotic recombination due to their sequence similarity. This may decrease genome stability when their chromatin environment is accessible, and therefore requires a more compact chromatin state (Vader *et al.*, 2011), alternatively a regular chromatin structure may be required to form a stable kinetochore. These compact chromatin fibres were first described as satellite bands isolated from bulk DNA in density gradients (John and Miklos, 1979). One of the most abundant, the α-satellite, is conserved across primates spanning 5% of the genome. α-satellite in primates comprises a core 171 bp repeat that hybridises to all human canonical centromeres (Fittler and Zachau, 1979). Within the central core of the centromere, sixteen α-satellite monomers are arranged sequentially head to tail forming a 2.7 kb higher order repeat unit propagated throughout. By contrast, the human pericentromere contains disordered adjacent monomers (Aldrup-MacDonald and Sullivan, 2014). Nucleosome positioning is strictly defined across α-satellites, first demonstrated in African green monkeys (Zhang, Fittler and Horz, 1983). Mice by contrast have only two centromeric repeats, major and minor satellites. The centric minor satellite has a shorter 120 bp repeat and the major pericentric repeat is 234 bp (Wong and Rattner, 1988).

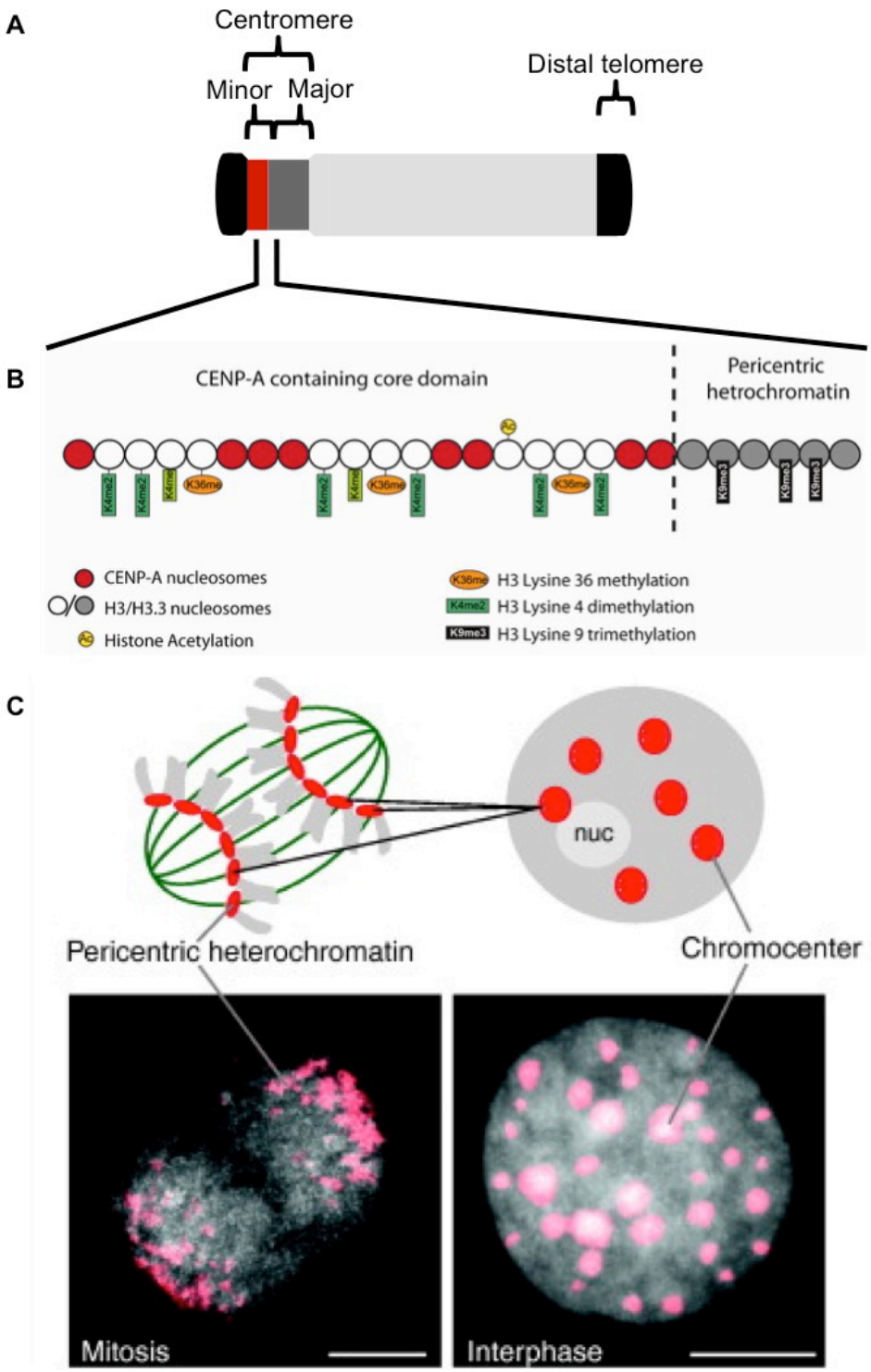

Figure 1.5 Centromere structure and organisation. (A) Typical acrocentric mouse chromosome, with pericentric major satellite and centric minor satellite (red) repeats. (**B)** Centromere identity components. The CENP-A core contains H3K36me, H3K4me2, and acetylation, whereas pericentric regions contain H3K9me3. (**C)** Major satellite organisation (red) in mouse 3T3 cells mitosis or interphase by DNA fluorescence *in situ* hybridisation (FISH). Scale is 10 μm. Adapted from Probst and Almouzni, (2011); Lyn Chan and Wong, (2012)

1.5.2 Centromere large-scale structure

The role of CENP-A in large scale chromatin fibre structure at centromeres, is limited by its low frequency of deposition (~400) within the core centromeric region contributing to just ~4% of nucleosomes (Bodor *et al.*, 2014). High-resolution microscopy of stretched chromatin fibres demonstrated that these were ordered into blocks of CENP-A or H3 containing nucleosomes from *Drosophila* to humans (Blower, Sullivan and Karpen, 2002; Ribeiro *et al.*, 2010). Electron microscopy experiments demonstrated that CENP-A nucleosomes are exclusively found at the surface of the cytological constriction. The CENP-A nucleosomes are not prevalent enough though to cover the entire surface of the restriction, occupying two thirds of the length, and one third of both the width and height of the surface (Marshall, Marshall and Choo, 2008). How the chromatin fibre is compacted to allow these CENP-A domains to lie on the surface of the fibre remains to be elucidated. Many models including; looping, solenoidal, planar sinusoids, and layered boustrophedon have been hypothesised. The repetitive nature of satellite sequences makes the use of capture-C methods problematic (Naumova *et al.*, 2013). Additionally, limitations of current microscopy techniques mean that the folding model of the core centromere remains an area of current debate.

Flanking the core centromere, the pericentromere contains canonical heterochromatic marks and is responsible for sister chromosome cohesion with high levels of cohesion (Glynn *et al.*, 2004). This process is mediated by the stabilisation of cohesion complexes throughout S phase (Yeh *et al.*, 2008). The heterochromatic nature of the pericentric regions directly mediates this process via H3K9me3. In *S. pombe,* HP1 homologues Swi6 and Chp2 which bind H3K9me3 provides a platform for cohesin recruitment (Bernard *et al.*, 2001; Nonaka *et al.*, 2002). Pericentric cohesin is protected from turnover by Swi6 recruiting shugoshin proteins (Yamagishi *et al.*, 2008). These recruit phosphatase PP2A preventing cohesin subunit phosphorylation and subsequent separase cleavage (Kitajima *et al.*, 2006). The role of H3K9me3 and HP1 in regulating mammalian cohesin remains controversial. While HP1 in humans recruits shugoshin proteins, they are not essential for cohesin protection and do not drive cohesin recruitment (Koch *et al.*, 2008; Serrano, Rodríguez-Corsino and Losada, 2009). However, Suv4-20 methyltransferase, tethered by HP1 isoforms significantly contributes to loading cohesin (Yang *et al.*, 2008; Shimura *et al.*, 2011; Hahn *et al.*, 2013). Loss of pericentric cohesin loading completely abrogates the cytological constriction known as heterochromatin repulsion (Whelan *et al.*, 2012). This occurs in the human disease Roberts syndrome, causing increased aneuploidy and abnormal nuclear morphology due to loss of genome integrity during mitosis (Jabs *et al.*, 1991). Despite the function of heterochromatin and cohesins during mitosis, the loss of Suv39 methyltransferases in mice does not lead to loss of their cytological constriction and remarkably are viable with few minor abnormalities (Peters *et al.*, 2001).

1.5.3 Neocentromeres

Despite the highly ordered nature of repetitive elements within the centromere, they are not essential. Centromeres can form sporadically over non-repetitive DNA, classed as neocentromeres. These were first found to occur naturally in humans by Voullaire *et al.*, (1993) and can be stably passed generation to generation (Tyler-Smith *et al.*, 1999). In *Drosophila* irradiation exposure was sufficient to produce acentric mini-chromosomes containing a neocentromere (Murphy and Karpen, 1995). These mini-chromosomes demonstrated the ability to recruit centromere specific protein ZW10, and formed a neocentromere from the sub-telomeric region of chromosome X (Williams *et al.*, 1998). This sub-telomeric sequence does not display the cytological restriction of a centromere when not attached to the X chromosome outside of this mini-chromosome environment, further demonstrating the epigenetic activation step required for centromere formation.

Dicentric chromosomes occur when a centromere naturally translocates within a chromosome resulting in inactivation of the original centromere locus. The dicentric (X;15) translocation in *Drosophila* first demonstrated the loss of centromeric proteins such as CENP-C from the inactive centromere (Page *et al.*, 1995). Additionally heterochromatic proteins HP1β and Suv39h1 are found pericentrically at all canonically active but not inactive centromeres (Aagaard *et al.*, 2000; Saffery *et al.*, 2000). The loss of these heterochromatic proteins elevates chromosome loss suggesting impaired kinetochore function (Taddei *et al.*, 1999; Rea *et al.*, 2000). Furthermore, inner centromere protein (INCENP) directly associates with HP1 (Ainsztein *et al.*, 1998) and binds to the spindle mid-zone as part of the chromosome

passenger complex for chromosome arrangement throughout mitosis (Mackay *et al.*, 1998). Despite INCENP's direct interaction with HP1, Ainszstein demonstrated this was not required for centromere targeting of INCENP, instead functioning in its transfer from chromosomes to the anaphase spindle. Recently the role of pericentric heterochromatin has come under debate as neocentromeres can occur without surrounding heterochromatic marks H3K9me3 and HP1, albeit with centromere cohesion defects (Alonso *et al.*, 2010). This demonstrates a functional but not essential role of heterochromatin for centromere formation.

1.5.4 Evolutionary New Centromeres

The ability to form non-repetitive centromeres appears across all forms of life. Some species, such as orangutan, horse and chicken, have both repetitive and non-repetitive centromeres within their genomes (Piras *et al.*, 2010; Shang *et al.*, 2010; Locke *et al.*, 2011). By comparing recently diverged evolutionary species these centromeres have been termed evolutionary new centromeres (ENCs) (Kasai *et al.*, 2003; Rocchi *et al.*, 2012). This centromere repositioning occurs without transposition of the surrounding genetic landscape (Montefalcone *et al.*, 1999). Intriguingly however a typical ENC acquires the molecular properties and satellite repeat sequences of 'old' centromeres. Macaques, in contrast to orangutans, have nine ENCs within their genome, each of which contains α-satellite duplications (Ventura *et al.*, 2007). Therefore, despite not being required for centromere formation, there is evolutionary pressure for their presence. Furthering this idea, the satellite arrays at old centromere positions decay once ENCs are formed (Kalitsis and Choo, 2012).

1.5.5 Mammalian Artificial Chromosomes

In order for a chromatin fibre to be a stable constituent of a genome, it requires the ability to undergo mitosis. In order to be correctly segregated in mitosis, a functioning centromere is required. Generation of *S. cerevisae* artificial chromosomes (YACs) was therefore relatively simple as the single CENP-A requires a specific underlying DNA sequence (Clarke, 1998). Human artificial chromosome production proved more intricate as the underlying factors of centromere formation remain unresolved. Pioneering work by Harington *et al.*, (1997) combined α-satellite arrays with telomeric and genomic DNA in human HT1080 cells to generate a 6-10Mb chromosome, further demonstrating the role of repetitive higher order units in centromere structure. Although the mechanism behind artificial centromere formation is yet to be fully elucidated, recent studies propose that α-satellite has a propensity for epigenetic marks that favour CENP-A deposition (Bergmann *et al.*, 2011; Ohzeki *et al.*, 2012).

1.5.6 Regional Centromere Determinants

For genomic sequences such as α-satellite to be a determining factor in centromere location, they must directly or indirectly recruit CENP-A and the constitutive centromere associated network (CCAN). In *S. cerevisiae* the single CENP-A nucleosome location is determined by the presence of the centromere DNA element III (CDEIII) recognised by Cbf3 (Lechner and Carbon, 1991).

Regional centromere sequences across species are conversely highly varied, unlike the components of CCAN. CCAN component CENP-C for instance has high homology with *S. cerevisiae* Mif2 protein (Meluh and Koshland, 1995). Ectopic recruitment of core CCAN components CENP-C, HJURP, and CENP-I individually is sufficient for CENP-A deposition and kinetochore assembly at centromeres (Hori *et al.*, 2013). This demonstrates that the targeting of core CCAN is the main determinant for centromere location. In contrast to the conservation of CCAN, the only conserved centromeric sequence from humans to mice is the 17 bp CENP-B box sequence (Muro *et al.*, 1992). The CENP-B box is present in the higher order repeats of the core minor satellite region in *M. musculus* and human α-satellite. CENP-B, which binds to this sequence, directly stabilizes CENP-A nucleosomes and their interaction with CCAN component CENP-C (Fachinetti *et al.*, 2015). While CENP-B increases the fidelity of centromere location, loss of the CENP-B box in mice is not lethal (Hudson *et al.*, 1998) Additionally other primate and rodent species have divergent sequences or lack the sequence entirely (Haaf *et al.*, 1995; Kipling *et al.*, 1995). As expected, CENP-B is not recruited to neocentromeres, and intriguingly Y chromosome centromeres lack the CENP-B box repetitive sequence and subsequent CENP-B binding

(Earnshaw, Ratrie and Stetten, 1989; Voullaire *et al.*, 1993). Repetitive elements from the Y chromosome however are not able to form HACs which require the CENP-B box (Grimes, Rhoades and Willard, 2002; Ohzeki *et al.*, 2002). This further demonstrates a functional if not essential role for the CENP-B box centromeric sequence.

In addition to the underlying genomic sequence at centromeres, specific epigenetic states are thought to be permissive to centromere formation. H3 variant CENP-A as mentioned is required for recruitment of kinetochore components. The effect of CENP-A deposition on a nucleosome's physical property at the centromere remains unclear. Whether CENP-A is found in an octamer or a tetramer hemisome *in vivo* is the crux of this debate (Dunleavy, Zhang and Karpen, 2013). Perceptive hydrogen-deuterium exchange experiments demonstrated that CENP-A--H4 tetramers are more compact due to a rotated interface between the two CENP-A molecules (Sekulic *et al.*, 2010). Additional studies have demonstrated the ability of CENP-A hemisomes to preferentially wrap DNA in a right handed manner (Furuyama and Henikoff, 2009). Contrary to this, crystal structures of octameric CENP-A nucleosomes do not perform this axis rotation and form more condensed arrays (Panchenko *et al.*, 2011; Tachiwana *et al.*, 2011). These views were unified recently by Falk *et al.*, (2015), who demonstrated that both forms are present in solution with the octameric form preferring CENP-C binding.

The local chromatin environment is proposed to regulate histone variant CENP-A deposition throughout the core centromere. Unlike normal nucleosome incorporation, CENP-A is uncoupled from replication and remains in a hemi state throughout mitosis (Shelby, Monier and Sullivan,

2000; Jansen *et al.*, 2007). Histone variant H3.3 incorporates where CENP-A is lost acting as a marker for new assembly of CENP-A nucleosomes in G1 (Dunleavy, Almouzni and Karpen, 2011). Incorporation of CENP-A is facilitated through chaperone complexes containing HJURP and MIS18 proteins. While not all MIS18 components are evolutionarily conserved, MIS18 complexes have been shown to interact with CENP-C across species (Moree *et al.*, 2011; Dambacher *et al.*, 2012). CENP-C has also been demonstrated to directly interact with CENP-A chaperone HJURP demonstrating its ability facilitate CENP-A—CENP-C interactions (Tachiwana *et al.*, 2015).

In addition to CENP-C and H3.3 presence at centromeres, surrounding chromatin signatures influence CENP-A deposition. For instance MIS16 and MIS18 have been proposed to prime the centromere for CENP-A deposition via DNA methylation and histone deacetylation (Hayashi *et al.*, 2004; Kim *et al.*, 2012). Pericentric regions as mentioned above canonically contain heterochromatic marks such as H3K9me3 and DNA methylation (Lehnertz *et al.*, 2003). Adversely, the CENP-A core region contains transcriptionally permissive marks, H3K4me2 and H3K36me2 (Sullivan and Karpen, 2004). This chromatin state has been demonstrated to directly influence CENP-A deposition by HJURP (Bergmann *et al.*, 2011). Eloquent studies on human artificial chromosomes demonstrated that the heterochromatinization of the inner centromere core abdicated centromere function and CENP-A deposition (Nakano *et al.*, 2008; Ohzeki *et al.*, 2012).

The requirement of this permissive chromatin state at centromeres has led to a hypothesis for transcription at the core centromere. Transcription machinery including FACT (facilitates chromatin transcription complexes),

RSF1, and helicase CHD1 have all been implicated in CENP-A deposition (Perpelescu *et al.*, 2009; Dudek *et al.*, 2010). Absence of FACT mediated transcription results in aberrant CENP-A deposition and centromere function, demonstrating a direct link between transcription and centromere function (Chen *et al.*, 2015).

The presence of RNA transcripts from these repetitive elements appears to be required. In *S. pombe* the RNA interference complex DICER cleaves pericentric transcripts, producing small interfering RNA (siRNA). These short transcripts and HP1 are required for correct CENP-A deposition (Folco *et al.*, 2008). The function of transcription at human centromeres has also been inferred by the presence of polymerase II and transcription during mitosis, while the Gilbert lab (unpublished) shows transcription during interphase at human neocentromeres (Chan *et al.*, 2012). Investigations using HACs has also shown the presence of α-satellite transcripts from its centromere (Bergmann *et al.*, 2011). Disrupting this transcription at the centromere results in kinetochore defects and aberrant CENP-A profiles (Quénet and Dalal, 2014; Liu *et al.*, 2015).

Together this body of work demonstrates that interplay of genomic sequences, local chromatin states, transcription and CCAN formation occurs. Exactly how these contribute to the spatial restriction of the centromere and its propagation remains elusive. This remains an area of current major scientific interest as the field looks to understand why some abnormal CENP-A deposition induces neocentromere formation, while other sites remain inert. Understanding this process will provide intriguing evolutionary insights in addition to understanding the relationship between epigenetic states and chromatin fibre structure.

1.5.7 Telomeres

Telomeres are heterochromatic regions that cap linear chromosomes. They were first identified as a distinctive feature of nuclear structure in *drosophila* by Herman Muller, who noted their requirement for faithful genome maintenance (Muller, H, 1938). These chromosome caps function to distinguish the chromosome ends from breaks. This allows cells to undergo mitosis without activating cell cycle checkpoint responses to chromosome breaks (Sandell and Zakian, 1993). The requirement of telomeres for cell cycle progression has promoted their evolutionary conservation (Meyne, Ratliff and Moyzis, 1989).

Vertebrates have large kb arrays of repeating telomeric associated sequences (TAS) to cap their chromosomes. Although mostly double stranded, the definitive end is a 3' single stranded overhang ranging from 50-400 nucleotides (Wright *et al.*, 1997). These exposed nucleotides are proposed to form a high order loop like structure, folding into the duplex region of the telomere, protecting chromosome ends from DNA repair mechanisms (Griffith *et al.*, 1999).

Loss or shortening of these capping sequences is associated with senescence, faithful chromatid separation, genome stability and oncogenesis (Lundblad and Blackburn, 1993; Greider, 1998; Blackburn, 2001). These phenotypes occur as DNA replication is not conservative and, therefore, completion to the chromosome end is not essential. Organisms must harbour mechanisms to restore lost telomeric sequences after every mitotic division to prevent loss of telomeric repeats. This is achieved by telomerase which uses RNA telomeric transcripts as a template for DNA restoration (Collins and Miller, 2002).

The stabilisation of the T loop structure and the accessibility of telomerase mediated repair is regulated by telosome or shelterin complexes (De Lange, 2005). Subunits TRF1/2 negatively regulate telomerase activity and in combination with POT1 facilitate T-loop formation (Stansel, De Lange and Griffith, 2001; Hockemeyer *et al.*, 2006). Although telomere structures are required to avoid activating the DNA damage response pathway, shelterin recruits many DNA damage proteins involved in signalling, nucleotide excision, helicases, homologous repair (HR) and non-homologous end joining (NHEJ). These interactions all have a functional role in telomere maintenance. Loss of ATM-TRF2 interaction in ataxia-telangiectasia patients, for instance, results in aberrant telomere length (Hande *et al.*, 2001; Karlseder *et al.*, 2004). This is mediated by excision of the 3' overhang followed by HR or NHEJ that also prevent chromosome end to end fusions (Zhu *et al.*, 2003; Myung *et al.*, 2004; Tarsounas *et al.*, 2004).

Werner and Bloom syndrome patients with helicase mutations first implicated the role of chromatin structure on telomere maintenance. WRN and BLM helicases have since been shown to interact with TRF2 causing the de-condensation of telomeric regions (Opresko *et al.*, 2002).

Mammalian chromatin condensation at telomeres was demonstrated by reduced nuclease accessibility in rats (Makarov *et al.*, 1993). Subsequent studies have demonstrated enrichment for: constitutive heterochromatic HMT's Suv39h1/2 and Suv420h1/2, their methylation marks H3K9me3 and H4K20me3, DNA methylation and HP1 (García-Cao *et al.*, 2003; Gonzalo *et al.*, 2006; Benetti *et al.*, 2007). The formation of constitutive heterochromatin reduces the accessibility of telomerase enzymes, therefore, regulating telomere length. This is demonstrated by loss of Suv39h1/2 or DNMT's causing telomere elongation, and HP1 overexpression instigating telomere erosion (García-Cao *et al.*, 2003; Sharma *et al.*, 2003; Gonzalo *et al.*, 2006). Similarly to centromeric regions, transcription of telomeric repetitive elements has recently been implicated in its regulation. Telomeric RNAs (telRNA) are transcribed by PolII from the 5' strand and therefore does not occur at the 3' overhang. telRNA's remain chromatin bound at telomeric regions by interacting with TRF1 and demonstrate the ability to inhibit telomerase activity (Schoeftner and Blasco, 2008). The role of these telRNA's on chromatin structure has yet to be properly investigated, but provides another function for ncRNA in regulating heterochromatin structure.

1.6 Thesis Aims

The advancement of sequencing technologies has resulted in a more refined understanding of genome organisation and the association of proteins and their modifications. However these studies have largely focused on euchromatin due to the repetitive nature of centromeric regions. The relationship between histone modifications and global chromatin structure is based on correlative rather than causative evidence, and a direct role continues to be debated. As such, whether both compaction and de-compaction are active processes also remains unresolved. Identifying factors that affect heterochromatin formation, consequently, remains an important research question today.

Additionally, epigenetic regulation has been suggested as important therapeutic cancer targets (Feinberg, Ohlsson and Henikoff, 2006). However drug development has largely focused on inhibiting oncogenes, rather than the re-expression of tumour suppressors, due to clarified mechanisms of action, and reduced potential off target effects. Heterochromatic abnormalities and mutations in repressive epigenetic factors are however associated in disease phenotypes, suggesting their therapeutic potential (Ehrlich *et al.*, 2002; Suzuki *et al.*, 2004; Birgisdottir *et al.*, 2006).

Thus this thesis aims to:

- Investigate any causality behind epigenetic regulation of chromatin structure correlations.
- Identify components of heterochromatin regulation
- Investigate the epigenetic regulation of acquired kinase signalling inhibitor resistance.

Chapter 2: Methods

2.1 General reagents, stock solutions and buffers

2.1.1 Sources of reagents

All solutions were prepared with deionised water and stored at room temperature unless stated otherwise.

Chemicals were purchased from Sigma Aldrich, Fischer Chemicals, GE healthcare, and VWR. Enzymes and antibodies were procured from New England Biolabs, Roche, Life Technologies, and Promega. Invitrogen manufactured all cell culture materials unless stated differently

2.1.2 Stock solutions and buffers

20 × TBE 1L:	108 g Tris-base, 27.5 g boric acid, 40 ml 0.5 M EDTA
20 × TPE 1L:	218 g Tris-base, 31 ml orthophosphoric acid (85%), 40 ml 0.5 M EDTA
20 × TEEP 0.2L:	40 ml 1 M Tris (pH 8), 8 ml 0.5 M EDTA, 40 ml 100 mM EGTA, 0.05% (w/v) NP40, 250 μ M PMSF
5 × DNA loading buffer:	50% glycerol, 5 mM EDTA pH 8, 0.3% orange G (w/v)
4 × SDS buffer:	40% glycerol v/v, 8% SDS v/v, 0.25 M Tris-HCl pH 6.8, 5 mM β-mercaptoethanol
Buffer 1:	0.5 M Tris pH 8, 0.15 M NaCl
Cell lysis buffer:	85 mM KCl, 0.5% NP-40, 5 mM HEPES
ChIP dilution buffer:	0.01% SDS, 1.1% Triton X-100, 1.2 mM EDTA, 16.7 mM Tris-HCl pH 8, 167 mM NaCl.

Chloroform-IAA:	Chloroform and iso-amyl alcohol were mixed at a 24:1 ratio
Colloidal Coumassie Stain:	0.25% (w/v) brilliant blue R-250, 45% methanol, and 10% glacial acetic acid.
Colloidal Coumassie Destain:	30% methanol, 10% glacial acetic acid
Chromatin elution buffer:	1% SDS, 0.1 M $NaHCO_3$
CSK buffer:	100 mM NaCl, 0.1% Triton X-100, 300 mM sucrose, 1 mM $MgCl_2$, 1 mM EGTA, 10 mM PIPES and 100 μ M PMSF.
Destaining solution:	30% methanol, 7% glacial acetic acid, 63% ddH_2O (v/v)
Denaturation buffer:	1.5 M NaCl, 0.5 M NaOH
Genomic lysis buffer:	150 mM NaCl, 1% (w/v) SDS, and 10 mM EDTA
Hybridisation buffer:	6 × SSC, 10 mM EDTA, 5 × Denhardt's solution, 0.5% SDS, 100 μ g/ml salmon sperm DNA.

In vitro click reaction mix:	3 μl 2 M triethylammonium acetate buffer, 30 μl DMSO, 6 μl 5 mM ascorbic acid, 3 μl 10 M CuTBTA, 1.2 μl 10 mM biotin azide
LiCl buffer	0.25 M LiCl, 1% NP-40, 1% deoxycholate, 1 mM EDTA, 10 mM Tris-HCl pH 8.
Luria-Bertani (LB) agar (1L):	10 g tryptone, 5 g yeast extract, 10 g NaCl, 15 g agar, pH 7.0 by sodium hydroxide. Prepared by the MRC HGU Technical Services.
Luria-Bertani (LB) broth (1L):	10 g tryptone, 5 g yeast extract, 10 g NaCl, pH 7.0 by sodium hydroxide. Prepared by the MRC HGU Technical Services.
MD Anderson lysis buffer:	1% Triton X-100, 50 mM HEPES, 150 mM NaCl, 1.5 mM $MgCl_2$, 1 mM EGTA, 199 mM NaF, 10mM sodium pyrophosphate, 1 mM Na_3VO_4, 10% glycerol, phosphatase inhibitor cocktail (Roche, cat no. 04 906 845 001)

Nuclear Buffer A (NB A):	85 mM KCl, 5.5% sucrose, 10 mM Tris pH 7.6, 0.5 mM spermidine, 0.2 mM EDTA, 250 μ M PMSF
Nuclear Buffer B (NB.B):	Nuclear buffer A supplemented with 0.2% NP-40 for differentiated cells, and 0.05% NP-40 for ESCs
Nuclear Buffer Release 2:	85 mM KCl, 5.5% sucrose, 10 mM Tris-HCl pH 7.6, 1 mM $CaCl_2$, 1 mM $MgCl_2$, 250 μ M PMSF.
Nupage transfer solution:	1 × Nupage transfer buffer, 10 or 20% methanol, 1% nupage antioxidant
Neutralisation buffer:	1.5 M NaCl, 0.5 M Tris-HCl pH 7.5
Optimal live cell click reaction:	0.5 mM $CuSO_4$, 0.25 mM THPTA, 250 mM sodium ascorbate
Phosphate buffer saline (PBS):	Dublecco's recipe (without calcium and magneisum), 10 mM Phosphate, 137 mM NaCl, 27 mM KCl. Prepared by MRC HGU Technical Services
Penecillin/Streptomycin:	10,000 U/ml penicillin and 650 μ g/ml streptomycin. Prepared by MRC HGU Technical Services

Propidium iodide solution:	PBS, 1 μg/ml propidium iodide, 4 μg/ml RNase A.
Proteinase K:	20 mg/ml (w/v) proteinase K, 1.5 mM calcium acetate, 50% glycerol, 50 mM Tris-HCl pH 7.
RIPA:	1% NP-40, 0.5% sodium deoxycholate (v/v), 0.1% SDS in water. Protein inhibitor cocktail added before use.
Saline sodium citrate (SSC):	0.5L 20 × stock prepared by MRC HGU Technical Services: 3 M NaCl, 0.3 M tri-sodium citrate, pH 7.
TEEP ΔNaCl:	20 × TEEP stock used to make 10 mM Tris-HCl pH 7.5, 1 mM EDTA, 1 mM EGTA, 250 μM PMSF, supplemented with 1 mM, 20 mM or 80 mM NaCl.
TBE:	90 mM Tris-borate, 2 mM EDTA prepared from 20 × stock
TBS-T:	50 mM Tris-HCl, 150 mM NaCl, 0.05% Tween-20

Tris EDTA (TE):	10 mM Tris-HCl, 0.1 mM EDTA. 50 ml stock was prepared by MRC HGU Technical Services.
TPE:	0.8 M Tris-phosphate, 0.02 M EDTA prepared from 20 × stock.
TSE-I buffer	0.1% SDS, 1% Triton X-100, 2 mM EDTA, 20 mM Tris-HCl pH 8, 150 mM NaCl
TSE-II buffer	0.1% SDS, 1% Triton X-100, 2 mM EDTA, 20 mM Tris-HCl pH 8, 500 mM NaCl

2.2 Bacterial Culture

2.2.1 Media

E. coli strains were grown at 37°C in a Luria-Bertani (LB) broth suspension by a shaking incubator (250 rpm) overnight. To select for plasmid containing bacteria, ampicillin or kanamycin was added as required. Ampicillin resistant *E. coli* colonies were grown on ampicillin containing L-agar plates poured by MRC HGU Technical Services.

2.2.2 Bacterial strains

DH5α competent cells (Invitrogen) were used for cloning experiments, and stored at -80°C.

2.2.3 Bacterial glycerol stocks

50% glycerol stocks were made for long-term bacterial storage. 500 μl of *E. coli* suspended in LB broth was added to 500 μl of glycerol and stored at -80°C.

2.2.4 Bacterial transformation

50 μl of DH5α competent cells (Invitrogen) and thawed on ice for 15 minutes then 50 ng of plasmid or ligation was added. Competent cells were heat-shocked at 42 °C for 30 seconds before being rested on ice for 2 minutes to reduce the temperature. 400 μl of SOC media was then added to the bacterial culture and incubated at 37 °C for 30 minutes. Cultures were diluted and spread on L-agar plates with antibiotics, as required.

2.3 DNA methods

2.3.1 Phenol/chloroform DNA purification

To purify mammalian genomic DNA, cells were trypsinised and suspended in genomic lysis buffer (GLB). RNase A/T1 mix (Cat No EN0551) was added to the GLB lysed solution to a final concentration of 5 μg/ml of RNase A and 12.5 U/ml of RNase T1. Samples were incubated at 37 °C for 30 minutes. Proteinase K at 150 μg/ml was added to the solution and further incubated at 55 °C for 2-16 hours. Phenol chloroform-IAA at a ratio of 25:24:1 was added in equal volume to the solution before inversion to mix. Samples were centrifuged at 12,000 g for 30 minutes at room temperature to separate the different phases. The aqueous phase was transferred to a new tube and re-extracted with chloroform-IAA, in order to remove residual phenol.

DNA was precipitated from samples by the addition of sodium acetate (pH 5.5) to 300 mM with 2.5 volumes of ethanol. 1 μl of glycogen 20 μg/ml (Sigma cat no G1508) was added as a carrier and incubated at -20°C for 1-16 hours. The DNA was collected by centrifugation at 12,000 g for 30 minutes at RT. The supernatant was removed and the pellet was washed with 1ml 70% ethanol to remove residual salt. The DNA was re-centrifuged at 12,000 g 10 minutes at RT. The supernatant was again removed and the pellet dried at room temperature. DNA was resuspended in TE and quantified by 260 nm absorbance on a Nanodrop 1000 UV-VIS spectrometer (Thermo Scientfic). The 260/280 ratio was used to determine sample purity with 1.85-2.15 considered free of contaminants.

2.3.2 Gel electrophoresis of nucleic acids

Small DNA fragments (<2 kb) were resolved by horizontal electrophoresis in a 1% agarose (Invitrogen cat no. 16500-500) 1 × TBE gel with 0.5 μg/ml ethidium bromide (VWR cat no. 443922U). 5 × DNA loading buffer (50% glycerol, 5 mM EDTA, 0.3% Orange G) was added to each sample to 1 × before gel loading. Unless stated otherwise, 500 ng of 1 kb plus DNA ladder (Invitrogen cat no. 10787018) was used as a reference and gels were visualised on a UV transilluminator.

DNA fragments >2 kb were resolved by horizontal electrophoresis in a 0.7% agarose 1 × TPE gel with 0.5 μg/ml ethidium bromide. Samples were prepared in 1 × DNA loading buffer before loading. 500 ng of 1 kb ladder (NEB cat no. #N0552) and 0.4 μg of 2.5 kb molecular ruler (Biorad cat no. #1708205) were used as DNA size markers. Gels were run at low voltage <35 V for 14-18 hours with recirculating buffer (Loening, 1969).

2.3.3 Plasmid purification

Single *E. coli* colonies from plasmid antibiotic containing agar plates were swabbed and incubated in 5 ml L-broth >6 hours 37 °C in a shaking incubator (250 rpm). Either a Qiaprep Miniprep Kit (Qiagen cat no. 27104) or E.Z.N.A Plasmid Mini Kit (Omega cat no. D6942-01) were used to purify >20 μg plasmid DNA from 5 ml *E. coli* cultures as per manufacturers' instructions and eluted into 30 μl TE buffer, and concentration measured on a Nanodrop 1000 UV-VIS spectrometer (Thermo Scientific). For 20-200 μg of plasmid DNA, a 5 ml *E. coli* culture was added to 200 ml L-broth overnight at 37 °C in a shaking incubator (250 rpm). Plasmid from 50 ml of culture was isolated using E.Z.N.A Plasmid Maxi Kit (Omega cat no. D6922) following the manufacturer's instructions and eluted into 50 μl TE. For larger plasmid amounts the E.Z.N.A Plasmid Maxi Kit was used in series, as per manufacturer's instructions.

2.3.4 Restriction digestion and ligation of DNA

Plasmid DNA was digested with the required restriction endonucleases (New England Bioloabs) following manufacturer's guidelines. 10-20 units of restriction enzyme was typically used per 1 μg of plasmid DNA at 37 °C for 2-12 hours. T4 DNA ligase (Cat No M0202S) was used to join DNA fragments. A 3:1 vector to insert ratio was used for ligation reactions, with 10 U T4 ligase per 200 ng of plasmid. Ligation reactions were incubated at room temperature of 4 hours.

2.3.5 Restriction digested DNA isolation

DNA fragments from restriction digestions were resolved by agarose gel electrophoresis with sybr safe (Invitrogen cat no. S33102). 1 μl of a 1:10 dilution of sybr safe stock was added to each sample before loading into each lane. Gels were viewed under blue light and a single edged razor blade was used to excise the desired DNA fragment. Gel fragments where transferred to 1.5 ml tubes and the DNA extracted with QIAquick Gel Extraction Kits (Qiagen cat no. #28704) as per manufacturer's instructions.

2.3.6 Cross linked chromatin immunoprecipitation

Approximately $5x10^7$ cells per ChIP were crosslinked with 1% formaldehyde (Sigma cat no. #F87750) in FCS free media for 10 minutes at room temperature. To stop crosslinking, formaldehyde was removed and cells were washed three times with ice-cold PBS containing 125 mM glycine for 5 minutes. Cells were removed from tissue culture flasks or 10 cm petri dishes using a cell scraper and centrifuged at 500 g for 4 minutes at 4°C. The supernatant was removed and the pellet resuspended in RIPA buffer and sonicated in 1 ml sequential batches. Fragmentation by sonication was performed on a Soniprep 150 for 15 cycles 20 s on and 40 s off at amplitude of 8 μm on ice.

Samples were centrifuged at 20,000 g for 20 minutes at 4 °C to pellet large cellular debris. Supernatant was collected and a 50 μl aliquot used to check fragmentation efficiency. The 50 μl aliquot was diluted with 50 μl cell lysis buffer (85 mM KCl, 0.5% NP-40, 5 mM HEPES pH 8.0) and 5 M NaCl at 65 °C for 4 hours to reverse the formaldehyde crosslinks and incubated with 1 μl RNase A/T1 (Ambion cat no. EN0551) at 37 °C for 30 minutes. Proteinase K was added and incubated at 55 °C for 1 hour and samples were analysed by gel electrophoresis. Only samples with DNA fragments between 100-1000 bp were used for immunoprecipitation.

The chromatin concentration of sonicated samples was measured at 260 nm on a UV-VIS Nanodrop 1000 (Thermo Scientific) and normalised across all samples to >200 ng/μl. The samples are then diluted 10 fold in ChIP dilution buffer (0.01% SDS, 1.1% Triton X-100, 1.2 mM EDTA, 16.7 mM Tris-HCl pH 7.5, 167 mM NaCl, and protein inhibitor cocktail) and 10% stored as input.

50 μl magnetic protein A dynabeads (Invitrogen cat no. #100-02D) per immunoprecipitation were preblocked in 5 mg/ml BSA in PBS, before antibody incubation in 500 μl ChIP dilution buffer with proteinase inhibitors for 4 hours rotating (15 rpm) at 4 °C. The Dynabeads were then washed with BSA 5 mg/ml in PBS, before incubation with samples overnight at 4 °C.

Magnets were used isolate the Dynabeads from the solution and washed with TSE-I and TSE-II buffers (0.1% SDS, 1% Triton X-100, 2 mM EDTA, 20 mM Tris-HCl, 150/500 mM NaCl) for 5 minutes at 4 °C. Samples were further washed with LiCl buffer (0.25 M LiCl, 1% NP-40, 1% deoxycholate, 1 mM EDTA, 10 mM Tris-HCl) and TE buffer for 3 minutes at 4 °C. Chromatin was eluted from Dynabeads in 250 μl elution buffer (1% SDS, 0.1 M $NaHCO_3$) for 1 hour at 65 °C with occasional vortexing, before 5 M NaCl was added to each sample (20 μl) and input sample (4 μl) for a further 5 hours at 65 °C. The supernatant was then incubated with RNase A/T1 for 30 minutes at 37 °C. The samples were then treated with proteinase K (2 μl proteinase K, 10 μl 0.5 M EDTA, 20 μl 1 M Tris-HCl) at 65 °C overnight. The samples were then purified using Qiagen PCR MiniElute Kits (Qiagen cat no. 28004) as per manufacturer's instructions. DNA concentrations were then quantified using a GE healthcare GeneQuant Pro RNA/DNA Spectrophotmeter (Cat no. 80-2114-98). Samples were analyzed by qPCR.

2.3.7 ChIP qPCR

To quantify the DNA abundance in each ChIP sample, real-time PCR with LightCycler™ SYBR green I Master Mix (Roche cat no. 04707516001) was used. 10 μl reactions were analysed for each sample with 0.4 μM of each primer in technical triplicates. A lightcycler 480 system was used to perform the PCR with 45 cycle amplification reactions as per SYBR green I Master Mix manufacture instructions (95 °C for 3 minutes, 45 × 95 °C for 15 s, 58 °C for 15 s, and 72 °C for 30 s). Melting curves were observed to ensure single annealing steps for each primer, with PCR products checked by 2% agarose gel electrophoresis. Ct values were used to determine amplification compared to input for each sample and antibody, using the $\Delta\Delta$Ct method.

2.3.8 Sanger sequencing DNA

Sanger sequencing of plasmids to check sequences were performed by the MRC HGU Technical Services using standard methods. BigDye (Thermo Fisher cat no. 4337455) was used in terminator sequencing reactions on an ABI 3730XL. Sequencing data was examined using Snapgene.

2.3.9 Nuclei preparation

To isolate nuclei for downstream experiments, Cereghini and Yaniv's, (1984) method was modified. Cells were washed with PBS before Trypsin/EDTA (Invitrogen cat no. 59427) was used to detach them for harvest. Trypsin was inhibited by adding 10 ml of 10% FCS/PBS to each sample. Samples were centrifuged at 1200 rpm for 3 minutes, and the pellet resuspended by pipette in 1 ml of NBA buffer (85 mM KCl, 5.5% sucrose, 10 mM Tris-HCl pH 7.6, 0.5 mM spermidine, 0.2 mM EDTA, and 250 μl PMSF) on ice. A further 4 ml of NBA buffer was then added. 5 ml of NBB buffer (NBA + Δ% NP-40) was added to each sample on ice for 4 minutes. The nuclei were quickly pelleted by centrifugation 2000 rpm for 4 minutes, to prevent lysis of the nuclei. The nuclei pellet was resuspended in 10 ml of NBR2 buffer (85 mM KCl, 5.5% sucrose, 10 mM Tris-HCl pH 7.6, 1 mM $CaCl_2$, 1 mM $MgCl_2$, and 250 μl PMSF) and quickly pelleted again by 2000 rpm for 4 minutes. The nuclei pellet was then resuspended in 500 μl NB.R2 buffer.

5 μl aliquot of each sample was then added to 95 μl NBR2 and 1 μl DNaseI for 4 minutes at room temperature. 400 μl of 5 M Urea / 2 M NaCl was added to each sample and quantified on a GeneQuant Pro spectrophotometer at 260 nm. Nuclei samples were normalised to 20 A260 units. 20 A260 units is equivalent to a DNA concentration of 1 mg/ml.

2.3.10 Southern Blotting

DNA was transferred from 0.7% agarose TPE gels to Hybond N+ membranes (GE Life Sciences cat no. 25005990) as first described by Southern, (1975). Agarose gels containing DNA were first exposed to UV light from a transilluminator for 3 minutes to cause double strand breaks and trimmed to size using a razor blade. Gels were incubated in 250 ml 0.25 M HCl for 20 minutes shaking at room temperature to depurinate the DNA. The gel was washed twice with 250 ml H_20 to remove residual HCl and incubated twice with 250 ml denaturing buffer (1.5M NaCl, 0.5M NaOH) for 15 minutes at room temperature shaking. Once the denaturation buffer was removed and the gel rinsed with H_2O, gels were twice soaked in 250 ml neutralisation buffer (1.5 M NaCl, 0.5 M Tris-HCl). Upward capillary transfer was used to transfer DNA from the gel to the Hybond N+ membrane using 20 × SSC solution overnight at room temperature. The Hybond N+ membrane was rinsed in 2 × SSC solution and exposed to UV on a transilluminator to immobilise the DNA.

[α -^{32}P] dCTP radiolabelled probes were then hybridised to the Hybond N+ membrane. Each membrane was incubated in 15 ml of hybridisation buffer (6 × SSC, 10 mM EDTA, 5 × Denhardt's solution (Thermo Fisher cat no. 750018), 0.5% SDS, 100 μg/ml salmon sperm DNA) for 30 minutes. Radiolabelled probe was then added to the hybridisation solution and incubated at 65°C overnight. Membranes were washed twice with 2 × SSC 0.1% SDS for 15 minutes at 65°C followed by two washes with 0.1 × SSC 0.1% SDS at 65°C for 15 minutes. Hybridised radiolabelled probes were then detected in autoradiography cassettes with phosphorimager screens overnight and analysed.

2.4 RNA methods

2.4.1 RNA purification

Total RNA was isolated from mammalian cell cultures using Qiagen's Rneasy Mini Kit (Qiagen cat no. 74104). Cells were washed with PBS, harvested by trypsinisation and counted using a Beckman Coulter Counter. More than 1×10^7 cells were pelleted per sample. Cell pellets were resuspended in 350-600 μl of RLT buffer with 1% β-mercaptoethanol depending on cell number. An equal volume of 70% ethanol was then added to the samples and mixed by pipetting.

Samples were transferred to Rneasy mini spin column and centrifuged at 12,000 g for 30 s. 10 μl of DnaseI was mixed with 70 μl of RDD buffer (Qiagen RNase-Free Dnase Set ; Cat no. 79254) and added to each column for 15 minutes at room temperature, for on column DNase digestion. RNA was eluted from the column in 50 μl of RNase-free water, quantified on a Nanodrop-1000 UV-VIS spectrometer and stored at -80°C.

2.4.2 cDNA library synthesis

Complementary DNA to first strand RNA was synthesised using SuperScript II Reverse Transcriptase (Invitrogen cat no. 18064-022). 1 μg of purified RNA was added to 250 ng of random hexamers, and 10 mM dNTP mix in RNase free water. Samples were the incubated at 65 °C for 5 minutes to melt secondary RNA conformations and quickly cooled on ice. SuperScript II buffer was added to each sample (1 × final conc First Strand Buffer, 0.1M DTT). Samples were gently mixed and incubated at 25 °C for 2 minutes. 200 units of SuperScript II reverse transcriptase was added into each sample and incubated at 25 °C for 10 minutes, followed by 42 °C for 50 minutes. Reactions were stopped by denaturation at 70 °C for 15 minutes.

2.4.3 Quantitative real time PCR

To evaluate the relative abundance of complementary DNA sequences indicative of relative gene expression, real time PCR was used. Lightcycler 480 SYBR Green I Master Mix (Roche cat no. 04707516001) was as described earlier for analysing ChIP DNA sequences (**Section 2.3.6**).

2.4.4 EU-RNA dot blotting

Mouse ESCs were incubated with 1 mM ethynyl uridine (EU) overnight at 37 °C 5% CO_2. Cells were rinsed 3 × with CSK buffer (100 mM NaCl, 0.1% Triton X-100, 300 mM sucrose, 1 mM $MgCl_2$, 1 mM EGTA, 10 mM PIPES and 100 μM PMSF) at room temperature for 5 minutes. Cells were then trypsinised and centrifuged at 1200 rpm for 5 minutes. mESC nuclei were isolated using NBA and NBbB buffers (**Section 2.3.7**). RNA was purified using Qiagens Rnasey kit (**Section 2.4.1**).

18 μl of RNA was added to an *in vitro* click reaction mix (3 μl TEA pH 7, 30 μl DMSO, 6 μl ascorbic acid, 1.2 μl biotin-azide (Thermo Fisher cat no. B10184), 3 μl 10 mM Cu-TBTA, and vortexed to ensure complete mixing. Samples were left overnight at room temperature for the click reaction to complete. RNA was precipitated using 150 μl of ethanol and 0.3 M sodium acetate pH 5.5 and 20 μg of glycogen at -20 °C for 2 hours. Centrifugation at 12,000 rpm for 30 minutes was used to pellet the RNA and samples were washed in 500 μl 70% ethanol. Samples were pelleted again and left to air dry to remove residual ethanol at room temperature. Samples were resuspended in 20 μl TE and the absorbance measured using a nanodrop 1000 UV-VIS spectrometer.

Nitrocellulose membranes were hydrated in water for 5 minutes followed by 20 × SSC for 20 minutes at room temperature. Excess 20 × SSC buffer was absorbed using filter paper and 2 × 1 μl of RNA TE was then spotted and dried at room temperature. The RNA was crosslinked to the membrane with 200 mJ of UV radiation and baked at 70 °C for 30 minutes.

The crosslinked membranes were then blocked with 50 ml of 3% BSA (w/v) in buffer 1 (0.5 M Tris, 0.15 M NaCl) at 60 °C for 30 minutes. For biotin detection membranes were incubated with Streptavidin-HRP (Thermo Fisher cat no. 89880D) at 1:1000 dilution for 2 hours rotating at room temperature. Membranes were washed twice with buffer 1 for 15 minutes with shaking to remove any unbound streptavidin-HRP molecules. Membranes were then developed with enhanced chemiluminescence detection kit (Pierce cat no. 32106) for 1 minute at room temperature before exposure to Hyperfilm ECL (GE Healthcare cat no. 28906837).

2.5 Protein analysis

2.5.1 Protein lysate preparation

Proteins were extracted from mammalian cell cultures by detergent mediated cell lysis. Cells were typically grown in T75 flasks or 6 cm dishes to 75% (max) density. Cells were washed with PBS and recovered by trypsinisation (Invitrogen cat no. 59427C). Non-adherent cells were collected and lysed with NuPage LDS sample buffer (Invitrogen cat no. NP0007) with 12.5 mM DTT as per manufacturer's instructions. Samples were incubated at 70 °C for 10 minutes before being stored at -20 °C.

2.5.2 SDS-PAGE

Nupage Novex precast gels were used to resolve protein lysates. Nuclear lysates were centrifuged at 12,000 g for 1-2 minutes to pellet any large cellular fragments. 10-20 μg was loaded per well on 4-12% gradient (Invitrogen cat no. NP0322BOX) or 10% (Invitrogen cat no. NP0315BOX) Bis-Tris gels. 4 μl of SeeBlue Plus2 prestained protein standard (Invitrogen cat no. LC5925) was run to determine molecular weights. For low molecular weight proteins such as histones, 1 × Nupage MES running buffer (Invitrogen cat no. NP0002) was used, while 1 × Nupage MOPS running buffer (Invitrogen cat no. NP0001) was used for high molecular weight proteins (>80 kDa). Proteins were resolved at 150 V for 50 minutes with MES buffer, and 80 minutes with MOPS running buffer.

2.5.3 Western blotting

Nuclear protein lysates resolved by SDS-PAGE electrophoresis were transferred to Immobilon-P polyvinylindine flouride (PVDF) membranes (Millipore cat no. IPVA00010). 'Wet' transfers were performed using the X Cell 11 Blot Module (Invitrogen cat no. EI9051). Blotting pads and filter paper were submerged in 1 × Nupage transfer solution (Invitrogen cat no. NP0006) supplemented with 20% methanol, 1% antioxidant (Invitrogen cat no. NP0005) and any air bubbles removed. PVDF membrane was cut to size and hydrated in 100% methanol before being soaked in transfer solution. Protein transfer was performed at 30 V for 60 minutes.

The protein bound PVDF membrane was incubated in 5% milk powder TBS-T buffer (50 mM Tris HCl pH 7.5, 150 mM NaCl, 0.05% Tween-20) for 30 minutes shaking at room temperature. PVDF membranes were washed with TBS-T for 10 minutes at room temperature. Membranes were then incubated with primary antibodies in 5% milk PBS-T overnight at 4 °C.

Primary antibody was removed and the membrane washed 3 × with TBS-T shaking at room temperature for 5-10 minutes. Antibody species specific conjugated horseradish peroxidase (HRP) secondary antibodies were diluted in 5% milk TBS-T and added to the membranes while shaking at room temperature for 1 hour. Membranes were briefly washed in TBS-T and incubated with an enhanced chemiluminescence detection kit (Pierce cat no. 32106) for 1 minute at room temperature. Membranes were place between acetate sheets and exposed to Hyperfilm ECL (GE lifesciences cat no. 28906837) and developed on a Konika SRX-101A processor. Films were scanned and densitometry performed on the required bands using ImageJ or AIDA image analysis software with background correction.

2.6 Cell Culture

2.6.1 Cell lines

Cell lines used were murine erthroleukeamia cells (Chapter 3), HCT116 cells and matched trametinib resistant TRAMR cells (Chapter 4), murine 3T3 fibroblasts, and mouse embryonic stem cells wild type (WT41) and Suv39h double null clones (DN57, DN72) (Chapter 5).

MEL cells with various GFP constructs inserted at the RL5 locus were obtained from the Larionov lab. p212 MEL cells lacked any heterochromatic sequences within the transgene, while RL5 MEL cells lacked the GFP construct entirely. α-MEL cells contained a human alpha satellite domain upstream of the GFP enhancers and promoter (**Figure 3.1, A**). HCT116 cells and matched trametinib resistant TRAMR (derived from HCT116) cells were obtained from John Dawson, who initially characterised the cellular phenotype. Mouse embryonic stem cells were obtained from the Jenuwein lab.

2.6.2 Adherent cell growth and passaging

HCT116, TRAMR and 3T3 cells were typically cultured in T75 flasks with 15 ml of Dulbecco's Modified Eagle Medium F12 (Gibco cat no. 12500-062) supplemented with 10% fetal calf serum, 1% penicillin/streptomycin and 1% L-glutamine. Cells were grown in 5% CO_2 at 37 °C in a humidified cell culture incubator. When confluent (> 70% coverage) cells were passaged by washing with PBS and treated with trypsin/EDTA (Gibco cat no. 5400054) and split 1:7 to 1:10 every 2-3 days.

2.6.3 Suspension cell growth and passage

MEL cells were also cultured in T75 flasks with 20-30 ml high glucose Dulbecco's modified eagle medium with L-glutamine (Gibco cat no. 11965084) supplemented with 10% fetal calf serum (FCS) and 1% penicillin/streptomycin. Cells were grown at 5% CO_2, 37 °C and split 1:10 to 1:20 for every other day.

2.6.4 mESC cell growth and passage

Mouse embryonic stem cells were only grown with low passage numbers (<50). WT41, DN57, and DN72 cell lines were cultured in Glasgow Minimal Essential Medium (Gibco cat no. 11710035) supplemented with 10% fetal calf serum, 0.1 mM β-mercaptoethanol, 1% penicillin/streptomycin, 1% L-glutamine, 1 mM sodium pyruvate, non-essential amino acids (Sigma cat no. M7145), and 1000 U/ml of human recombinant LIF (prepared in MRC HGU). mESC flasks (Corning cat no. 430639) were pre-treated with 0.1% gelatin/PBS for 5 minutes. The excess gelatin was removed and 5 ml of mESC media was added to prevent the gelatin layer drying out. mESCs suspended in 20 ml of media were added to each flask.

2.6.5 Freezing cells

For cell storage, >80% confluent cell flasks were washed with PBS, incubated with typsin/EDTA (Gibco cat no. 5400054) for 5 minutes, collected by centrifugation at 1200 rpm for 5 minutes. Cells were resuspended in 1-2ml freezing media (50% fetal calf serum, 10% DMSO, 40% ES cell growth media). 500 μl aliquots were frozen at -80°C and transferred to liquid nitrogen after 24 hours for long term storage.

2.6.6 Thawing cells

Cell lines retrieved from liquid nitrogen or -80°C storage were kept on dry ice before being rapidly thawed at 37 °C in a water bath. Once thawed the contents was added to 10 ml of normal growth media pre-warmed to 37 °C and centrifuged at 1200 rpm for 5 min. Cell pellets were resuspended in 15 ml of growth medium in a T75 flask stored at 5% CO_2 and 37 °C. After 12-24 hours flasks were rinsed with PBS and 15 ml fresh growth media added. Media was replaced every 1-2 days and cells passaged every 72 hours or whenever mESC colonies were enlarged.

2.6.7 Stable mammalian cell transfection

Mouse embryonic stem cells were seeded at 50,000 cells/ml on 0.1% gelatin coated 6-well plates overnight at 37 °C in antibiotic free growth media. 1 μg of the vector construct was incubated with 200 μl of Opti-MEM (Gibco cat no. 31985070) for 10 minutes, whilst 5 μl lipofectamine 2000 (Invitrogen cat no. 11668019) was added to a separate 200 μl Opti-MEM aliquot per transfection. The pre-mixed lipofectamine 2000 and DNA constructs were mixed by inversion and incubated at room temperature for 30 minutes. This mix was then added to 2 ml of fresh antibiotic free media and used to refresh the media on a mESC culture. mESC's were then grown with appropriate antibiotic (Zeocin) prior to experiments.

2.6.8 Generating drug resistant cell lines

Cells were initially treated with log dose curves of JQ1 for 5 days and viability determined by PrestoBlue reagent (Invitrogen cat no. A13261). Cells were seeded at 10,000 cells/ml in 96 well plates with 200 μl of media in each well. Cells were left over night to adhere to the well bottom, and the media was then aspirated and replaced with JQ1 containing media for 4 days. The media was removed and fresh media with 10% PrestoBlue (v/v) was added to each well for 90 minutes. 540/590 nm fluorescence was assayed on a PerkinElmer Victor3 multilabel reader.

The concentration of JQ1 that inhibited growth by 50% (195 nM) was then added to the growth media for two weeks. Cell viability in response to a log dose concentration of JQ1 was then reanalysed with PrestoBlue reagent, and the JQ1 dose adjusted for the next two-week period. After ~3 months cells could tolerate 1 μM JQ1 treatment and were considered resistant. JQ1 was then removed from the growth media and viability re-analysed after two weeks. Cells presented no loss of resistance to JQ1 demonstrating a permanent state of resistance. Cells were periodically retested to check JQ1 resistance was not lost.

2.6.9 Immunofluorescence

To analyse the cellular distribution of proteins and their modifications cells were immunostained with appropriate antibodies. Cells were seeded on Superfrost plus slides (Thermo Fisher cat no. J1800AMNZ), pre-coated in 0.1% gelatin for mESC's, for 6-8 hours at 37 °C 5% CO_2 in chambers with 5 ml of growth media.

To observe chromatin bound protein distribution slides were treated with CSK buffer (100 mM NaCl, 0.1% Triton X-100, 300 mM sucrose, 1 mM $MgCl_2$, 1 mM EGTA, 10 mM PIPES and 100 μ M PMSF) for 10 minutes on ice.

Slides were carefully washed with PBS to prevent loss of adherent cells and fixed with 4% paraformaldehyde (Sigma cat no. 158127) for 10 minutes at room temperature. Slides were carefully removed and submerged in PBS twice to remove any residual paraformaldehyde and permeabilised in 0.5% Triton X-100 (Sigma cat no. T8787) for 10 minutes at room temperature.

Slides were then blocked in 5% donkey serum in PBS for 30 minutes at room temperature. Primary antibodies were then added to the slides diluted in 5% donkey serum and incubated for 1 hour at room temperature in a dark humidified chamber. Slides were washed 3 × in PBS/ 0.02% Tween-20 5 minutes each at room temperature. Fluorophore conjugated secondary antibodies (Jackson Immuno Research) were incubated on the slides for 1 hour at room temperature in a dark humidified chamber, diluted 1:500 with 5% donkey serum/PBS. Slides were kept in the dark and washed carefully 3 × with PBS 0.02% Tween-20 for 5 minutes at room temperature. For nuclei staining the final wash was supplemented with 50 μ g/ml of DAPI at room

temperature. Slides were mounted in Vector Shield (Vector Laboratories cat no. H-1000). Standard and deconvolution epifluorescent microscopes using 63x or 100x plan-APOCHROMAT (1.4 NA) objectives were used to image slides. Deconvolution analysis was performed using iVision software.

2.6.10 Chromatin bound protein distribution analysis

To determine chromatin bound protein distribution, samples were washed with CSK buffer prior to fixation and imaged on a deconvolution epifluorescent microscopes as stated above (**Section 2.6.8**). Image stacks were initially deconvolved on iVision software per standard protocols. Image stacks were then transferred to ImageJ. A macro in Javascript was written to split the channels, identify the single plane for analysis, restack the channels for the plane of interest, and save the stack.

A second macro was written to use edge segmentation to make a mask of the DAPI channel. The DAPI channel was first applied with a rolling ball background subtraction, unsharpen mask to rescale the contrast to the original image, and processed with a gaussian blur to smooth the image further. The image was then made binary with a black background. The classic watershed function was applied to edge segment the image and particles under 500 pixels excluded. This created the region of interests (ROI) around each nucleus in each image. This mask was then applied to the FITC channel, where the area mean integrated intensity for each pixel was calculated within the ROI, determining the radial pixel intensity and exported to excel.

Each radial pixel number was divided by the max radial pixel number per ROI and multiplied by 100 to turn pixel number in percentage distribution. This enabled the data of multiple cells to be binned together into radial decile pixel intensities, which were then plotted by box plot.

2.6.11 Cell cycle analysis with propidium iodide

Propidium Iodide (PI) is a DNA intercalator that has 20 times the fluorescence when bound to DNA (Wilson *et al.*, 1986). As DNA content changes as a cell progresses throughout the cell cycle, PI staining was used to investigate cell cycle dynamics. Cell cultures were first washed with PBS and harvested by trypsinisation. Cells were centrifuged at 1200 rpm for 5 minutes, resuspended in PBS and counted using a Z2 Coulter counter. Cell counts were normalised to 1.5×10^6 cells/ml and 2.5 × volume of 100% ethanol was pipetted dropwise while samples were vortexed. Cells were incubated on ice for >2 hours to allow fixation, centrifuged at 2000 rpm for 5 minutes at room temperature and resuspended in PBS. Samples were then recentrifuged and cells resuspended in propidium iodide staining solution (1 μ g/ml PI, 4 μ g/ml RNase A, PBS) at a count of 2.5×10^6 cells/ml for 2 hours at room temperature.

Flow cytometry was used to measure PI staining on a BD LSR Fortessa cell analyser. Filters limited fluorescence detection to 695-740 nm. Data analysis of cell population was performed using Flow-Jo single-cell flow cytometry software.

2.7 Radioactive nucleotide labelling

2.7.1 DNA probe labelling

25 ng of oligomers or DNA molecular ladders in 11 μl DNase free water were boiled for 5 minutes and placed on ice to cool. 4 μl of High Prime Kit (Roche cat no. 11585584001) supplemented with 125 mM dATP, dGTP, and dTTP was added to each sample as per manufacturer instructions. 5 μl of [α-^{32}P] dCTP 3000 Ci/mmol was also added and incubated at 37 °C for 30 minutes. 80 μl of DNase free water was added to each sample and transferred to a G-25 sephadex spin column (Roche cat no. 27532501).

2.7.2 Unincorporated label removal

Unincorporated free nucleotides dATP, dGTP, dTTP and [α-^{32}P] dCTP were removed from DNA probes by passing through sephadex G-25. Columns were prepared by vortexing and then the cap loosened ¼ turn and centrifuged >700 g for 1 minute. 100 μl of radiolabelled samples were then carefully transferred to the column without disturbing the G-25 grade F resin. Samples were then centrifuged >700 g for 2 minutes at room temperature. The [α-^{32}P] dCTP labelled DNA was recovered in the eluate and stored for hybridisation.

2.7.3 RNA metabolic labelling

Cells were grown in T75 flasks to 60% confluency and treated with JQ1 1 μM for 24 hours. 5 μl/ml of 1 mCi [5-^{3}H] Uridine (Perkin Elmer cat no. NET174250UC) was added to the culture media for 30 minutes at 37 °C 5% CO_2. Media was aspirated from the cells and washed with PBS. Cells were trypsinised, collected and washed again with PBS. RNA was extracted from the cells using the RNeasy Mini Kit as previously described (**Section 2.4.1**). Samples were quantified on a nanodrop 1000 UV-VIS spectrometer 260 nm absorbance and 5 μl of each sample was then added to 4 ml of scintillant. Radiation from the tritiated RNA causes the scintillant to fluoresce allowing the quantity to be analysed using a Beckman LS 6500 scintillation counter. Samples were counted for 30 minutes at room temp in technical triplicates.

2.8 Chromatin analysis

2.8.1 Chromatin fibre extraction

In order to release chromatin fibres from isolated nuclei, chromatin was partially digested with micrococcal nuclease (Mnase). Nuclei at 20 A260 in NBR2 buffer were incubated with RNase A/T1 (Ambion cat no. EN0551) for 2 minutes at room temperature. Each sample was then digested with 400 units/ml of MNase for 8 minutes at room temperature. 125 mM glycine final concentration was used to stop the MNase digestion, and samples were quickly pelleted at 12,000 g for 1 minute and resuspended in 500 μl TEEP-20 or TEEP-80 buffer at 4°C overnight. Samples were centrifuged at 12,000 g for 5 minutes at room temperature to remove nuclear fragments from the supernatant.

Samples fixed with 1% formaldehyde for 10 minutes before or after MNase digestion, were released into TEEP-20 (+/- 0.5% SDS) and transferred to Visking tubing. The samples were then dialysed in 5 litres TEEP-80 or TEEP-1 at 4 °C overnight to remove excess formaldehyde molecules.

2.8.2 Chromatin purification – Sucrose step Gradients

Chromatin fibres and chromatin bound proteins can be isolated from nuclear components by centrifugation onto a TEEP-80 50% sucrose boundary as described in Gilbert, *et al*, (2007). A 1.5 ml layer of 50% sucrose TEEP-80 was added to a SW55 Beckman tube. 10% sucrose TEEP-80 was then slowly layered on without mixing, resulting in a boundary between the 10-50% sucrose. Chromatin samples released from nuclei were loaded on the 10% TEEP-80 and centrifuged 48,000 rpm for 90 minutes. 60% sucrose TEEP-80 was pumped in the bottom of the centrifuge tubes, using upward displacement to fractionate the gradient into 500 μl aliquots. DNA from chromatin containing fractions was then purified by phenol chloroform extraction.

2.8.3 Isokinetic sucrose gradient fractionation

Sucrose density centrifugation is a technique used to fractionate macromolecules that has been adapted to distinguish between chromatin states (Brakke, 1953; Gilbert, Thomson, Boyle, Allan, Ramsahoye and Wendy A Bickmore, 2007). Micrococcal nuclease released chromatin fibres were resolved in 6-40% isokinetic sucrose TEEP gradient centrifugation in Beckmann SW41 tubes. 6% sucrose TEEP ΔNaCl was mixed with 40% sucrose TEEP ΔNaCl solution at room temperature in a constant volume mixing chamber and loaded bottom up as first described by Noll, (1967). Gradients were then left overnight at 4 °C to settle. 0.5 cm was left free at the top of each SW41 tube sucrose gradient, and 500 μl of soluble chromatin was loaded. Samples were centrifuged in a Beckman ultracentrifuge using a

SW41 Ti swinging bucket rotor at 41,000 rpm, 4 °C for 4.5 hours. Gradients were fractionated using upward displacement with 50% sucrose TEEP-80 and samples were passed through an inline UV spectrometer and collected in 500 μl aliquots. The UV absorbance was used to detect which fractions contained chromatin fibres, which were then purified by phenol chloroform. DNA samples were fractionated on 0.7% agarose TPE gels.

2.8.4 Micrococcal Nuclease accessibility digestion

To assess micrococcal nuclease accessibility, isolated nuclei (**Section 2.3.7**) were diluted to 4 A260 (200 μg/ml) in NBR2 buffer. Samples were incubated with 1 μl of RNase A/T1 for 2 minutes at room temperature. 800 units/ml of micrococcal nuclease was then added to the samples at room temperature. At 1, 2, 4, 8, and 16 minutes aliquots were added to EDTA to stop the MNase digestion. Each time point sample was then added to genomic lysis buffer 1 × final concentration and incubated with 1 μl proteinase K at 55 °C overnight. Samples were phenol chloroform purified and ethanol precipitated before being resolved on 1% agarose TBE gel with a 1 kb plus ladder.

2.9 Reverse phase protein arrays

α-MEL cells were treated with 0.1% DMSO, 1 μM IBET151 for 24 hours in normal cell culture conditions. Cells were washed in PBS, trypsinised and resuspended in MD anderson buffer (1% Triton X-100, 50 mM HEPES, 150 mM NaCl, 1.5 mM $MgCl_2$, 1 mM EGTA, 199 mM NaF, 10 mM Na pyrophosphate, 1 mM Na_3VO_4, 10% glycerol, phosphatase inhibitor cocktail - Roche cat no. 04 906 845 001) for 30 minutes at room temperature with intermittent vortexing.

Protein concentrations were analysed by Coomassie Plus staining (Pierce cat no. 23236). A BSA serial dilution was used as a standard (0, 0.05, 0.1, 0.15, 0.2, 0.3, 0.4, and 0.6 mg/ml). 2.5 μl of each sample were diluted 1:20 to 50 μl and transferred to opaque 96 well plates in addition to 10 μl of standards. 240 μl of Coomassie Plus reagent was added to each well for 30 s while shaking and further incubated at room temperature for 10 minutes. 595 nm filter microplate reader was then used to measure absorbance. Lysates were normalised to 1 mg/ml and 150 μl aliquots transferred to fresh tubes.

50 μl of 4x SDS buffer was then added to each sample (40% glycerol v/v, 8% SDS v/v, 0.25 M Tris-HCl pH 6.8, 5 mM β-mercaptoethanol). Samples were incubated at 80 °C for 5 minutes and rapidly cooled by 15 s max speed centrifugation. Samples were then transferred to a 96 well plate in duplicate. Samples were half log serial diluted with MD Anderson lysis buffer (1% Triton X-100, 50 mM HEPES, 150 mM NaCl, 1.5 mM $MgCl_2$, 1 mM EGTA, 199 mM NaF, 10mM Na pyrophosphate, 1 mM Na_3VO_4, 10% glycerol, phosphatase inhibitor cocktail -Roche cat no. 04 906 845 001) supplemented

with 1 × SDS buffer (2% SDS, 62.5 mM Tris-HCl pH 6.8, 1.25 mM β-mercaptoethanol). Samples were spotted onto arrays at 70% humidity using an Aushon 2470 microarray printing platform and samples were left at room temperature 70% humidity for 2 hours to allow the samples to dry. Once the arrays were removed from the printing platform, they were incubated with SuperBlock TBS (Pierce cat no. 37535) for 4 hours at room temperature on a rocker.

Each array was placed in ArrayIt hybridisation cassettes and rinsed 3 × with 130 µl TBS-T, followed by incubation with TBS-T at room temperature for 10 minutes. Primary antibodies diluted in SuperBlock were added to the array cassettes and incubated overnight at 4 °C with rocking. The cassettes were rinsed 3 × with TBS-T and incubated 3 × with TBS-T for 10 minutes. Secondary antibodies and IgG control were incubated in the array cassettes for 1 hour at room temperature in the dark. The array cassettes were then further rinsed 3 × with TBS-T and submerged in 50 ml of dH_2O. The arrays were then spun at 200 g for 5 minutes to remove any residual water and left overnight in the dark at room temperature. Arrays were imaged on an Innopsys Innoscan 710 using 785 nm excitation.

Sample spotting concentrations were quality controlled and normalised for analysis using fast green staining. Arrays were first washed in 50 ml dH_2O for 5 minutes at room temperature before incubation with 0.25 M sodium hydroxide for 15 minutes and washed 3 × in dH_2O for 10 minutes at room temperature. Arrays were then incubated in destain solution (30% methanol, 7% glacial acetic acid, dH_2O) for 15 minutes at room temperature. Arrays were incubated with 1x Fast Green destain solution (250 μ g Fast Green FCF (Sigma cat no. F7252), 30% methanol, 7% glacial acetic acid, dH_2O) for 3 minutes at room temperature with shaking. Arrays were submerged 3 × in 50 ml dH_2O and centrifuged at 200 g for 5 minutes to remove residual water. Arrays were scanned again with Innoscan 710 at 785 nm.

2.10 Compound screening

2.10.1 FACS screening

MEL cells were washed with PBS and concentration analysed by a Coulter counter. Cell concentrations were normalised to 333,000 cells per ml in fresh media and 300 μl added to each well of a 96 well plate resulting in 100,000 cells per well. Cells were incubated at 37 °C in 5% CO_2 for 6 hours before compounds were added.

Compounds were first diluted to 1000 × final concentration in DMSO (1 mM unless stated otherwise) in V-bottomed 96 well plates in the required final layout. Plates were sealed and kept at 4 °C in the dark for replicate use.

The 1000 × final concentration (1 mM) compounds were then diluted 100 × in fresh growth media in an intermediary 96 well plate. 33 μl of the 10 × probe compounds were added to 300 μl of MEL cell growth media in each well. Cells were incubated for 48 hours at 37 °C in 5% CO_2 before being pelleted at 1200 rpm for 5 minutes and resuspended in 100 μl ice cold PBS. Cells were kept on ice and immediately analysed on a BD FACSAria flow cytometer analyser. Samples were initially gated on side scatter height and area to ensure only single cells were analysed. Forward scatter and side scatter area was gated to remove cellular debris. GFP transgene expression was determined by 488 nm excitation and 525-550 nm emission filters. RFP expression was determined by 561 nm excitation and 610-620 nm emission filters.

2.10.2 IncuCyte growth screening

MEL cells with GFP and RFP expression constructs were quantified on a coulter counter. Cells were seeded in clear-bottomed 96 well plates at 50,000 cells/ml in 180 μl of prewarmed growth media. Each well was supplemented with 20 μl of 2 mg/ml of Corning matrigel (Cat no. 354263), previously stored at 4 °C was added to each well of 96 well plates. Plates were inserted into an IncuCyte Zoom microscope at 37 °C and 5% CO_2.

Matrigel is the base components from Engelbreth-Holm-Swarm mouse sarcoma extracellular membrane extract (Laminin, Collagen IV, Heparin sulfate proteoglycans, entactin/nidogen). As the matrigel warms to 37 °C it solidifies to form a hydrogel preventing the MEL cells from moving between focal planes allowing live cell imaging. The IncuCyte Zoom was used to image bright field, GFP and RFP every 6 hours for the length of the experiment. Four 10 × images were taken per well per time and collated.

Probe compounds were then prepared as 10 × final concentrations in fresh growth media as described for FACS screening (**Section 2.10.1**). After 12 hours at 37 °C, 22 μl of 10x concentration probe compounds were then added to each well. Cells were grown at 37 °C in 5% CO_2 and imaged every 6 hours up to 84 hours. Quantitative data analysis was performed using the IncuCyte Zoom analysis software. Brightfield images were used for edge segmentation, with the processing definition adjusted manually for each experiment. This mask was then applied to the GFP and RFP channels. The mean fluorescent pixel intensity for all cells within each image mask were then calculated and exported to excel. At each time point samples were compared to untreated DMSO controls.

2.10.3 Presto Blue viability assays

Single agent and drug combinations effects on viability were analysed using PrestoBlue reagent (Invitrogen cat no. A13261). Adherent HCT116 and TRAMR cells were washed with PBS, trypsinised and concentrations adjusted to 10,000 cells/ml of growth media. 200 μl aliquots were added to each well and incubated at 37 °C overnight.

Single agent log dose concentrations were first prepared 1000 × final concentrations in V-bottomed 96 well plates. 10 mM of each compound was serial diluted to 100 μM in DMSO. Trametinib was also serial diluted from 300 μM to 100 nM. Each drug concentration was added in separate wells to every concentration of the other drug, reducing the concentration of each drug 2-fold. An equal volume of DMSO was therefore added to each single agent drug dose range to halve the concentration.

Drug matrix intermediary plates were diluted 50-fold in fresh growth media. 22 μl was added to each well of a 96 well flat bottomed plate containing cells incubated overnight. Cell were then incubated for 48 hours at 37°C in 5% CO_2. 10% (v/v) PrestoBlue reagent was then prepared in fresh growth media. Each well was then aspirated and replaced with 200 μl of 10% PrestoBlue growth media, and incubated for 90 minutes. A Victor3 multilabel plate reader was then used to detect 540/590 nm fluorescence.

Readings were normalised to DMSO control readings producing relative changes to cell growth. 3D plots of relative cell growth across the combination and antagonism/synergism analysis was performed using the combenefit platform (Di Veroli *et al.*, 2016). Combination matrices were

analysed in parallel using Loewe's model, the Bliss model and the Highest Single Agent (HSA) model. Synergy, antagonisms or neutrality modelling was similar across all three models, so HSA model was used across all figures to allow direct comparison.

2.11 Copper assisted azide-alkyne cycloaddition

2.11.1 Single nucleotide HPLC-UV spectrometry

Cells were washed in PBS, trypsinised and resuspended in genomic lysis buffer (150 mM NaCl, 1% SDS, 10 mM EDTA). Samples were then incubated with 10 μl/ml proteinase K and incubated at 55 °C overnight shaking at 500 rpm. An equal volume of phenol chlorofom:IAA was then added to each sample and centrifuged at 12,000 rpm for 30 minutes at 4 °C. The aqueous phase was then transferred to a fresh tube and retreated with an equal volume of chloroform in the same fashion. The aqueous phase was added to 2.5 × volume of 100% ethanol and 0.3 M sodium acetate pH 5.5 at -20 °C for 2 hours. Samples were precipitated and collected by 12,000 rpm centrifugation for 15 minutes. The supernatant was then removed and the samples air-dried at room temperature. Samples were resuspended in 400 μl TE and 6 μl RNase A/T1 added at 37 °C overnight.

Samples were again precipitated with 2.5 × volume of 100% ethanol and 0.3 M sodium acetate pH 5.5 at -20 °C for 2 hours. Samples were pelleted and allowed to air dry, before being suspended in 400 μl TE. 6 μl RNase A/T1 was again added at 37 °C for 6 hours. Samples were re-precipitated by the same method described and resuspended in 25 μl of TE. 3 μl of DNaseI and 10 × reaction buffer were added to each sample and incubated overnight at 37 °C shaking at 500 rpm. Zinc sulphate and sodium acetate were added to each sample at 1 mM and 30 mM final concentrations respectively. 3 μl of

nuclease P1 and 48 μl TE was also added and samples were incubated for 6 hours at 37 °C. Samples were then centrifuged at 12,000 rpm for 5 minutes and transferred to fresh tubes before loading onto the HPLC column. Bernie Ramsahoye ran samples on the HPLC-UV spectrometer.

2.11.2 Single nucleotide HPLC-MS-MS

Single nucleotide solution was prepared following the same protocol as HPLC-UV analysis (**Section 2.11.1**). Cells were lysed in genomic lysis buffer, and the nucleic acids isolated by phenol chloroform:IAA extraction. RNA was then digested by RNase A/T1 and centrifugation used to purify DNA molecule from the mono RNA nucleotides. The DNA was digested to mononucleotides by sequential digestions with endo- and exonucleases, DNaseI and Nuclease P1. Samples were run on a Thermo Q-Exactive Orbitrap coupled with a Dionex UPLC column, by Andrew Finch.

2.11.3 Click optimisation coumarin assay

3T3 cells were resuspended at 50,000 cells/ml and 100 μl added to each well of a 96 well plate. Media was supplemented with 20 μM of EdU for 24 hours, allowing for EdU to be incorporated in DNA during replication. 3-azido-7-hydroxycoumarin [Coumarin-azide] (Baseclick cat no. BCFA-047-5) fluorescence was used to determine the rate of azide-alkyne copper assisted cycloaddition.

Cells were incubated with 200-250 mM coumarin-azide with a dose curve of each click reaction component in turn, across the 96 well plates. EdU treated cells were supplemented with 0.25-1 mM Δ metal (copper sulphate, ruthenium, magnesium chloride, and copper bromide), 0.01-1 mM Δ chelating agents (THPTA, TBTA), and 0.1 mM – 1 M sodium ascorbate.

The plates were imaged using the IncuCyte Zoom, with four 10x images per well imaged every 30-60 minutes with brightfield and GFP 400 ms channels for up to 72 hours. Images were processed with edge segmentation using IncuCyte Zoom software as described before (**Section 2.10.2**). Total integrated intensity values for edge-segmented cells was exported to excel and plotted over time between reaction conditions.

To determine if cellular membrane disruption enhanced azide-alkyne copper assisted cycloaddition kinetics, cells were treated with optimal click conditions supplemented with Triton X-100 or lipofectamine. 3T3 cells incubated with 20 μM EdU for 24 hours as described above were treated with 250 mM coumarin-azide, 250 mM NaAsc, 250 μM THPTA, with 0.001-1% Triton X-100 for 6 hours. 500 μM $CuSO_4$ was then added to start the click reaction.

To investigate the effect of lipofection on click reaction kinetics, optimal click reaction final concentration conditions (250 mM NaAsc, 250 mM Coumarin-azide, 250 μM THPTA) was made at 2 × concentration in opti-MEM for 10 minutes at room temperature. Lipofectin, Lipofectamine 2000 and Lipofectamine 3000 were separately incubated in an equal volume of opti-MEM for the same time period at room temperature. Click reaction opti-MEM was then mixed 1:1 with lipofectin, lipofectamine 2000 or 3000 and incubated on 3T3 cells for 6 hours. 500 μM $CuSO_4$ was then added to each well to start the click reaction, and cells were imaged on the IncuCyte Zoom as per coumarin-azide click optimisation.

2.11.4 Naked DNA *in vitro* click crosslinking reaction

E. coli transfected with pUC57-Recon2 was grown in 5 ml of Luria-Burtani broth (L-broth) overnight in a shaking incubator (250 rpm). Cultures were then supplemented with 5 ml of additional L-broth and 20 μM of EdU for 3 hours in the shaking incubator. EdU incorporated plasmid was isolated and an aliquot digested and analysed by HPLC-UV as described above (**Sections: 2.3.3, 2.11.1**). pUC57-Recon2 was then digested with *Xho*I at 37 °C overnight with shaking (500rpm). Optimal live cell click conditions (0.5 mM $CuSO_4$, 0.25 mM THPTA, NaAsc 250 mM) and 100 mM of PEG-bis-azide ~5000 M.W. (Sigma cat no. 689580) were then added to the digested plasmid at room temperature for 1-8 hours. Samples were then resolve by 1% agarose TBE electrophoresis.

2.11.5 Live cell click crosslinking reaction

Mouse fibroblast 3T3 cells were incubated with 20 μM EdU and 100 mM PEG-bis-azide (~5000 M.W) for 24 hours in normal cell culture conditions. Optimal live cell click conditions (0.5 mM $CuSO_4$, 0.25 mM THPTA, 250 mM NaAsc) was then added to the growth media for 1 hour at 37 °C in 5% CO_2, Growth media was then aspirated, and cells were washed in PBS, trypsinised and resuspended in NBA for nuclei isolation and chromatin released as described previously (**Sections: 2.3.7, 2.8.1**). MNase released chromatin fibres were released into TEEP-20 buffer before being dialysed in Visking tubing into TEEP-80 or TEEP-1 overnight at 4 °C. Samples were then centrifuged on TEEP-80 or TEEP-1 6-40% isokinetic sucrose gradients respectively at 41,000 rpm for 4.5 hours at 4 °C as described in **Section 2.8.3**.

Chapter 3: Screening for heterochromatin factors

Mis-regulation of epigenetic mechanisms has been attributed to the aberrant phenotypes of numerous conditions, including cancer. The study of altered gene regulation has largely focused on gene activation, as this provides an obvious mechanism of action, and therefore a validated target for therapeutic inhibition, but gene silencing also contributes to disease phenotypes. Within a cancer setting, genes that require silencing for oncogenesis to occur are termed tumour suppressors. Expression of repetitive DNA elements from normally heterochromatic loci are also linked to genomic instability and disease phenotypes (Kazazian *et al.*, 1988) whilst loss of pericentric heterochromatin and expression of underlying satellite repeats occurs in human and mouse tumours across cancer types (Ting *et al.*, 2011). Therefore, identifying the fundamental mechanisms of chromatin condensation both at constitutive and facultative loci remains an important biological question, with under- appreciated potential therapeutic benefit.

3.1 A synthetic model of heterochromatic silencing

To identify factors affecting heterochromatin formation and gene silencing, an artificial P212 construct, developed by Kim *et al.*, (2009), was used to screen a library of drugs. This system uses isogenic murine erythroleukaemia cells with different elements inserted at the Scl/Map17 (RL5) locus on chromosome 4, via the LoxP/Cre system (Feng *et al.*, 2005). The *Scl* gene encodes for a transcription factor, and is expressed in pluripotent haemopoietic stem cells, and is required for haemopoietic lineage differentiation. Lineage specific DNaseI hypersensitivity sites at the locus correlate with *Scl* expression, and therefore regulated disruption to the chromatin fibre have been proposed to modulate local transcription (Gottgens *et al.*, 1997; Göttgens *et al.*, 2001). Other studies have identified a downstream CTCF site that acts as an insulator from the *Cyp* gene cluster expressed in the liver. While not a tissue specific enhancer, this CTCF site is required to separate *Scl* and *Cyp* regulation (Follows *et al.*, 2012). As MEL cells have a haemopoietic lineage, the local chromatin environment is therefore considered to be normally permissive of transcription.

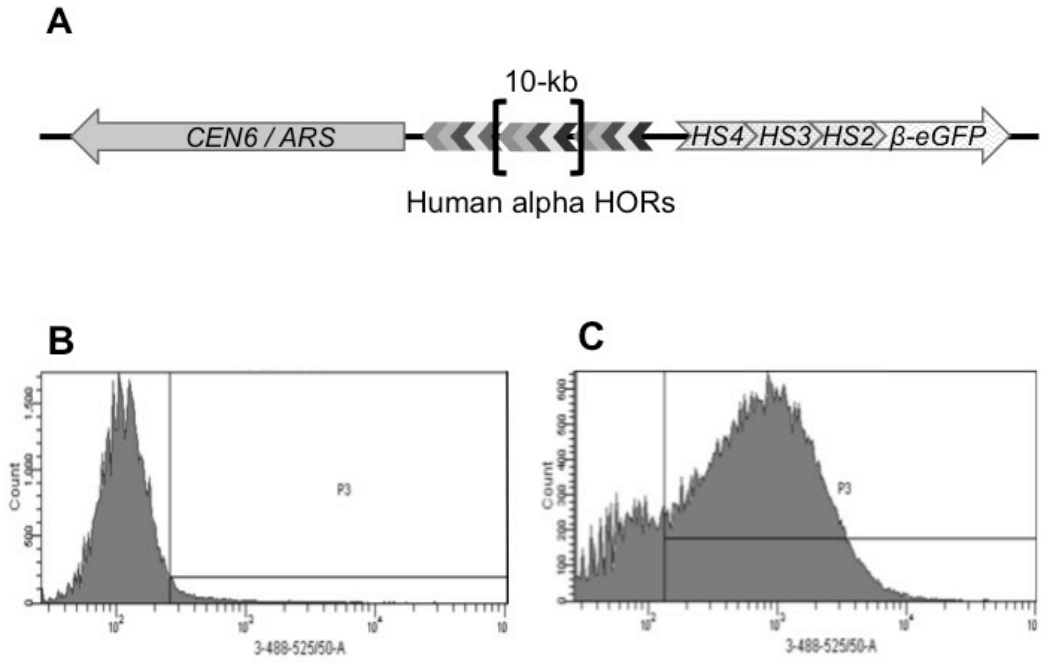

Figure 3.1. Organisation and dynamics of an artificial heterochromatic transgene. **(A)** Organisation of an artificial insert at the RL5 locus in a murine erytholeukeamia (MEL) cell clone. Construct consists of yeast centromere region from chromosome 6, a 10 kb array of human alpha satellite, and a GFP transgene with a human β-globin promoter and enhancer hypersensitivity sites. **(B-C)** Histograms showing GFP fluorescence of cells on the x-axis. **(B)** Basal GFP expression level of α-MEL cells **(C)** GFP expression in α-MEL cells after 1 μM TSA treatment for 48 hours.

The inserted P212 cassette encodes an enhanced GFP gene under a human β -globin promoter and a series of hypersensitivity sites 2, 3, and 4 (HS2, -3, -4) from the human β -globin locus control region (LCR) was inserted at the RL5 locus (**Figure 3.1**). Activation via HS2 is mediated by the histone acetyltransferase CREB binding protein (CBP) (Johnson, Norton and Bresnick, 2002) whilst HS3 is the binding site for the required transcription factors GATA-1 and Oct1 (Molete *et al.*, 2002). HS4 in contrast acts as a terminal differentiation insulator of HS2 from the β-globin promoter, mediated by CTCF (Zhao *et al.*, 2006). The β-globin promoter, when interacting with HS2, facilitates chromatin remodelling via SWI/SNF

complex HLTF, activating globin transcription (Mahajan and Weissman, 2002). By varying the artificial insert, Feng *et al,* (2005) demonstrated that eGFP with hypersensitivity sites 2 and 3 is permissive of both active and silenced states. Kim *et al*, (2009) showed that the basic eGFP cassette with hypersensitive sites, when inserted at the RL5 locus stably expressed eGFP for longer than 6 months without selection. This demonstrated a stably accessible chromatin environment at the RL5 locus within this cell line.

A modified p212 cassette, with a flanking YAC/BAC centromeric element from yeast chromosome 6, Kim (2009), silenced transgene expression (Chen *et al.*, 2004; Suzuki, Kasai and Saeki, 2006). This cassette was further modified by inserting a 10 kb array of 11 monomer higher order α-satellite repeats from the human centromere of chromosome 21 **(Figure. 3.1A)**. This pYB-α insert showed the strongest silencing that Kim, (2009) tested and was decorated with H3K9me3 and H3K27me3, marks present at repressive pericentric heterochromatin (Peters *et al.*, 2003). The expression of eGFP within pYB-α MEL cells was therefore considered to be a good system to identify compounds, which disrupt heterochromatic silencing and could give a clear phenotypic output.

To analyse basal eGFP expression in pYB-α cells, GFP levels were analysed by flow cytometry. The cells had a normal distribution, with only a few cells with elevated eGFP fluorescence (**Figure 3.1B)**. To test the effect of changes in histone acetylation cells were treated with 1 μM Trichostatin A, an inhibitor of histone deacetylases, for 48 hours. The majority of cells maintained an elevated eGFP fluorescence however the distribution was biphasic, suggesting some heterogeneity within the cell population, which was consistent over time and treatments **(Figure 3.1C)**. Flow cytometry

gating for GFP expression was defined by using MEL RL5 cells that lacked any eGFP transgene. The level of eGFP fluorescence within this reporter system is influenced by the underlying eGFP transgene transcription, and the amount of time after treatment that is required to change gene expression. Consequently, genes essential for heterochromatin formation after mitosis would take longer to activate eGFP transcription and have lower eGFP fluorescence. Therefore, for the purpose of this screen, a significant change in eGFP fluorescence after drug treatment was considered as a potentially relevant compound.

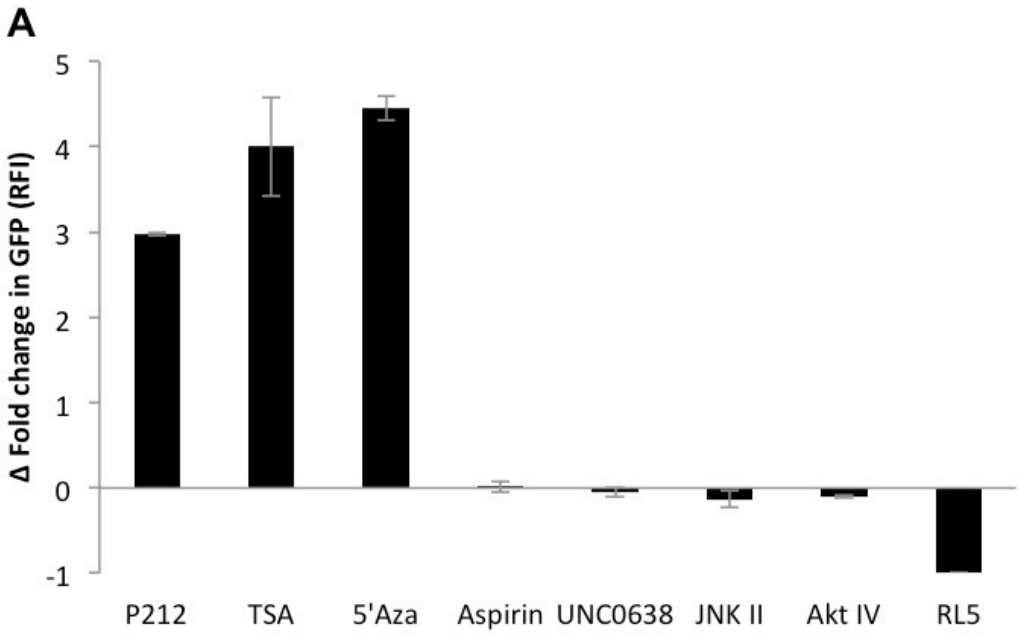

Figure 3.2. Opitmisation of eGFP transgene reactivation in MEL cells. Graph showing fold change in GFP expression in α-MEL cells, containing the heterochromatic construct after drug treatment measured by flow cytometry. P212 untreated cells (left) lack the yeast centromeric sequences and α-satellite repeats, and GFP is constitutively expressed. RL5 untransfected loci (right) lack the eGFP construct entirely providing a negative control for background fluorescence. Fluorescence was normalised to α-MEL cells DMSO treated controls. Six compounds; 5' Azacytidine, Aspirin, UNC0638, JNK II and Akt IV, were tested in α-MEL cells at 1 μM for 72 hours.

To investigate the reproducibility of this assay, 6 compounds (1 μM for 48h) were screened and compared to the expression level of the p212 cassette lacking any centromeric sequences; the RL5 cell line lacking any eGFP transgene was used as a negative control **(Figure 3.2)**, and all samples were normalised to the 0.01% DMSO control samples. Canonical inhibitors of gene silencing, TSA and 5′ azacytidine (5′Aza) altered eGFP expression. Expression was more than the p212 eGFP expression suggesting that the effect goes beyond the repressive properties of the pYB-α-satellite insert, promoting gene activation.

Cells were also treated with 1 μM aspirin and UNC638. Aspirin, while still poorly understood, is known to inhibit NF-kB which has been shown to act as a transcriptional activator at the β-globin locus in erythroleukaemia cells (Moitreyee *et al*, 1998). As aspirin did not affect eGFP expression this suggests that NF-kB does not influence the human β-globin promoter in this repressed state, and suggests that the repressed state of this transgene prevents transcription factor binding. UNC0638 also did not affect eGFP expression. UNC0638 is a highly specific inhibitor of G9a/GLP methyltranferases responsible for H3K9 -mono and -dimethylation. G9a/GLP function has been associated with selective looping between foetal and adult globin genes (Chaturvedi *et al.*, 2009; Deng *et al.*, 2013) and UNC0638 G9a/GLP inhibition has previously been used to facilitate looping to foetal globin promoters reducing β-globin expression (Krivega *et al.*, 2015). Therefore, UNC0638 would be expected to inhibit eGFP expression if any looping occurred between the LCR hypersensitive sites and the human β-globin promoter. As UNC0638 had no effect on eGFP expression, chromatin looping is unlikely to function within this repressed construct. Investigating the signalling pathways associated with β-globin expression is also

important; JNK kinase activation regulates haemopoietic transcription factor degradation (Lee *et al.*, 2010). Therefore, JNK2 inhibition should increase TF availability for gene activation. Limited re-activation of eGFP after JNK II inhibition suggests it is not involved in maintaining the repressive chromatin environment at the eGFP transgene. AKT also negatively regulates PLC kinase mediated β-globin expression (Follo *et al.*, 2008, 2012). The lack of re-expression of eGFP after AKT inhibition provides further evidence that this model of gene silencing is not primarily mediated by transcription factors.

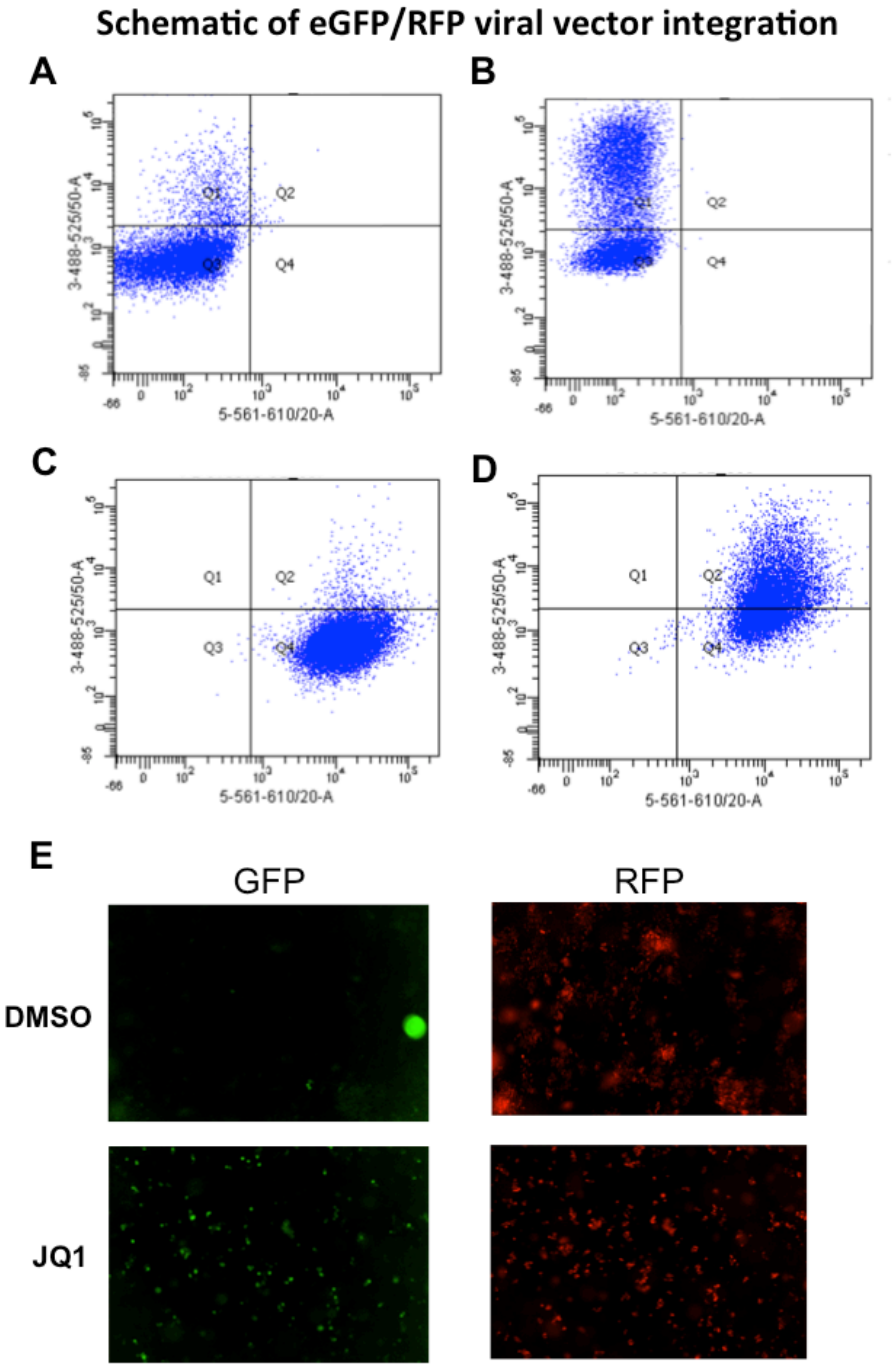

Figure 3.3. RFP and heterochromatic eGFP expression dynamics. α-MEL cells with a randomly inserted RFP lentiviral construct (Sigma. Cat No. SHC012V). Flow cytometry plots showing GFP on the y-axis and RFP fluorescence on the x-axis. **(A-B)** Silenced lentiviral RFP α-MEL clone, treated with **(A)** DMSO **(B)** 1μM TSA for 72 hours. **(C-D)** Expressed RFP α-MEL clone, treated with **(C)** DMSO **(D)** Chaetocin 1 μM for 72 hours **(E)** 10x images of RFP expressing α-MEL cells after 72 hours with DMSO or $JQ1^{+/-}$ treatment showing GFP and RFP fluorescence.

To control for compounds, which generally affected gene expression, from heterochromatic modulators, and to improve this model system, a lentiviral system was used to insert an RFP gene under a CMV promoter across the genome (Sigma, Cat No. SHC012V). The random integration of this construct resulted in MEL clones that varied in eGFP and RFP fluorescence. Clones were selected that maintained a silenced eGFP with a silent or expressed RFP construct (**Figure. 3.3A, C)**. When eGFP was re-expressed in the silenced RFP clone with TSA (1 μ M 24hours) there was no increase in RFP indicating that the transgene is silenced (**Figure. 3.3B)**. This effect was also demonstrated in RFP expressing clones (**Figure. 3.3D)**. However, RFP expressing clones did not see similar levels of eGFP activation but cells with higher RFP levels also had higher eGFP levels, limiting the sensitivity of the primary reporter. Therefore, for the initial FACS screen MEL clones with the silenced RFP construct were used, and validated using the RFP expressing clone. Of the compounds that significantly activated eGFP expression in **Table 3.1** only Cdk inhibitor CR8 and Nicotinamide, which is thought to function in DNA methylation, affected RFP expression. When selected hit compounds identified using the RFP expressing clone were validated by live cell imaging, there was no significant change in RFP pixel intensity compared to the increase in eGFP fluorescence **(Figure. 3.3E)**. This suggests that the compounds affect heterochromatic silencing, rather than regulators of transcription.

3.2 Screening for heterochromatic modulators

In the primary screen, over 250 compounds were tested with known and unknown targets **(Appendix 1)**. Each compound was tested at 1 μM for 24 hours and compared to a DMSO control. 30 compounds showed significant and consistent eGFP expression **(Table 3.1),** and can be broadly grouped by target; HDAC, histone demethylase, SIRT-HDACs, signalling kinases, cell cycle, bromodomain, and unknown.

The most prominent of these was the HDAC group. This was not surprising as many HDAC inhibitors exist and are being investigated as therapeutics in a range of malignancies (Ceccacci and Minucci, 2016), and were prevalent in our library. Surprisingly, the level of eGFP expression differed significantly between the compounds. M344, an HDAC3 inhibitor with an IC50 of 100 nM, was less effective than broad HDAC inhibitors (S)-HDAC-42 and CAY10433, which are active in the μM range. This could suggest that HDAC3 is less important for eGFP reactivation than HDAC1/6. This is perhaps not surprising, as HDAC3 is known to deacetylate H3K27 to enable subsequent methylation. H3K27me3 mediated silencing tends to be mutually exclusive from constitutive H3K9me3 silencing, as was shown to be enriched over the pYB-α construct (Kim *et al.*, 2009). This therefore suggests that inhibtors of polycomb mediated silencing, will be less effective than H3K9me3 linked mechanisms.

Table 3.1. α-MEL eGFP reactivation compound screen. eGFP expression after α-MEL cells were screened with each compound in turn for 48 hours, and fluorescence determine by flow cytometry. Table of compounds that by a bonferroni corrected two tailed t-test significantly affected GFP fluorescence after treatment for 48 hours at 1 μM (unless stated otherwise). n = >3.

Drug	P Value	Mean fold change in GFP expression	Target
MS-275	0.004925982	18.63136934	HDAC 1
CAY10603	0.013633511	13.29898959	HDAC6
N-oxalylglycine	0.009706582	11.3134046	A-ketoglutarate analogue
JQ1 +/-	0.001075345	9.919194763	Brd2/3/4/t
JNK IX	0.012350805	8.203121959	JNK kinase 2/3
EGFR CAY	0.00519797	6.847546494	EGFR
Nicotinamide	0.0007832	6.766163463	DNA methylation
CR8	0.045432001	6.024891933	Cdk1/2/3/5/7/9
Gemcitabine	9.11794E-05	5.747655185	Cytadine analogue
PKC CAY	3.48946E-08	5.395956518	Protein kinase C
Aurora A I	0.000114125	5.306265754	Aurora kinase
S-HDAC-42	0.008520126	4.495340903	HDAC
Polo CAY	0.015638502	4.443171944	Polo -kinase
Tubastatin A	0.000425538	4.159496234	HDAC6
CAY10433	1.60398E-05	3.236466453	HDAC
IOX1	4.4807E-06	2.875600431	JmJC demthylase
Cy19	0.030144393	2.771185384	Unknown
Emi1 (10uM)	0.021528568	2.72710909	Unknown
Dg19	0.001608853	2.554656165	Unknown
Dg16	0.000713801	2.405384254	Unknown
CAY10398	0.020074572	2.220820726	HDAC1
trans-Resveratrol	0.00085766	2.125363958	SIRT1 activator
AG-014699	9.02063E-09	1.958926292	PARP
JGB1741	0.000356006	1.408895944	SIRT1 - HDAC
Bromosporine	0.002356856	1.079811982	Bromodomain family
M 344	0.002270078	0.780450208	HDAC 3
Tenovin-1	0.00045872	0.624920819	SIRT1/2 HDAC
Capecitabine	0.006403966	0.563737847	DNA synthesis
Phthalazinone pyrazole	0.004715884	0.443206574	Aurora A kinase
SAHA	0.000341222	0.385392863	HDAC

The high level of eGFP expression as a result of MS-275, and CAY10603 treatment is likely due to their high selectivity, and that HDAC1/6 have been implicated in haematopoiesis and could have a greater role in regulating gene expression in an erythroleukaemia background. Furthermore, HDAC1 functions in the NuRD complex and inhibition could suppress HP1 deposition (Huang *et al.*, 2013; Shearstone *et al.*, 2016).

The role of class III HDACS, known as Sirtuins (SIRT*)*, remains unresolved (Kozako *et al.*, 2014). In the MEL system both SIRT inhibitors and activators promoted eGFP expression (**Table 3.1**), although trans-resveratrol is reported as a SIRT1 activator, the mechanism is not direct and could function differently in this artificial system. The reactivation by SIRT1 inhibition/activation is significant but is below the basal expression of the p212 cassette suggesting a relatively weak effect on heterochromatic silencing. SIRT1 canonically functions to deacetylate H4K16 and H3K9 allowing for H3K9me3 and facilitates linker histone H1 binding and heterochromatin formation (Vaquero *et al.*, 2004).

JmjC demethylases have recently been implicated in heterochromatin formation and JARID2 can recruit PRC2 complexes although this normally occurs in non-cycling cells (Son *et al.*, 2013). JmjC demethylases can remove all three methylation states giving them broad functionality, initially demonstrated at H3K36. They have subsequently been shown to directly demethylate pericentric H3K9me3 (Klose *et al.*, 2006; Whetstine *et al.*, 2006). For JmjC domain containing proteins to demethylate substrates they require cofactors Fe(II) and α-ketoglutarate (Tsukada *et al.*, 2006). JmjC inhibitors such as N-oxalyglycine and IOX1, promote eGFP expression, and could function by competitively inhibiting α-ketoglutarate binding to Fe(II) within

the domain. As this catalytic domain is conserved across the family this means inhibitors are non-specific. It is therefore surprising that catalytic inhibition of a family of demethylases known to directly affect pericentric heterochromatin, should cause eGFP expression.

Poly(ADP-ribose) polymerases (PARP) are known to bind at active promoters and at heterochromatic regions including α-satellite sequences, however this paradoxical function in gene regulation is not understood. At promoters, PARP1 binding excludes linker H1 association but PARP1 loss only affects a subset of bound genes that are both up- and down-regulated (Krishnakumar *et al.*, 2008). Heterochromatic PARP1 interacts with the Nucleolus repressor complex (NoRC) (Strohner *et al.*, 2001) and recruitment of PARP1-NoRC is facilitated by nascent RNA which acts as a substrate for parylation (Mayer *et al.*, 2006). Research has demonstrated that this is a transient event after the passage of a replication fork to facilitate heterochromatin formation in mid-to-late S phase (Guetg *et al.*, 2012). As MEL cells were treated for 48 hours with each compound, this would normally allow multiple complete cell cycles to take place so PARP inhibition could inhibit heterochromatin reformation explaining eGFP activation.

Perturbation to the cell cycle also resulted in eGFP expression. Inhibition of cyclins by CR8 and nucleotide analogues such as gemcitabine and capecitabine significantly de-repress the RL5 locus. Feng, (2005) demonstrated that insertion of p212 cassette with silenced or expressed eGFP, replication timing shifts from late-to-early. The relationship of gene expression, replication timing and chromatin is unclear, but by altering the length of S-phase via Cdk inhibition or nucleotide analogues could affect the replication timing of the eGFP transgene which may in turn regulate its chromatin environment.

A broad range of kinase inhibitors were found to activate eGFP expression: JNK II/III, EGFR, PKC, Polo, and Aurora (**Table 3.1)**. As mentioned above the JNK pathway is thought to be antagonistic to β-globin expression (Lee *et al.*, 2010). JNK II inhibition in **Figure. 3.2**, did not, however, reactivate the eGFP transgene. JNK IX inhibitor of JNK II/III however resulted in an 8-fold increase in eGFP fluorescence. JNK III is known to function as a stress induced pro-apoptotic pathway independent of JNKI/II transcriptional regulation (Yang *et al.*, 1997). Stress related proteins such as heat shock factor 2-β, are regulated by the JNK pathway and are involved in erythroid differentiation (Hietakangas *et al.*, 2001). Although exactly how JNK functions in differentiation remains undefined, JNK3 is known only to be expressed in a tissue specific manner in the brain, heart and testes. The three JNK genes are spliced to form 10 JNK isoforms that regulate TF activity independently of each other (Gupta *et al.*, 1996). More recently, JNK kinases have been shown to directly phosphorylate H3S10 in interphase (Tiwari *et al.*, 2012) whilst the combined and adjacent marks H3K9me3 and H3S10p have been associated with modulating heterochromatin through differentiation (Ribeiro-Mason *et al.*, 2012). The effect of JNK IX inhibition on eGFP

expression may provide an insight to heterochromatin regulation in the MEL background.

During mitosis, H3S10 phosphorylation occurs via Aurora B rather than JNK (Hirota *et al.*, 2005). The function of mitotic H3S10p on chromatin condensation remains unclear, as its presence causes HP1 proteins to dissociate during mitotic compaction. Aurora kinase inhibition by Aurora-A, or Phthalazinone pyrazole, caused eGFP expression. When viewed in combination with JNK inhibitions effect on eGFP expression, this suggests that H3S10p is required for maintaining the transgene silencing, even if the mechanism is indirect.

EGFR, PKC and PLC inhibition triggered eGFP expression. EGFR is a membrane receptor that can stimulate multiple kinase pathways, including PI3K/Akt. Akt inhibition, downstream of EGFR, does not however induce expression of the eGFP transgene. This suggests that the PKC/PLC pathway of the EGFR response is modulating the transgene expression. PLC is directly activated by EGFR, and results in downstream PKC activation (Hofmann *et al.*, 1999). PKC once activated is a potent stimulator of the Ras/Raf/MEK/ERK pathway (Schönwasser *et al.*, 1998). ERK activation is required to maintain haematopoietic undifferentiated cell states demonstrating it as a key regulator within an erythroid setting (Chan, Gu and Neel, 2013). How ERK modulates differentiation is not fully understood, although it has been shown to regulate key haematopoietic transcription factors including c-myc (Chen and Sytkowski, 2001). Additionally, PKC has been implicated in heterochromatin modulation directly via interacting with transcriptional intermediary factor 1B (TIF1B). TIF1B regulates KAP1/TRIM28 chromatin remodelling complex recruitment to chromatin.

TIF1B is recruited to heterochromatin by directly binding to HP1 proteins, but this is abrogated by its phosphorylation at Ser473 by PKC (Chang *et al.*, 2008). Inhibiting PKC therefore could directly result in the loss of heterochromatin condensation via KAP1/TRIM28. This is most likely the mechanism behind eGFP expression, as ERK inhibitors by contrast did not result in eGFP activation (**Appendix 1)**.

Intriguingly, bromodomain inhibition by JQ1 also caused eGFP expression; the effect was specific as the inactive enantiomer of JQ1 did not change expression (**Appendix 1)**. Additionally, the less selective bromosporine compound also activated the eGFP transgene. These results were surprising as bromo-extra terminal (BET) proteins inhibited by JQ1 are known transcription factors found at active enhancers (Chapuy, McKeown and Lin, 2013). The role of BET proteins in haematological malignancies has been widely studied with its function in oncogene activation attributed to activation at super enhancers (Lovén *et al.*, 2013). Therefore, the role of BET proteins in regulating heterochromatic silencing differs from their canonical role.

3.3 BET mediated eGFP expression

To better understand the role of BET inhibitors MEL cells were treated with bromosporine for 48 hours at 0.05 μM to 1 μM, prior to analysis by FACS in the same method as described earlier **(Figure. 3.4A)**. eGFP was upregulated after 0.5 μM treatment, and re-expression correlated with increased cell death. This suggests that the function of BET proteins in heterochromatin condensation is essential for cell viability.

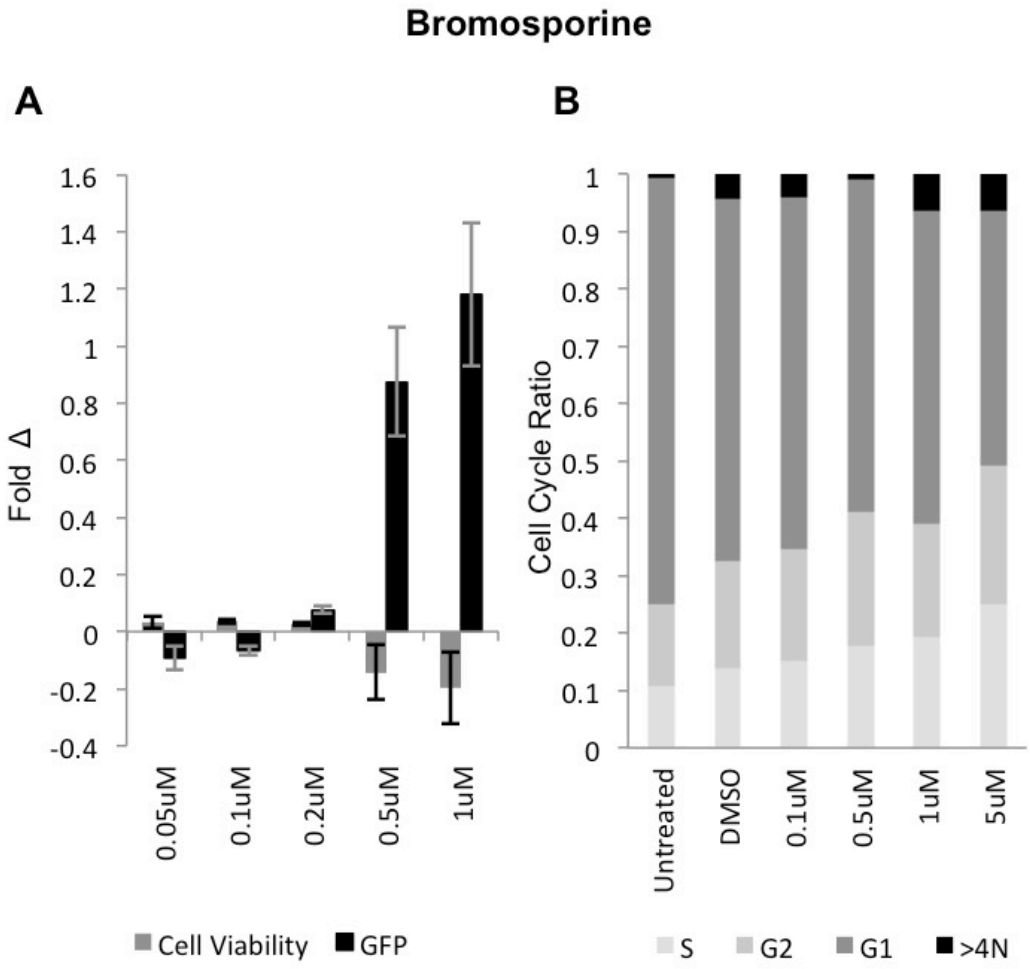

Figure 3.4. Bromosporine eGFP reactivation and cell cycle arrest. (A) MEL cells treated with increasing concentrations of *pan* BET inhibitor, bromosporine for 48 hours. GFP fluorescence and cell death was determined by flow cytometry. (n=3) **(B)** Stacked bar plot showing cell cycle analysis by high content imaging on ScanR platform. MEL cells were grown on gelatin coated dishes and treated with bromosporine at various doses for 48 hours prior to imaging. Error bars = SEM between biological repilicates.

As these cells are non-adherent, plates were coated with 0.1% gelatin, to facilitate cell adhesion and access to microscopy techniques. MEL cells were treated with 0.1 μM to 5 μM bromosporine for 48 hours, as this covered the reactivation of eGFP detected by FACS (**Figure. 3.4A).** The ScanR analysis platform was used to determine cell cycle stage of more than 500 cells per treatment. Bromosporine caused a dose dependent increase in G2/S phase after treatment **(Figure. 3.4 B)** which suggests that replication is impaired and cells are therefore not allowed to progress through mitosis.

To analyse the relationship between eGFP expression and cellular proliferation, cells were treated with a log-dose range of selective BET inhibitor I-BET151 **(Figure 3.5)**. MEL cells were treated with I-BET151 for 48 hours before the addition of cell viability reagent PrestoBlue for 3 hours prior to measuring the fluorescence at 590-615 nm. Independent samples were normalised to a DMSO 0.01% control. 10-1000 nM I-BET151 gives an 80% reduction in cell viability **(Figure 3.5 A)** and 50-5000 nM I-BET151 affects eGFP levels measured by FACS **(Figure 3.5 B)**. This suggests that the effect on cell viability precedes BET inhibitions effect on condensed heterochromatin.

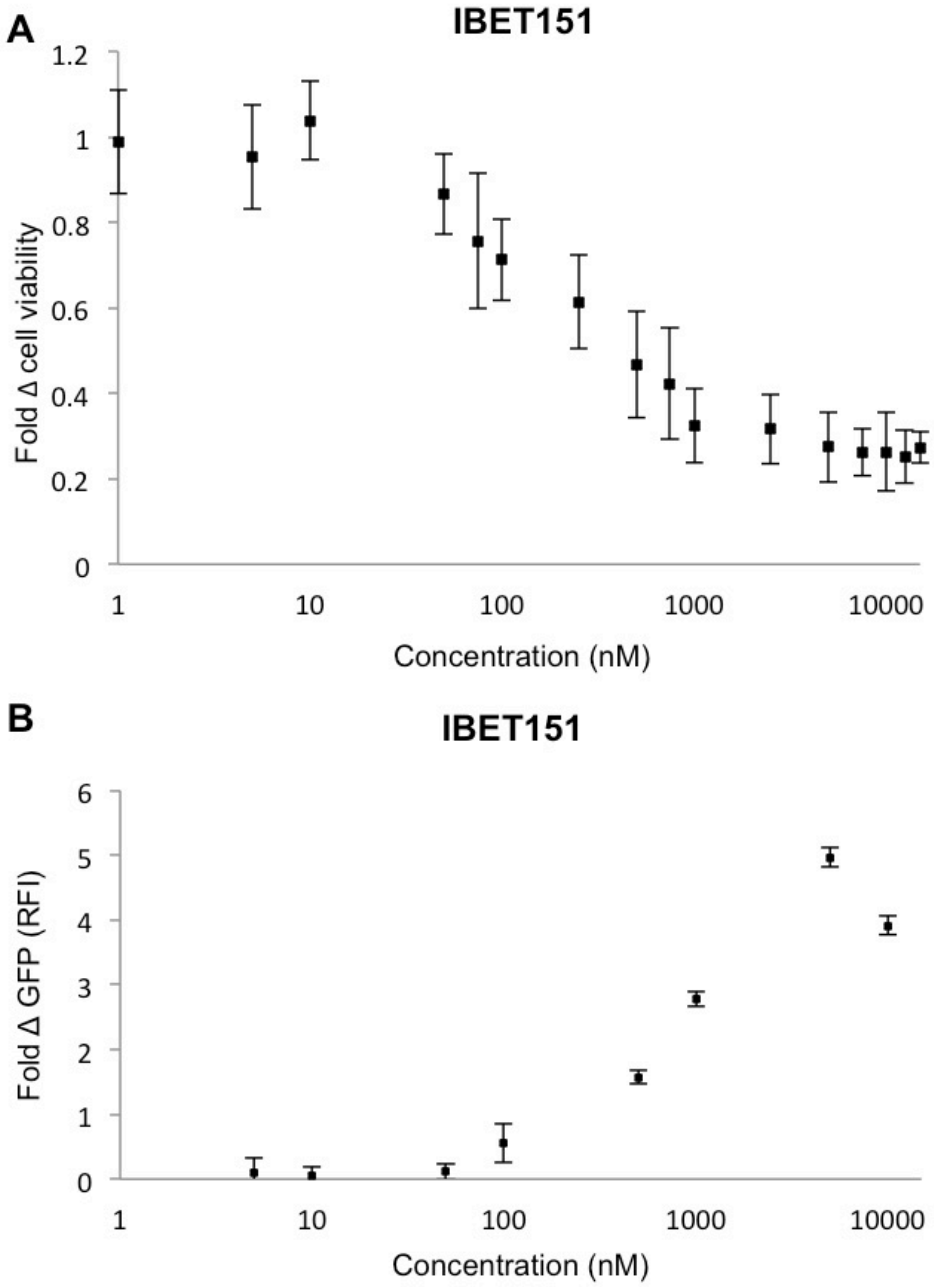

Figure 3.5. Relationship between IBET151 eGFP reactivation and cell viability. α-MEL cells treated for 48 hours with a log-dose range of I-BET151. **(A)** Cell viability was determined using a Presto Blue™ assay (n=6) **(B)** Fold change in GFP fluorescence in response to IBET151 measured by flow cytometry.

As the previous experiments investigating eGFP involved 48-hour treatments, which affect multiple cell cycles, it seemed desirable to investigate the kinetics of eGFP expression post treatment. While coating wells in gelatin was sufficient for cell attachment before fixation for standard microscopy, this method still resulted in cellular detachment over time. This led to a change in the depth of field for individual cells preventing tracking over time. To reduce this movement, cells were seeded in matrigel (Hughes, Postovit and Lajoie, 2010). When incubated post seeding the matrigel polymerizes preventing the movement of the non-attached MEL cells and enabled imaging of wells at 10x over 84 hours to investigate the kinetics of eGFP expression. To investigate kinetics of eGFP expression a MEL clone expressing RFP was also used **(Figure 3.3 C-E)** which allowed a comparison of eGFP expression to general gene activation.

To exclude compound specific effects cells were treated with a half-log dose range of the three BET inhibitors, previously identified to cause eGFP expression: Bromosporine, JQ1$^{+/-}$, and I-BET151 **(Figure 3.6)**. Cells were also treated with dose ranges of 5'Azacytidine and Chaetocin, which inhibit DNA methylation and H3K9me3 respectively. DNA methylation, while not affecting chromatin condensation, regulates endogenous β -globin transcription in MEL cells at the LCR and down-stream of the 3' end (Yisraeli *et al.*, 1988; Kotkow and Orkin, 1995).

For analysis, the change in RFP expression was subtracted from eGFP expression. RFP pixel intensity was however only affected after chaetocin treatment. This resulted in a decrease in eGFP/RFP expression ratio after low dose chaeotcin **(Figure 3.6 B)**. Intriguingly, the speed of eGFP activation differed between 5'Azacytidine and Chaetocin. Re-expression from chaetocin was first detected at 12 hours post treatment. 5'Azacytidine by contrast required 36 hours post treatment for activation of the eGFP transgene **(Figure. 3.6 A-B)**. Also unexpectedly, low dose chaetocin resulted in increased silencing.

All three selective BET inhibitors: I-BET151, JQ1$^{+/-}$, and Bromosporine caused eGFP expression 24 hours after treatment which sits in-between Chaetocin and 5'Azacytidine eGFP activation. Additionally, the pan BET inhibitor Bromosporine required a higher dose to achieve the same level of eGFP expression compared to JQ1$^{+/-}$ and I-BET151 **(Figure 3.6 C-E) with** JQ1$^{+/-}$ having a 2.5 fold greater effect than Bromosporine. I-BET151 was approximately 0.6 fold more effective at eGFP reactivation than JQ1$^{+/-}$; as JQ1 and I-BET151 are known to be active at inhibiting BET proteins with the similar potency, this effect is most likely due to differences in selectivity within the BET family.

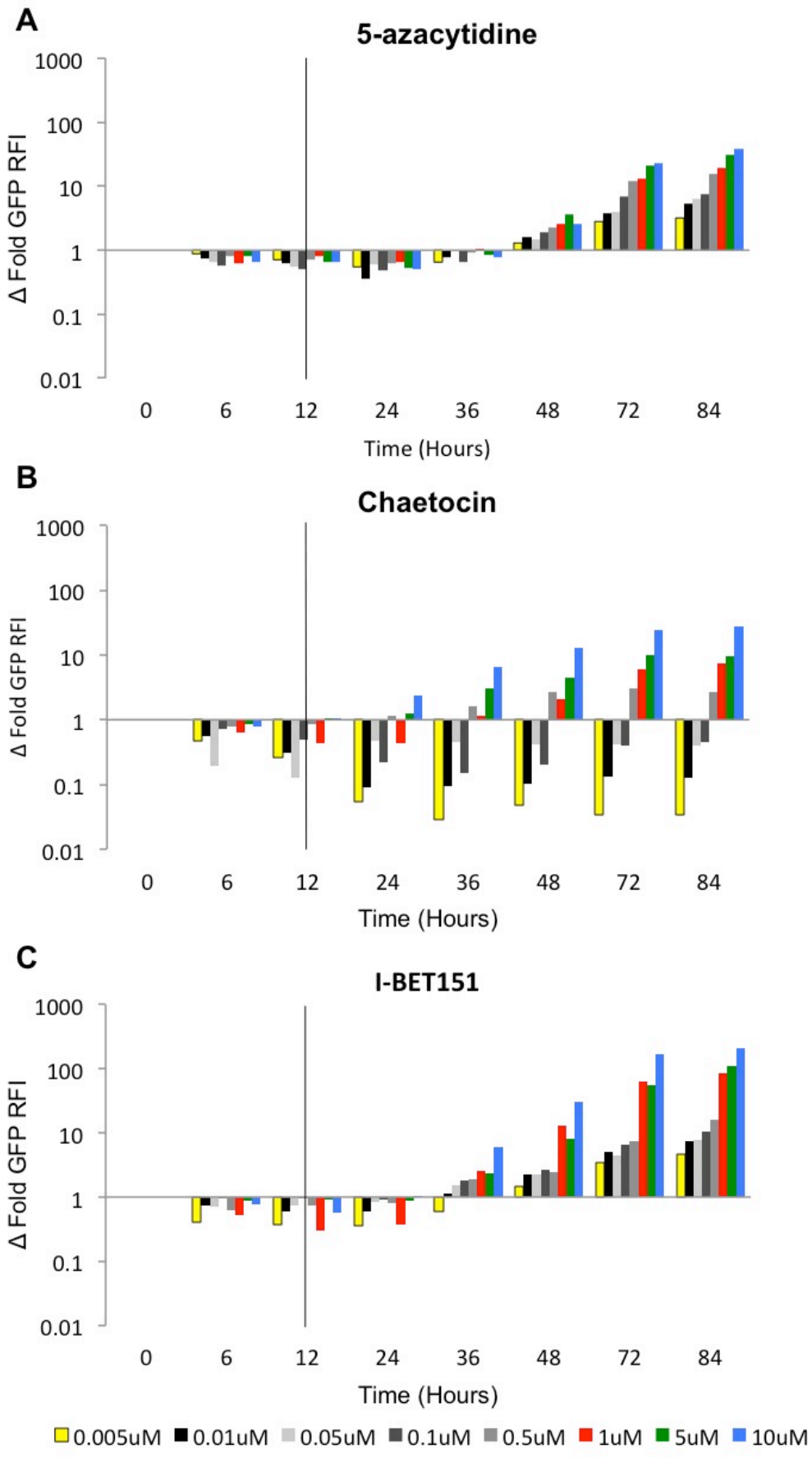
A
5-azacytidine
1000
100
10
1
0.1
0.01
Δ Fold GFP RFI
0
6
12
24
36
48
72
84
Time (Hours)
B
Chaetocin
1000
100
10
1
0.1
0.01
Δ Fold GFP RFI
0
6
12
24
36
48
72
84
Time (Hours)
C
I-BET151
1000
100
10
1
0.1
0.01
Δ Fold GFP RFI
0
6
12
24
36
48
72
84
Time (Hours)
0.005uM
0.01uM
0.05uM
0.1uM
0.5uM
1uM
5uM
10uM

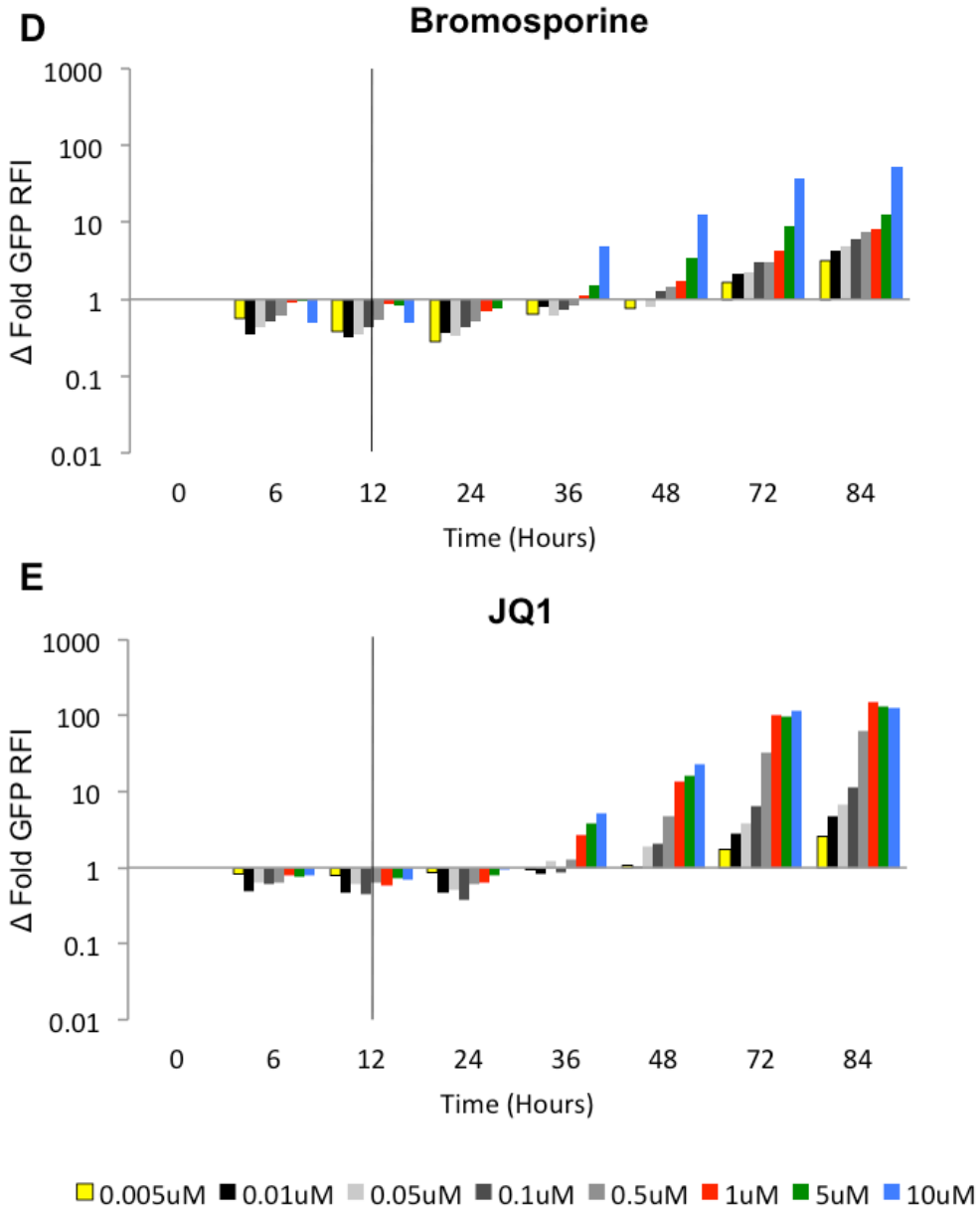

Figure 3.6. Heterochromatic eGFP activation kinetics. α-MEL cells embedded in Matrigel™ were imaged over 84 hours using an Incucyte microscope. GFP fluorescence is relative to DMSO controls at each time point. Fold change in GFP fluorescence in shown for cells treated with compounds 12 hours after seeding. **(A)** 5'Azacytidine **(B)** Chaetocin **(C)** I-BET151 **(D)** Bromosporine and **(E)** $JQ1^{+/-}$.

To investigate the effect of BET inhibition on epigenetic marks, samples treated with BET inhibitors were analysed by reverse phase protein arrays. Protein lysates were spotted onto arrays in triplicate serial dilutions **(Figure 3.7)**, the arrays were clamped into 12 chambers per array and incubated with primary and secondary antibodies. The R^2 value, used to determine how close data fits a line of regression, was measured for signal intensity across the duplicate spot serial dilution was checked as a quality control.

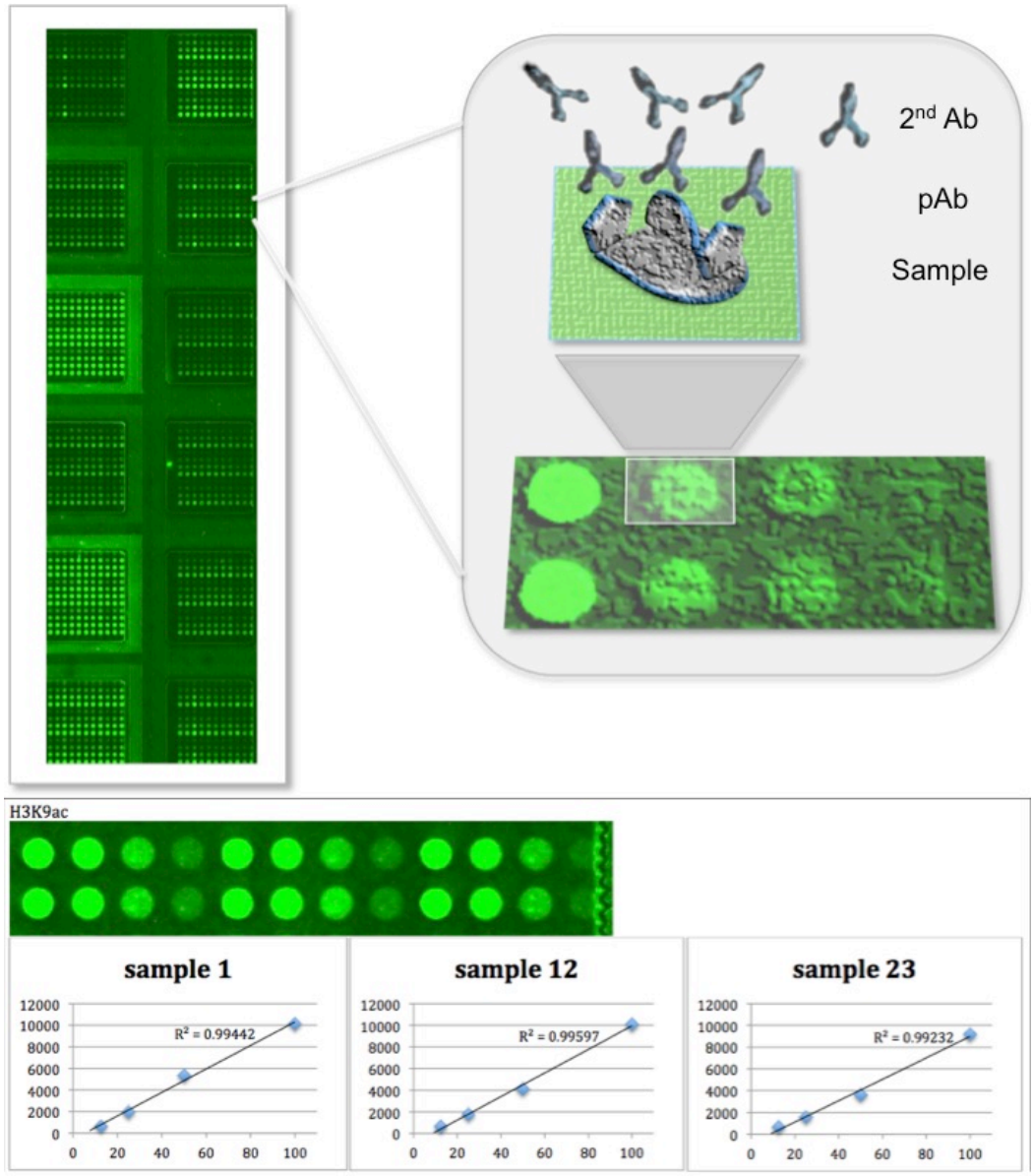

Figure 3.7. Reverse phase protein arrays. Protein array methodology. Lysates were spotted onto arrays in a four series dilution in duplicate. Primary and secondary antibodies were sequentially incubated in the chambers and imaged. Antibody fluorescence signal was quality controlled by analysing the R^2 of the serial dilution. Samples 1, 12, and 23 represent the H3K9 acetylation serial dilutions above, indicative of the sample spotting order (number shown on graph). All samples with R^2 value <0.95 were excluded.

33 histone modifications or chromatin binding proteins were assayed after 1 μM I-BET151 treatment for 6 hours and 24 hours. The 6 hour and 24 hour treated samples were collated to determine significant changes that were sustained over time (**Figure. 3.8**). The only significant changes after BET inhibition were elevated levels of unmodified and dimethylated H3K4. Although not significant (p=0.064), H3K4 monomethylation correlated with the elevated signals from H3K4me2 and unmodified antibodies. This correlation would be expected with loss of H3K4me3, a mark of active transcription and is not surprising given the role of BET proteins as transcription factors (Kyoo Jang *et al.*, 2005; W. Zhang *et al.*, 2012). As expected there were no significant change in global levels of H3K9 methylation states or BET proteins Brd2, and Brd3, but of interest were a near significant loss of H3K27me3 (p=0.059) with elevation of H3K27me2, and the general trend for a subtle increase in histone acetylation (H4K16ac, H4K12ac, H4K5ac). BET proteins are known to bind to acetylated H4, so a compensatory increase in H4 acetylation is possible (Filippakopoulos *et al.*, 2012) although it remains unknown whether a general increase in histone acetylation would affect heterochromatin.

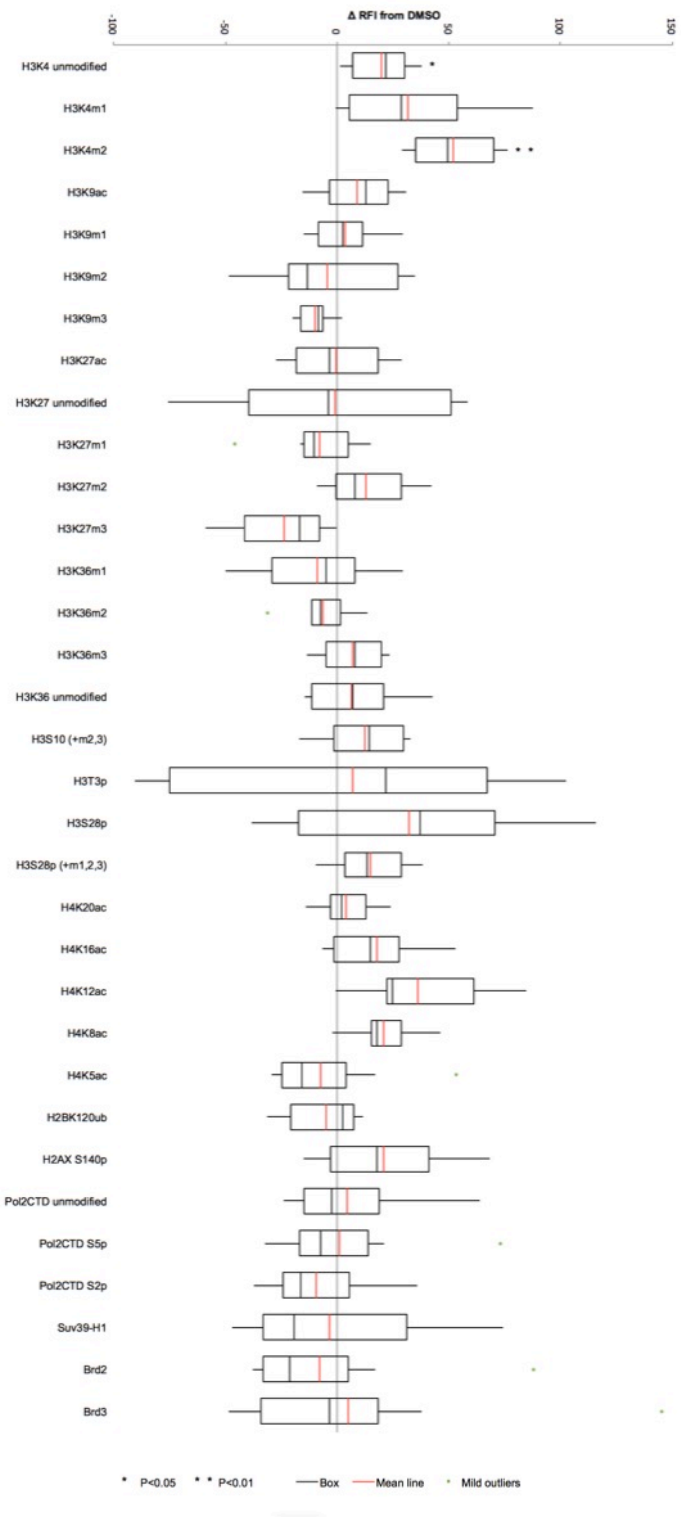

Figure 3.8. Global Epigenetic modification changes with IBET151. Boxplots showing changes in global epigenetic marks after BET inhibition in α-MEL cells, measured by reverse phase protein arrays. Cells treated with 1 μM IBET151 for 24 hours (n=9) and analyzed by Bonferroni corrected 2-way ANOVA to calculate significance.

The eGFP transgene is known to be marked with H3K9me3 (Kim *et al.*, 2009). Therefore, the levels of H3K4me3, and H3K9me3 at the eGFP transgene were evaluated, given the global changes in H3K4 methylation detected by RPPA **(Figure 3.8)**. Chromatin immunoprecipitation was used to analyse the effect of BET inhibition at the amylase, eGFP, murine β-globin, and major satellite **(Figure 3.9)**. Amylase is constitutively repressed throughout normal haematological differentiation, whilst a subset of haematological tumours have ectopic amylase expression independent of genetic translocations (Weiss, Edmondson and Wertman, 1951; Ohtsuki *et al.*, 1989). However, amylase is repressed in MEL cells, providing a locus of potential facultative heterochromatin (Kim *et al.*, 2009). The endogenous β-globin gene is in a poised state in undifferentiated MEL cells and undergoes chromatin de-condensation and expression upon differentiation (Smith and Yus, 1984) providing a poised silent loci in these MEL cells. Finally, major satellite repeats are pericentromeric and are packaged as constitutive heterochromatin.

Both $JQ1^{+/-}$ and I-BET151 treatment caused a large reduction in H3K9me3 over the eGFP transgene **(Figure 3.9 B)**. There was also an enrichment of H3K4me3 compared to control. This change in histone modifications correlates well with gene activation, although treatment with BET inhibitors did not consistently increase Brd4 occupancy at the transgene. Treatment of BET inhibitors decreased H3K9me3 and H3K4me3 at the poised β-globin gene **(Figure 3.9 C)** and Brd4 occupancy was also reduced especially after IBET151 treatment.

Control facultative and constitutive loci, amylase and major satellite showed reductions in H3K9me3 after BET inhibition which was exacerbated after

IBET151 treatment **(Figure 3.9 A,D)**. Unlike at the eGFP transgene there was no elevation of H3K4me3 at amylase or Major satellite, nor a consistent increase in Brd4 after BET inhibition.

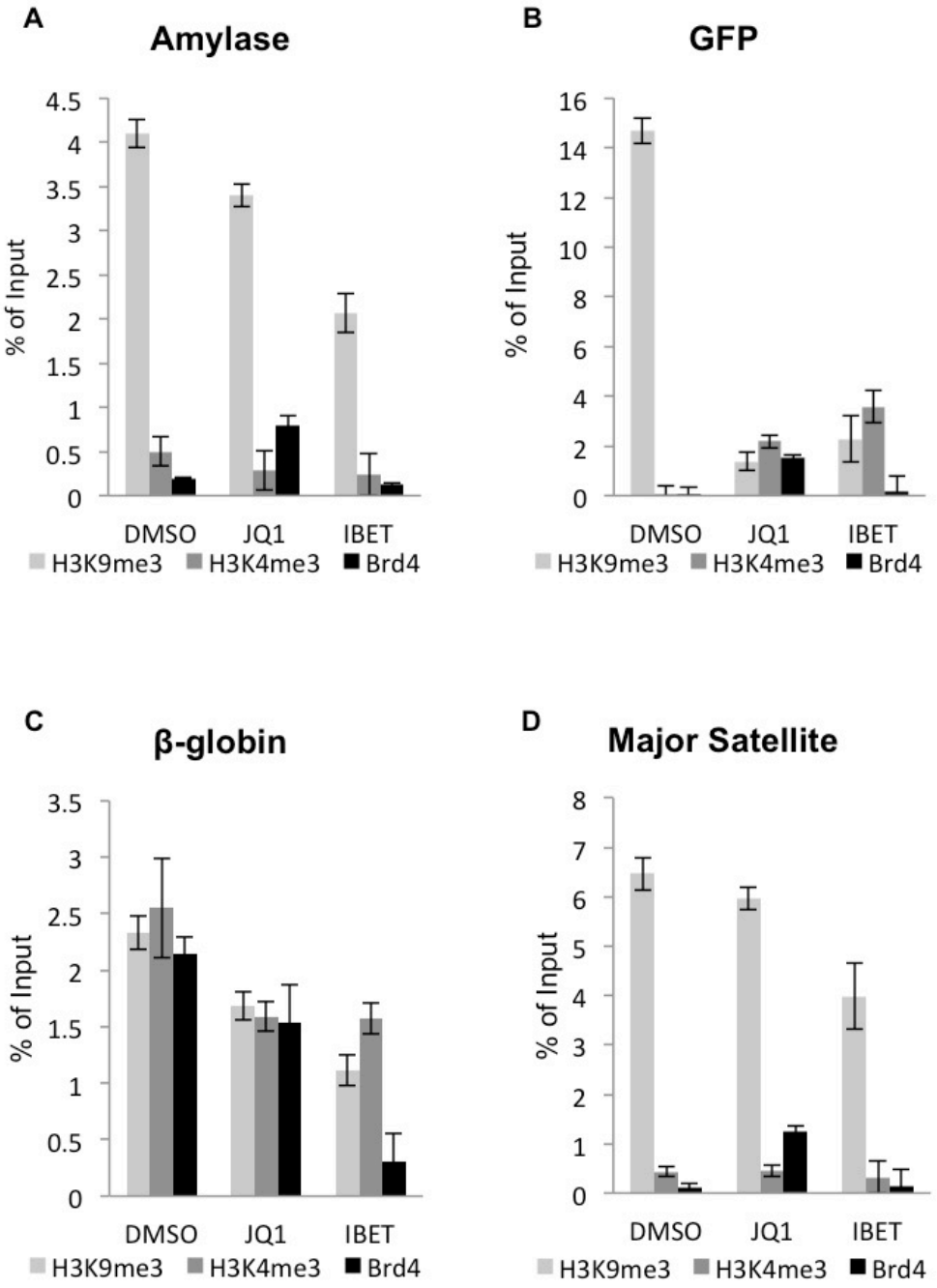

Figure 3.9. Chromatin immunoprecipitation for H3K9me3, H3K4me3, and Brd4 after BET inhibition. MEL cells were treated for 24 hours with DMSO, $JQ1^{+/+}$, or IBET151. qPCR's were performed at four loci and compared to ChIP input samples **(A)** Amylase **(B)** GFP transgene **(C)** Murine β-globin and **(D)** Major Satellite.

3.4 BET inhibition affects cell signalling

Cellular epigenetic profiles represent the programmed state, and their adaption to the cellular environment (Ravelli *et al.*, 1998; Borengasser *et al.*, 2013). Inhibiting an epigenetic process such as acetyl-lysine binding is therefore likely to alter a cell's response mechanism. Either compensatory changes to signalling pathways could occur to overcome a BET protein reduction or cellular adaption to signalling will be altered. To investigate if BET inhibitors affected cellular signalling, MEL cells were treated with $JQ1^{+/-}$ or I-BET151 1 μM for 24 hours. Cell lysates were prepared and spotted onto Zeptozen™ arrays for 87 antibodies. $JQ1^{+/-}$ and I-BET151 samples were collated to reduce off target drug specific effects and compared to controls **(Figure 3.10, Appendix 2)**. Significant consistent changes with BET inhibition are summarised in **Table 3.2**.

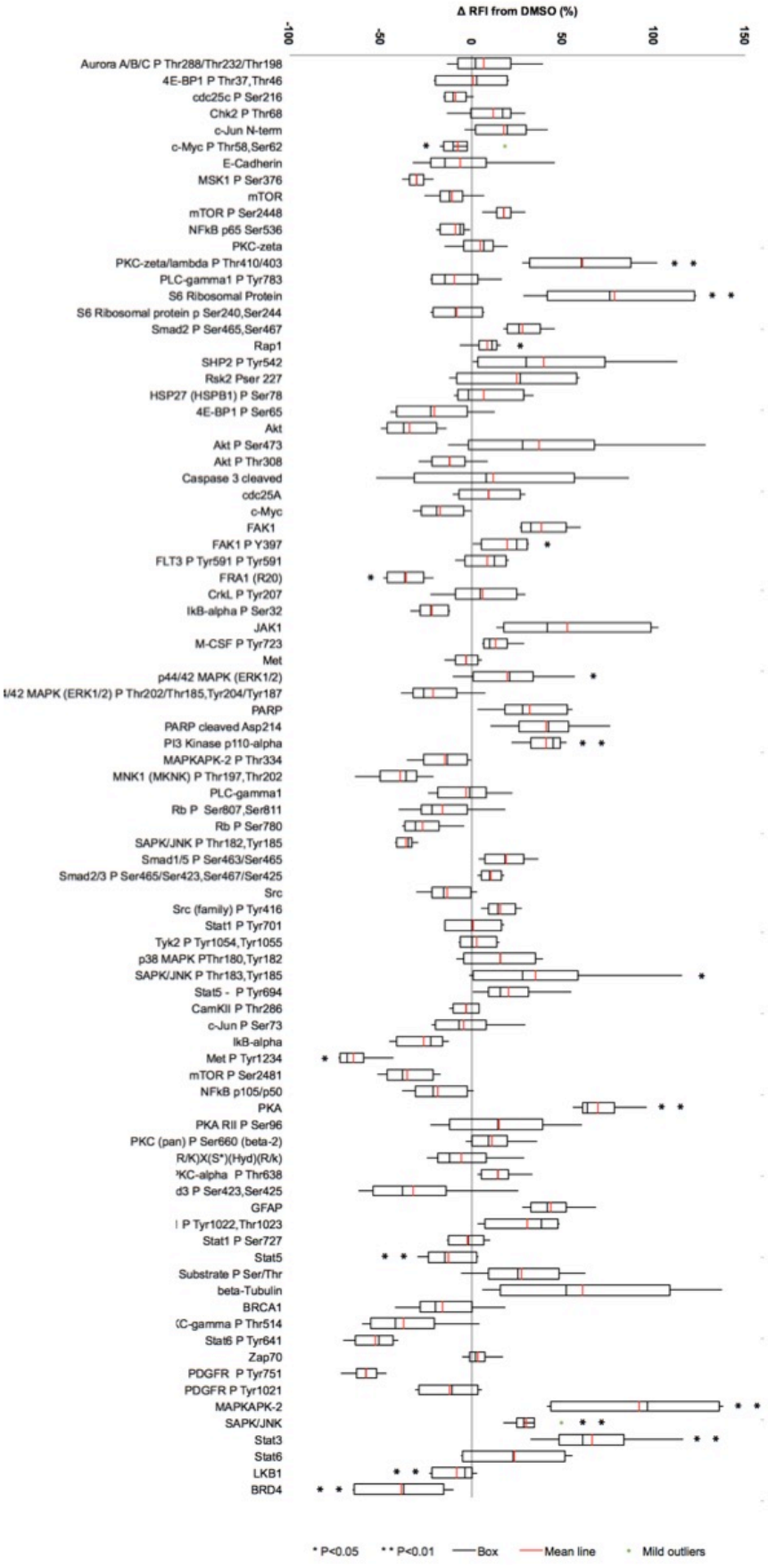
Δ RFI from DMSO (%)
-100
-50
0
50
100
150
Aurora A/B/C P Thr288/Thr232/Thr198
4E-BP1 P Thr37,Thr46
cdc25c P Ser216
Chk2 P Thr68
c-Jun N-term
c-Myc P Thr58,Ser62
E-Cadherin
MSK1 P Ser376
mTOR
mTOR P Ser2448
NFkB p65 Ser536
PKC-zeta
PKC-zeta/lambda P Thr410/403
PLC-gamma1 P Tyr783
S6 Ribosomal Protein
S6 Ribosomal protein p Ser240,Ser244
Smad2 P Ser465,Ser467
Rap1
SHP2 P Tyr542
Rsk2 Pser 227
HSP27 (HSPB1) P Ser78
4E-BP1 P Ser65
Akt
Akt P Ser473
Akt P Thr308
Caspase 3 cleaved
cdc25A
c-Myc
FAK1
FAK1 P Y397
FLT3 P Tyr591 P Tyr591
FRA1 (R20)
CrkL P Tyr207
IkB-alpha P Ser32
JAK1
M-CSF P Tyr723
Met
p44/42 MAPK (ERK1/2)
I/42 MAPK (ERK1/2) P Thr202/Thr185,Tyr204/Tyr187
PARP
PARP cleaved Asp214
PI3 Kinase p110-alpha
MAPKAPK-2 P Thr334
MNK1 (MKNK) P Thr197,Thr202
PLC-gamma1
Rb P Ser807,Ser811
Rb P Ser780
SAPK/JNK P Thr182,Tyr185
Smad1/5 P Ser463/Ser465
Smad2/3 P Ser465/Ser423,Ser467/Ser425
Src
Src (family) P Tyr416
Stat1 P Tyr701
Tyk2 P Tyr1054,Tyr1055
p38 MAPK PThr180,Tyr182
SAPK/JNK P Thr183,Tyr185
Stat5 - P Tyr694
CamKII P Thr286
c-Jun P Ser73
IkB-alpha
Met P Tyr1234
mTOR P Ser2481
NFkB p105/p50
PKA
PKA RII P Ser96
PKC (pan) P Ser660 (beta-2)
R/K)X(S*)(Hyd)(R/k)
KC-alpha P Thr638
d3 P Ser423,Ser425
GFAP
I P Tyr1022,Thr1023
Stat1 P Ser727
Stat5
Substrate P Ser/Thr
beta-Tubulin
BRCA1
C-gamma P Thr514
Stat6 P Tyr641
Zap70
PDGFR P Tyr751
PDGFR P Tyr1021
MAPKAPK-2
SAPK/JNK
Stat3
Stat6
LKB1
BRD4
* P<0.05
** P<0.01
Box
Mean line
Mild outliers

Figure 3.10. Signaling kinase changes after BET inhibition. Boxplots of kinase proteins and their phosphorylated states after BET inhibition in α-MEL cells. Treatments with 1 μM $JQ1^{+/-}$ or IBET151 for 24 hours were collated together to remove off target compound specific effects. 2-way Bonferroni was performed to determine significance.

As one might expect BET inhibition resulted in a decrease in Brd4 protein levels, whilst changes in kinases suggest that BET inhibition and loss of Brd4 adversely affects canonical EGFR signalling.

The canonical EGFR pathway is Ras/Raf/MEK/ERK, which up regulates multiple transcription factors including c-myc and Elk-1. Importantly, the downstream component ERK1/2 shows a significant loss in phosphorylation after BET inhibition **(Table 3.2)**. MEK is upstream of ERK and shows a significant increase in phosphorylation after BET inhibition indicating the cell is stimulating ERK signalling. Hyper-phosphorylation of ERK signalling is a known resistance mechanism to loss of ERK signalling via receptor tyrosine kinase (RTK) or Ras/RAF/MEK inhibition.

BRAF can be alternatively activated by PKA or PKC independently of Ras, both of which are phosphorylated after BET inhibition. Both these pathways are stimulated by metabolic compounds cAMP and PIP^2 respectively. Increased cAMP stimulates PKA mediated Rap1 phosphorylation both of which are up-regulated by BET inhibition. Rap1 can then directly activate BRAF independently of Ras and is known to regulate multiple haematological response pathways (Katagiri *et al.*, 2002). PKC can also directly activate BRAF. PKC activity is modulated by PLC that requires the PIP^2 metabolite. PIP^2 also acts as the substrate for PI3K signalling, which is also stimulated by BET inhibition and activation of the PI3K/Akt pathway, and is a well characterised mechanism to mediate loss of ERK signalling (Vergani *et al.*, 2011; Cante-Barrett *et al.*, 2016).

Table 3.2. Significant kinase changes to BET inhibition. List of two-tailed t-test significant changes to kinase signaling in α-MEL cells. α-MEL cells were treated with 1 μM I-BET151 or $JQ1^{+/-}$ for 24 hours and the signaling affects binned together and normalised from DMSO controls. Bonferoni corrected ANOVA (*, $p < 0.05$) (**, $p < 0.01$).

Antibody	Δ from DMSO (%)	p-value (Bonfferoni)	
MAPKAPK-2	91.92744	3.82085E-9	**
PKC-zeta/lambda P Thr410/403	60.84479	1.4041E-8	**
Stat3	65.87927	3.4141E-6	**
PKA	68.94439	6.83351E-6	**
S6 Ribosomal Protein	78.53622	7.21852E-6	**
BRD4	-38.67678	0.00026	**
PI3 Kinase p110-alpha	41.10582	0.00032	**
LKB1	-8.39205	0.00245	**
SAPK/JNK	30.08464	0.00565	**
Stat5	-12.56719	0.00665	**
Rap1	8.55371	0.01055	*
c-Jun N-term	17.69132	0.01145	*
Met P Tyr1234	-64.97844	0.01494	*
SAPK/JNK P Thr183,Tyr185	34.97637	0.01578	*
p44/42 MAPK (ERK1/2) P Thr202/ Thr185,Tyr204/Tyr187	-21.25869	0.01666	*
FAK1	38.03102	0.03026	*
FRA1 (R20)	-36.14749	0.03756	*

PIP^2 is also known to modulate the targeting of Src (Corte, Gettemans and Vandekerckhove, 1997; Benesch *et al.*, 2002) which in turn phosphorylates Stat3 resulting in increased invasion and poor prognosis in lung cancer (Carretero *et al.*, 2010). Src upstream receptor Met has significantly reduced phosphorylation after BET inhibition whereas, its downstream effector Stat3 protein level is up-regulated. LKB1, which normally inhibits Src activation, is known to be supressed by elevated cAMP and is reduced by BET inhibition. This suggest that normal up-regulation of Src signalling after loss of EGFR is also prevented upon BET inhibition (Mueller *et al.*, 2008) and a recent study implicated Brd2 as a regulator of Stat signalling hinting at a potential mechanism (Liu *et al.*, 2014).

Stress activated MAPK signalling (SAPK/JNK) is also up-regulated after BET inhibition **(Table 3.2)** and the SAPK/JNK downstream partner c-Jun is more phosphorylated. SAPK/JNK when activated normally functions to activate p53 dependent cell arrest but after oncogenesis is known to mediate mesenchymal endothelial transition (MET), and pluripotency (Schramek *et al.*, 2011; Neganova *et al.*, 2016). One mechanism functioning in these pathways is the stabilisation of c-myc preventing its degradation after SAPK/JNK activation (Alarcon-vargas and Ronai, 2004). The modulation of ERK/Stat3/PI3K/JNK pathways after BET inhibition suggests that BET proteins function in regulating ERK mediated c-myc transcription, for which Brd4 is well known (Lovén *et al.*, 2013).

3.5 Discussion

In the compound screens undertaken here multiple targets were identified as modulating heterochromatic silencing of an eGFP transgene. This synthetic model system generated by the Larionov lab, was previously use to investigate the ability of the underlying genetic sequence in modulating heterochromatin formation and gene silencing (Ebersole *et al.*, 2005; Kim *et al.*, 2009). This system is clearly regulated by the HDAC inhibitor TSA, and DNA methylation inhibitor 5'Azacytidine (**Figure 3.2)**. TSA treatment both elevates histone acetylation and gene activation and has been shown to disrupt heterochromatin formation by mediating loss of H3K9me3 and HP1 proteins (Taddei *et al.*, 2001). Loss of DNA methylation does not normally lead to chromatin de-condensation (Gilbert, Thomson, Boyle, Allan, Ramsahoye and Wendy A Bickmore, 2007) but DNA methylation is known, however, to regulate β-globin expression, and the eGFP transgene is under a human β-globin promoter. Given that MEL cells are of an undifferentiated haematological background, the β-globin promoter is normally poised **(Figure. 3.9 C)**. Upon differentiation α- and β- globin genes are up-regulated in these MEL cells (Friend *et al.*, 1971) suggesting that differentiation factors may also influence eGFP expression **(Figure. 3.9 C)**.

The positive results in **Table. 3.1**, further validated this model, as multiple inhibitors of heterochromatic factors resulted in eGFP activation (HDAC, JmjC demethylases, PARP). An increase in eGFP expression by BET inhibition ($JQ1^{+/-}$ and Bromosporine) is surprising as BET proteins are universally accepted as transcriptional activators across cell types and lineages (Korb *et al.*, 2015; Roe *et al.*, 2015; Najafova *et al.*, 2017). As BET

proteins bind to acetylated lysines, this contradicts the role of CBP mediated acetylation at HS2 to activate the β-globin promoter (Johnson, Norton and Bresnick, 2002).

As demonstrated in **figures 3.4 A** and **3.5,** eGFP activation by BET inhibition correlates with cell death. As these cells are stressed and BET protein Brd4 is known to stay bound to chromatin throughout mitosis, cell cycle stalling in **Figure 3.4 B** is expected (Zhao *et al.*, 2011), however a correlation with cell death is not necessarily causal.

To investigate the kinetics of eGFP activation, MEL cells were embedded in Matrigel with the ratio of eGFP to RFP pixel intensity measured by live cell imaging **(Figure 3.3 E)**. BET inhibition, resulted in decreased confluence as expected from **Figure 3.4 B**, whilst RFP pixel intensity remained constant. 5'Azacytidine treatment required multiple cell cycles to give eGFP expression **(Figure 3.6 A)** which is in line with DNA methylation in haematopoiesis causing globin gene expression (Lessard et al., 2015). Chaetocin, an inhibitor of Suv39 methyltransferases, was used as a drug to directly alter heterochromatin **(Figure 3.6 B)**. Chaetocin did promote eGFP expression in the primary screen, but was toxic causing high levels of cell death. The further suppression of eGFP by low-level chaetocin treatment was due to an increase in RFP expression, which affected the GFP/RFP ratio, however eGFP activation was detected after 12 hours treatment, indicating loss of heterochromatin repression.

BET inhibition caused dose dependent eGFP expression 24 hours after treatment using a pan inhibitor bromosporine **(Figure 3.6 D)** and selective inhibitors JQ1$^{+/-}$ and I-BET151 **(Figure 3.6 C, E).** Bromosporine was the least effective, followed by I-BET151 and JQ1$^{+/-}$. As a pan BET inhibitor bromosporine binds to proteins including CECR2, CBP and EP300 in addition to Brd- proteins (Picaud *et al.*, 2016). As CBP mediated histone acetylation at HS2 greatly enhances normal β-globin expression, eGFP expression after inhibition of these proteins is intriguing (Johnson, Norton and Bresnick, 2002). eGFP expression from selective inhibitors JQ1$^{+/-}$ and I-BET151 would suggest that eGFP activation is independent of pan BET inhibition, and that this process is dominant over CBP-EP300 mediated acetylation. As CBP acetylation and GATA-1 recruitment is required for differentiation dependent globin expression, this suggests that Brd- protein loss directly causes heterochromatin loss (Cho *et al.*, 2008). BET specific inhibition, while causing eGFP expression to a greater level than chaetocin treatment, was only detected 24 hours post treatment. The loss of heterochromatin therefore could require replication. This supports work from the Spector lab, where artificial tethering of Brd4 to heterochromatin did not cause HP1 loss and gene activation, but accelerates post mitotic de-compaction (Zhao *et al.*, 2011).

The only histone modifications globally affected by BET inhibition were H3K4 unmodified, mono- and di-methylated **(Figure 3.8)** whilst at the eGFP transgene H3K4me3 is enriched **(Figure 3.9 B)**. Together this data infers a loss of H3K4 acetylation, which is normally found upstream of active promoters (Wang *et al.*, 2008). Promotion of H3K4me2 –me3 over H3K4 acetylation is mediated via the Set-1 containing complex (COMPASS), although the explicit function of H3K4 acetylation is poorly understood

(Guillemette *et al.*, 2011). This may be functional however as the tandem bromodomains (BD1 and BD2) in Brd- proteins have different specificities (Wu and Chiang, 2007). Although highly conserved, the two bromodomains only share ~44% homology and have been demonstrated to form homodimers (BD1-BD1, BD2-BD2) in solution (Nakamura *et al.*, 2007). This has also been inferred in Brd4 where BD1 preferentially binds to the di-acetylated H4K5acK8ac motif; in contrast Brd4 BD2 preferentially binds to H3K4acK9ac over single H3K4 acetylation (Filippakopoulos *et al.*, 2012). This indicates that BET protein binding to H3 or H4 is mediated by different bromodomains, where H3 needs to be acetylated. If BD2 binding to H3K4 acetylation is inhibited this would increase the exposure of the modification to turnover by COMPASS further preventing Brd- protein binding. However, H3K4 acetylation is associated with gene activation and as such would not be expected to affect heterochromatic regions.

ChIP-qPCR data shows BET inhibition causes a loss of H3K9me3, and enrichment of H3K4me3 at the eGFP transgene **(Figure 3.9 B)** whilst endogenous facultative and constitutive heterochromatin loci, amylase and Major satellite, respectively, show moderate loss of H3K9me3 but no enrichment of H3K4me3 **(Figure 3.9 A, D)**. This suggests that the BET proteins role in heterochromatin maintenance is not limited to the artificial transgene, and appears to be a universal property of heterochromatin, even without gene activation. At a poised promoter, such as the endogenous β-globin, there is no significant change in H3K9me3/H3K4me3 ratio suggesting that this locus remains poised, although both marks are reduced **(Figure 3.9 C)** suggesting that BET inhibition does not induce erythroid differentiation within this system.

Aside from differentiation, BET proteins have been implicated in multiple signalling cascades. Brd4 interacts with the activated NF-kB subunit RelA and is required for its activation in the inflammation response (Huang *et al.*, 2009). Brd4 can also act to insulate loci from signalling process such as DNA damage processes by recruiting condensin II complexes maintaining silencing (Floyd *et al.*, 2013).

c-myc is a master regulator of haematopoiesis and its expression is regulated by Brd4. At the murine erythroid developmental stage, Myc is normally supressed by GATA-1 (Rylski *et al.*, 2003) but MEL cell proliferation is driven by aberrant up-regulation of c-myc that is lost upon differentiation (Lachman and Skoultchi, 1984; Coppola and Cole, 1986).

To elucidate the effect of BET inhibitors on kinases, reverse phase protein arrays were used to analyse multiple signalling pathways in parallel **(Figure 3.10)**. BET inhibition leads to increased Brd4 turnover, while Brd2 and Brd3 were previously shown to be unaffected **(Figure 3.8)**. This would suggest that Brd4 mediates the effect of BET inhibition on heterochromatin.

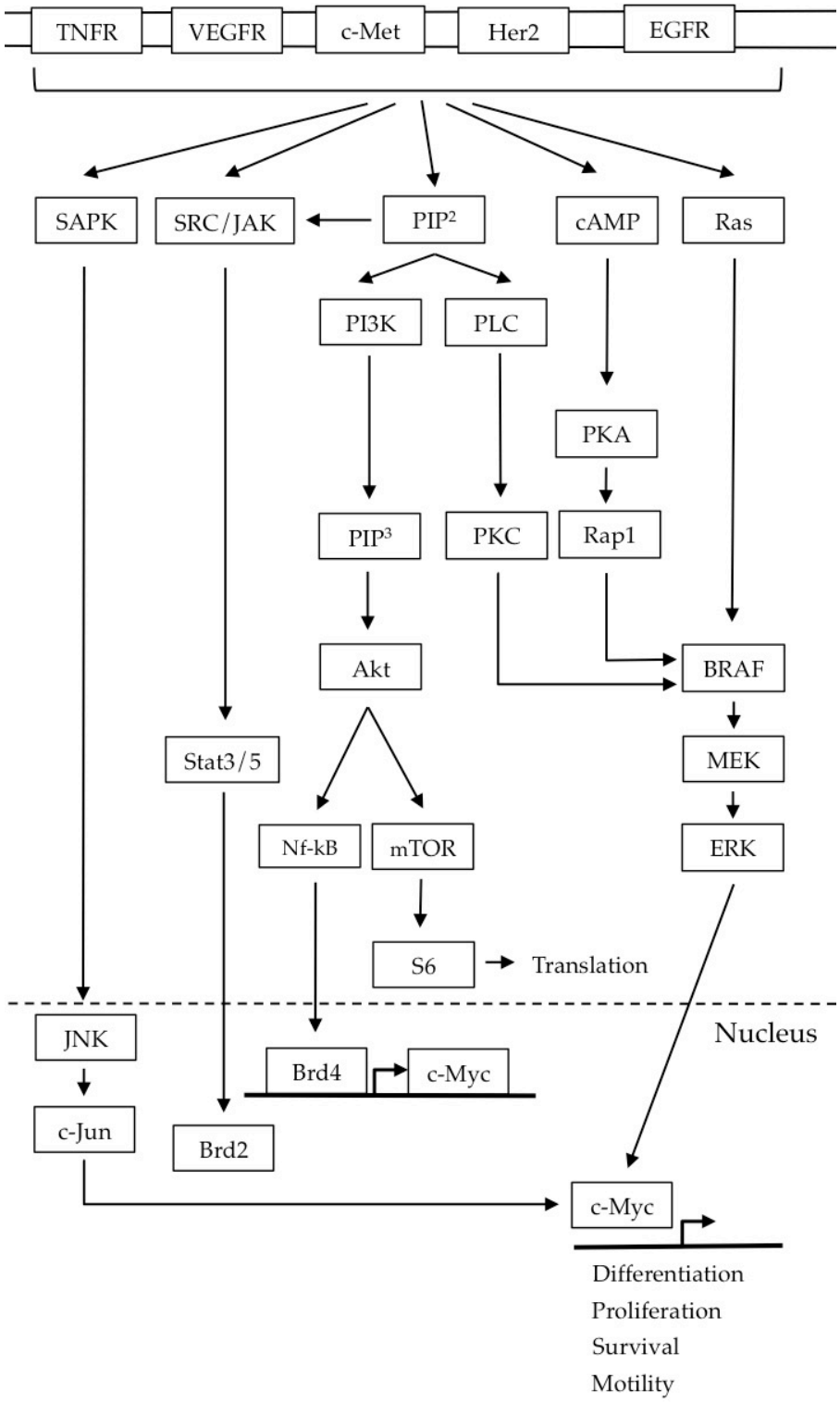

Figure 3.11 MAPK signaling pathways. Diagram showing signaling pathways affected by 1 μM BET inhibition, for 24 hours. Canonical MAPK signaling pathway (right side) stabilises c-Myc. Compensatory PI3K/Akt signaling (center) can also lead to ERK mediated c-Myc stabilisation, which can also increase c-Myc expression. JNK/SRC signaling (left) associated with loss of cell adhesion factors and EMT-like transitions involving c-Myc stabilisation.

BET inhibition also caused significant loss of MAPK signalling from membrane receptors (Met) to downstream ERK **(table 3.2)**. MEK and PKA, components upstream of ERK have increased protein levels but phosphorylation levels are not significantly altered. Protein level increase would remove their abundance as a factor regulating MAPK signalling, a logical response to loss of phosphorylation. Upon BET inhibition, alternative signalling pathways I3K and PKC are hyper-phosphorylated. This suggests that PIP^2 signalling has been up regulated. PKC can act as an alternative method for ERK activation, while PI3K pathway is an alternative method of stimulating c-myc expression (Chen and Sytkowski, 2001). The stimulation of these pathways in addition to STAT and SAPK signalling suggested in **figure 3.11**, indicates that BET inhibition leads to a loss of MAPK signalling, for which the cell compensates through alternative pathways. Intriguingly, inhibitors of these pathways (SAPK/JNK, EGFR/MAPK, PKC) also lead to eGFP expression in the preliminary screen.

To conclude the MEL eGFP system proved to be a robust synthetic system of heterochromatin. Multiple signalling kinases and BET inhibitors, in addition to classical heterochromatic mechanisms, were identified as inducing eGFP expression. The effect of BET inhibition was not compound specific, suggesting it was not due to off-target effects. eGFP activation correlated with G2 arrest and cell death. Heterochromatic marks were also lost from endogenous facultative and constitutive heterochromatic loci. The loss of H3K9me3 at the eGFP transgene was accentuated compared to the endogenous loci, likely due to the gene transcription, for which active marks were not found at the endogenous loci. There was a global increase in H3K4 methylation by BET inhibition suggesting a global increase in transcription, which suggests an alternative role from transcriptional activation for BET proteins.

This is supported by recent work from the Escaffit lab, that recently demonstrated Brd2 binding to pericentric heterochromatin (Grézy *et al.*, 2016). They demonstrated that TIP60 histone acetyltransferase deposits H4K12ac that acts as a binding site for Brd2 and depletion of TIP60 or Brd2 leads to pericentric satellite transcription, conducive to a de-condensed chromatin structure. The work presented here in MEL cells suggests that Brd4 has a role as it is the only Brd- protein depleted, although this requires further investigation to rule out Brd2. Loss of Brd4 has also been shown to globally increase accessibility to nucleases indicative of a de-condensed chromatin fibre, although not specifically demonstrated at heterochromatin loci (Wang *et al.*, 2012a). Together this suggests BET proteins function at silenced loci in addition to their role in transcriptional activation.

Chapter 4: Epigenetic factors in tumor drug resistance and invasion

4.1 Introduction

The previous work in MEL cells identified MAPK signalling as a method of modulating heterochromatin structure (Chapter 3) but aberrant MAPK signalling is also a hallmark of oncogenesis. Hahn and Weinberg (2002) first modelled human cells *in vitro* proposing six essential steps to oncogenesis: independence from proliferative and anti-growth extracellular signals, freedom from replication limitation, apoptotic/senescence evasion, and gaining invasion and angiogenesis abilities. Through human intervention, acquiring drug resistance can also be considered an essential trait of tumour development. MAPK signalling cascades have been associated with each of these processes, and their mis-regulation is a common occurrence in a tumour setting, as suggested by Downward, (2003).

ERKs upstream effectors Ras and Raf have high mutational frequency in multiple malignancies, with Ras mutations found in 20-30% of all human tumours (Bos, 1989). These are invariably found in protein regions involved with GTP hydrolysis, causing constitutive activation. Importantly, this information has led to the development of multiple highly specific Ras/Raf/MEK inhibitors, to prevent ERK driven tumour survival. These can provide a significant benefit to melanoma patients where 45% present with BRAF mutations whilst another 20% harbour NRAS mutations (Hocker and

Tsao, 2007; Flaherty *et al.*, 2012), but unfortunately, ERK driven tumours rapidly develop resistance leading to less than five months increased survival. In ~82% of BRAF V600E patients, resistance to BRAF/MEK inhibition is linked to reactivation of MAPK, PI3K and ERK signalling (Long *et al.*, 2014). Of these V600E BRAF patients amplification only occurs in 20% of MEK resistant cases, whereas hyper-phosphorylation induced by V600E BRAF overexpression is in 80% of cases (Shi *et al.*, 2012). Therefore the largest share of acquired resistance to MEK inhibition is not due to *de novo* genetic mutation, rather it is through an epigenetic response.

Many transcriptional regulators have been implicated in MEK inhibition (MEKi) acquired resistance. PTEN, a negative regulator of PI3K signalling is lost upon MEKi, while MITF (a PI3K activator) is upregulated (Wee *et al.*, 2009; Ferguson *et al.*, 2017). Additionally Ras activator ERBB3 is also upregulated leading to Ras hyper-phosphorylation (C. Sun *et al.*, 2014).

Recent work has demonstrated that acquired resistance to ERK signalling inhibition correlates with large scale alterations in genome regulation similar to epithelial mesochymal transition (EMT) (Jakobsen *et al.*, 2016; Byeon *et al.*, 2017). This leads to a more invasive tumour type and poor patient survival. Altered polycomb silencing has been implicated in an EMT-like transition in oestrogen receptor positive breast carcinoma background, demonstrating epigenetic processes within EMT (Javaid *et al.*, 2013). Understanding how MAPK signalling influences genome regulation inducing an EMT-like transition is therefore fundamental to understanding how ERK driven tumours acquire resistance.

4.2 Development of acquired resistance MEK inhibition model

Trametinib is a highly selective MEK inhibitor, that prevents ERK phosphorylation in a dose dependent manner <100 nM in HCT116 cells (Abe *et al.*, 2011). In order to identify epigenetic mechanisms important for MEKi acquired resistance, HCT116 cells were treated with trametinib in increasing doses up to 100 nM over three months. HCT116 cells that could survive in 100 nM trametinib were considered to have overcome MEKi. Invasion assays (John Dawson, Neil Carragher lab) demonstrated that trametinib resistant cells had altered cellular morphology, decreased cell-to-cell contact, and increased motility **(Figure 4.1 A)**. Trametinib treatment in sensitive HCT116 cells caused a decreased thickness of the cell layer in addition to reduced haematoxylin and eosin (H&E) staining, indicative of reduced cell density (**Figure 4.1, A)**. HCT116 cells resistant to MEKi (TRAMR) maintain matrix invasion and cell layer thickness after trametinib treatment and H&E staining was slightly reduced. The decreased cell-to-cell contact and increased motility mimics the patient phenotype of MEKi acquired resistance due to an EMT-like transition (Byeon *et al.*, 2017). TRAMR cells had increased survival at less than 100 nM trametinib treatment but similar cell survival to the sensitive HCT116 cells at concentrations about 100 nM **(Figure 4.1 B)** suggesting that resistance is acquired by hyper-activation of the Ras/Raf/MEK/ERK pathway. This was sustained even after the removal of trametinib stimulation for two weeks, demonstrating a new stable cellular state.

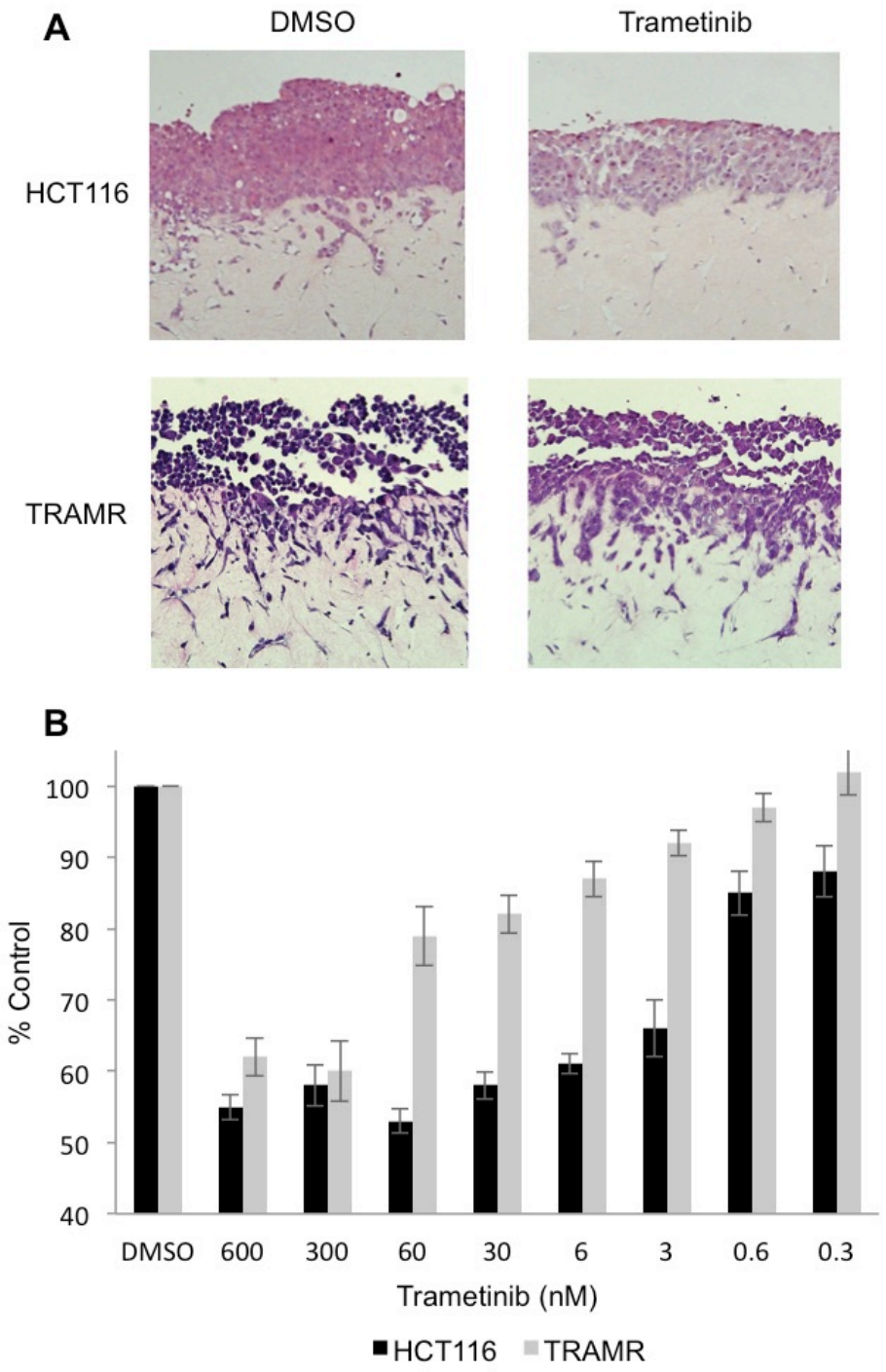

Figure 4.1. Development of Trametinib resistance. (A) Organotypic invasion assay (carried out by John Dawson). HCT116 or TRAMR cells were cultured on fibroblast-collagen matrices for 7 days with DMSO or 5 nM Trametinib. Images are H&E stained cross sections. **(B)** Cell viability data after trametinib treatment in HCT116 or TRAMR cells. Cells were treated with a log-dose of trametinib with viability determined by Presto Blue reagent after 48 hours and imaged on a Victor3 multi-label plate reader at 540/590 nm.

HCT116 and TRAMR cells were treated with 300 nM trametinib for 24 hour. Cell extracts were prepared by John Dawson, spotted onto reverse phase protein (RPPA) arrays and analysed using 185 antibodies against multiple signalling pathways. All the experimental data was collected and analysed **(Appendix 3)**. Significant changes between samples are listed in **table 4.1**. The only significant change between DMSO treated HCT116 and TRAMR cells was ERK1/2 phosphorylation, which was upregulated in TRAMR cells (2.43 fold increase, p = 0.015), an expected result for a resistance mechanism linked to ERK hyper-phosphorylation.

Table 4.1. Significant kinase signaling changes in response to trametinib. List of bonferroni corrected t-test significant changes in antibody fluorescence between either; **(1)** basal states of HCT116 and its trametinib resistant sister cells TRAMR, **(2)** HCT116 cells treated with 300 nM trametinib for 24 hour compared to DMSO controls, or **(3)** TRAMR cells treated with 300 nM trametinib for 24 hour compared to DMSO controls.

Antibody	Basal Δ TRAMR	*p-value*	HCT116 Δ Trametinib	*p-value*	TRAMR Δ Trametinib	*p-value*
ErbB-2/Her2/EGFR *P Tyr1248/Tyr1173*	0.97	0.958	3.79	<0.001	2.09	0.021
Met *P Tyr1234*	0.99	0.980	2.66	0.018	1.94	0.048
PLC-gamma1 *P Tyr783*	1.04	0.939	3.29	0.001	1.83	0.078
SHP2 *P Tyr542*	1.30	0.610	3.26	0.001	1.91	0.053
FLT3 P Tyr591 *P Tyr591*	0.98	0.974	3.13	0.002	1.91	0.055
p44/42 MAPK (ERK1/2) *P Thr202/Thr185, Tyr204/Tyr187*	2.43	0.015	0.65	0.616	0.72	0.000
SAPK/JNK *P Thr183,Tyr185*	1.06	0.913	2.66	0.018	1.66	0.161
p53 *P Ser15*	0.93	0.906	1.40	0.564	1.97	0.041

Similar to previous studies, trametinib treatment in both cell lines triggered upregulation of ERBBs activation (C. Sun *et al.*, 2014). Significant increases in phosphorylation after trametinib treatment were also found in HCT116 cells for: Met and FLT3 receptors, downstream PLC-gamma and SHP2, and SAPK/JNK **(table 4.1)**. Met and FLT3 cell membrane receptors can activate PI3K signalling via PLC-gamma and SHP2 and are known to be upregulated in resistance to MAPK inhibition increasing cell motility (Usatyuk *et al.*, 2014; Nogami *et al.*, 2015). SAPK/JNK stimulation has also been implicated in EMT transition by inhibiting EZH2 mediated polycomb gene silencing, and is further evidence that trametinib treatment in this *in vitro* system is a good model for trametinib response (Li *et al.*, 2016). While these proteins are also upregulated in TRAMR cells after trametinib treatment, only Met phosphorylation is significant. Additionally p53 Ser15 phosphorylation is also upregulated after trametinib treatment in both cell lines, indicating p53 mediated transcription (Loughery *et al.*, 2017). Together these data suggest that trametinib treatment in HCT116 and TRAMR cells provides a useful model for analysing before and after acquired drug resistance in an EMT-like manner.

4.3 Identifying epigenetic components of acquired trametinib resistance

To identify mechanisms involved in acquired MEKi resistance, compounds were screened in a dose matrix with MEK inhibitor trametinib **(Figure 4.2)**. If the compounds are synergistic then the combination of both drugs will increase cell death when compared to each compound singularly. Identifying differences in responses between HCT116 and TRAMR cells can be used to infer that the compound's target protein is implicated in acquiring trametinib resistance. 42 selective inhibitors were screened in a dose matrix across 21 target classes identified as regulating synthetic heterochromatin in **Table 3.1**, in combination with trametinib. These included selective inhibitors of heterochromatin components, BET inhibitors and the kinase inhibitors identified in the MEL screen as modulating heterochromatin structure. Eight compounds were identified, as having combinatorial effects with trametinib or altered effects between HCT116 and TRAMR cells **(Figures 4.3, 4.4)**. Two kinase inhibitors demonstrated altered profiles in TRAMR cells compared to HCT116. One of them, GW843682X is a selective inhibitor of PLK kinase (Lansing *et al.*, 2007). In normal HCT116 cells PLK inhibition demonstrates no combinatorial effect with trametinib and limited efficacy singularly **(Figure 4.3 A)**. TRAMR cells demonstrate increased sensitivity to PLK inhibition singularly **(Figure 4.3 B)**. However, GW843682X has 100-fold selectively towards PLK1 and PLK3 (2.2 nM and 9.1 nM) compared to other kinases. The increased sensitivity required 500 nM treatment to affect cell growth in TRAMR cells and is therefore likely to be due to inhibition of off

target kinases. This also applies to the antagonistic affects with low-level trametinib treatment and high GW843682X dosage synergism **(Figure 4.3 B)**.

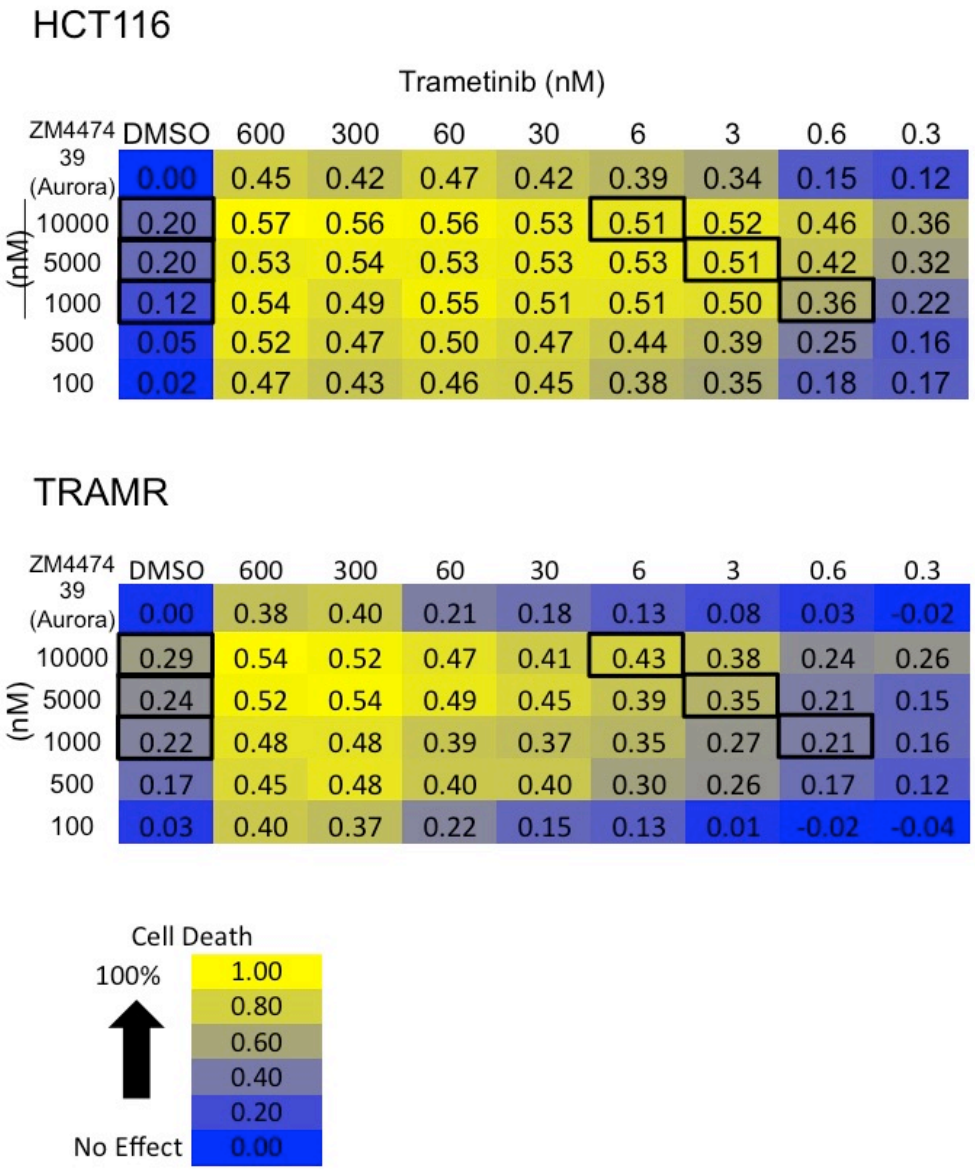

Figure 4.2. Drug combination dose matrix. Layout of a dose matrix experiment with Aurora kinase inhibitor ZM447439. HCT116 cells or their resistant sister cells were treated with a log-dose range of two compounds independently of each other (far left column and top row). Other wells were treated with every combination of the two compounds dose range. Cells were then incubated for 48 hours and cell viability analyzed using PrestoBlue™. Comparison of concentration combinations were then compared to the singular compounds to determine synergistic and antagonistic effects. Further comparison between the sister cells identified combinations or targets pertinent to MEK inhibition resistance.

ZM447439 is a potent inhibitor of Aurora A and B kinases (Ditchfield *et al.*, 2003) and had an altered combinatorial effect with trametinib treatment **(Figure 4.3 C, D)**. In trametinib sensitive HCT116 cells Aurora inhibition had little effect on cell viability as a single agent **(Figure 4.3 C)**, while high dose ZM447439 (5-10 μM) is synergistic at low trametinib levels; this is lost at higher doses. This suggests that trametinib has a dominant effect in this combination. In trametinib resistant HCT116 cells (TRAMR) Aurora inhibition had a moderate effect as a single agent. The combination with trametinib demonstrates combinatorial synergism, limiting cell viability at higher concentrations to a similar level to sensitive HCT116 cells **(Figure 4.3 C, D)**. Together this indicates a minor role for Aurora kinase in acquired resistance to trametinib.

UNC642 is a highly selective inhibitor of G9a and GLP methyltransferases (IC50 <2.5 nM). It has >2,000 times selectivity toward these H3K9 mono- and di- methyltransferases compared with H3K27me3 HMT Ezh2 and H3K9me3 HMT Suv39h enzymes (F. Liu *et al.*, 2013). High dose treatment of G9a/GLP inhibitor UNC642 resulted in low levels of cell viability in both HCT116 and TRAMR cells **(Figure 4.3 E, F)**. At low doses UNC642 promotes cell growth as a single agent in HCT116 cells **(Figure 4.3 E)**. However, there is no significant synergism or antagonism with trametinib treatment. This suggests that H3K9me2 does not have a significant role in ERK driven cell proliferation. In trametinib resistance cells, UNC642 combination is highly antagonistic **(Figure 4.3 F)** and suggests that H3K9me2 has an altered function in cells that have undergone the EMT-like transition to acquire trametinib resistance. Proliferation within these conditions is enhanced over controls, suggesting that in TRAMR cells this function of H3K9me2 limits cell growth when proliferative MAPK signalling is reduced.

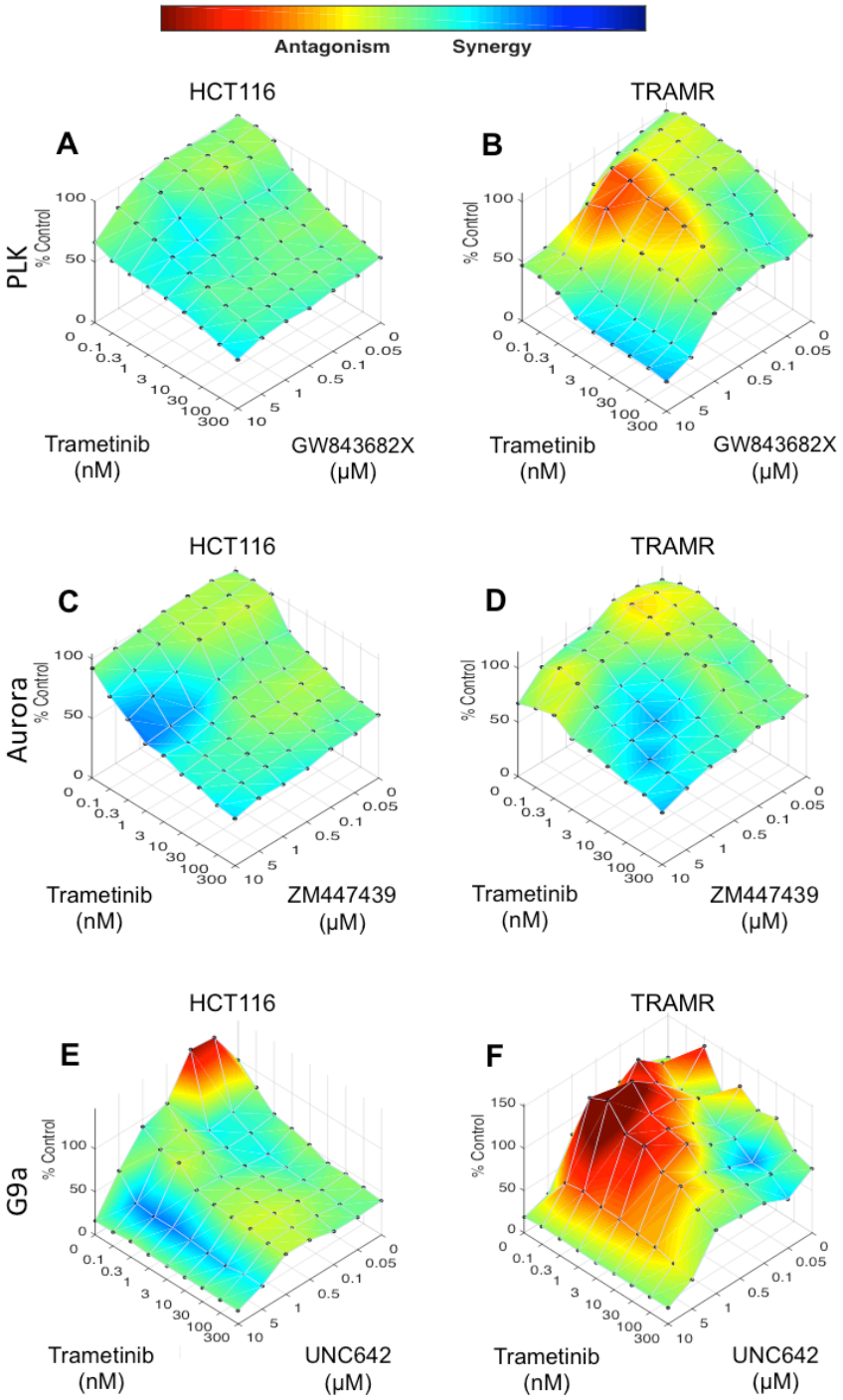

Figure 4.3. Trametinib 3D HSA dose matrix plots for kinase inhibitors. Fraction affected 3D dose combination plots overlaid with the HSA model for synergism with MEK inhibitor trametinib. HCT116 or TRAMR cells were treated with a log-dose matrix between trametinib and another compound for 48 hours followed by PrestoBlue™ cell viability assay. **(A-B)** Combination plots of for PLK inhibitor GW843682X. **(C-D)** Combination plots for Aurora kinase inhibitor ZM44739. **(E-F)** Combination plots of G9a, GLP inhibitor UNC642.

H3K9me2 has been implicated in the formation of facultative heterochromatin during differentiation at genic regions in addition to its deposition pericentromerically (Wen *et al.*, 2009). Recent work has indicated that H3K9me2 functions to allow transcriptionally permissive pericentric heterochromatin, maintained by argonaute mediated transcriptional silencing (Jih *et al.*, 2017). Maintenance of pericentric heterochromatin in the absence of RNAi mechanisms requires the transition to H3K9me3, demonstrating an independent role for H3K9me2 in heterochromatin formation. The antagonistic effect of G9a/GLP inhibition in TRAMR cells, therefore suggests that H3K9me2 has altered function in ERK signalling response after acquired resistance, that may indicate altered heterochromatin regulation and/or altered heterochromatic transcription.

Polycomb mediated silencing via the formation of facultative heterochromatin, is known to also function in differentiation mediated gene regulation as an alternative to H3K9me mediated heterochromatin (Gilbert *et al.*, 2003). To determine if polycomb functions in trametinib acquired resistance, HCT116 and TRAMR cells were treated with selective inhibitors of Ezh2 (PRC2 subunit) and L3MBTL (PRC1 subunit), GSK343 and UNC 699 respectively **(Figure 4.4)**. For both inhibitors in sensitive HCT116 cells, inhibition had no effect on proliferation until the highest dose of 10 μ M; additionally there was no combinatorial effect with trametinib in HCT116 cells (**Figure 4.4 A, C**). However, the trametinib resistant cells, TRAMR, showed increased sensitivity to both inhibitors when used as single agents. This effect is accentuated in UNC 699 treated TRAMR cells suggesting that PRC1 and subsequent PRC2 recruitment may be altered.

In combination with trametinib both inhibitors, GSK343 and UNC 699, have antagonistic effects at low concentrations (**Figure 4.4 B, D**). This suggests that MAPK signalling interacts with polycomb regulation after developing MAPKi resistance. Canonical PRC1 complexes have a tight association to PRC2 and H3K27me3, and the common subunit Cbx7 is known to be phosphorylated by MAPK signalling (Kassis and Brown, 2012; Wu *et al.*, 2013). This would suggest a synergistic relationship with MAPK inhibition. However, atypical PRC1 complexes with Cbx6 and L3MBTL2 subunits are known to be essential for ES cell differentiation functioning independently of PRC2 and repressing MAPK expression (Qin *et al.*, 2012; Santanach *et al.*, 2017). Together these data suggest that inhibition of PRC1 subunits would need to be highly specific in order to target a single PRC1 function.

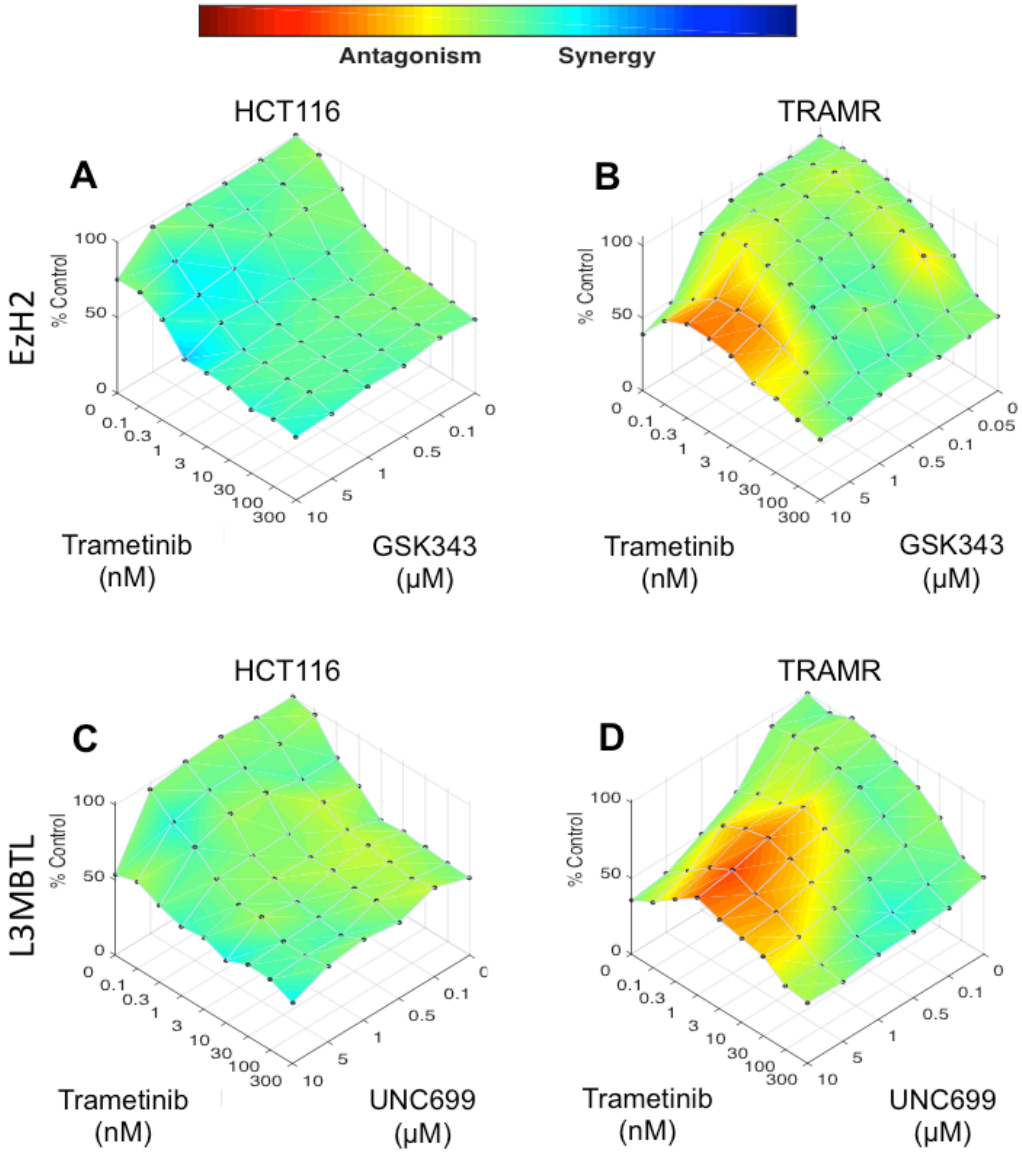

Figure 4.4. Trametinib 3D HSA dose matrix plots for polycomb inhibitors. Fraction affected 3D dose combination plot overlaid with the HSA model for synergism with MEK inhibitor trametinib and polycomb subunit inhibitors. HCT116 or TRAMR cells were treated with a log-dose matrix of trametinib and another compound for 48 hours followed by PrestoBlue™ cell viability assay. **(A-B)** Combination plots of for EZH2 inhibitor GSK343. **(C-D)** Combination plots for L3MBTL inhibitor UNC699

PRC2 is also known to have both tumour suppressor and oncogenic functions depending on the tumour type. Many tumours overexpress PRC2 proteins including breast and colon (Bracken *et al.*, 2003), but in contrast recurrent somatic loss of function mutations of PRC2 components are enriched in diffuse large B cell lymphoma and acute lymphoblastic leukaemia (Ernst *et al.*, 2010). Subsequent studies have demonstrated that PRC2 loss in solid tumours has cooperative effects with MAPK signalling in driving tumour progression (De Raedt *et al.*, 2014; Zhang *et al.*, 2014). Taken together this suggests that PRC2 has tumour suppressor functions specifically acquired when developing trametinib resistance.

Intriguingly, Thomas De Raedt's (2014) work also suggests that loss of PRC2-MAPK tumour suppressor functions results is linked to BET protein function. To investigate this HCT116 and TRAMR cells were treated with multiple BET inhibitors to determine the function of BET proteins in trametinib resistance development (**Figure 4.5)**. JQ1, I-BET151, and I-BET762 are selective inhibitors of Brd2, Brd3, Brd4 and Brdt (Filippakopoulos *et al.*, 2010; Nicodeme *et al.*, 2010; Mirguet *et al.*, 2013). While selectivity differs between compounds, in HCT116 cells, BET inhibition has moderate affect as a single compound (**Figure 4.5 A, C, E**). Low dose of IBET762 and IBET151 was antagonistic to trametinib, and, although this only occurred at one dose, it was reproducible (n=3). This antagonistic effect aside, there was no combinatorial effect with trametinib in HCT116 cells. Resistant TRAMR cells were more sensitive to all three BET inhibitors as single agents (**Figure 4.5 B, D, F**) while JQ1 was highly antagonistic in combination with trametinib. IBET151 and IBET762 by contrast showed moderate antagonism with trametinib at higher dosages. Unlike JQ1, which is a pan inhibitor across the

BET proteins, IBET151 and IBET762 have differing selectivity across the class. IBET151 has decreased selectivity towards Brd2 and further decreased selectivity towards Brd3 *in vitro*. IBET762 is most selective towards Brd2 followed closely by Brd4, and decreased binding to Brd3 *in vitro* (Dawson *et al.*, 2011). This suggests that the antagonistic properties come either from inhibiting all three BET proteins or is specifically linked to Brd2 and Brd3 rather than canonical Brd4 inhibition.

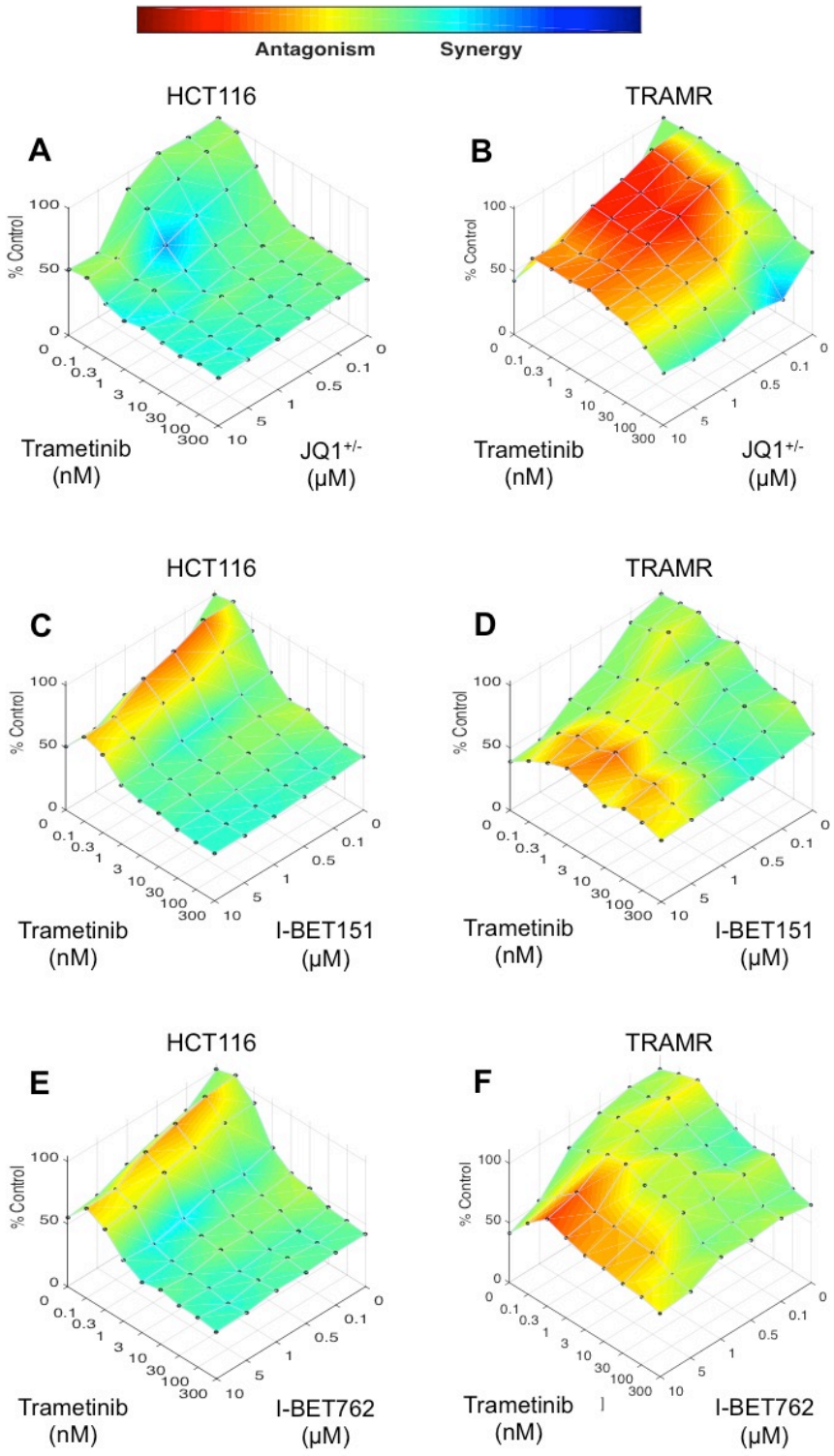

Figure 4.5. Trametinib 3D HSA dose matrix plots with BET inhibition. Fraction affected 3D dose combination plot overlaid with the HSA model for synergism with MEK inhibitor trametinib and BET inhibitors. HCT116 or TRAMR cells were treated with a log-dose matrix with trametinib and a BET inhibitor for 48 hours followed by PrestoBlue™ cell viability assay. **(A-B)** combination plots for JQ1$^{+/-}$. **(C-D)** combination plots for I-BET151. **(E-F)** Combination plots for I-BET762.

BET proteins bind to acetylated chromatin via tandem bromodomain hydrophilic pockets (Dhalluin *et al.*, 1999). JQ1, IBET151 and IBET762 act as competitive inhibitors to acetylated lysines releasing BET proteins from chromatin without affecting protein structure. To determine whether acetylation changes were affecting BETi sensitivity, HCT116 and TRAMR cells were treated with a dose matrix of HDAC inhibitor trichostatin A and JQ1 (**Figure 4.6**). In HCT116 cells TSA and JQ1 are highly synergistic, indicative of inhibitors targeting the same pathway (**Figure 4.6 A**). Trametinib resistant cells sensitivity to the TSA single agent treatment was similar to that of HCT116 cells. However, JQ1-Trametinib combinations had a weak antagonistic effect, suggesting altered BET protein function after acquiring trametinib resistance (**Figure 4.6 B**). As TSA is a pan HDAC inhibitor this could be due to altered acetylation of non-chromatin substrates or acetylation independent recruitment of BET proteins. Recent work has demonstrated that structural chromatin protein CTCF can recruit Brd2 to determine transcriptional and architectural boundaries (Hsu *et al.*, 2017). Additionally BET proteins Brd2 and Brd4 c-terminal domain interaction with viral DNA is known to cause recruitment to heterochromatin (You *et al.*, 2004; Viejo-borbolla *et al.*, 2005).

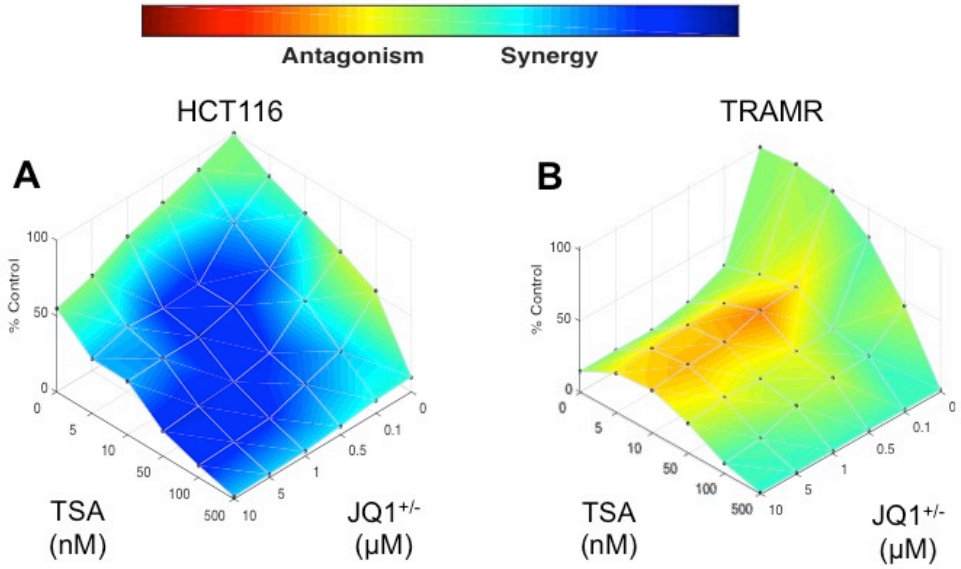

Figure 4.6. Trichostatin 3D HSA dose matrix with BET inhibition. Fraction affected 3D dose combination plot overlaid with the HSA model for synergism with HDAC inhibitor trichostatin A (TSA). HCT116 or TRAMR cells were treated with a log-dose matrix with TSA and JQ1$^{+/-}$ for 72 hours followed by PrestoBlue^{TM} cell viability assay. **(A)** combination plot of for HCT116 cells. **(B)** combination plot of for TRAMR cells

To investigate which BET proteins or bromodomains were implicated in trametinib-acquired resistance, further BET inhibitors were compared (**Figure 4.7**). OTX015 is another pan BET inhibitor similar to JQ1 with little selectivity between Brd2, Brd3 and Brd4 (Coudé *et al.*, 2015). RVX-208 by contrast has 10-100 fold selectivity to BET proteins second bromodomain. Additionally RVX-208 has decreased selectivity towards Brd4 when compared to Brd3 and Brd2 (Picaud *et al.*, 2013). All BET inhibitors apart from RVX-208 demonstrated increased sensitivity in TRAMR cells, indicating that both bromodomains are essential to this acquired function. The order of sensitivity across the BET inhibitors also correlates with selectivity towards Brd3 and Brd2 in contrast to Brd4 suggesting that one or both of these proteins may be involved in the acquired resistance to MAPK inhibition.

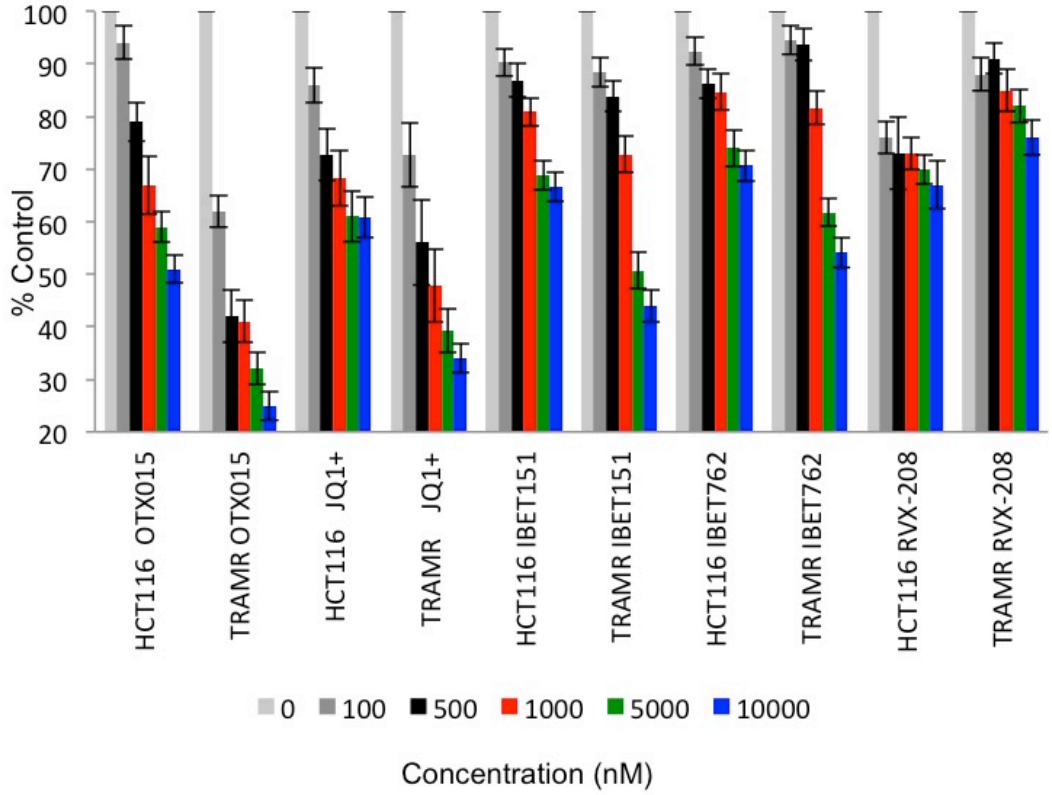

Figure 4.7. BET inhibition and cell viability. Bar charts showing cell viability using a PrestoBlue™ assay. HCT116 and TRAMR cells were treated with a half-log dose curve of BET inhibitors for 48 hours, independently. Viability was determined by Presto Blue reagent incubation and 540/590 nm measured on a Victor3 multi-label plate reader.

4.4 The role of BET proteins in acquired resistance to ERK inhibition

In order to further investigate the function of BET proteins, both HCT116 cells and TRAMR were treated with increasing doses of JQ1 up to 1 μM over three months to develop resistance also known to occur in patients (Kurimchak *et al.*, 2016). HCT116 and TRAMR cells resistant to JQ1 treatment (HJQ1R and TJQ1R) were treated with dose curves of trametinib +/- 1 μM JQ1, and JQ1 as a single agent along with their parental cell lines (**Figure 4.8**). With trametinib treatment HCT116 cells were the most sensitive. Intriguingly, both JQ1 resistant cell lines had similar tolerance of trametinib, beyond that of TRAMR cells (**Figure 4.8 A**). When treated with a log dose range of JQ1, both JQ1 resistant cell lines demonstrated negligible reduction. Reaffirming the drug combination matrix results TRAMR cells were more sensitive to JQ1 treatment than HCT116 cells (**Figure 4.8 B**).

1 μM JQ1 combined with a log dose range of trametinib was however synergistic in both JQ1 and trametinib resistant cells (**Figure 4.8 C**) which suggests that BET inhibition is able to overcome MEK inhibition, reverting resistant cells to a sensitive state. Additionally, the synergism of JQ1 and trametinib in JQ1 resistant cells suggest that these act as a switch between molecular states, and not just as an upregulated multidrug resistance pathway. Together these results suggest that BET/MEK inhibition would be a viable drug combination, as they prevent acquired resistance to each other. This hypothesis has been further established by recent studies demonstrating that a Tip60/Brd4/Twist complex is required for nuclear reorganisation in an endothelial mesenchymal like transition (Shi, Cao and Zhou, 2015).

The antagonistic combination shown previously in **figure 4.5 B** was not observed here at these comparatively higher dosages. Hyperphosphorylation at multiple protein residues is known to reduce the affinity of trametinib to MEK1, decreasing its efficacy, resulting in the stabilisation of phosphorylated c-myc, preventing its ubiquitination (Gilmartin *et al.*, 2011; Tsai *et al.*, 2012). Subsequent studies have demonstrated that c-myc, known to be regulated by BET proteins, contributes ERBB2/3 suppression, thus acting as a negative feedback loop (C. Sun *et al.*, 2014). As such, BET inhibition and downstream reduction of c-myc will partially compensate for trametinib MEK1 inhibition. Further studies demonstrated that more extensive RTK inhibition was, however, able to overcome this myc driven feedback loop, demonstrated by higher doses used in **figure 4.8 C** (Lito *et al.*, 2012).

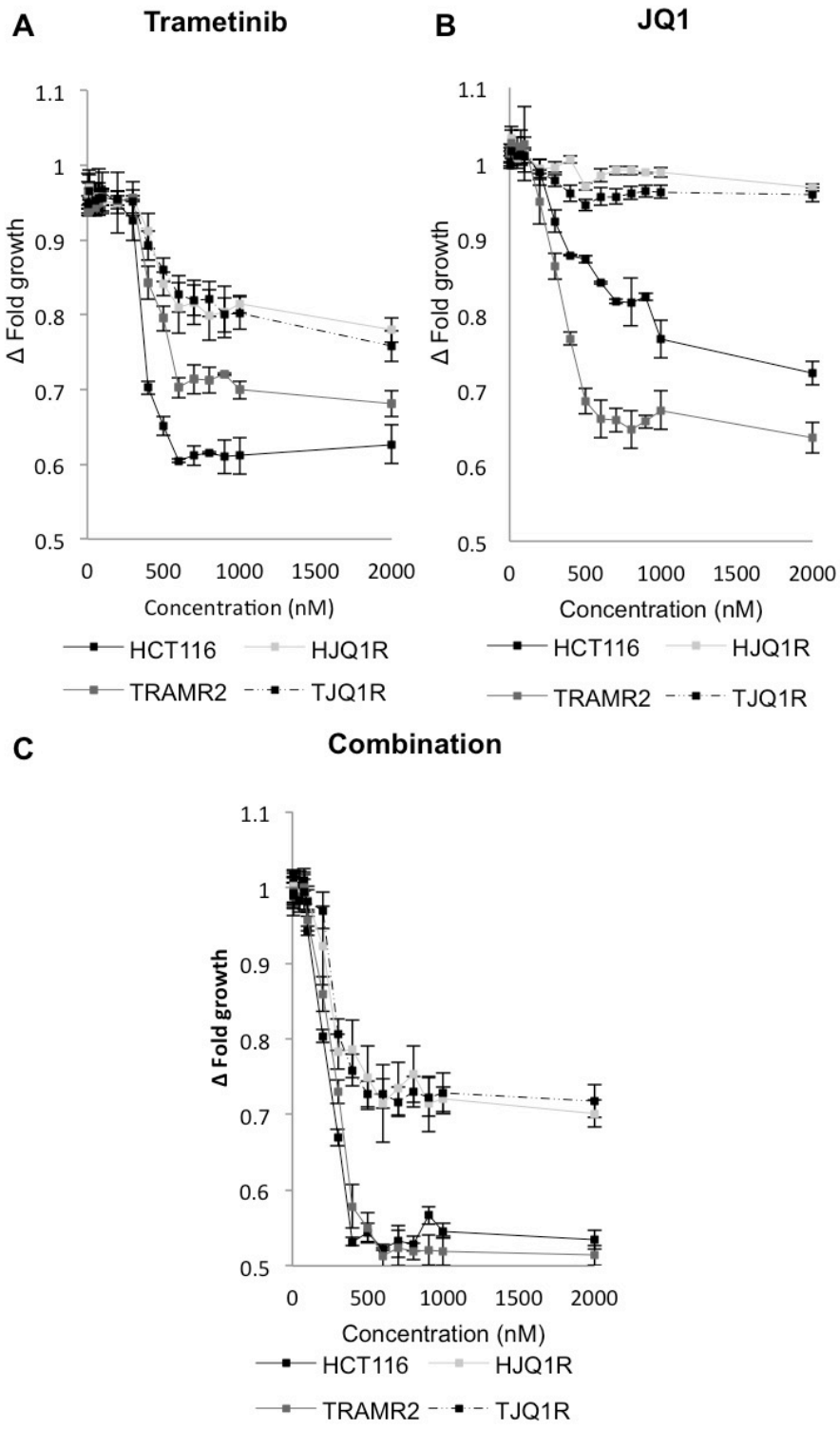

Figure 4.8. Development of JQ1 resistance in combination with trametinib. Comparison of HCT116 cells and their sister cells with trametinib or JQ1$^{+/-}$ acquired resistance cells. Cell viability was assayed by PrestoBlue^{TM} incubation and measured at 540/590 nm. **(A)** Cells treated with a log-dose range of trametinib for 24 hours. **(B)** Cells treated with a log-dose range of JQ1$^{+/-}$ for 24 hours. **(C)** Cells were treated with a singular dose of 1 μM JQ1$^{+/-}$ and a log-dose range of trametinib for 24 hours.

BET proteins have multiple functions modulating cell cycle progression. Brd4 stays bound to chromatin through mitosis, and is known to interact with condensin II and insulate chromatin from the DNA damage response. Loss of this function induces relaxed chromatin compaction and rapid cell-cycle checkpoint recovery (Floyd *et al.*, 2013). Brd2 was first identified as a regulator of cyclin A transcription and subsequent cell cycle progression (Sinha, Faller and Denis, 2005). To determine whether cell cycle alterations occur when HCT116 cells develop resistance to trametinib and JQ1 that could alter BET inhibition efficacy, propidium iodide cell cycle flow cytometry analysis was performed (**Figure 4.9**). HCT116, TRAMR, and HJQ1R cells were tested with 1 μM JQ1 for 48 hours. Untreated TRAMR cells had a similar cell cycle profile to untreated HCT116 cells, suggesting that the development of resistance to trametinib had no effect on cell cycle progression. Untreated HJQ1R cells however had elevated levels of cells in S phase and G2 indicating that the development of JQ1 resistance alters cell cycle progression. In all cell lines however JQ1 treatment resulted in an increase of cells in G1 (**Figure 4.9 G**) and suggests that development of resistance to JQ1 is an inherent property of "resistant" cells and not just an altered response to JQ1 treatment.

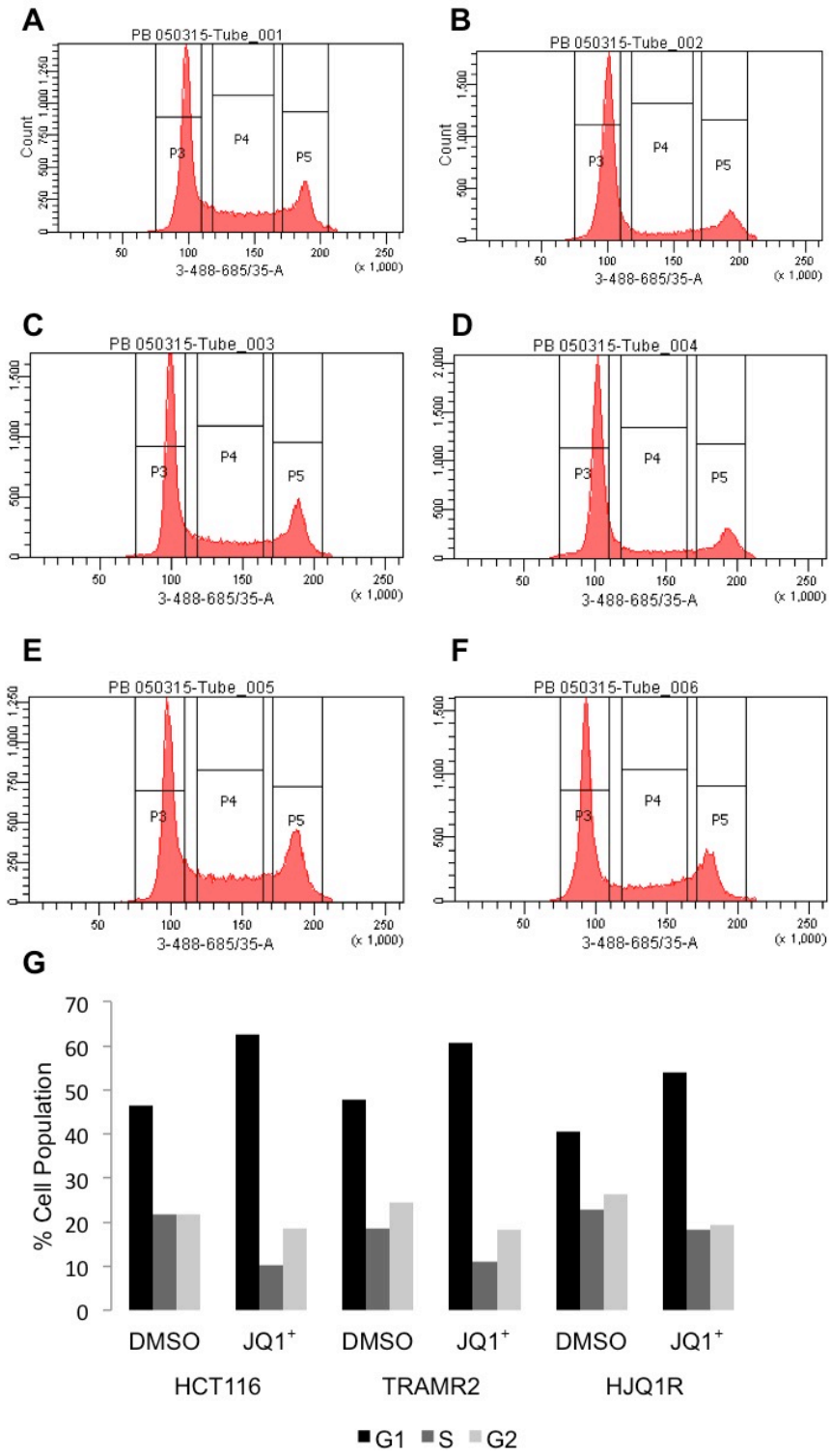

Figure 4.9. BET inhibition and the cell cycle. Frequency distributions for propidium iodide (PI) stained cells analyzed by flow cytometry. Treated cells were ethanol fixed and stained with 1 µg/ml of PI for 2 hours at room temperature. PI fluorescence was detected at 695-740 nm by flow cytometry **(A-B)** HCT116 cells treated with DMSO or 1 µM $JQ1^{+/-}$ for 48 hours **(C-D)** TRAMR cells treated with DMSO or 1 µM $JQ1^{+/-}$ for 48 hours **(E-F)** HJQ1R cells treated with DMSO or 1 µM $JQ1^{+/-}$ for 48 hours. **(G)** Cell cycle stage ratios from **A-F**.

To determine if there was a change to the spatial distribution of Brd4, Brd4 was analysed by immunofluorescence after 1 μM JQ1 treatment for 24 hours (**Figure 4.10**). In untreated HCT116 and TRAMR cells Brd4 had a diffuse staining pattern but HJQ1R cells by contrast had a diffuse staining pattern in addition to some punctate spots. The appearance of punctate Brd4 also occurred in each cell line after JQ1 treatment. To determine if Brd4 was redistributed from a central to more peripheral position, DAPI images were used in conjunction with edge segmentation to determine nuclear boundaries for each nucleus. These were then applied to the linked Brd4 image and the average radial pixel intensity was calculated and binned into deciles for each cell. At least 20 cells were analysed for each treatment and cell line and plotted (**Figure 4.10 B-G)**. Both HCT116 and TRAMR untreated cells had Brd4 radial distributions weighted to more central positions, in line with canonical functions of Brd4 within euchromatin, and JQ1 treatment in HCT116 cells did not significantly alter Brd4's distribution (**Figure 4.10 B-C**). TRAMR cells by contrast saw a significant shift in Brd4 signal towards the periphery, which could be indicative of Brd4 being recruited to heterochromatic regions (**Figure 4.10 D-E**). HJQ1R cells differed from HCT116 and TRAMR cells as untreated Brd4 was evenly distributed from the centre to the periphery. JQ1 treatment of HJQ1R cells also did not significantly alter this distribution despite the signal being more variable (**Figure 4.10 F-G**) which might suggest that a Brd4 distribution associated with the nuclear periphery is not dependent on bromodomain function.

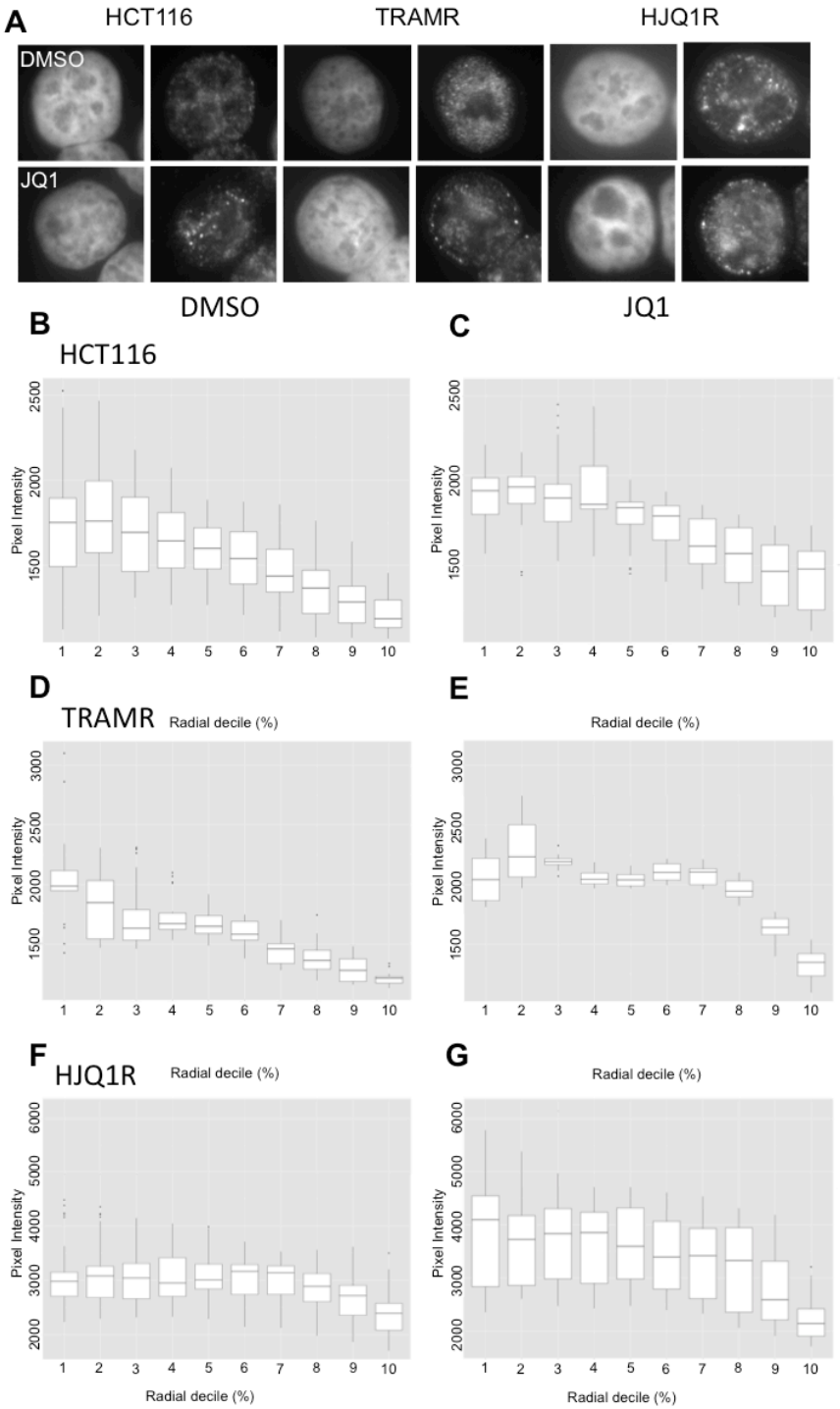

Figure 4.10. Brd4 distribution in nucleus after BET inhibition. HCT116, TRAMR and HJQ1R cells were treated with DMSO or 1 μM $JQ1^{+/-}$ for 24 hours. Cells were washed before fixation to remove unbound proteins, and stained with DAPI and Brd4 antibodies. **(A)** DAPI and Brd4 images of cell nuclei. **(B-G)** Radial distribution of Brd4 pixel signal intensity binned into deciles from more central positioning to the nuclear periphery. **(B-C)** HCT116 cells treated with DMSO or $JQ1^{+/-}$ **(D-E)** TRAMR cells treated with DMSO or $JQ1^{+/-}$ **(F-G)** HJQ1R cells treated with DMSO or $JQ1^{+/-}$

To determine if the increased sensitivity to JQ1 in TRAMR cells was directly due to BET protein transcription, RT-qPCR normalised to MRIP was used to analyse RNA levels (**Figure 4.11**). In HCT116 cells, JQ1 1 μM treatment for 6 hours resulted in no significant changes in Brd3 and Brd4 transcription, with a minor decrease in Brd2. C-myc, the canonical downstream effector of Brd2 and Brd4, also showed no significant increase in transcription after JQ1 treatment. Untreated TRAMR cells by comparison had a 4-fold increase in c-myc transcription. This could implicate c-myc as a driver of resistance within TRAMR cells. Importantly, this increase in c-myc transcripts is lost upon JQ1 treatment, directly implicating BET proteins in regulating MEK inhibition resistance. Untreated TRAMR cells also had a 2-fold increase in Brd2 transcription. JQ1 treatment did not affect Brd3 and Brd4 transcription but Brd2 decreased 4-fold. This suggests that the only immediate change in transcription post JQ1 treatment is a reduction in Brd2.

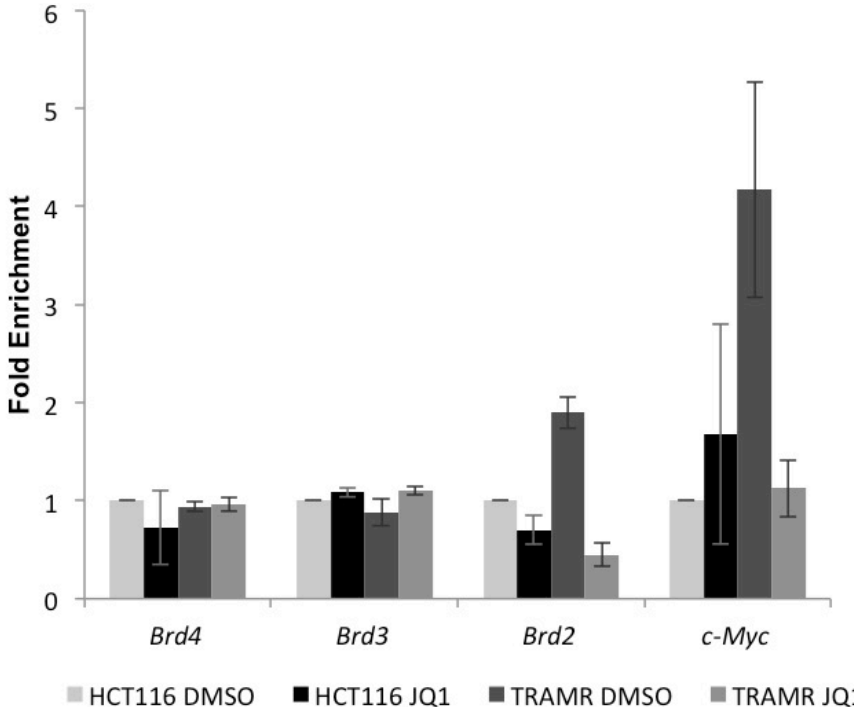

Figure 4.11. Transcriptional response to BET inhibition. HCT116 and TRAMR cells were treated with DMSO or 1 μM JQ1$^{+/-}$ for 24 hours. Transcription of c-Myc, Brd4, Brd3, and Brd2 was quantified by qPCR. Amplification was normalized to the house-keeping gene MRIP.

RT-qPCR was also used to determine if these transcriptional changes were sustained out to 24 hours and determine the effect on HJQ1R cells (**Figure 4.12**). HCT116 and TRAMR BET protein transcription broadly mirrored the changes at 6 hours, except a two-fold reduction in Brd2 after JQ1 treatment in HCT116 cells. Untreated HJQ1R cells had no significant changes in all BET proteins when compared to HCT116 cells. JQ1 treatment however resulted in decreased transcription (30-70%) across the BET proteins. Intriguingly, 7sk RNA levels were also elevated in TRAMR cells. 7sk functions in a complex to sequester P-TEFb, regulating its binding to Brd4 and its function in transcriptional elongation (Prasanth *et al.*, 2010). Together this suggests that BET proteins have altered post-transcriptional regulation in TRAMR cells.

The radial distribution of Brd4 in TRAMR cells after JQ1 treatment and HJQ1R distribution suggests a role at the nuclear periphery (Figure **4.10**). HP1 proteins play an important role in the maintenance and propagation of heterochromatin (Nakayama, Klar and Grewal, 2000; Hall *et al.*, 2002). Therefore RT-qPCR was used to determine if BET proteins regulate heterochromatin via HP1 proteins (**Figure 4.12**). Upon JQ1 treatment HCT116 cells showed no significant change to HP1α transcripts, while HP1β and HP1γ are elevated by 48% and 68%, respectively. Untreated TRAMR cells however showed no major change in any HP1 isoform transcripts after JQ1 treatment or to HCT116 cells. Untreated HJQ1R by contrast had decreased levels of HP1α accentuated by JQ1 treatment. HP1β was also reduced after JQ1 treatment in HJQ1R cells suggesting that acquiring resistance to JQ1 alters HP1 transcription.

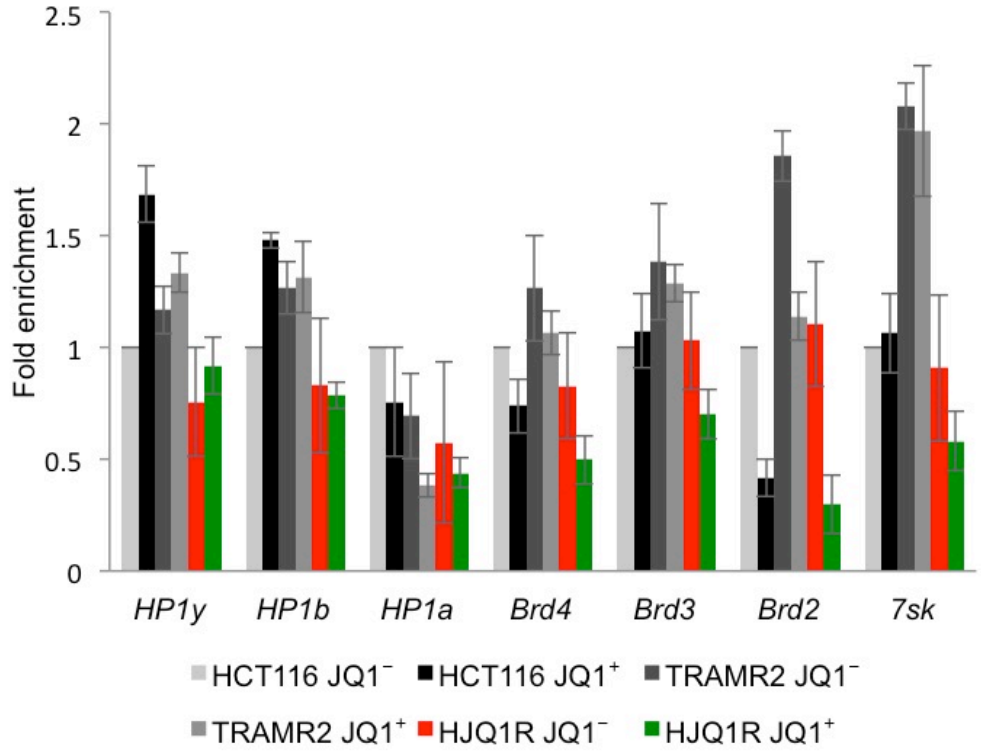

Figure 4.12. HP1 α/β/γ protein expression in response to BET inhibition. HCT116, TRAMR, and HJQ1R cells were treated with 1 μM inactive $JQ1^{-/-}$ or active $JQ1^{+/-}$ for 24 hours. Transcription of 7SK, BET proteins and HP1 proteins were quantified by qPCR. Amplification was normalized to the house-keeping gene MRIP.

Western blotting was used to assess whether JQ1 treatment and acquired resistance affected protein levels (**Figure 4.13**) and densitometry was performed to quantify protein levels in HCT116, TRAMR and HJQ1R cells. Brd4 total protein levels were only elevated in HJQ1R cells upon JQ1 treatment. This indicates that HJQ1R cells may overcome JQ1 treatment by preventing Brd4 degradation, as transcription is not supressed (**Figure 4.12**). Brd3 nuclear protein levels were stable across all three cell lines and treatment conditions, suggesting that it is not involved in acquired resistance to BET or MEK inhibition but Brd2 nuclear protein levels by comparison were altered in the resistant cell lines. Although HCT116 cells showed no major changes in Brd2 levels after JQ1 treatment, TRAMR cells presented with a significant reduction. Untreated HJQ1R cells also had significantly lower Brd2 levels when compared to TRAMR and HCT116 cells. Upon JQ1 treatment however Brd2 levels are restored to levels similar to HCT116 and TRAMR cells. Taken together this implicates Brd2 in the phenotypic switch between JQ1 and trametinib resistance implicated in **figure 4.8**.

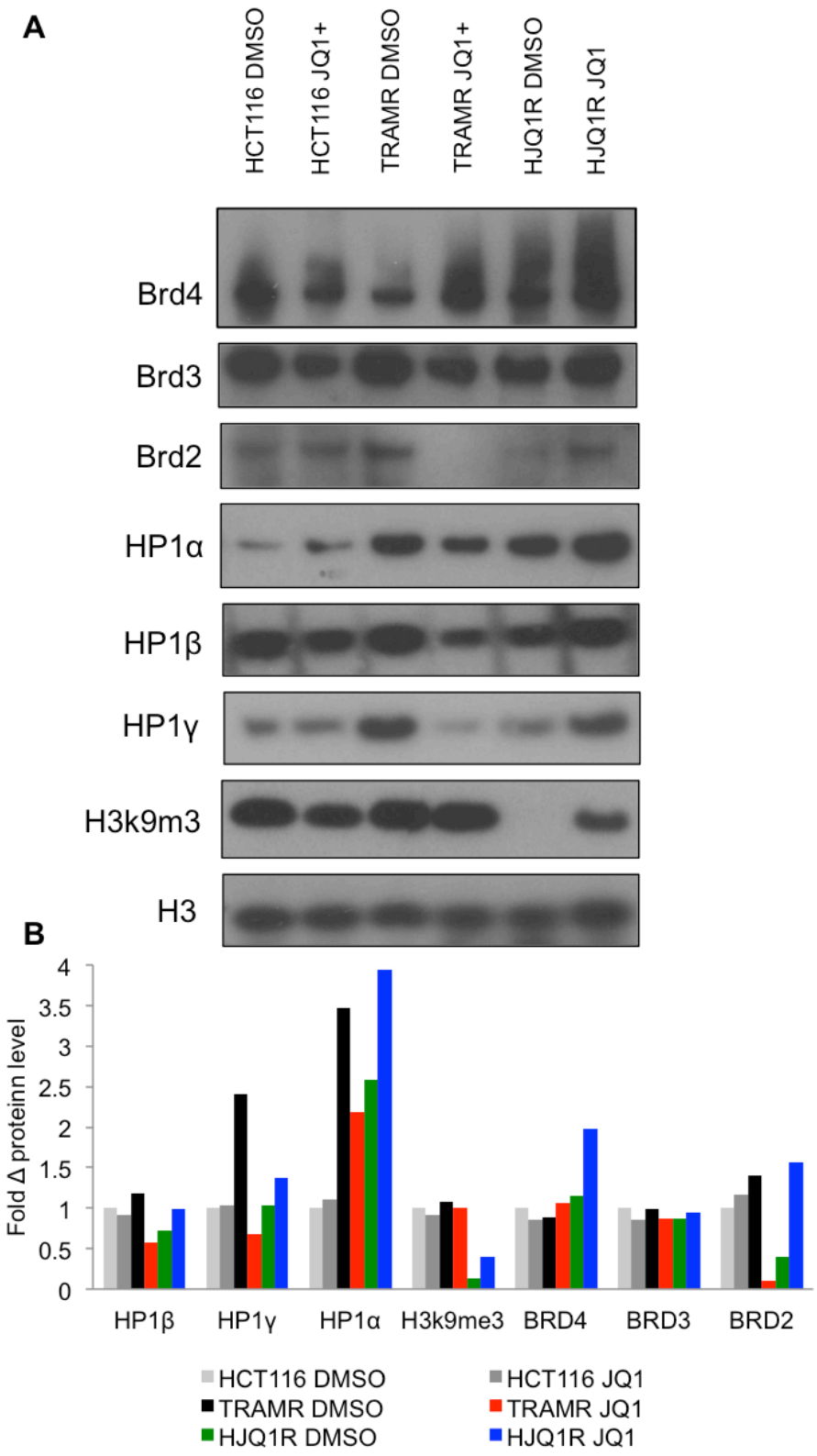

Figure 4.13. Nuclear protein levels after BET inhibition. (A) Westerns of HCT116, TRAMR, and HJQ1R nuclear lysates after 48 hour treatment with DMSO or $JQ1^{+/-}$ 1uM. **(B)** Bands were quantified by 2D densitometry and normalised to total histone H3. Relative protein levels determined by comparison to HCT116 DMSO controls.

HP1 nuclear protein levels were also analysed by western blotting (**Figure 4.13**). JQ1 treatment in HCT116 cells had no effect on any HP1 isoform nuclear concentration. Untreated TRAMR cells presented elevated levels of HP1α and HP1γ when compared to HCT116 cells and this effect was partially negated by JQ1 treatment. Untreated HJQ1R cells also had increased HP1 α nuclear levels, but no significant changes to HP1β or HP1γ levels. In contrast, JQ1 treatment in TRAMR cells resulted in a further increase in HP1α levels. This suggests that HP1α may function in acquiring resistance to JQ1 and trametinib in addition to Brd2. Intriguingly, H3K9me3 levels appear to be severely depleted in HJQ1R cells. As H3K9me3 and HP1α are hallmarks of pericentric heterochromatin, this also suggests an altered chromatin state at the nuclear periphery in response to developing resistance.

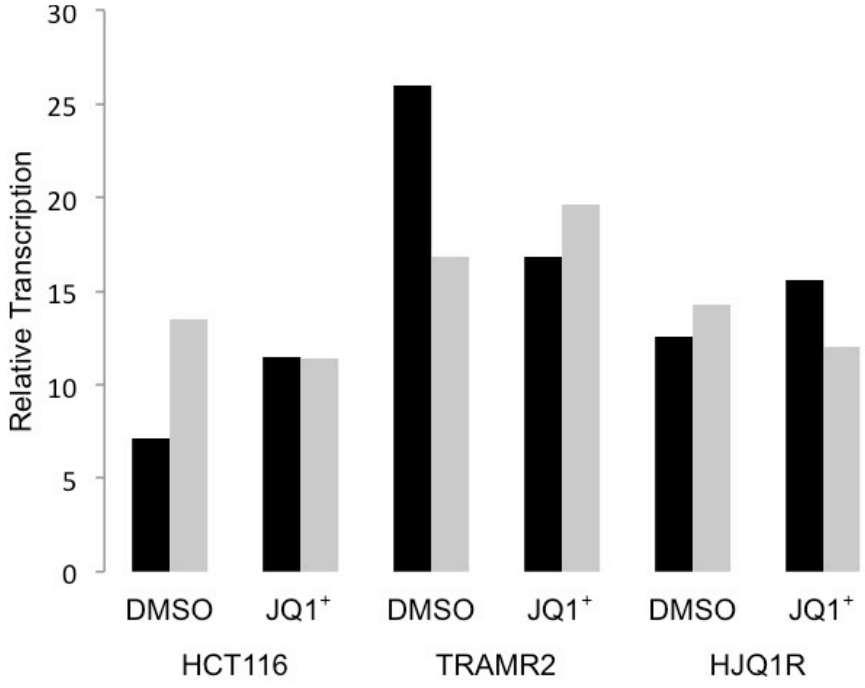

Figure 4.14. Transcriptional response to trametinib resistance. Global transcription levels determined by the incorporation of 5 µl per ml of [5-3H]-uridine within 30 minutes. HCT116, TRAMR, and HJQ1R were treated with DMSO or 1 µM JQ1$^{+/-}$ for 24 hours prior to [5-3H]-uridine exposure (n = 3 technical replicates). RNA was purified and incorporation determined via scintillation counting (n = 2).

HP1 proteins have been associated with RNA at pericentric heterochromatin, and are known to have a non-specific RNA binding site. To determine if global transcription levels were affected by JQ1 or resistance the incorporation of tritiated thymidine was assayed. 5 μ l [^{3}H]-Thymidine was added per ml of media for each sample for 30 min to allow incorporation into RNA polymerase transcripts. Purified RNA was added to scintillant and measured on a scintillation counter (**Figure 4.14**). While biological replicates showed some variation, there was no consistent effect of JQ1 on global transcription in any cell type, for this short period of time. Untreated HJQ1R cells showed a minor increase (30%) in global transcription levels compared to HCT116 cells, however given the variation in untreated HCT116, this was not likely to be significant. Untreated TRAMR cells in contrast have a 2-fold increase in global transcription levels. This suggests that in addition to elevated Brd2 and 7sk levels (**Figure 4.12**), there is a significant but subtle global change in transcriptional regulation after acquiring trametinib resistance.

4.5 Discussion

Epithelial to mesenchymal transitions (EMT) are driven by specific transcription factors SNAIL and TWIST, and typified by the loss of E-cadherin (Cano *et al.*, 2000; Yang *et al.*, 2004). Rapid development of acquired resistance to MAPK inhibitors is associated with an EMT-like transition across tumour types (Byeon *et al.*, 2017; Kitai and Ebi, 2017) and EMT tumour progression is known to result in genome wide chromatin reorganisation. This chromatin reprogramming encompasses distinct alterations of H3K9 methylation and HP1 binding to heterochromatin (McDonald *et al.*, 2011; Millanes-Romero *et al.*, 2013). Therefore, the inhibitors identified as modulating synthetic heterochromatic domains (**Table 3.1**), were investigated within a MAPK inhibitor resistant model system.

The initial studies characterising the altered phenotype to prolonged MEK inhibition (**Figure 4.1**) demonstrated that this *in vitro* cell line model mirrored the patient phenotype for overexpression/hyperphosphorylation of the Raf/Ras/MEK/ERK pathway (Montagut *et al.*, 2008; Long *et al.*, 2014). Trametinib resistance resulted in more invasive cells and basal levels of ERK phosphorylation were upregulated, whilst the adaptive signalling response was tempered in trametinib resistant cells (**Table 4.1**).

To determine if drugs could modulate pathways associated with an EMT-like transition to a drug resistant state, they were screened in a dose-matrix combination with MEK inhibitor trametinib (**Figure 4.2**). Two specific kinase inhibitors of PLK and Aurora B (**Figure 4.3**) were identified as having an altered phenotypic effect in MEKi resistant cells. PLK, a known regulator of chromosome segregation correlates with tumour grade and invasiveness across Ras driven tumours (X. G. Zhang *et al.*, 2012; W. Sun *et al.*, 2014) and the elevated sensitivity towards PLK inhibition suggests increased dependence on PLK in MEKi resistant cells. PLK is also a downstream effector of Akt driven EMT, while hyperphosphorylation of Ras has been linked to Akt crossover activation (Carracedo and Pandolfi, 2008; Cai *et al.*, 2016; Ferrarotto *et al.*, 2017). The antagonism between GW843682X and trametinib however suggests that trametinib promotion of EMT and acquired MEKi resistance is not dependent on PLK phosphorylation.

Aurora kinases also plays a key role in chromosome segregation during mitosis, with Aurora A being implicated in activating EMT (D'Assoro *et al.*, 2014). Increased sensitivity to Aurora A/B inhibition by ZM447439 as a single agent in TRAMR cells is therefore expected. Additionally the weak synergism with trametinib treatment is likely due to the direct activation of Aurora A by MAPK signalling previously reported, further demonstrating the dependence of EMT and heterochromatin regulation in acquired drug resistance (Wan *et al.*, 2008).

Three epigenetic target classes (EZH2, L3MBTL, and BET) from the inhibitor panel (**Table 3.1)** also had altered sensitivity in TRAMR cells. UNC642, a potent inhibitor of G9a/GLP methyltransferases was more sensitive as a single agent in resistant cells, but had significant antagonism with MEK inhibition (**Figur**e **4.3**). G9a/GLP are responsible for H3K9 mono- and di-methylation. These histone modifications are thought to regulate the formation of facultative heterochromatin and gene silencing via HP1 recruitment (Ogawa *et al.*, 2002; Lyons *et al.*, 2014). G9a has previously been associated with EMT-like phenotype by interacting with SNAIL in MAPK driven tumours (Dong *et al.*, 2012). This suggests that G9a/GLP inhibition would be synergistic with trametinib. However, G9a has been identified as a direct regulator of Sprouty4 which in turn negatively regulates MAPK signalling and the mesenchymal phenotype (Taniguchi *et al.*, 2009; Hua *et al.*, 2014). This regulation is likely to contribute to large antagonistic effect with G9a/GLP-MEK combinations.

The EZH2 inhibitor, GSK343, demonstrated a weak increase in response to treatment in TRAMR at high concentrations only (**Figure 4.4 B**). Equally, in combination with trametinib it showed a weak antagonistic effect. UNC699, an inhibitor of the PRC1 subunit, L3MBTL, showed a large increase in response to treatment as a single agent at low dosage, by contrast. However, UNC 699 was also antagonistic in combination with trametinib (**Figure 4.4 D**). As discussed previously, canonical and atypical PRC1 complexes have been linked with driving EMT and repressing MAPK signalling, demonstrating its dual role and subsequently antagonism with MEK inhibition (Kassis and Brown, 2012; Santanach *et al.*, 2017).

BET protein inhibitors were also identified as having increased sensitivity in TRAMR cells (**Figure 4.5**) and were antagonistic in combination with trametinib. Recent studies have demonstrated that RTK-driven cancers' resistance mechanism converge on MYC activation supporting this result (Ma *et al.*, 2017; Singleton *et al.*, 2017; Zawistowski *et al.*, 2017). These studies also present evidence that MEK inhibition is enhanced with the addition of JQ1, however they did not comprehensively analyse the synergism of the combinations. While BET-MEK combination therapy may not be synergistic, the additive effects presented in these studies and ability to resensitise MEKi resistance was demonstrated at higher trametinib concentrations (Figure **4.8**). Singleton, *et al* (2017) and Zawistowski, *et al* (2017) studies were also performed on *in vivo* models over prolonged treatment which would accentuate any cytostatic effects of the combination. This was not be identified with the combination matrixes analysed in **figure 4.5** or **figure 4.8** which were performed over 24-48 hours treatment but these studies do, however, validate findings that BET inhibition has altered effects in cells that have adaptive resistance to MAPK inhibition.

Variations in sensitivity towards different BET inhibitors gave an indication of which BET proteins had the dominant effect on acquired resistance (**Figure 4.5** and **4.7**). The results shown here suggest that selectivity towards Brd2 influenced cell survival. However Brd4 nuclear distribution was significantly altered after JQ1 treatment in TRAMR cells, with increased association with distinct loci at the periphery (**Figure 4.10**). No clear change in Brd2 pattern was observed (data not shown), suggesting that the change in Brd4 distribution occurs with general loss of Brd2. This interplay between Brd2 and Brd4 supports the current studies indicating a partial overlap in function (Cheung *et al.*, 2017). Recent studies have also indicated that isoform

switching between Brd2 and Brd4 drives lineage specific differentiation (Fernandez‐Alonso *et al.*, 2017). Cell cycle analysis showed no difference between HCT116 and TRAMR cells suggesting that the atypical Brd4 distribution was not due to mitotic defects (**Figure 4.9**). The potential role of Brd2 was further linked to this response, attributable to its elevated transcription in TRAMR cells. Supporting the recent studies indicating MYC-driven resistance to MAPK inhibition, c-myc was also elevated in TRAMR cells; elevated levels of c-myc and Brd2 are both lost upon JQ1 treatment. Brd3 and Brd4 levels remained unchanged further implicating Brd2 as the driver of JQ1 sensitivity. Consistently, loss of Brd2 transcripts also translates to protein levels (**Figure 4.13**).

Intriguingly, HP1 isoform levels were significantly altered by acquiring trametinib resistance and JQ1 treatment. Untreated TRAMR cells had significantly increased abundance of nuclear HP1α and HP1γ (**Figure 4.13**) but JQ1 treatment caused significant reductions in all HP1 isoforms. This suggests that BET proteins play a significant role in regulating HP1 transcription and consistently in cells resistant to JQ1 treatment these changes to BET and HP1 proteins were broadly reversed, providing further

evidence of BET protein regulation in switching of phenotypic states.

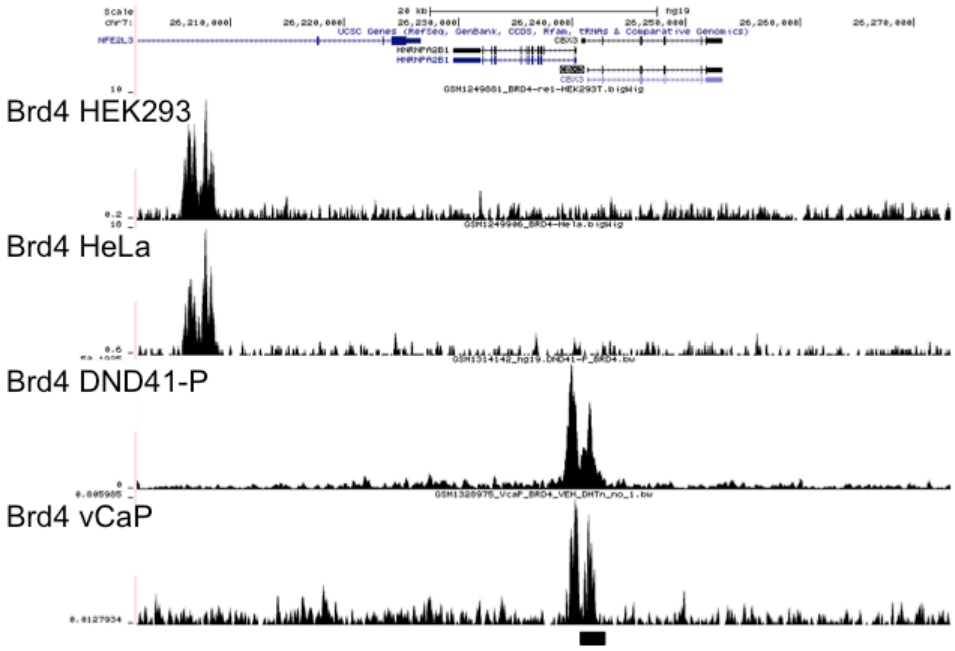

Figure 4.15. BET proteins distribution at HP1 promoters. Brd4 ChIP-seq tracts from Asangani (2014), W. Liu (2013), and Knoechel (2014) on epithelial cell lines HEK292 and HeLa compared to mesenchymal drug resistant prostrate cell line VCaP and T-ALL cell line DND41-persistors. Black bar highlights the promoter region of HP1γ.

Comparison of publically available Brd4 ChIP-seq data sets further supports this position. Epithelial cell lines HEK293 and HeLa (W. Liu *et al.*, 2013) lack Brd4 binding at HP1 promoters while mesenchymal and drug resistant DND-41 and vCaP cells (Asangani *et al.*, 2014; Knoechel *et al.*, 2014) have distinct Brd4 peaks over HP1 promoters (**Figure 4.15**). JQ1 treatment of the castration resistant VCAP cells resulted in a significant decrease in Brd2 occupancy over HP1 promoters when compared to Brd3 and Brd4, further suggesting a Brd2 specific role in acquired MAPK resistance (**Figure 4.16**).

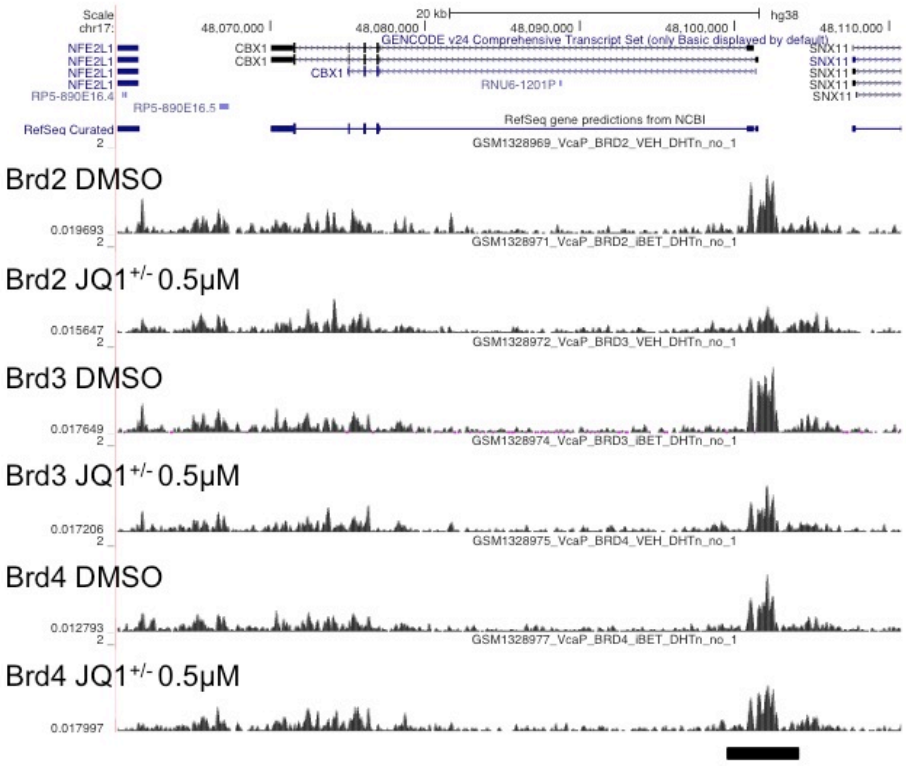

Figure 4.16. BET chromatin binding at HP1 promoters with JQ1 treatment. ChIP-seq tracts from Asangani (2014), depicting Castration resistant mesenchymal prostate cancer cells VCaP. VCaP cells were treated with DMSO or 0.5 μM JQ1$^{+/-}$ and immune-precipitated for Brd2, Brd3, and Brd4. HP1β gene CBX1 shows reduced BET protein occupancy after JQ1$^{+/-}$ treatment, representative of the HP1 family. Black bar highlighting HP1β promoter.

Together the results shown here further support the concept that relates EMT-like phenotypes with acquired MAPK inhibitor resistance, and the identification of BET proteins as a potential therapeutic agent to resistant cell types. Additionally, this work suggests that BET proteins are associated with heterochromatin regulation in acquired MAPKi resistance. There is evidence suggesting that Brd2 drives BET proteins function at heterochromatin. This could be indirect via regulating HP1 transcription or direct by TIP60 mediated recruitment to pericentric repeats (Grézy *et al.*, 2016). Although the regulation of pericentric heterochromatin, is not well understood, TIP60 is known to acetylate H4K12 at satellite repeats, recruiting Brd2 to maintain chromatin compaction and suppress transcription, while loss of Brd2 association via BET inhibition leads to aberrant satellite expression that could explain the Brd4 punctate recruitment to the nuclear periphery (**Figure 4.10**). Investigations of heterochromatin compaction and its impact on cellular phenotype will provide an exciting avenue of future research.

Chapter 5: The role of H3K9me3 in heterochromatin regulation

5.1 Introduction

A well-defined model of constitutive heterochromatin is mouse embryonic stem cells (mESCs). Mouse centric and pericentric heterochromatin is easily visualised by DNA staining, as it co-locates to form chromocenters unlike most primate cells. Pericentromeric regions are comprised of A-T rich repetitive elements such as minor and major satellites in mouse cells; major satellites form large arrays of a 234 bp core monomer (Vissel and Choo, 1989), whilst minor satellite forms a 120 bp repeat. Due to the role of centromeric chromatin in correct kinetochore assembly, chromatin abnormalities in constitutive heterochromatin can lead to mitotic defects (Ekwall *et al.*, 1997). In *Drosophila* and mammalian cells constitutive heterochromatin also spreads to adjacent euchromatic regions mediating transcriptional suppression (Muller, H, 1930) and position effect variegation. The constitutive heterochromatin at these suppressive regions of variegation are characterised by DNA methylation, general hypoacetylation, H3K9 methylation and association of HP1 proteins (James and Elgin, 1986; Jeppesen *et al.*, 1992; Jeanpierre *et al.*, 1993; Peters *et al.*, 2001).

The interplay between HP1 proteins, H3K9me3, and Suv39h1/2 methyltransferases has been extensively studied at constitutive heterochromatic regions. HP1 isoforms are highly conserved across species from Swi6 in *S. pombe* to HP1α/β/γ in mammalian cells (Singh *et al.*, 1991). HP1 proteins are regulators of gene expression by position-effect variegation (Eissenberg *et al.*, 1990). Although they do present some variation in their distribution (Minc, Courvalin and Buendia, 2000; Nielsen *et al.*, 2001), the differential functions of the HP1 isoforms have yet to be fully elucidated. The HP1 protein encodes a chromo domain that facilitates its binding to H3K9me3 (Jacobs and Khorasanizadeh, 2002; Nielsen *et al.*, 2002) in a process that requires dimerisation of HP1 proteins via its chromoshadow domain (Cowieson *et al.*, 2000; Sadaie *et al.*, 2008). Subsequent studies on the *S.pombe* HP1 homologue Swi6 suggest that proximity of two H3K9me3 enables two HP1 proteins to tetramerise on a nucleosome which, in addition to the formation of homodimers, enables oligomerisation of HP1 across large H3K9me3 domains facilitating heterochromatin propagation (Canzio *et al.*, 2011).

The disordered hinge region of HP1 proteins is the least conserved and has been shown to interact with both RNA and DNA (Meehan, Kao and Pennings, 2003; Keller *et al.*, 2012). As RNase treatment triggers the dissociation of HP1 from heterochromatin (Maison, Bailly, Peters, J.-P. Quivy, *et al.*, 2002) it suggests an RNA component to HP1 recruitment or stabilisation. In *S.pombe* DICER mediated RNAi produces short transcripts from pericentric regions that stabilise the recruitment of HP1 proteins, while in humans lncRNA TERRA has been implicated in HP1 recruitment to telomeric constitutive heterochromatin, however a similar mechanism at pericentric heterochromatin has yet to be found (Arnoult, Van Beneden and Decottignies, 2012; Keller *et al.*, 2013).

HP1 canonical recruitment to heterochromatin is driven by Suv39 histone methyltransferase through the deposition of H3K9me3. This was proposed when Suv39h double null knockout fibroblast cells showed a loss of H3K9me3 and HP1 from heterochromatin (Lachner *et al.*, 2001). However, HP1 affinity for trimethylated H3K9 is particularly low suggesting that additional factors are directly involved in its recruitment (Jacobs and Khorasanizadeh, 2002). This is further supported by studies on the X-chromosome where inactivation leads to H3K9me3 deposition but not HP1 recruitment (Chadwick and Willard, 2003), but to complicate the picture Suv39h1 and Suv39h2 have also been implicated in directly recruiting HP1 proteins (Hall *et al.*, 2002). Due to the cooperativity between H3K9me3 deposition, HP1 and Suv39h recruitment, recent studies have focused on identifying the causal seeding event on unmethylated H3K9 domains.

Suv39h methyltransferases contain an N-terminal chromodomain and a C-terminal SET domain (Horita *et al.*, 2001; Min *et al.*, 2002) which are highly conserved across species and protein classes. SET domains are catalytic sites for S-adenyl-methionine (SAM) mediated methylation (Trievel *et al.*, 2002). whereas chromodomains were identified as a consensus motif between polycomb and HP1 proteins in *drosophila* (Paro and Hogness, 1991). Site directed mutagenesis experiments showed that these chromodomains functioned in gene repression (Messmer, Franke and Paro, 1992). This was confirmed by *in vitro* studies demonstrating their reactivity towards di- and tri-methylated lysines (Hughes *et al.*, 2007). Suv39h chromodomains however are more specific towards trimethylated states (Schalch *et al.*, 2009). This specificity however suggests that Suv39h chromodomain is not involved in its recruitment for *de novo* heterochromatin formation.

Given that RNase treatment leads to loss of the H3K9me3/HP1/Suv39h complex from heterochromatin, back to back studies in eLife suggested that recruitment of Suv39h enzymes can be mediated by RNA (Johnson *et al.*, 2017; Shirai *et al.*, 2017; Velazquez Camacho *et al.*, 2017). However, these studies do not completely validate each others' findings. They present conflicting data around the specificity of Suv39h binding to specific RNA transcripts and general RNA/DNA binding affinity. Despite the controversial claims of these studies, they do provide strong evidence for a direct interaction between Suv39h and nucleic acids, and that pericentric transcripts can associate with local chromatin and concentrations correlate with Suv39h association.

In addition to RNA and H3K9me3, HP1 SUMOylation has been implicated in regulating RNA associated *de novo* heterochromatin formation and maintenance (Shin *et al.*, 2005). Maison *et al.* (2011) demonstrated that HP1 proteins are only associated with major satellite RNA transcripts when SUMOylated at the hinge region, and that this only occurs at low levels (>1%) *in vivo*. In Suv39h double null mouse cells, constitutively SUMOylated HP1α, HP1 was weakly associated with the pericentromere despite the lack of its binding partners H3K9me3 and Suv39h. However the exact method of *de novo* chromatin recruitment remains elusive, with recent evidence implicating Suv39h as recruiting Ubc9 to SUMOylate HP1 proteins (Maison *et al.*, 2016). While SUMOylated HP1 proteins are chromatin associated at *de novo* heterochromatin sites, the SUMO protease SENP7 is required to maintain HP1 enrichment across established heterochromatin domains by reducing its mobility (Maison *et al.*, 2012). SENP7 has two HP1 binding motifs that have been suggested to recruit SENP7 to sites of oligomeric HP1 in contrast to *de novo* HP1 recruitment, demonstrating how SUMOylation is removed from established heterochromatin (Romeo *et al.*, 2015).

The interplay between H3K9me3, Suv39h, and HP1 in their binding of chromatin is complex; Suv39h double null cells also lose H4K20me3 and DNA methylation while presenting chromosome instability with increased tumour risk in mice (Peters *et al.*, 2001). Knock out of DNA methylation enzymes by contrast does not result in the loss of Suv39h mediated H3K9me3 or chromatin compaction, implying that Suv39h is the master determinant of hertochromatin modifications (Martens *et al.*, 2005; Gilbert, Thomson, Boyle, Allan, Ramsahoye and Wendy A Bickmore, 2007). Despite an absence of extensive epigenetic marks Suv39-/-mice cells still form cytological chromocenters, questioning the perceived role of histone

modifications and their binding partners in being able to regulate the compaction state of the underlying chromatin. Therefore, before investigating the role of histone modifiers such as BET inhibitors on HP1 proteins and chromatin compaction, the regulators of chromatin compaction need to be further characterised.

5.2 Characterising the chromatin state of Suv39h double null mESC's

To maintain mouse embryonic stem cells in an undifferentiated state, different growing conditions were first analysed (**Figure 5.1**). mESCs were grown on gelatin coated Corning orange capped flasks and yellow capped Sarstedt cell+flasks for sensitive adherent cell types . 10X magnification bright field images show that growth in yellow capped flasks resulted in more round distinct colonies, similar to the morphology of ES cells grown in 2i medium (information from Richard Meehan lab). This was regardless of Suv39h phenotype (**Figure 5.1, A**). Transcription of key pluripotency factors Nanog and Oct4 were then analysed by qPCR. Nanog and Oct4 levels were elevated in the orange capped Corning flasks indicative of increased stem cell characteristics (Chambers *et al.*, 2003; Niwa, Miyazaki and Smith, 2016) (**Figure 5.1, B**). Therefore cells were grown on gelatinised corning flasks for cell line maintenance.

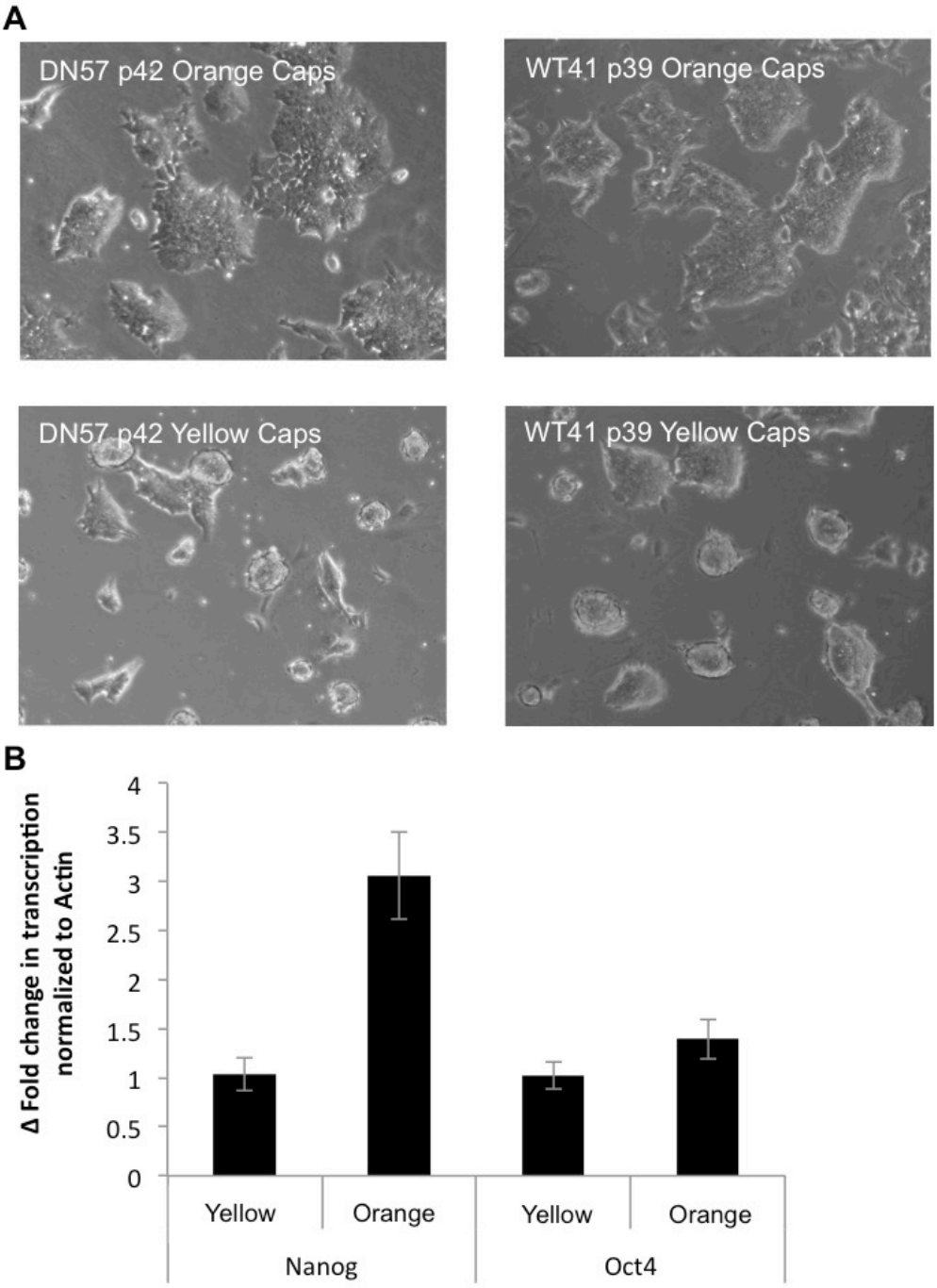

Figure 5.1. Mouse embryonic stem cell phenotype. (A) 10X bright field images of mouse ESC colonies from wild type [WT41] and Suv39h1/2 double knockout cells [DN57]. "Orange Caps" are Corning CellStar flasks manually coated in 0.1% gelatin for 5 minutes, "Yellow Caps" are Sarsted Cell+ pre-coated flasks. **(B)** RNA from mESC's was harvested using an RNeasy kit and cDNA libraries prepared. QPCR for stem cell factors Nanog and Oct4, normalized to actin for cells grown on Corning orange capped flasks coated in gelatin and Sarstedt Cell+ yellow capped pre-coated flasks. Error bars = SEM of biological replicates (n=3).

To analyse the effect of Suv39h1 and Suv39h2 double knock out (DN57) on heterochromatic makers in ES cells, nuclei were isolated and analysed by western blotting compared to wild-type cells (WT41) (**Figure 5.2**). Double null cells (DN57) showed a 20% decrease in H4K20me3 and a significant increase in mono-methylation. This supports evidence linking Suv39h regulation of H4K20me3 at the pericentromere (Peters *et al.*, 2001; Yang *et al.*, 2008). H3K27me3 was also elevated in the knockout cells at the expense of H3K27me2. This suggests that polycomb activity is increased in the absence of Suv39h. Intriguingly, repressive H3K9 di- and tri-methylation were not completely lost. This suggests some redundancy with other methyltransferases at least on a global scale. HP1α and HP1β levels, were also reduced, possibly as a feedback from their disassociation from chromatin. Together these data suggest that Suv39 double knockout mESCs mimic phenotypes described previously (Peters *et al.*, 2001).

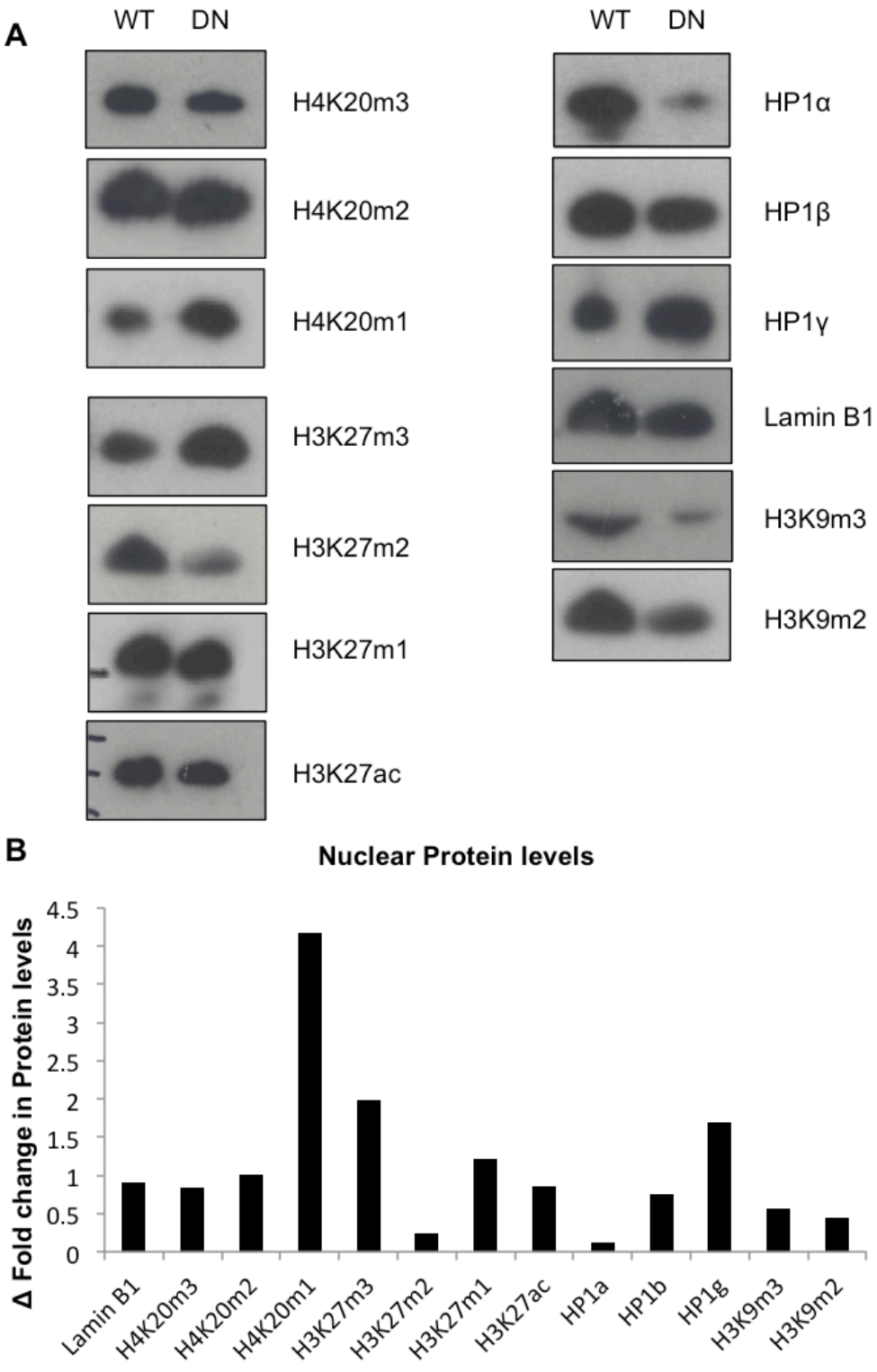

Figure 5.2. Heterochromatic histone modifications response to Suv39h1/2 loss. (A) Nuclei were isolated and protein lysates prepared from WT41 and DN57 mouse ES cells. Samples were run on a 4-12% Bis-Tris Nupage gel and western blots performed for multiple heterochromatin components. **(B)** Densitometry quantification of the blots. Results show the relative levels of DN57 to WT41 samples.

As global levels of H3K9me3 and H4K20me3 were not completely lost in the double knockout cell lines, immune-fluorescence was used to determine their nuclear distribution **(Figure 5.3**). Both H3K9me3 and H4K20me3 signal in wild type cells were concentrated at chromocentres as visualised by DAPI staining and this was lost in the knock out cell lines.

To investigate changes in chromatin compaction at the level of the 30-nm chromatin fibre after loss of Suv39h, chromatin was analysed by sucrose gradient sedimentation and Southern blotting (**Figure 5.4**). This technique was used previously to measure compaction in a Dnmt3a/b null background (Gilbert *et al*, 2007). Nuclei were first isolated from the cells and digested with RNase A/T1 and micrococcal nuclease, in order to release soluble chromatin fibres from the nucleus under physiological salt conditions. In this approach RNase digestion is used to stop nuclear RNAs competing for binding of H1 to chromatin, which would otherwise affect the structure. However, this does have the disadvantage of degrading potential nuclear RNAs that might otherwise affect chromatin structure. In addition, micrococcal nuclease also attacks the 5'phosphodiester backbone of RNA so even in the absence of RNase the enzyme will digest potential chromatin associated RNAs and this might affect conclusions that have been drawn in studies implicating RNA in Suv39h recruitment (Cunningham, 1959; Velazquez Camacho *et al*., 2017). After soluble chromatin is released from the nucleus over-night it is fractionated on an isokinetic sucrose gradient in an ultra-centrifuge.

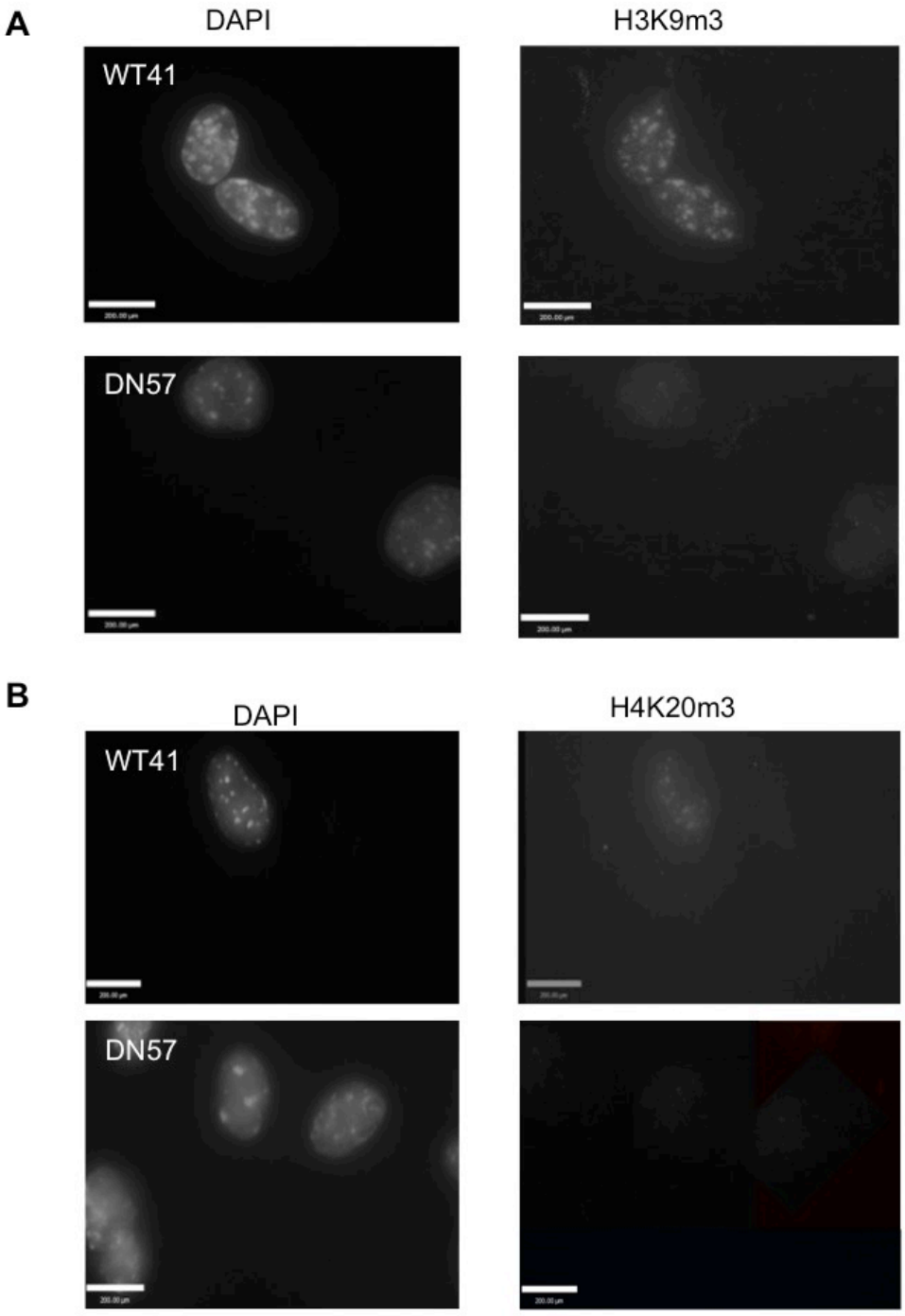

Figure 5.3. Distribution of histone modifications in SUV-/- cells. Wild type (WT41) and Suv39h1/2 knockout (DN57) mouse ES cells imaged for the methylation modifications attributed to Suv39h and Suv420h enzymes (H3K9me3, and H4K20me3). **(A)** images of DAPI and H3K9me3 immunofluorescence **(B)** Images of DAPI and H4K20me3 immunofluorescence. Scale bar is 20 μm.

The sedimentation rate of chromatin is determined by the fragment size (mass) and its structure. More disrupted chromatin fibres sediment at a slower rate than a more regular compact fibre of the same DNA length due to differences in friction. After sedimentation the gradient is fractionated by upwards displacement while measuring the DNA content via an inline UV spectrometer. Chromatin fibres of the same size (mass) but different compaction states will therefore be in different sucrose gradient fractions. Proteinase K treatment and phenol:chloroform extraction is then used to purify the DNA in each fraction before fractionating the DNA on a 0.7% Tris-phosphate gel at a low voltage to improve resolution (**Figure 5.4, B**).

In order to detect specific DNA regions the gel is Southern blotted onto a membrane and probed with radioactive DNA fragments described in Section 2.8. Essentially the agarose gel is UV nicked on a transilluminator and depurinated using HCl. NaOH treatment is used to induce DNA strand separation to single stranded DNA. Neutral Southern blotting is used to transfer single stranded DNA fragments to a nitrocellulose membrane, and complementary radiolabelled oligonucleotide fragments are used to analyse where individual DNA fragments sediment in the sucrose gradient (**Figure 5.4, C**).

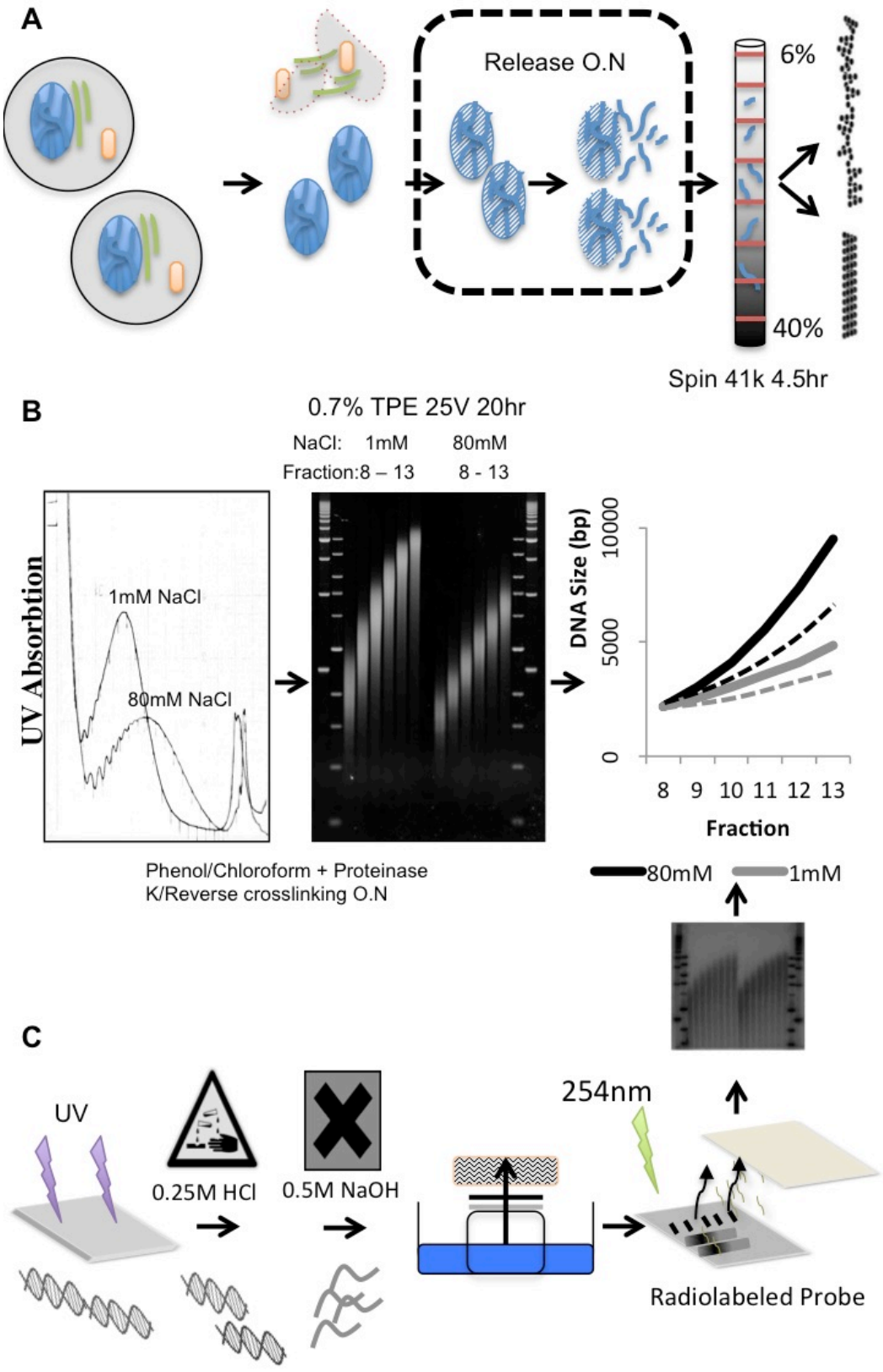
A
Release O.N
6%
40%
Spin 41k 4.5hr
B
0.7% TPE 25V 20hr
NaCl: 1mM 80mM
Fraction:8 – 13 8 - 13
UV Absorbtion
1mM NaCl
80mM NaCl
DNA Size (bp)
10000
5000
0
8 9 10 11 12 13
Fraction
80mM
1mM
Phenol/Chloroform + Proteinase
K/Reverse crosslinking O.N
C
UV
0.25M HCl
0.5M NaOH
254nm
Radiolabeled Probe

Figure 5.4. Sucrose gradient chromatin analysis methodology. Process of isolating chromatin fibers and performing compaction analyses. **(A)** Nuclei are prepared from cells under physiological conditions. Micrococcal nuclease partial digest allows chromatin fragments to be released from the nuclei. This chromatin solution is then spun through an isokinetic sucrose gradient. **(B)** The sucrose gradient is fractionated and passed through a UV spectrometer to determine the DNA content of each fraction. Each fraction undergoes a phenol/chloroform extraction to purify the DNA and run on a 0.7% TPE gel. The maxima intensity for each fraction is used to determine the DNA fragment size for each fraction and plotted to compare samples. **(C)** The DNA gel is treated with UV and HCl to fragment the DNA. Afterwards the gel is treated with NaOH to separate the DNA strands and single stranded DNA is transferred to a nylon membrane by Southern blotting. This membrane is then hybridized to radio labeled DNA probes for heterochromatic repeats and compared to the total DNA fragment position on the gel to assess chromatin compaction.

Gradient fractions containing chromatin fibres ranging from 2.5 kb to 12 kb were compared between wild type (WT41) and Suv39h double null (DN57) mESCs (**Figure 5.5**). As chromatin fibres get longer the number of possible disruptions increases, therefore, increasing the differences in sedimentation between the chromatin fibres. To facilitate a comparison in chromatin structure the sedimentation rate of chromatin fibres at 9 kb were contrasted. By reading across from 9 kb it is apparent that DN57 chromatin is sedimenting more slowly that WT41 chromatin (**Figure 5.5, B**). Reading the graph the other way, the bulk chromatin fragment size at Fraction 17 from WT41 cells was 8588 bp compared to 9328 bp in DN57 cells. This 8.6% discrepancy is a very surprising result that indicates that chromatin fibres in DN57 cells are on average more disrupted across the entire genome.

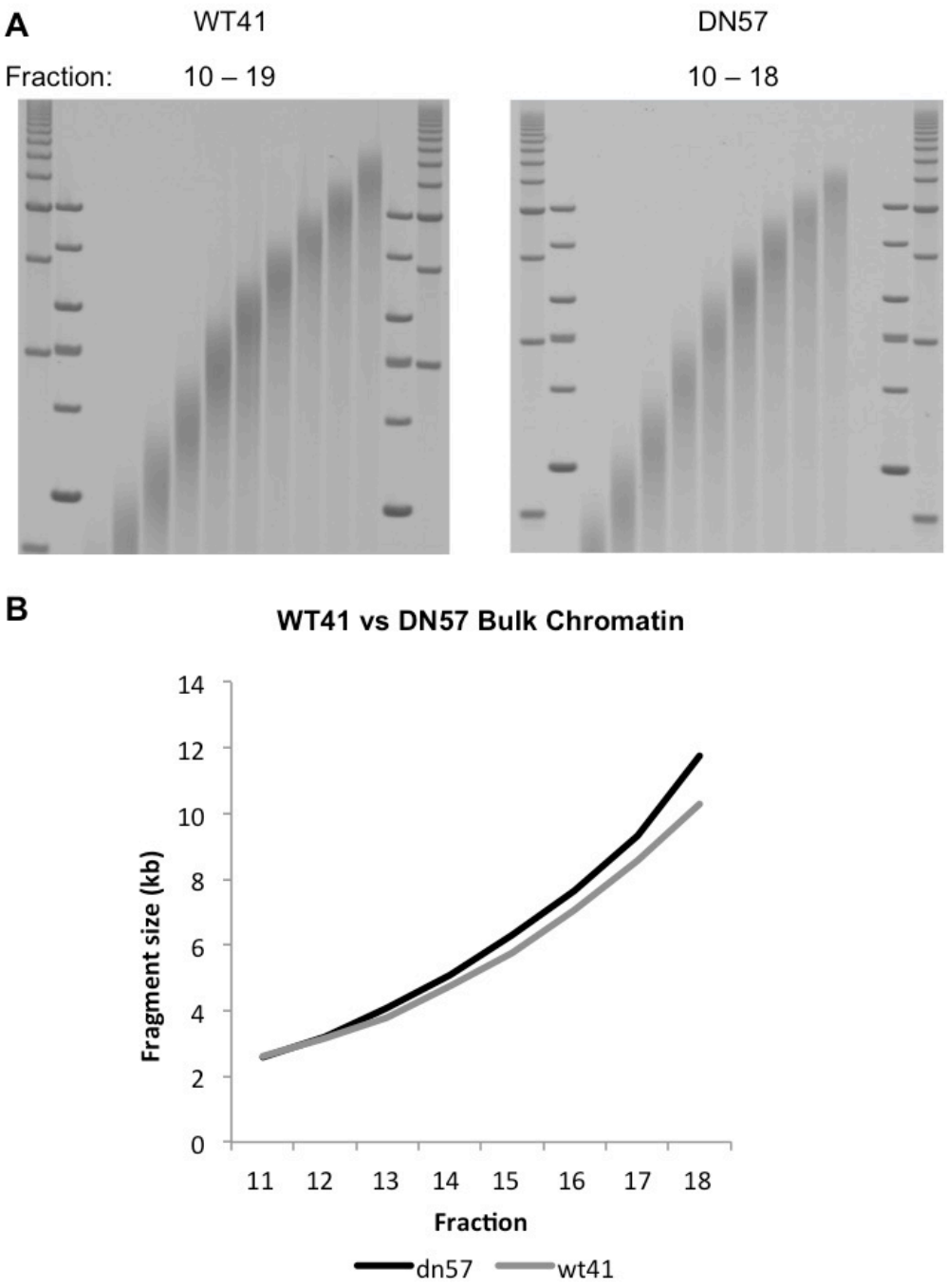

Figure 5.5. Effects of Suv39h1/2 loss of global large scale chromatin structure. Chromatin fibers were prepared from WT41 and DN57 nuclei preps in physiological NaCl conditions (80 mM) and resolved by sucrose sedimentation **(A)** DNA from sucrose gradient fractions were phenol chloroform purified and resolved on a 0.7% TPE gel at 25V for 16 hours. Left image – WT41 cells, Right image – DN57 cells. **(B)** Lane 2D densitometry was used to determine the position of the fraction intensity maxima. Maxima across fractions was plotted and compared between WT41 and DN57 chromatin.

The distribution of signal intensity throughout each lane represents the variation of compaction states in each fraction. The fragment size measurements are determined by the intensity maxima in each lane. In order to determine the effect of Suv39h1/2 knock out on pericentric and centric heterochromatin, fractions from the sucrose gradient were blotted and probed for major and minor satellite (**Figure 5.6**). Regions of constitutive heterochromatin are more compact than bulk chromatin as previously reported (Gilbert and Allan, 2001). This results in similar fragment sizes appearing in different fractions in bulk chromatin compared to heterochromatic regions. Major satellite DNA from WT41 and DN57 cells sediments into fraction 19 with 9624 bp and 10965 bp respectively. Bulk WT41 and DN57 chromatin fragments sedimented into fraction 18 with 9511 bp and 10266 bp sizes by comparison. The change in bulk chromatin sedimentation in DN57 was at similar levels to the previous experiments (7-9%) demonstrating that this change in compaction state is relatively stable. Major Satellite chromatin of similar fragment size (WT41: 9642 bp, DN57: 10965 bp) presents more disrupted sedimentation (13.7% change in 9 kb fragment size) in the Suv39h knockout system, than in bulk chromatin. This could be due to either a global de-compaction to a similar state, therefore accentuated in more compact chromatin regions; or that de-compaction is only occurring in pericentric heterochromatin.

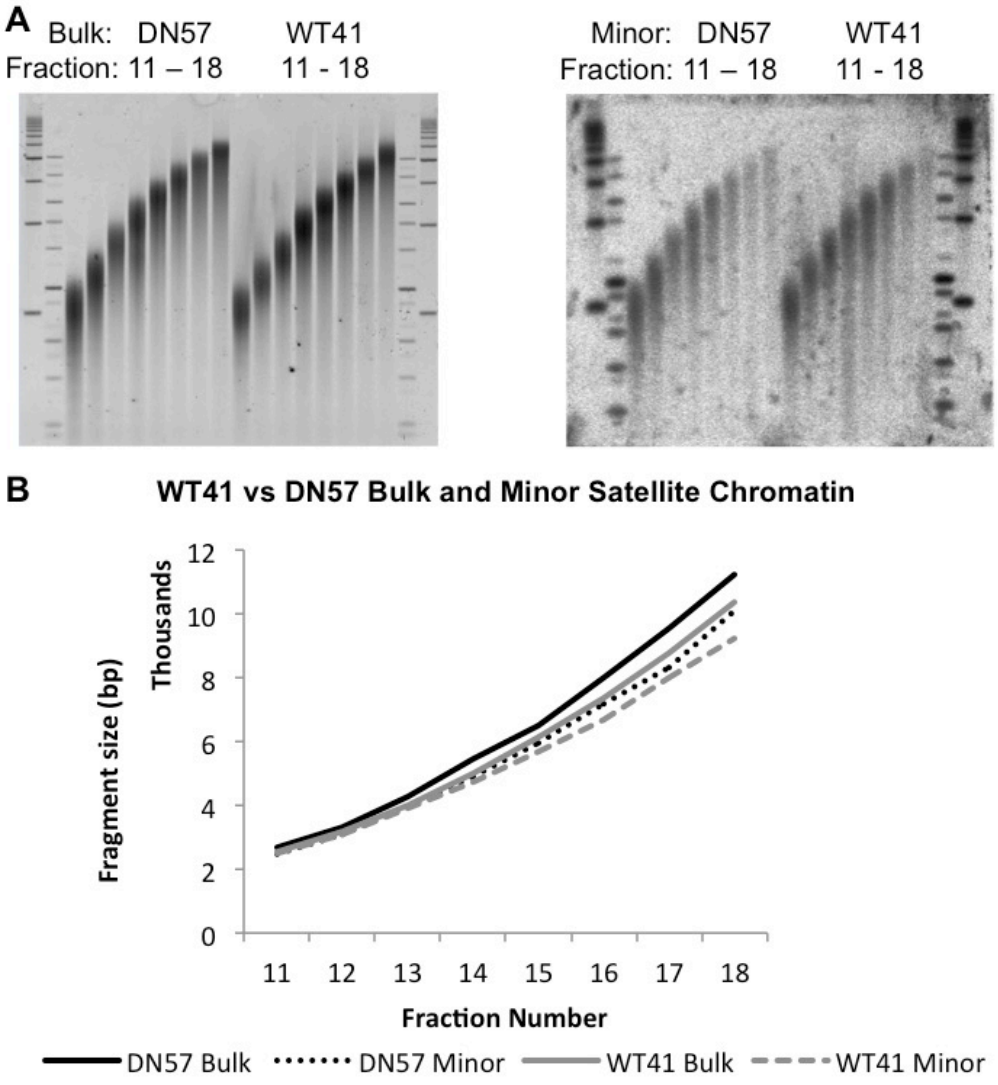
A
Bulk: DN57 WT41
Fraction: 11 – 18 11 - 18
Minor: DN57 WT41
Fraction: 11 – 18 11 - 18
B
WT41 vs DN57 Bulk and Minor Satellite Chromatin
Thousands
Fragment size (bp)
0
2
4
6
8
10
12
11 12 13 14 15 16 17 18
Fraction Number
DN57 Bulk
DN57 Minor
WT41 Bulk
WT41 Minor
C
WT41 vs DN57 Bulk and Major Satellite Chromatin
Thousands
Fragment size (bp)
0
2
4
6
8
10
12
14
11 12 13 14 15 16 17 18 19
Fraction Number
DN57 bulk
DN57 Major
WT41 bulk
WT41 Major

Figure 5.6. Effect of Suv39h1/2 loss on interphase centromere chromatin structure. Chromatin fibers were isolated from WT41 and DN57 nuclei and resolved by sucrose sedimentation. DNA from sucrose gradient fractions were phenol chloroform purified and fractions run on 0.7% TPE gels. Gels were then southern blotted and probed for Major and Minor satellite repeats. **(A)** Images of TPE gels with chromatin fractions from WT41 and DN57 cells. Left – all (Bulk) chromatin. Right – Minor satellite chromatin from southern blot. **(B)** Fraction peak intensity maxima from WT41 and DN57 cells, of total (bulk) chromatin **(C)** Fraction peak intensity maxima from WT41 and DN57 cells, Minor satellite probed chromatin.

To investigate if this was limited to major satellite heterochromatin, chromatin fraction for minor satellite DNA was also radiolabelled (**Figure 5.6**). Again bulk chromatin DNA fragment sizes in DN57 cells was 8.5% larger in fraction 17 (WT41: 8769 bp, DN57: 9523 bp). Minor satellite DNA, similar to major satellite was significantly more de-compacted than bulk in DN57 cells. WT41 cells fraction 18 DNA size was 9222 bp compared to 10353 bp in DN57 cells. This represents a 12.3% shift in DNA fragment size sedimentation of 9 kb chromatin fibres, similar to the 13.7% in major satellite DNA. This suggests that chromatin de-compaction is not limited to specific satellite repeats. Seminal studies by Kit, (1961, 1962) used CsCl gradients to quantify the satellite composition of mouse cells (10%) which has now been validated by sequencing techniques (Komissarov *et al.*, 2011). Given the 10% nuclear abundance of satellite chromatin, if the chromatin de-compaction was limited to satellite repeats in DN57 cells, and then the global effect should be a 10th of major and minor satellite de-compaction. As this is not the evident (Bulk: 7-9%, Major: 13.7%, Minor: 12.3%) this suggests significant chromatin de-compaction at euchromatic regions.

5.3 Investigating Suv39h double null cells global chromatin compaction

Sedimentation rate would be expected to alter if the mass of the chromatin fibre between WT41 and DN57 was different. In order to determine if the histone composition along the chromatin fibres was altered in DN57 cells, a step gradient was utilised to separate chromatin associated proteins (**Figure 5.7**). Chromatin fibres released after micrococcal nuclease treatment were loaded on a 50-10% sucrose step gradient described in Section 2.8.2. This forms a boundary between the two different sucrose concentrations and results in an accumulation of chromatin fibres of all sizes at the sucrose phase boundary. As unbound proteins will not sediment during centrifugation, this allows the separation of proteins bound to chromatin fibres from their soluble nuclear counterparts. Chromatin bound histone proteins were not consistently altered in the DN57 cells compared to wild type (**Figure 5.7 C**). This suggests that histone protein levels are not altered in DN57 chromatin fibres compared to WT41 cells.

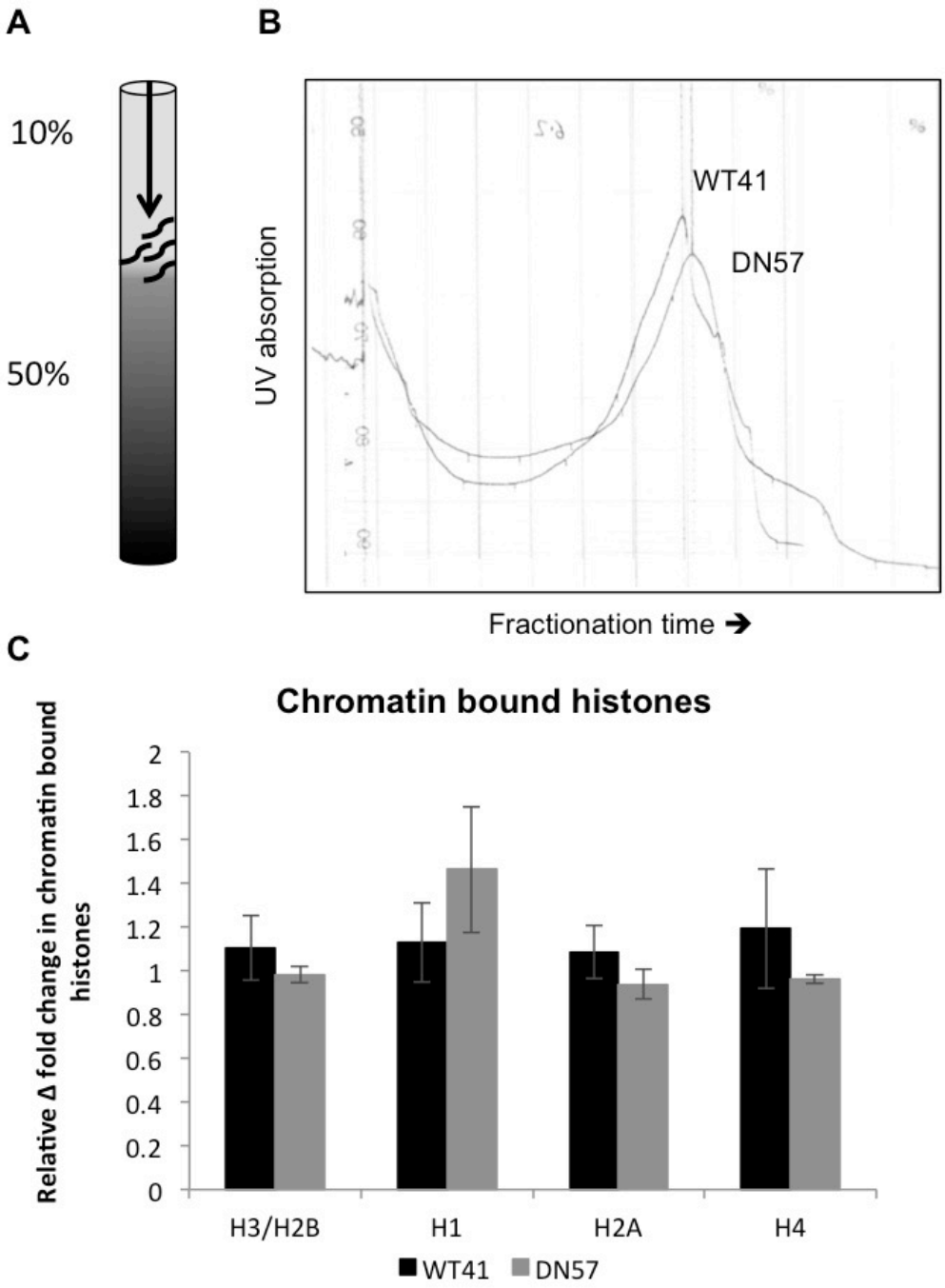

Figure 5.7. Chromatin incorporated histone levels after Suv39h1/2 loss. Chromatin fibers released from WT41 and DN57 were purified by sucrose step gradient sedimentation. **(A)** 10-50% sucrose SW55 step gradient preparation and centrifugation of chromatin fibers. **(B)** UV absorbance traces during the step gradient fractionation process. **(C)** Protein lysates from chromatin containing fractions were resolved on a 10% Bis-Tris Nupage and coomassie stained to visualise histone proteins. Relative 2D densitometry was used to compare chromatin bound histone levels from WT41 and DN57 mES cells.

Chromatin accessibility to nucleases has long been used as a method used to distinguish between chromatin structures (Huebner *et al.,* 1981). A micrococcal nuclease (MNase) timecourse digest was used to determine whether DN57 cells have altered accessibility to their DNA compared to WT41 (**Figure 5.8**). High molecular weight material is digested over time with MNase; DNA is cut between nucleosomes to form shorter nucleosomal fragments. DN57 cells high molecular weight material has accentuated digestion of high molecular weight DNA. Two minutes of MNase treatment reduces high molecular weight material by 18% and four minute treatment resulted in a 19% decrease compared to controls. This suggests that chromatin fibres in DN57 are more accessible to micrococcal nuclease, supporting the sucrose sedimentation experiments indicating that chromatin has a more disrupted or open configuration (**Figure 5.5**).

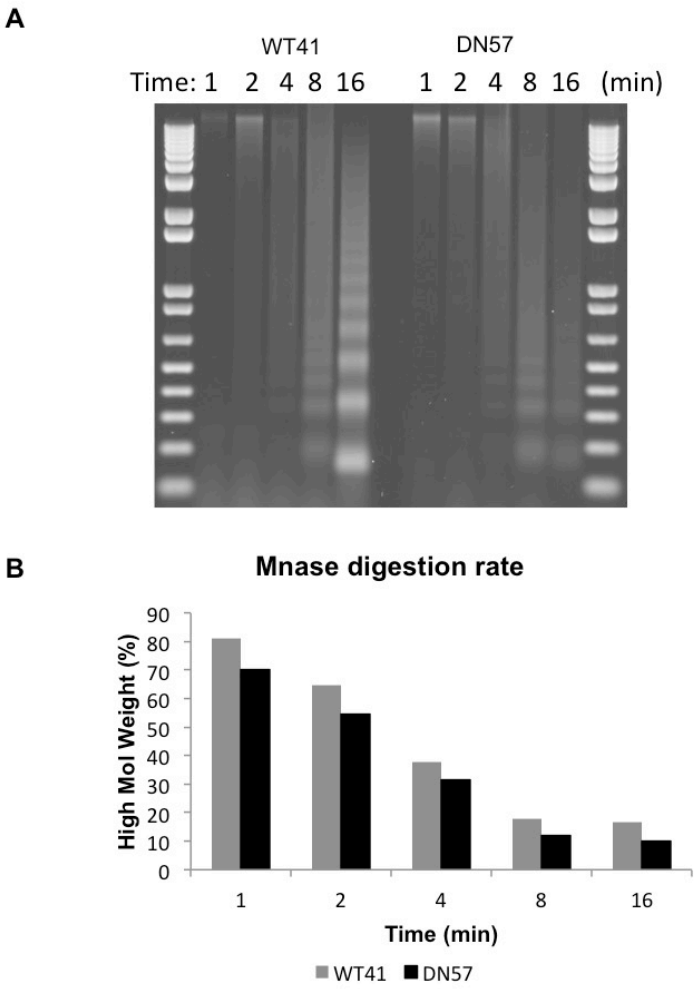

Figure 5.8. Chromatin accessibility with Suv39h1/2 loss. Nuclei were isolated from WT41 and DN57 cells, and a partial MNase digestion time course performed. Digestion was resolved on a 1% acrylamide gel. **(A)** Micrococcal Nuclease digest timecourse of WT41 and DN57 nuclei. 1-16 minutes. **(B)** Percentage of lane total pixel intensity above 4 kb for WT41 and DN57 cells, across 1-16 minutes micrococcal nuclease digest.

However as these mESCs were derived from a single clone, it was important to determine if this change in global compaction was restricted to this specific clone. Therefore, the chromatin compaction of another Suv39h double null clone was analysed. DN72 cells also presented a global change in chromatin compaction (**Figure 5.9**). In fraction 18, DN72 chromatin had an average DNA size of 9390 bp compared with WT41 chromatin DNA size of 8809 bp. This represents a 6.5% shift in DNA fragment size sedimentation in line with similar levels in the DN57 clone (**Figure 5.5**).

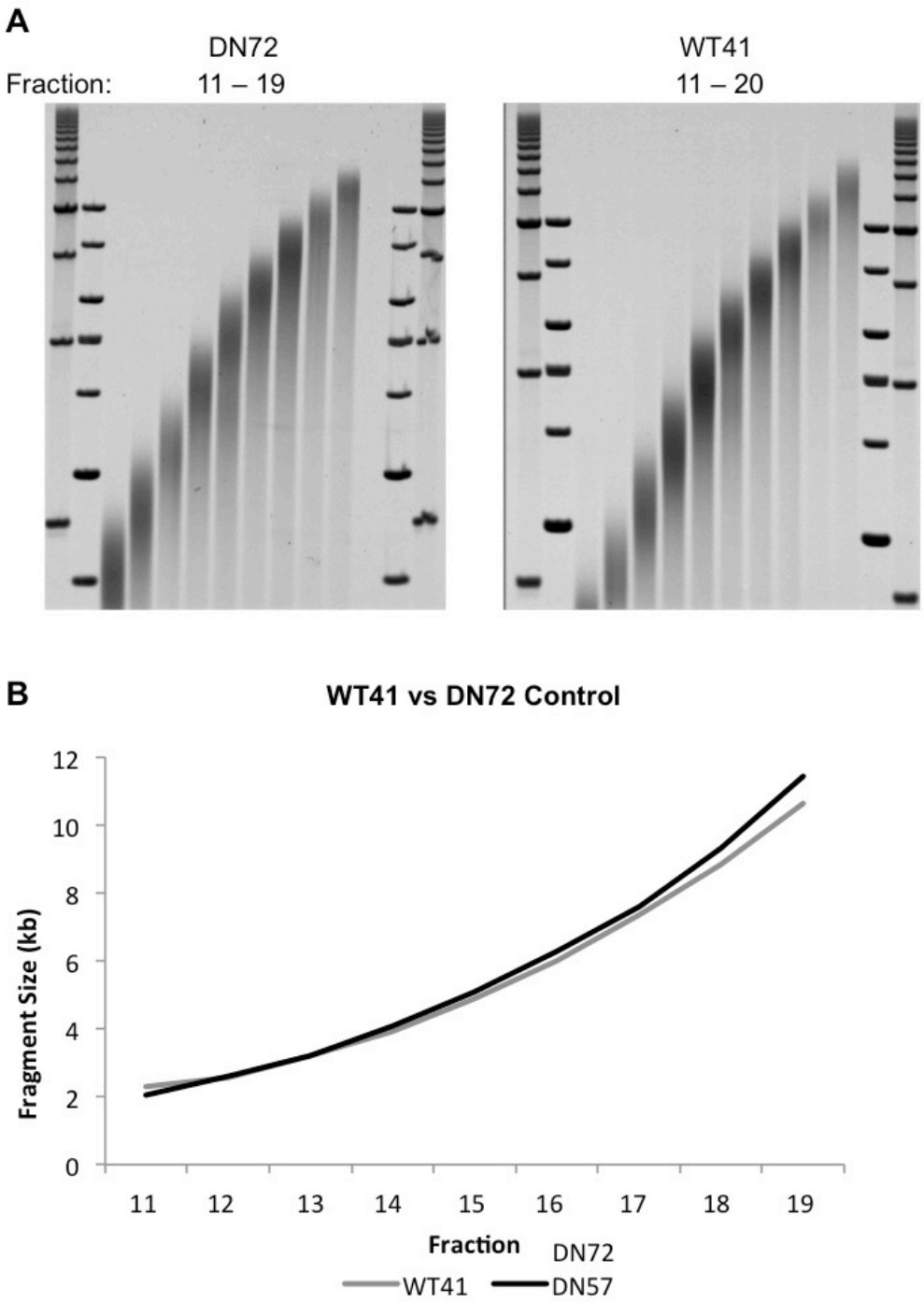

Figure 5.9. Bulk large scale chromatin compaction states of DN72 Suv39h1/2 clone. Chromatin fibers were purified from WT41 and DN72 nuclei and resolved by sucrose sedimentation **(A)** DNA from sucrose gradient fractions was phenol chloroform purified and run on 0.7% TPE gels at 25V for 16 hours. Left – DN72 cells, Right – WT41 cells. **(B)** Comparison of fraction peak maxima determined by 2D densitometry in WT41 and DN72 total (bulk) chromatin.

To determine if the relationship between Suv39h loss and chromatin de-compaction was direct, human Suv39h1 was reinserted into DN72 cells. Suv39h1 was cloned into the pPyCAGASIZ cassette and transfected into DN72 cells for stable expression under internal ribosome entry site (IRES) controlled zeocin resistance. To determine if Suv39h1 was stably expressed after transfections, western blots were used to quantify protein levels (**Figure 5.10, A**). In each DN72 clone selected, Suv39h1 was stably expressed. While exogenous human Suv39h1 was stable in these cells, expression levels were clearly below that of wild type mESCs. Despite the lower re-expression levels of Suv39h1, this was sufficient to recover H3K9me3 at chromocenters (**Figure 5.10, B**) and indicates that exogenous human Suv39h1 was properly recruited to chromocenters and maintained its catalytic activity.

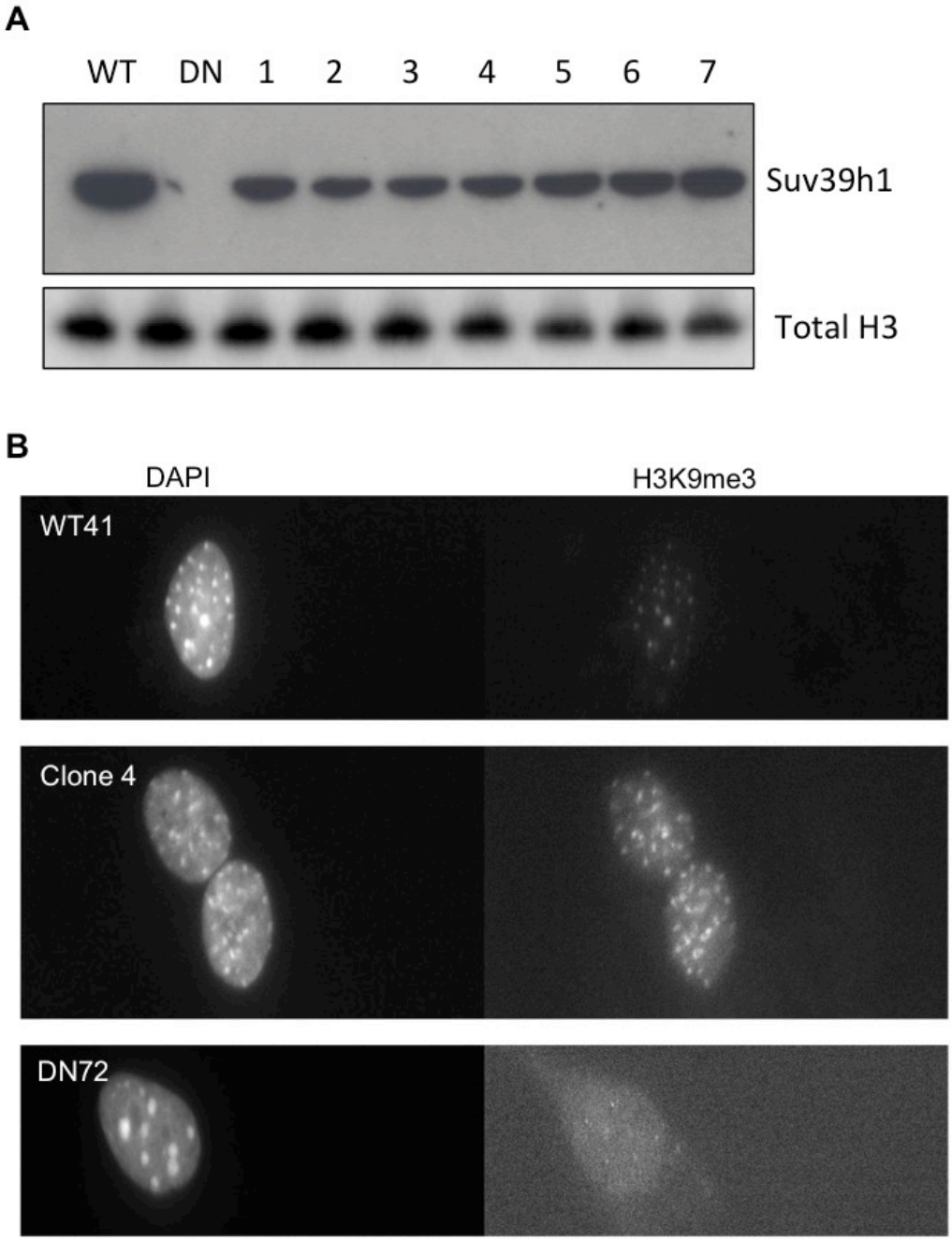

Figure 5.10. Exogenous Suv39h1 expression and restoration of H3K9me3 at constitutive heterochromatin. (A) Western of nuclei protein lysates of Suv39h1 rescue clones from DN72 knock out cells compared to wild type and the DN72 parental cells. **(B)** DAPI and H3K9me3 Immunofluorescence of wild type, Suv39h1/2 knockout cells and a Suv39h1 rescue clone. 100X magnification.

In addition to H3K9me3 deposition, it was important to determine if HP1 is also recruited to chromocenters. Immunofluorescence was used to determine recruitment of HP1α to chromocenters in wild type (WT41), Suv39h double null (DN72) and exogenous Suv39h1 rescued DN72 cells (**Figure 5.11**). HP1α demonstrated distinct recruitment to chromocenters in the majority of Suv39h1 rescued cells. The lack of recruitment in every cell may be indicative of some cells losing the exogenous Suv39h1 construct, or its expression being slightly lower. However, the correct recruitment of HP1α in the majority of Suv39h1 rescued cells, suggest that this is sufficient for correct establishment of the Suv39h/HP1/H3K9me3 complex at constitutive heterochromatin.

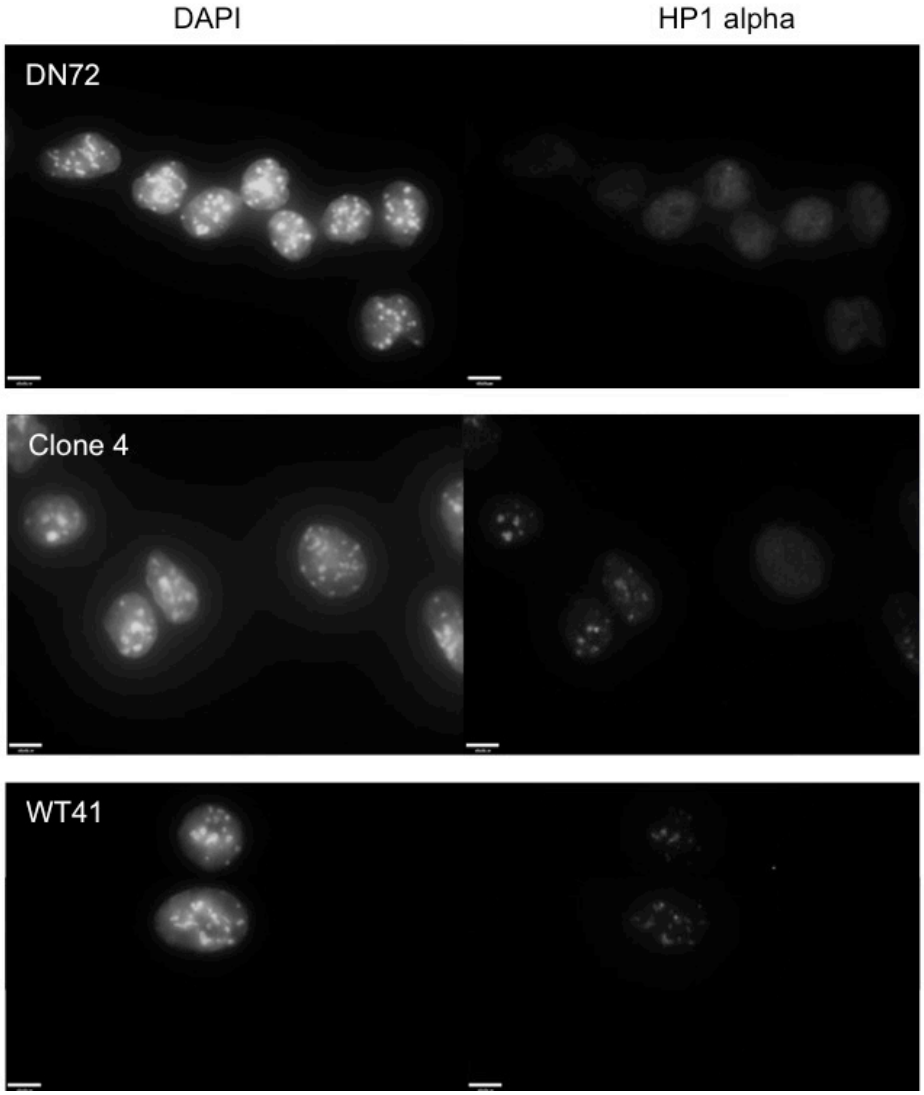

Figure 5.11. Recruitment of HP1α with exogenous Suv39h1 expression. Immunofluorescence of DAPI and HP1 alpha distribution in mES cells. Wild type (WT41), parental Suv39h1/2 knockout cells (DN72) and a daughter Suv39h1 rescue clone (Clone4) were analysed after fixation. 63X magnification. Scale bar is 10 μm.

Chromatin fibre sucrose sedimentation was used to determine if the Suv39h1 re-expression in the DN72 background was sufficient to ablate the global chromatin de-compaction phenotype (**Figure 5.12**). At larger chromatin fragment sizes, DN72R chromatin was more compacted when compared to WT41, completely reversing the original phenotype. At fraction 17, DN72R chromatin was 9067 bp compared while WT41 chromatin was 9487 bp in size. This suggests that DN72R chromatin is 4.4% more compact at this fragment size. This result was repeated (N=2) to validate the altered global compaction state of Suv39h1 rescued mESCs.

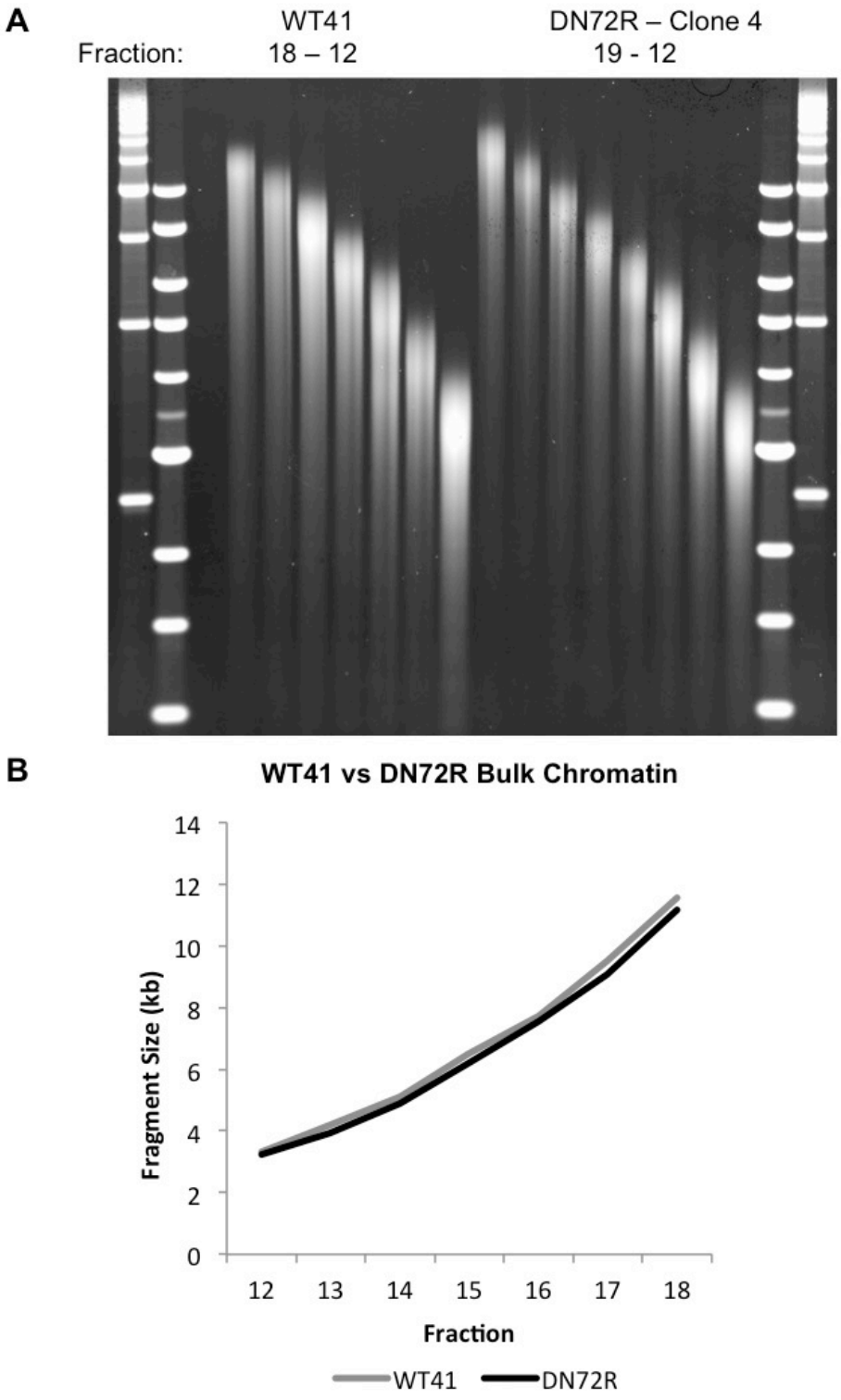

Figure 5.12. Reversal of global decompaction with exogenous Suv39h1 expression. Chromatin fibers were isolated from WT41 and DN72R nuclei and resolved by sucrose sedimentation. **(A)** DNA from sucrose fractions of WT41 and Suv39h1 rescue cells from DN72 parental cells run on a 0.7% TPE gel **(B)** Comparison of fragment intensity maxima from sucrose fractions of WT41 and DN72R chromatin

Given the growing evidence of an RNA component in heterochromatin formation (Maison, Bailly, Peters, J.-P. Quivy, *et al.*, 2002; Maison *et al.*, 2012; Keller *et al.*, 2013), RNA distribution was analysed by EU incorporation (**Figure 5.13**). Cells were treated with 1 mM EU so that the majority of EU transcripts would have EU incorporation. Cells were then washed with CSK buffer in order to remove free non-chromatin associated RNA and proteins from the nucleus and fixed with 4% PFA. A click reaction was used to covalently attach a biotin-azide to EU overnight before immunofluorescence was used to determine chromatin RNA distribution. Neither WT41, DN72, of DN72Rescue cells presented any distinct pattern to their chromatin associated RNA. However, DN72 cells did appear to have an increased intensity of EU-biotin signal.

In order to quantify chromatin bound RNAs, RNA was isolated from each cell line and analysed by dotblot (**Figure 5.14**). Similar to EU immunofluorescence experiments; each cell line was incubated with 1 mM EU overnight to incorporate EU into RNA. Cells were washed to remove non-chromatin bound RNA, before being trypsinised and the nuclei isolated, before further NB.B buffer incubation to remove the nuclear membrane. The Biotin-azide was then clicked onto the RNA overnight at room temperature before samples were normalised to the DNA concentration and spotted onto a nitrocellulose membrane. Avidin-HRP incubation was then used to quantify EU-RNA concentration. DN72 cells showed a 25% increase in chromatin associated RNA when compared to WT41. Additionally, the Suv39h1 rescue cell line had a further 10% reduction in chromatin associated RNA. These results correlate with the chromatin compaction states between the cell lines and suggest that Suv39h/HP1/H3K9me3 heterochromatin recruitment directly affects the global levels of chromatin associated RNA

and chromatin compaction states. While this data demonstrates an altered level of chromatin associated RNA, this does not explain the full de-compaction of chromatin fibres after sucrose sedimentation, as these fibres have be prepared in the presence of RNase and MNase. However, this provides further evidence towards to a regulatory role of chromatin associated RNA in heterochromatin formation and beyond in the genome.

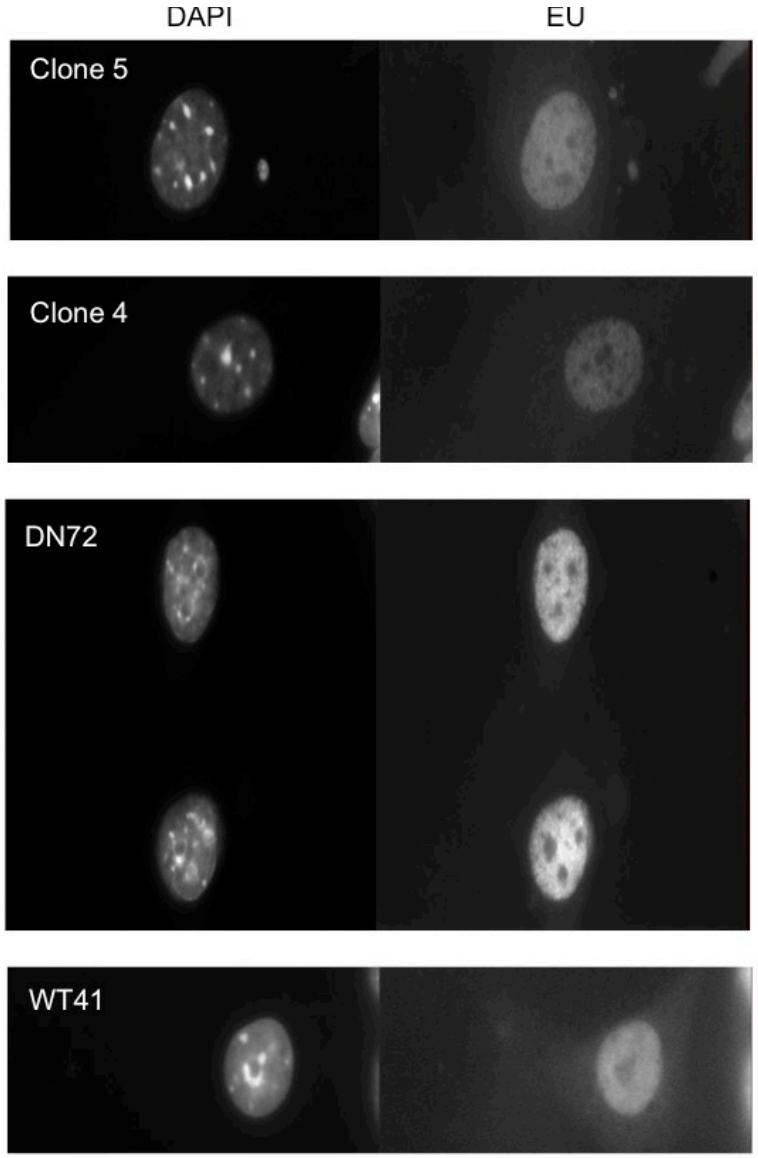

Figure 5.13. Suv39h1/2 loss/rescue and chromatin associated RNA. mES cells treated with 1 mM EU O.N, then washed in CSK buffer and fixed in 4% PFA for 10 minutes, further washed in 0.5% Triton-X for 10 minutes, before click reaction with an azide flourophore and DAPI stained for 3 minutes at room temperature. Chromatin associated RNA was imaged from wild type (WT41), Suv39h1/2 double null (DN72) and human suv39h1 rescue (Clone 4, 5) mouse ES cells. 100X magnification.

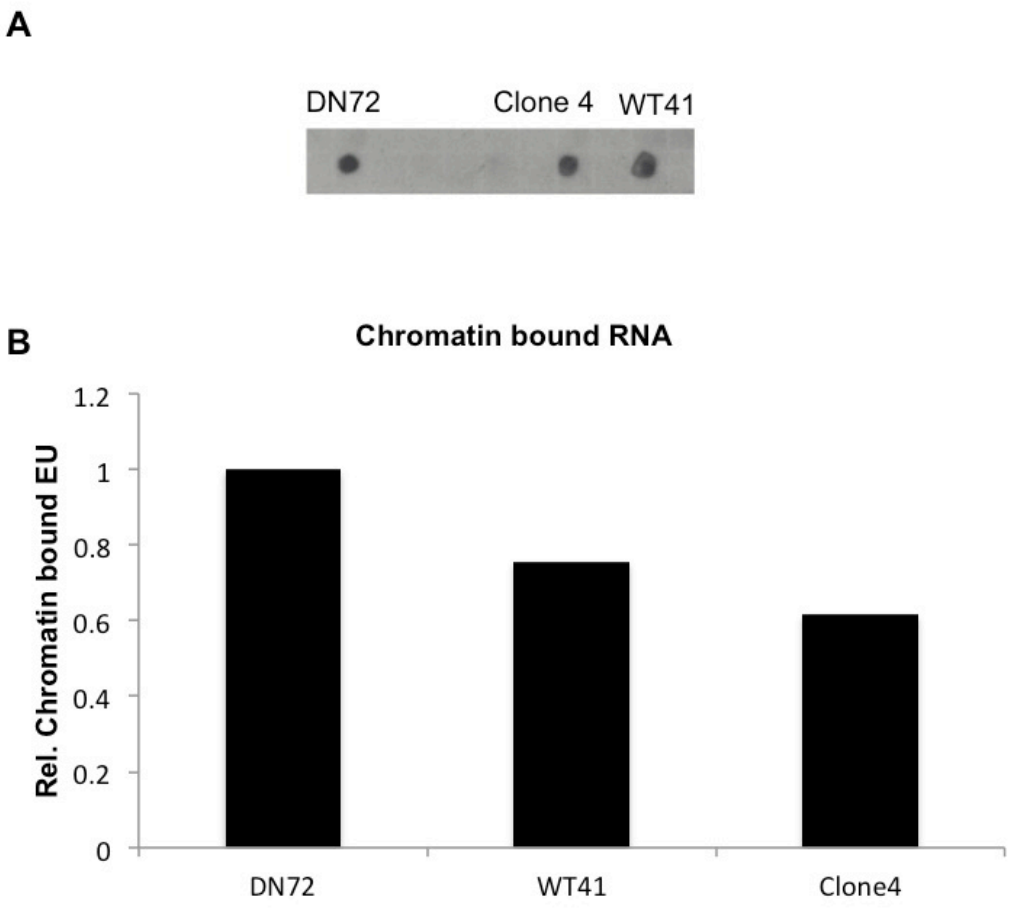

Figure 5.14. Effect of Suv39h methyltransferase expression on global chromatin associated RNA levels. (A) mES cells treated with 1 mM EU O.N before 3 x CSK washes for 5 minutes and nuclei isolation. RNA was prepared using Qiagen RNeasy kit instructions, and a biotinylated azide added via click chemistry. Samples were spotted on nitrocellulose membranes and incubated with avidin-HRP for detection. **(B)** 2D densitometry of chromatin bound RNA dotblot for wild type, Suv39h1/2 knockout DN72 cells, and a DN72 Suv39h1 rescue clone (clone 4).

5.4 Click chemistry DNA fixation: method optimisation

While the chromatin compaction studies, such as sucrose gradient sedimentation, are able to distinguish between chromatin fibres with different structures, but whether these are representative of *in vivo* chromatin is still not clear. As previously mentioned, the inevitable digestion of potential chromatin-associated RNAs by MNase could alter chromatin compaction (Maison, Bailly, Peters, J.-P. Quivy, *et al.*, 2002), and as the chromatin fibres released are not fixed, any torsional forces (such as DNA supercoiling) within the chromatin fibre will be lost. Finally, the process of releasing soluble chromatin fibres may directly alter their structure, despite physiological salt conditions being used, as this environment cannot compensate for the local hydrophobicity of the surrounding liquid state that is caused by protein and RNA concentrations in the nucleus (Larson *et al.*, 2017).

By comparison, altered salt conditions affect the ionic interactions between nucleosomes, and therefore can significantly affect chromatin compaction (**Figure 5.15**). Release of 3T3 chromatin into 1 mM NaCl compared to 80 mM NaCl (physiological levels) and subsequent characterisation of chromatin structure by sucrose gradient sedimentation shows that chromatin in low salt has a significantly more open or disrupted chromatin fibre structure.

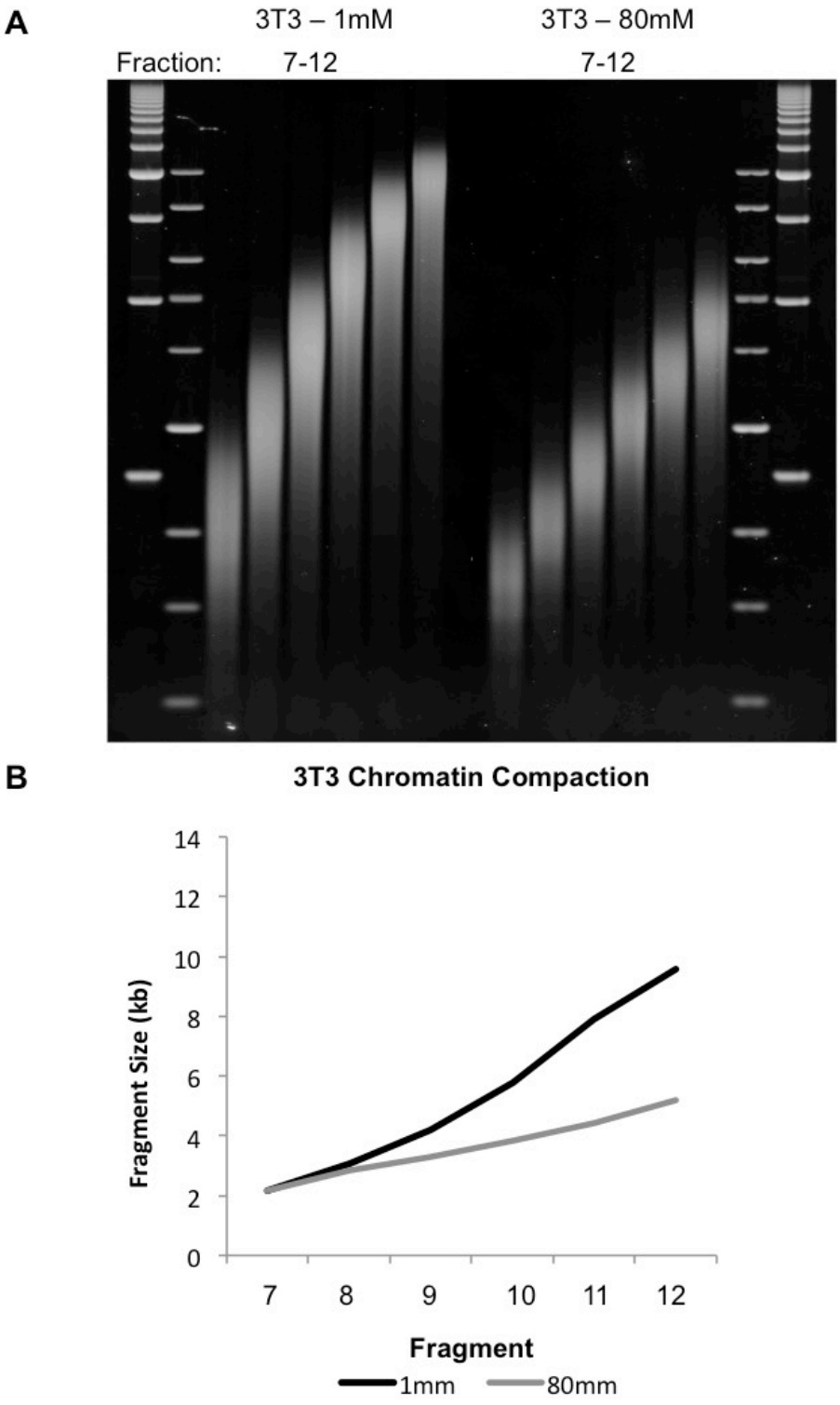

Figure 5.15. Decompaction of unfixed chromatin in low NaCl conditions. Chromatin fibers were isolated from mouse 3T3 cells and resolved by sucrose sedimentation in physiological (80 mM) and low (1 mM) NaCl conditions. **(A)** purified 3T3 cell DNA from 80 mM and 1 mM sucrose gradient fractions resolved by 0.7% TPE gel electrophoresis. **(B)** Comparison of fraction fragment intensity maxima identified by 2D densitometry of chromatin in physiological and low NaCl conditions.

Although formaldhyde is a commonly used and fast fixation method it is very indiscriminate and after cross-linking MNase can no longer efficiently digest chromatin and soluble fibres cannot be released (**Figure 5.16, A-B**). Treatment of 1% formaldhyde prevents any MNase digestion within 16 minutes, while 1% FA treatment after MNase digestion requires SDS addition to release chromatin fibres. Unfortunately, detergent treatment also disrupts chromatin fibre compaction and chromatin no longer sediments well in sucrose gradients indicative of heterogeneous and disorganised fibres. This could suggest that chromatin fibres have dramatically more diverse structures within the genome, or more likely that 1% FA treatment crosslinks between chromatin fibres of different sizes. This would result in shorter chromatin fibres 'piggybacking' on the larger chromatin fibres altering the sedimentation rate and fibre size distribution.

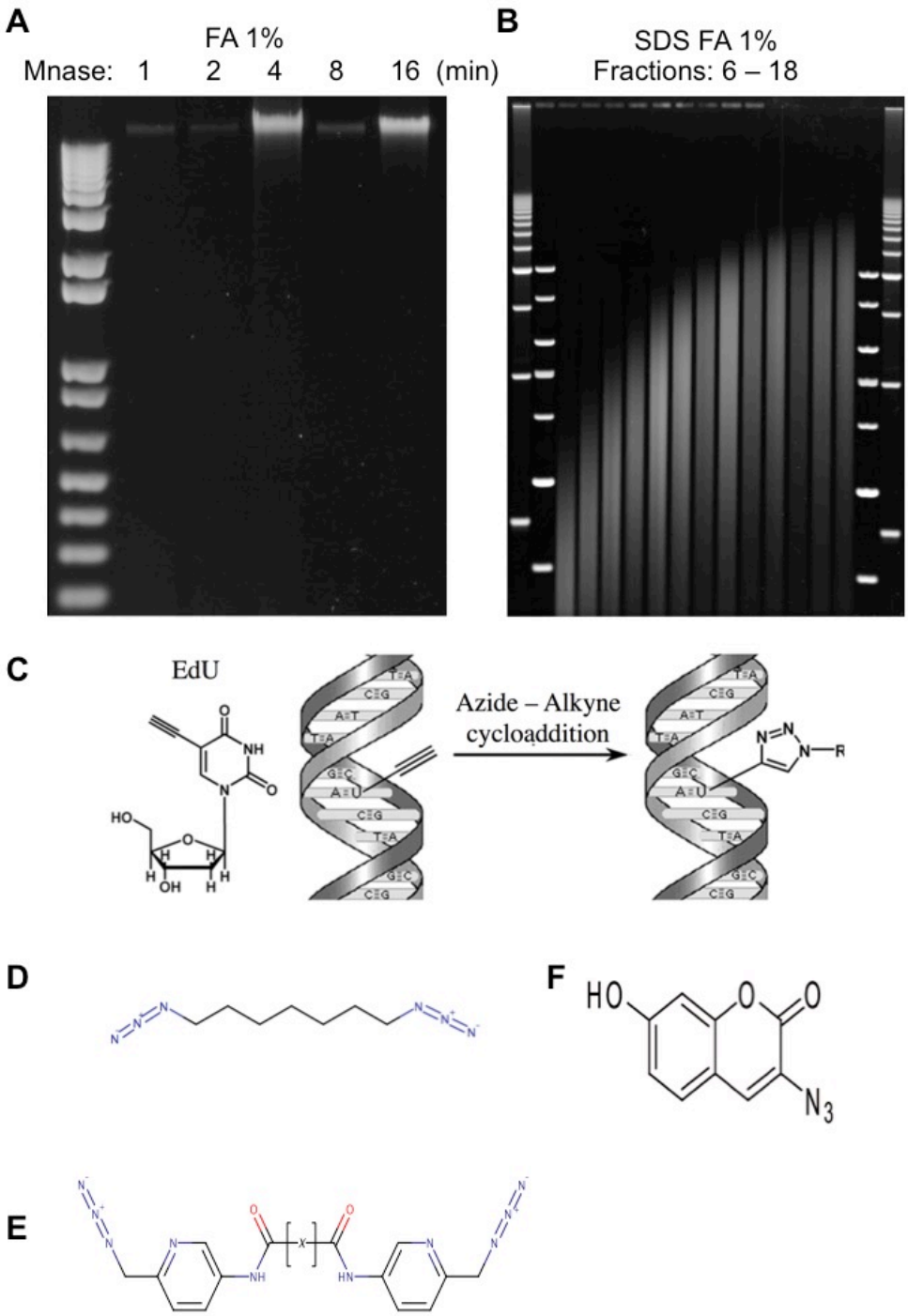

Figure 5.16. Difficulties of fixed chromatin preparation and click chemistry. Chromatin fibre release under formaldhyde (FA) fixed conditions. **(A)** Micrococcal digest of nuclei FA 1% fixed for 10 minutes RT. **(B)** DNA from sucrose gradient fractions with nuclei FA 1% fixation after micrococcal digest, treated with 0.5% SDS to release chromatin fibers. **(C)** DNA analogue EdU incorporation and alkyne click reaction **(D)** PEG-Bis-azide **(E)** Picolyl-bis-azide linker **(F)** 3-azido-7-hydroxycoumarin

Instead of using formaldehyde as an indiscriminate cross-linker we investigated the idea of specifically crosslinking DNA as it might still allow MNase accessibility and maintain chromatin fibres' flexibility in order to be released from the nucleus (**Figure 5.16, C**). Click chemistry could be used as a method to cross-link DNA-DNA due to its highly specific reaction conditions. In a click reaction an alkyne group is covalently attached to an azide group forming a triazole (Jiang *et al.,* 2014). A copper ion initially attacks the alkyne group weakening the triple bond. This allows another copper ion to associate with the alkyne group. The positive charge of the second copper ion then attacks the base nitrogen atom of a nearby azide group. Through electron pushing this causes the electron pair in the alkyne initially interacting with the second copper ion to switch to third nitrogen in the azide group resulting in the covalent bonding between the two groups (**Figure 5.17**). This click reaction has already been extensively used *in vitro* to covalently attach molecules to nucleic acids (Kumar *et al.,* 2007; Gramlich *et al.,* 2008).

Additionally this click reaction has been used to crosslink fluorophores to cellular membranes *in vivo* but has not been presented within the nucleus of live cells (Uttamapinant *et al.,* 2012; Jiang *et al.,* 2014). As free metals are toxic in cells, the free copper ion cellular availability inside cells must be highly regulated. Copper ions are therefore added to cells in the form of $CuSO_4$ to reduce initial toxicity. In order to release copper ions, sodium ascorbate is used as a weak reduction catalyst. To further reduce free copper ion toxicity a sequestering partner such as THPTA or TBTA is added and this enabled fluorophore labelling within zebrafish (Clavadetscher *et al.,* 2016).

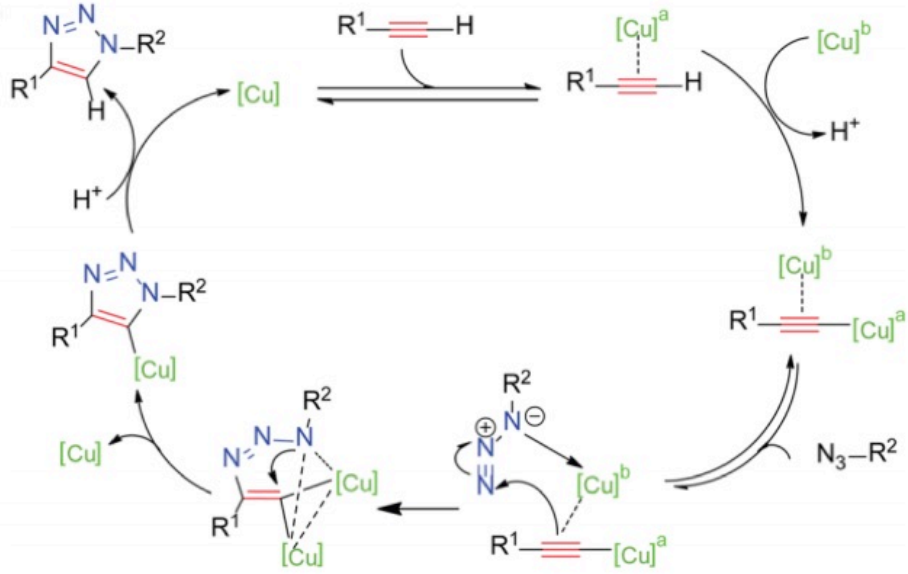

Figure 5.17. Click Chemistry azide-alkyne reaction. Mechanistic rational for copper assisted akyne-azide cycloaddition (CuAAC). Diagram adapted from Jiang, *et al.* (2014)

However, in order to fix chromatin fibre structure in cells the density of cross-links must be high and the reaction speed fast enough to prevent the likelihood of trans-fibre crosslinking. In order to determine if nucleotide analogues conjugated to an alkyne could be incorporated at a high enough density to facilitate chromatin fixation, cells were treated with EdU and EdC at 20 μM for up to 72 hours (**Figure 5.18, A**). The DNA was purified, digested to mononucleotides, analysed by HPLC and quantified using UV spectroscopy. The retention times and absorption profiles of the uridine analogues were determined via input standards. Under these conditions both EdC and EdU were detectable as being incorporated into the genome. In our hands the EdU derivative F-ara-EdU incorporation was barely detectable (data not shown) despite being sufficient for click based immunofluorescence (Neef and Luedtke, 2011). F-ara-EdU has been proposed as a less toxic tool

than EdU and BrdU however this may be due to significantly reduced incorporation rates during replication. F-ara-EdU was therefore rejected as a potential analogue for click-mediated chromatin fixation.

EdU and EdC had similar incorporation rates to each other with over 15% of all nucleotide incorporated after 72 hours. EdC incorporation plateaued between 24 and 48 hours, suggesting that replication rate after EdC incorporation was affected (**Figure 5.18, A**). To determine how stable analogue incorporation was and if they were excised by the repair process, cells were treated with 20 μM EdC or EdU for 72 hours, washed out and then a further 48 hours without analogue incorporation (**Figure 5.18, B**). Both EdU and EdC presented a partial decrease in analogue incorporation after free analogue nucleotides were removed. This would be expected, as future replication cycles would dilute the analogue nuclear concentration. The relatively stable incorporation of EdU and EdC analogues suggest that both would be suitable candidates for a click-based fixation method.

To determine if nucleotide analogue incorporation affected the ratio of endogenous nucleotide (A-T, C-G), Nucleotide ratios to dG were compared over dose ranges of EdU and EdC (**Figure 5.18, C-D**). Given that EdU and EdC are thymidine and cytidine analogues respectively, the levels of adenine and guanine should not be affected by analogue incorporation. With both EdU and EdC treatment: dG, dA, and methyl dC levels were not affected. Both EdU and EdC incorporation levels were inversely correlated with thymidine levels, suggesting that both are incorporated in place of thymidine. The fact that adenine and guanine ratios were unaffected by EdC treatment also implies that when EdC is incorporated instead of a thymidine, it is still paired correctly with an adenine nucleotide.

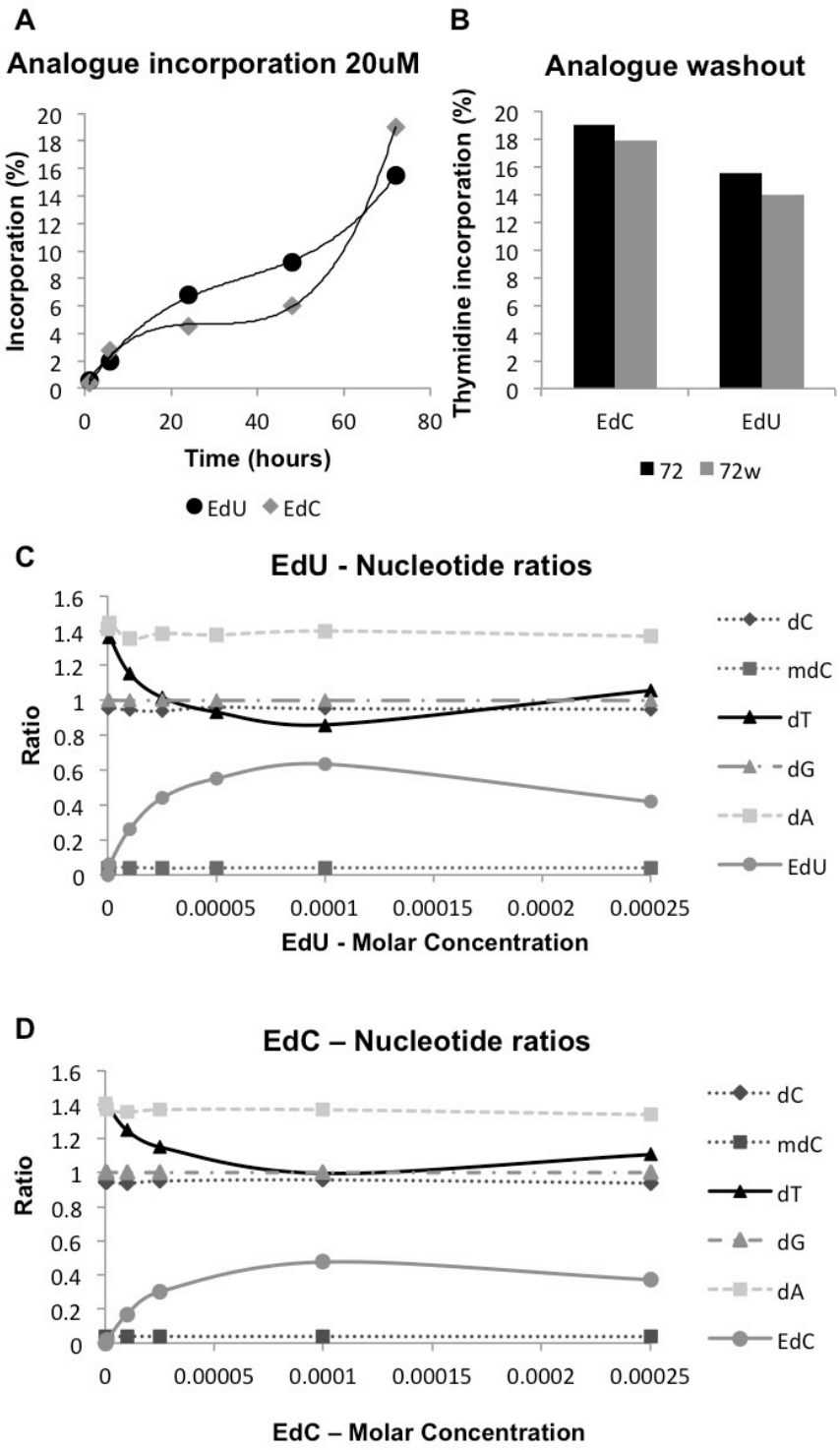

Figure 5.18. Alkyne nucleotide analogue incorporation. 3T3 cells incubated with DNA analogues and their DNA digested to mononucleotides for HPLC-UV analysis. **(A)** Percentage of DNA analogues [EdU and EdC] incorporation into mESc DNA at 20 μM over time. **(B)** DNA analogue incorporation density at 20 μM for 72 hours and after an additional 48 hours without DNA analogue treatment. **(C)** Individual mononucleotide ratios to dG after EdU dose range exposure **(D)** Individual nucleotide ratios to dG after EdC dose range exposure.

To determine if EdC was incorporated after being modified, the spectrometry profiles of incorporated EdC was compared to EdU and EdC standards. Incorporated nucleotides will always have a slightly altered spectrometry profile however due to the attached phosphate group required for incorporation into the DNA backbone. Despite this the EdC profile absorption peaks were more aligned with EdU than EdC standards (**Figure 5.19, A**). To further understand how EdC is modified when it is incorporated, EdC and EdU treated cells' nucleotides were analysed by HPLC-MS-MS (**Figure 5.19, B-C**). Peaks for the predicted EdU-monophosphate mass were detected in both EdU and EdC treated cells. The MS/MS fragmentation of these peaks revealed identical profiles for EdU and EdC. Together these data demonstrate that EdC is deaminated to an EdU molecule before its incorporation into DNA. This is an important finding as many studies (Petryk *et al.*, 2016) use EdC instead of EdU to control for sequence bias.

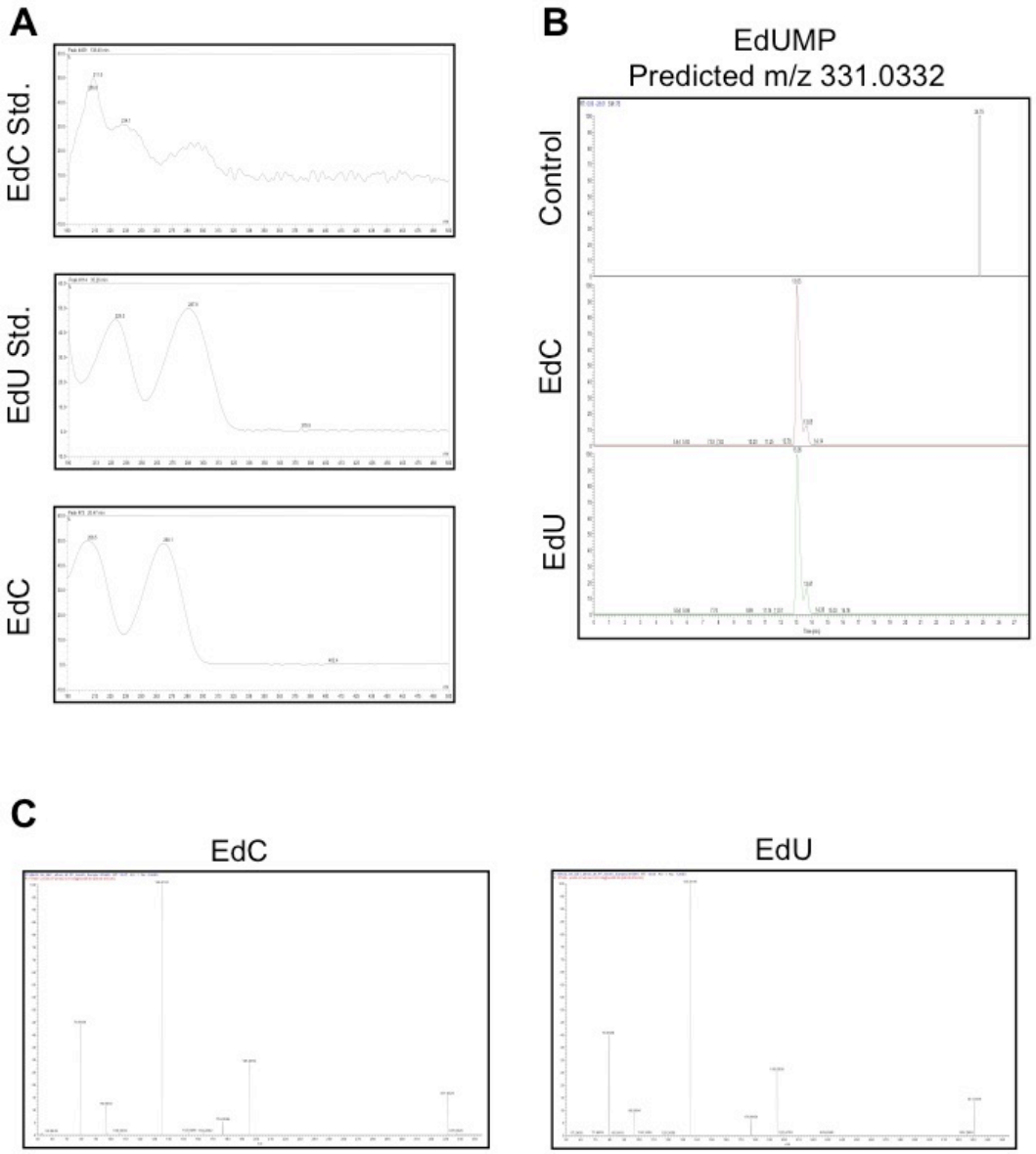

Figure 5.19. DNA analogues EdU and EdC UV spectra and MS fragmentation profiles. 3T3 cells were incubated with 20 μM DNA analogues for 24 hours before their DNA was digested to mononucleosomes. Samples were analysed by HPLC-UV or Mass spectrometry and compared to purified standards. **A)** DNA analogue UV spectrometer intensity profiles resolved by HPLC retention time. Comparison between incorporated EdC and the purified standards for EdU and EdC. **B)** Retention time profiles of incorporated DNA analogues of predicted EdUMP m/z by HPLC-MS **C)** MS/MS fragmentation profiles of incorporated EdC and EdU DNA analogues.

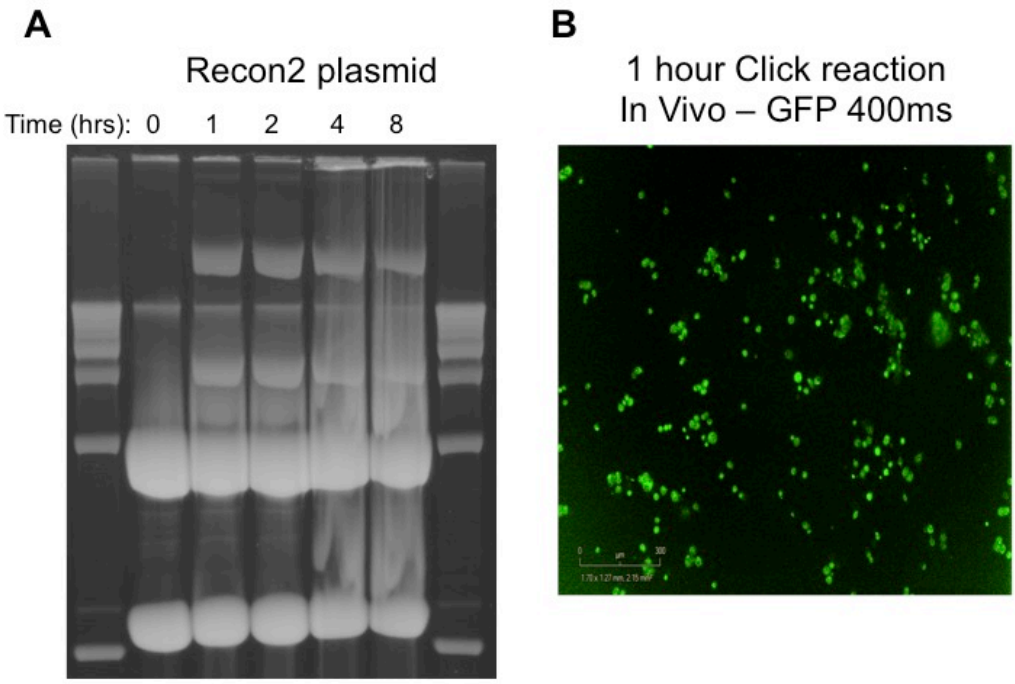

Figure 5.20. Azide-alkyne *in vitro* plasmid click reaction and clicked coumarin-azide fluorescence. A) *In vitro* click reaction of EdU incorporated Recon2 plasmid digested with Xho1. E.coli with Recon2 plasmid were incubated with 20μM EdU for 3 hours at 37°C. Plasmid was purified using the Qiagen mini prep protocol and digested O.N with Xho1 at 37°C. Click reaction was then added at RT: CuSO4 0.5mM, THPTA 0.25mM, NaAsc 250mM, 100mM PEG-bis-azide (5000) **B)** 10X 400ms 488nm of mouse 3T3 cells incubated with 20μM EdU O.N before click reaction added for 60 minutes: CuSO4 0.5mM, THPTA 0.25mM, NaAsc 250mM, 200mM Coumarin-azide.

As the incorporation of exotic nucleotides into DNA is normally unwanted during replication, the effect of EdU/EdC incorporation on the cell cycle was investigated (**Figure 5.21**). Propidium Iodide staining and FACS analysis showed that both a 24 hour 20 μ M EdU and EdC treatment increased the number of cells in S-phase. Significantly though, cell numbers in G2 that have exited S-phase was elevated in EdC but not EdU treated cells. This suggests that the deamination process required for EdC incorporation resulted in replication stress causing cellular arrest. By contrast, EdU treatment increased the time in S-phase but did not result in stalling of cells in G2, nor a significant increase in polyploidy. Together this evidence indicates that EdU is the analogue of choice for incorporating an alkyne tag into genomic DNA for click chemistry based cross-linking.

In order to optimise the click chemistry reaction *in vivo* a 3-azido-7-hydroxycoumarin compound was used (**Figure 5.16 D-F**). 7-hydroxycoumarin is a blue wavelength fluorophore between 404 and 480 nm and its fluorescence is quenched in the presence of the 3-azido sidechain. This quenching by the side group is however lost when the azide reacts with an alkyne to form a triazole (Gierlich *et al.*, 2006) and results in an order of magnitude (15x) increase in fluorescence in the clicked coumarin form (Li *et al.*, 2010). The use of a coumarin-azide fluorophore therefore allows the monitoring of click reaction kinetics in live cells for optimisation (**Figure 5.20, B**).

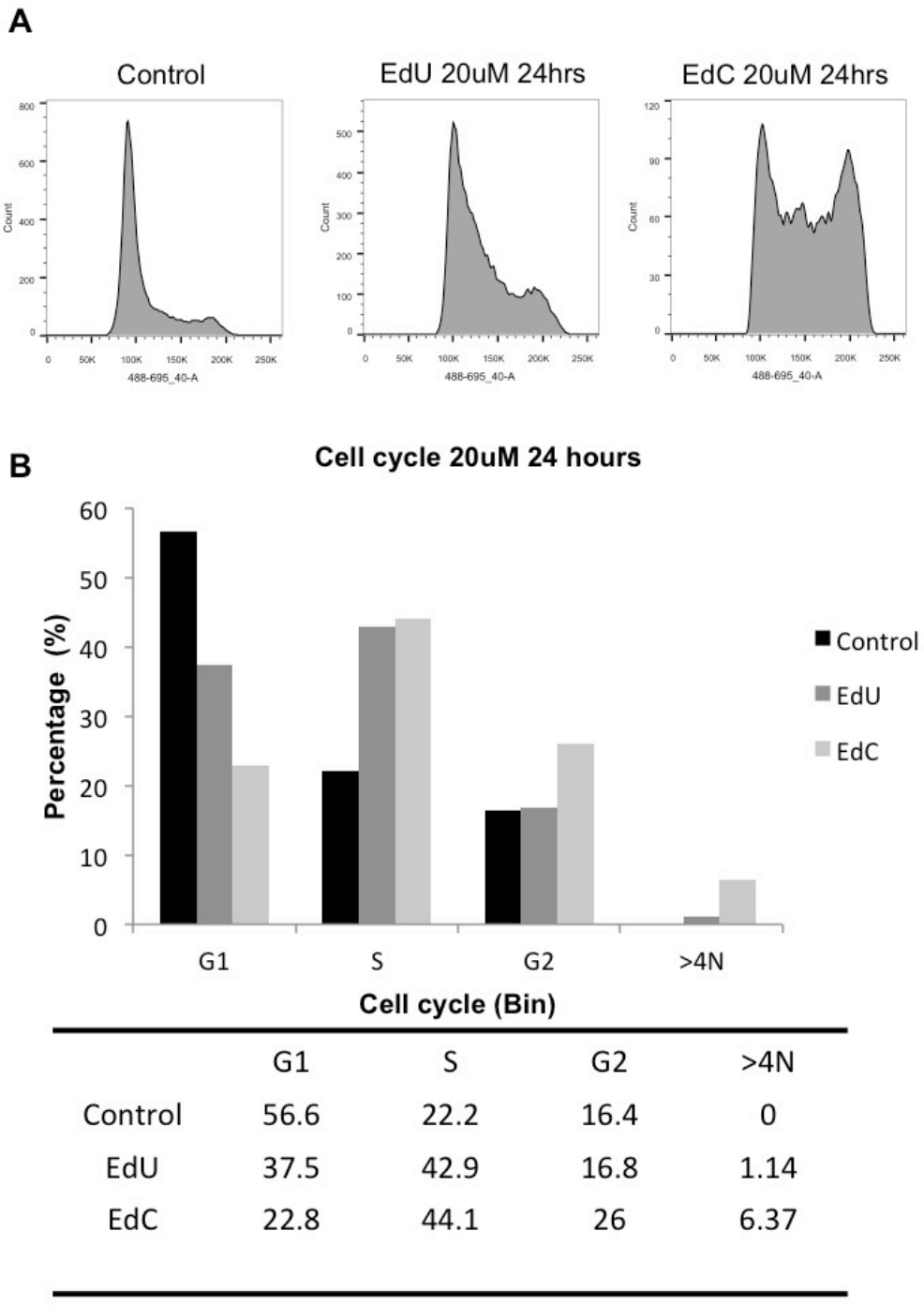

	G1	S	G2	>4N
Control	56.6	22.2	16.4	0
EdU	37.5	42.9	16.8	1.14
EdC	22.8	44.1	26	6.37

Figure 5.21. Effect of nucleotide analogue incorporation on the cell cycle. 3T3 cells treated with 20 μM of DNA analogues for 24 hours, ethanol fixed and propidium iodide (PI) stained for flow cytometry. **(A)** PI stain cell cycle analysis after EdU or EdC 20 μM treatment of mES cells for 24 hours and controls. Histogram plots of PI fluorescent intensity. **(B)** Gated cell cycle stages ratios from flow cytometry PI plots, analysed by FlowJo.

In order to determine if the coumarin-azide was detectable in cells, 3T3 cells were treated with EdU for 24 hours and were fixed with 1% paraformaldehyde. After fixation cells were with incubated with coumarin-azide in a click reaction (**Figure 5.22**) and a dose dependent incorporation was observed. In live 3T3 cells however an increase in coumarin fluorescence was only detectable at 500 μM $CuSO_4$. This suggests that live cells actively inhibit the click reaction mechanism, which is possibly due to native cellular copper chelators evicting free copper ions efflux transporters (Petris, 2004).

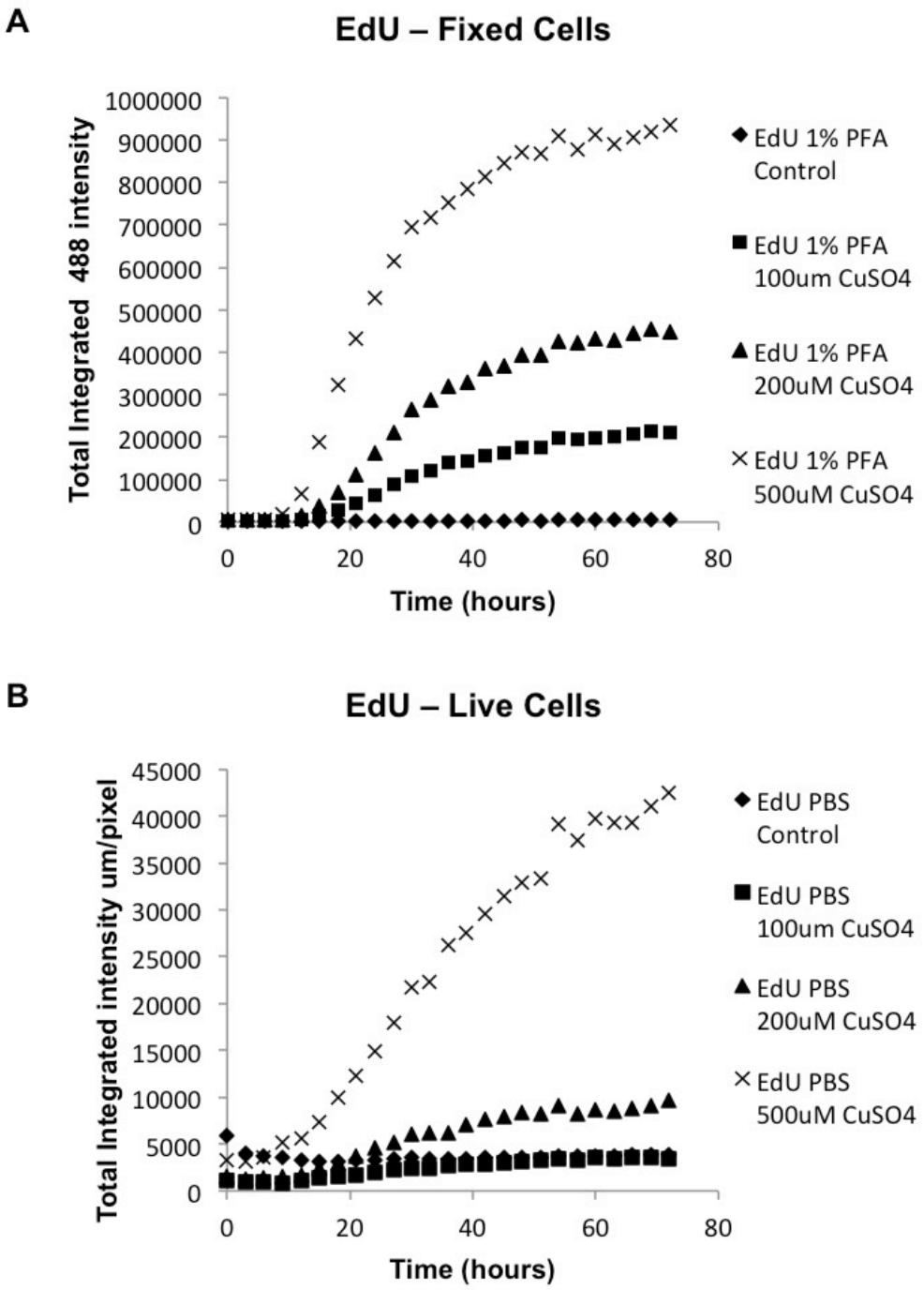

Figure 5.22. Coumarin-azide click reaction kinetics in live cells. 3T3 cells were incubated with 20 μM EdU for 24 hours. **(A)** Intensity of coumarin-azide fluorescence in 3T3 cells 1% formaldehyde fixed before click reaction. 3T3 cells were washed with CSK buffer prior to fixation. Click reaction: ΔμM CuSO4, 10 mM NaAsc, 200 mM coumarin-azide added to PBS. **(B)** Intensity of coumarin-azide fluorescence in 3T3 cells after click reaction in the presence of PBS: ΔμM CuSO4, 10 mM NaAsc, and 200 μM Coumarin-azide.

For click reactions to be conducive to fixing chromatin structure it must be efficient, fast, accurate, and non-toxic to the host cell. To achieve this the metal, chelating agent, and catalyst need to be optimised. Different metals and concentrations were first tested on 3T3 cells incubated with 20 μ M EdU for 24 hours (Figure **5.23**). In addition to $CuSO_4$; Ruthenium, $MgCl_2$ and $CuBr_2$ have previously been used as metal agents in click reactions and their efficacy was analysed (Pérez-Balderas *et al.*, 2003; Boren *et al.*, 2008). Cells were incubated with 250 mM coumarin-azide, 10 mM sodium ascorbate in the presence of each metal salt. Both ruthenium and magnesium chloride had delayed onset of coumarin fluorescence and did not present the expected sigmoidal reaction kinetics. Contrastingly $CuSO_4$ and $CuBr_2$ demonstrated dose dependent increases in fluorescence kinetics. At lower concentrations this dose dependent effect was more sensitive in $CuSO_4$ suggesting that it may be the optimal click reaction catalyst within this setting.

To determine if a chelating agent would accelerate or slow the reaction rate, a dose range of THPTA was added to 200 μM $CuSO_4$, 200 mM Coumarin-azide, and 10 mM sodium ascorbate (**Figure 5.24**). Increasing the THPTA concentration increased the reaction speed up to 100 μM, after which higher concentrations resulted in decreased reaction kinetics. This suggests that the chelating agent's ability to prevent free copper ion excretion increases the reaction speed up to a 1:2 ratio with $CuSO_4$. As the chelating agent's concentration increases above this ratio, the increased kinetics from preventing excretion is offset by the sequestering of the free copper ions from catalysing the click reaction. While other chelating agents were tested (TBTA, BTTP) THPTA presented the fastest click reaction kinetics (data not shown).

A

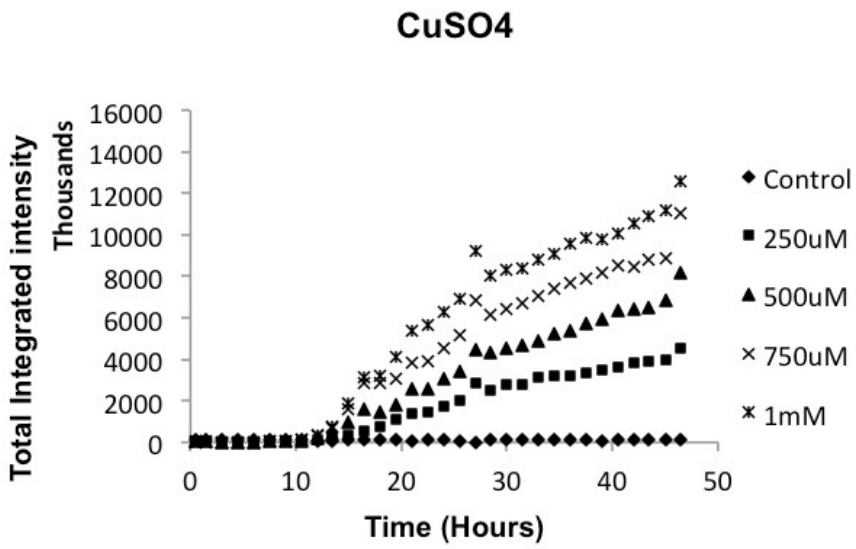
CuSO4
Total Integrated intensity
Thousands
16000
14000
12000
10000
8000
6000
4000
2000
0
0
10
20
30
40
50
Time (Hours)
Control
250uM
500uM
750uM
1mM

B

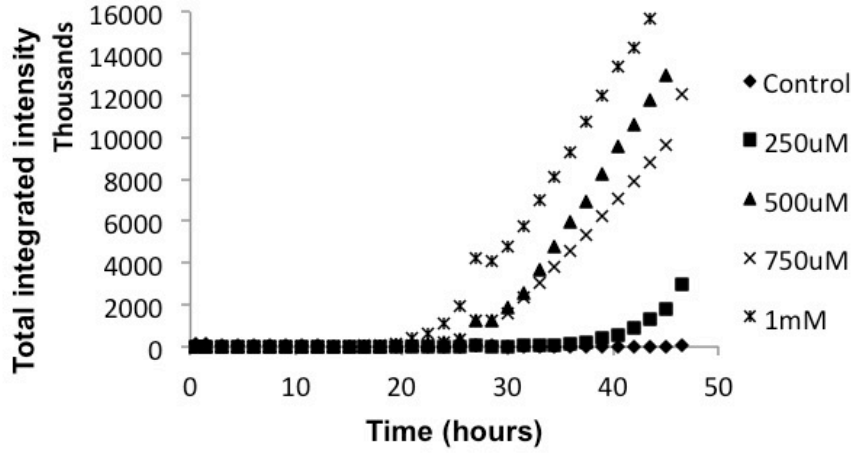
Ru
Total integrated intensity
Thousands
16000
14000
12000
10000
8000
6000
4000
2000
0
0
10
20
30
40
50
Time (hours)
Control
250uM
500uM
750uM
1mM

C

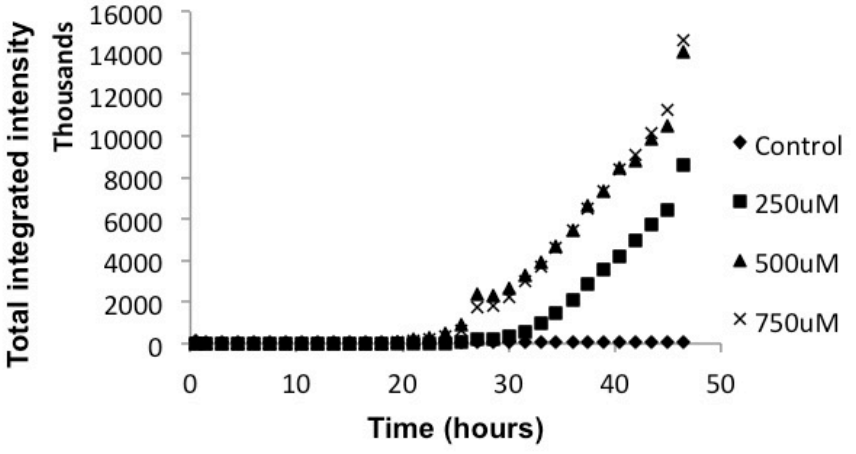
MgCl2
Total integrated intensity
Thousands
16000
14000
12000
10000
8000
6000
4000
2000
0
0
10
20
30
40
50
Time (hours)
Control
250uM
500uM
750uM

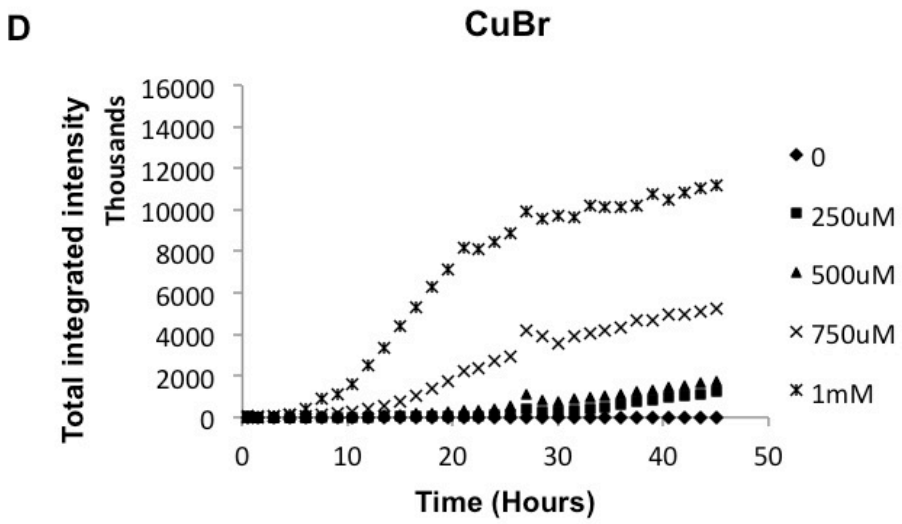

Figure 5.23. Live cell click chemistry metal catalyst optimisation. Comparison of different metals as click reaction catalyst. 3T3 cells were incubated with 20 μM EdU for 24 hours prior to click reaction. Click reaction conditions: Δ μM Metal, 250 mM Coumarin-azide, 10 mM NaAsc. And normal mESc growth media. Metals tested were; **(A)** $CuSO_4$, **(B)** Ruthenium, **(C)** $MgCl_2$, and **(D)** $CuBr_2$.

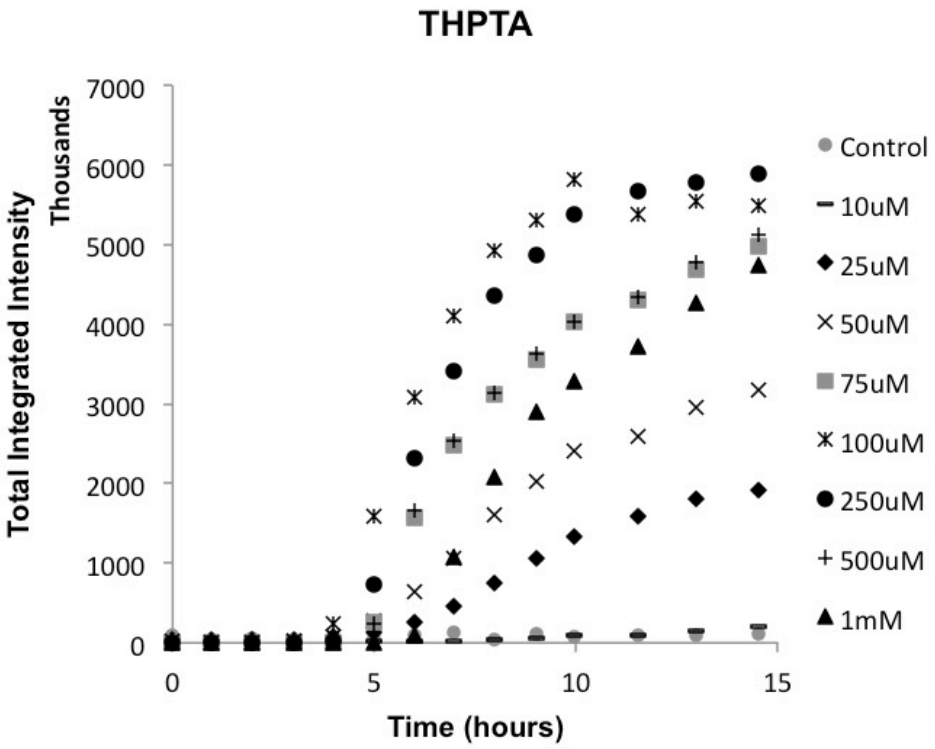

Figure 5.24. Live cell click chemistry metal chelator optimisation: chelating agent. Optimization of chelating agent THPTA concentration. 3T3 cells were incubated with 20 μM EdU for 24 hours prior to click reaction. Click reaction conditions: 200 μM CuSO4, Δ μM THPTA, 200 mM Coumarin-azide, 10 mM NaAsc.

For free copper to be chelated by THPTA and used in a click reaction, it must first be reduced from the $CuSO_4$ source. Sodium ascorbate (NaAsc) and ascorbic acid have traditionally been used as the reducing agent for free copper ions (Himo *et al.*, 2005). As NaAsc is less toxic than ascorbic acid a dose range of NaAsc was added to 500 μM $CuSO_4$, 200 mM coumarin-azide, 250 μM THPTA (Figure **5.25**). NaAsc increased the click reaction kinetics in a dose dependent manner up to 250 mM. Concentrations above 250 mM of NaAsc did not present any increase in reaction speed. This implies that after a NaAsc:CuSO4 ratio of 500:1, the reduction of $CuSO_4$ to free copper ions is not the limiting factor to the reaction speed. However, under these conditions the click reaction was complete in 5 hours. To try and increase the reaction speed further, lipofectin or Triton-X100 was used to disrupt the cell membrane to prevent copper ion excretion. However, Triton-X100 and lipofectin conditions had no benefit to click reaction kinetics (**Figure 5.26**).

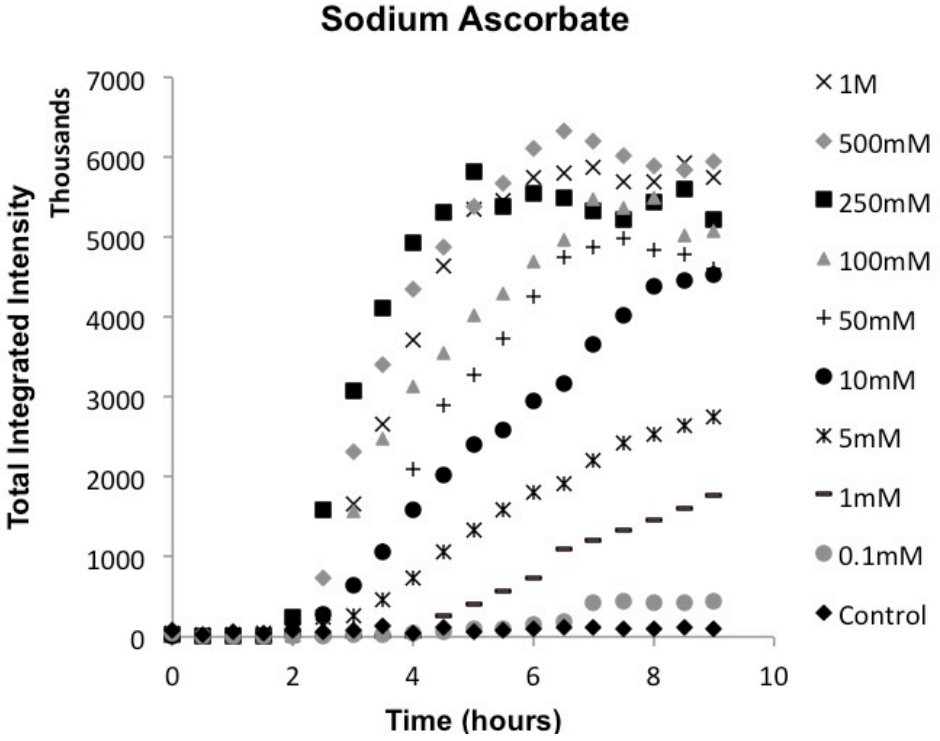

Figure 5.25. Live cell click chemistry reducing agent optimisation: reduction agent. Optimization of catalyst NaAsc concentration. 3T3 cells were incubated with 20 μM EdU for 24 hours prior to click reaction. Click reaction conditions: 500 μM $CuSO_4$, Δ mM NaAsc, 200 mM coumarin-azide, 250 μM THPTA.

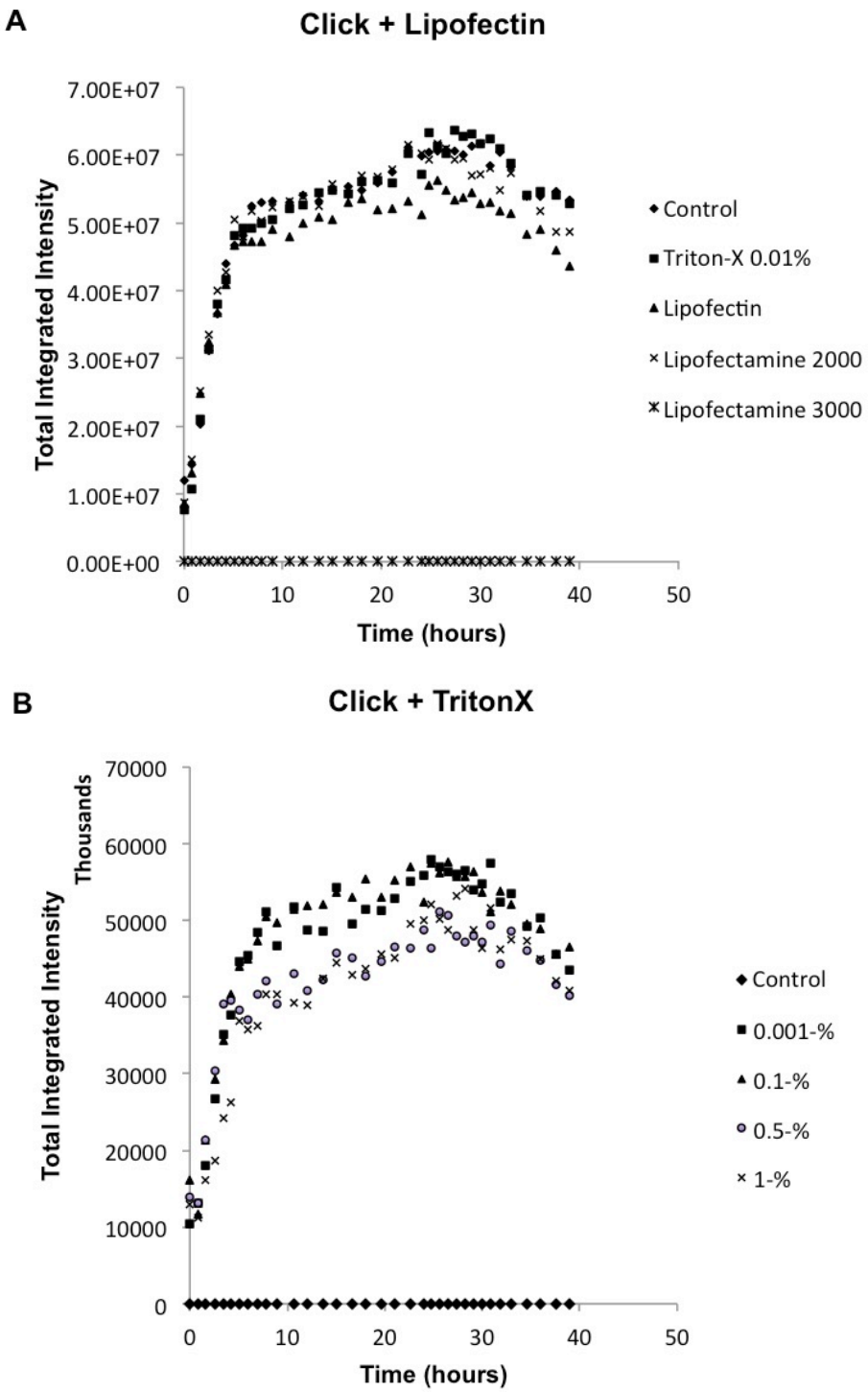

Figure 5.26. Live cell click chemistry, cell membrane disruption optimisation. A) Optimization of click reagent transfection. 3T3 cells incubated with 20μM EdU for 24 hours before the addition of 250mM coumarin-azide, 250mM NaAsc, and 250μM THPTA. 500μM CuSO4 addition after 6 hours to start the click reaction. **B)** Optimisation of detergent addition to EdU click reaction. Δ% Triton-X added to click reaction mix: 250mM Coumarin-azide, 250mM NaAsc, 250μM THPTA, and 500μM CuSO4.

This timeframe for reaction completion (5 hours) is biologically relevant due to the incorporation levels of EdU (**Figure 5.18, A**). As each nucleosome is wrapped around 147 bp of DNA, and mouse cells have a GC content of 51.24%, there should be ~70 AT nucleotide pairs on each nucleosome (Romiguier *et al.*, 2010). With 20 μ M EdU treatment for 24 hours, 7% of all nucleotides are EdU molecules, representing 14.35% of all thymidines. Together these data indicate that each nucleosome will have 7-14 alkyne tags. To maintain chromatin structure, crosslinking each nucleosome to its adjacent neighbours once should be sufficient to maintain fibre structure. Therefore only 20% of the total reaction potential (1 hour) should be needed to fix chromatin structure. This reaction time can theoretically be reduced further by the use of a picoyl-azide crosslinker (**Figure 5.16, E**) which should decrease the reaction time by an order of magnitude (Uttamapinant *et al.*, 2012; Jiang *et al.*, 2014).

Having optimised the click reaction conditions, the use of a bis-azide crosslinker to covalently bond two DNA fragment was investigated *in vitro* (**Figure 5.20**). E.coli cells transformed with a pUC57-Recon2 plasmid were grown overnight. 20 μM EdU was added for 3 hours before cells were lysed and plasmids extracted and purified. 3 hour 20 μM EdU treatment was previously determined to be sufficient for >10% EdU incorporation by HPLC-UV spectrometry (data not shown). Two DNA fragments were prepared by digesting the EdU containing pUC57-Recon2 plasmid with XhoI restriction endonuclease. Optimised click reaction conditions (24 hours of 20 μM EdU incubation, 250 mM NaAsc, 250 μM THPTA, and 500 μM $CuSO_4$) with an bis-azide PEG-linker (average M.W 5000 Da) were added to the digested Recon2 plasmid for 1 – 8 hours. Within 1 hour interstrand crosslinking had occurred resulting in two additional DNA bands and after 4

hours intrastrand crosslinking resulted in smearing of the DNA bands. This suggests that a click reaction can crosslink between naked DNA strands *in vitro*.

To establish if these click reaction conditions would be sufficient to fix chromatin fibre structures in live cells, sedimentation rates of clicked chromatin fibres were compared in sucrose gradients with 1 mM or 80 mM salt (**Figure 5.27**). 3T3 cells were incubated with 20 μ M EdU and 100 mM PEG-bis-azide for 24 hours. Cells were then crosslinked via a click reaction with 500 μ M $CuSO_4$, 250 μ M THPTA, and 250 mM NaAsc for 1 hour. Chromatin fibres were digested with MNase and then released as presented in **figure 5.4**. The clicked chromatin fibres were loaded onto isokinetic sucrose gradients in TEEP buffer with either 80 mM NaCl or 1 mM NaCl buffer. As 1 mM NaCl causes 3T3 chromatin fibres to de-compact substantially (Figure **5.15**), if click crosslinking had fixed the chromatin structure the sedimentation rate should have been the same in 80 mM or 1 mM NaCl gradients.

Unfortunately, 3T3 click fixed chromatin unfolded in 1 mM NaCl, suggesting that cross-linking was not sufficient to stabilise the chromatin structure (**Figure 5.27**). In fraction 13, 80mM salt conditions had an average DNA fragment size of 5213 bp compared to 6728 bp in 1 mM NaCl conditions. This represents a 29% shift in DNA fragment size sedimenting in fraction 13. This suggests a significantly slower sedimentation rate in 1mM NaCl conditions. However, unfixed 3T3 chromatin sedimenting in fraction 12 in 80 mM NaCl buffer had an average fragment size of 5176 bp whilst in 1 mM NaCl the chromatin sedimenting in fraction 12 was 9595 bp (Figure **5.15**). Therefore unfixed chromatin of similar fragment sizes to fixed chromatin presents an

85% shift in DNA fragment size. This suggests that a click-based cross-linking approach can fix chromatin fibres to an extent but cannot prevent other physiological properties from partially altering the chromatin compaction state.

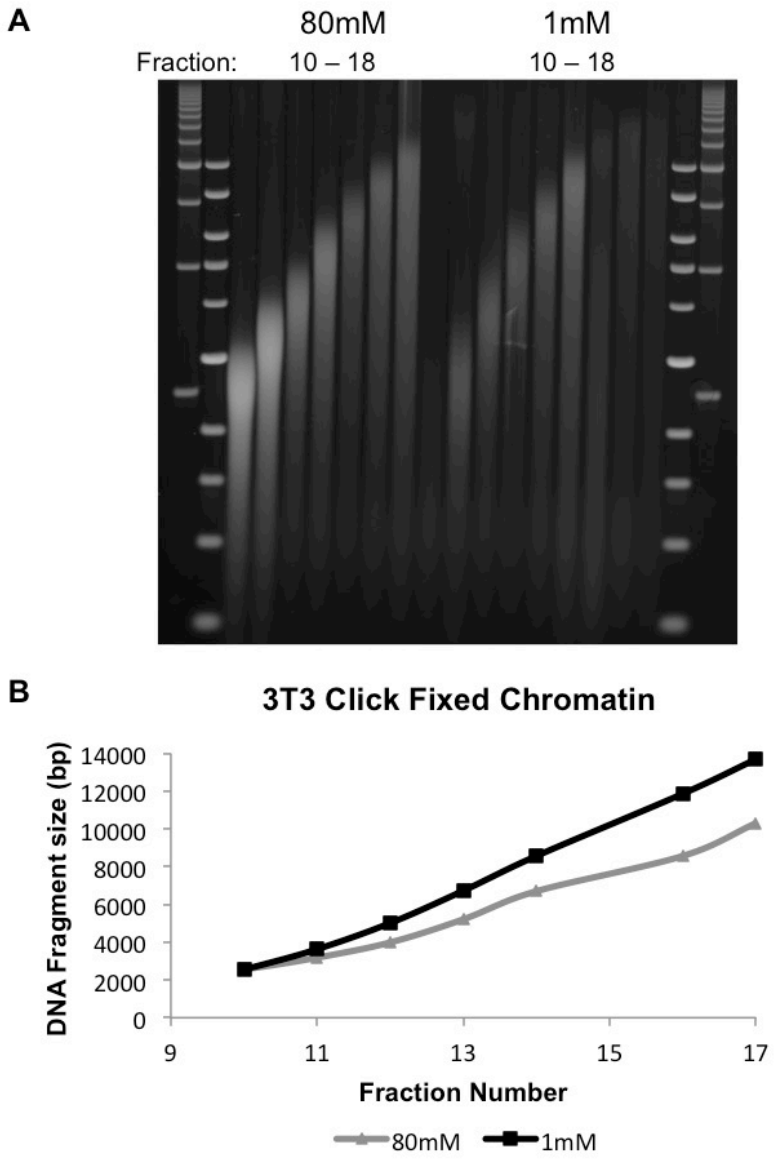

Figure 5.27. Azide-alkyne click reaction link chromatin stability in low NaCl conditions. Azide-alkyne clicked chromatin fibers were released from 3T3 nuclei into physiological (80 mM) and low (1 mM) NaCl conditions and resolved by sucrose sedimentation. 3T3 mouse fibroblast cells incubated with EdU 20 μM EdU and 100 mM PEG-Bis-azide (5000 MW) for 24 hours prior to click reaction. Click conditions: $CuSO_4$ 0.5 mM, THPTA 0.25 mM, 250 mM NaAsc for 1 hour **(A)** DNA from 3T3 cell clicked chromatin sucrose fractions, at 80 mM or 1 mM NaCl buffer conditions. Fractions 10-18 run on a 0.7% TPE gel. (**B)** Comparison of fragment intensity maxima from fractions in each lane of 1 mM or 80 mM treated clicked chromatin**.**

5.5 Discussion

5.5.1 H3K9me3 and chromatin compaction

Suv39h1 and Suv39h2 are the main methyltransferases responsible for H3K9me3 (Hall *et al.*, 2002). H3K9me3 is specifically limited to regions of constitutive heterochromatin including pericentric chromatin, telomeres and retrotransposons across the genome (Arnoult, Van Beneden and Decottignies, 2012; Bulut-Karslioglu *et al.*, 2014). This has led to a long-standing hypothesis that H3K9me3 has an important functional role in heterochromatin formation. Loss of Suv39h enzymes results in the loss of Suv39h, H3K9me3, H4K20me3, DNA methylation and HP1 proteins from constitutive heterochromatin regions (Peters *et al.*, 2001). However DNA methylation levels at heterochromatin have been shown to have no functional role in regulating heterochromatin compaction (Gilbert, Thomson, Boyle, Allan, Ramsahoye and Wendy A Bickmore, 2007). Given that Suv39h double null mice are viable, still form nuclear chromocenters, and only have a mild genome instability phenotype, the function of H3K9me3 in having a causal role in chromatin compaction remains unclear (Peters *et al.*, 2001). Furthermore, no epigenetic modifications have been directly demonstrated to have a causal role in chromatin fibre compaction, even histone acetylation.

Initial experiments shown here were focused on confirming that Suv39h double null mESC cell line presented the same profile of epigenetic marks as previously reported. H3K9me3, H4K20me3 and HP1α were all shown to be lost from chromocenters in Suv39h double null ES cells (**Figure 5.3, 5.10**). This supports the current view that Suv39h HMTs' specificity to H3K9me3 deposition results in the recruitment of Suv420 HMTs and HP1 proteins to constitutive heterochromatic domains (Schotta *et al.*, 2004).

In addition to H3K9me3 nuclear distribution, total levels of H3K9me2 and H3K9me3 were significantly reduced along with its pericentric heterochromatin recognition partners HP1α and HP1β (**Figure 5.2**). HP1γ levels were increased in the double null cells. However HP1γ is thought to function exclusively in euchromatin and therefore does not function at the pericentromere outside of S-phase (Minc, Courvalin and Buendia, 2000). Interestingly, H3K27me3 levels were significantly elevated suggesting an expanded regulatory role for polycomb silencing in Suv39h double null cells. Recent studies have begun to implicate PRC2 function with DNA methylation and HP1 chromatin stabilisation. Reddington *et al.*, (2013) demonstrated that a loss of DNA hypomethylation led to a global redistribution of DNA methylation, while comprehensive studies by Manzo *et al.*, (2017) described the detailed function of H3K27me3 and H3K4me3 in excluding DNMT3 isoforms from their bivalent chromatin domains but recruiting DNMT3A1 to their periphery.

While H3K27me3 is not found at pericentric regions, the principle of mutual exclusivity with H3K9me3 has been demonstrated to be false. Mass spectrometry of H3K27me2 and H3K27me3 containing nucleosomes from HeLa, mESC, and MEF cells consistently had H3K9me2/me3 and H4K20me2 marks (Voigt *et al.*, 2012). Additionally, chromatin immunoprecipitation experiments have found co-occupation of H3K9me3 and H3K27me3 at repetitive elements, telomeres, and bivalent promoters (Zeng *et al.*, 2009; Hawkins *et al.*, 2010; Arnoult, Van Beneden and Decottignies, 2012). Further studies have demonstrated that PRC2 subunits Ezh2 and Suz12 are required for HP1α recruitment to heterochromatin but not H3K9me3 deposition (Boros *et al.*, 2014). In the absence of H3K9me3, DNA methylation and HP1 heterochromatin recruitment, a compensatory increase in PRC2 mediated H3K27me3 deposition would not be unexpected and may cause the relatively mild mouse model phenotype (Peters *et al.*, 2001).

Having demonstrated that DN57 cells lacked H3K9me3, HP1α, and H4K20me3 at chromocenters, the effect of this altered epigenetic state on chromatin compaction was investigated. Unlike DNA methylation (Gilbert, Thomson, Boyle, Allan, Ramsahoye and Wendy A Bickmore, 2007), loss of the H3K9me3/HP1/Suv39h complex from heterochromatin results in the de-compaction of pericentric (major satellite) and centromeric (minor satellite) chromatin (**Figure 5.6**). However, this chromatin de-compaction was not limited to pericentric and centromeric domains, as Suv39h double null cells presented global de-compaction of chromatin fibres when compared to wild type (Figure **5.5**). This altered the sedimentation rate by 7-9% for 9 kb DNA fragments compared to 13.7% for Major satellite and 12.3% for minor satellite chromatin fibres of similar size.

As <10% of the mouse genome is made up of major and minor repetitive elements, if chromocenter de-compaction was solely responsible for the global effect, the de-compaction effect would be expected at a 10th of the effect at pericentric regions (Kit, 1962; Komissarov *et al.*, 2011). This therefore suggests changes in chromatin compaction beyond the normally H3K9me3 marked chromocenters. A possible mechanism for the global de-compaction may come from interspersed repetitive elements. Around 38% of the mouse genome is composed of interspersed repetitive elements, with 19% of the genome being LINEs, 8% SINEs, and 10% LTR elements (Waterston *et al.*, 2002). Recent studies have demonstrated Suv39h mediated H3K9me3 at ~5% of repetitive elements in mESCs (Bulut-Karslioglu *et al.*, 2014). However, in order for repetitive elements to result in the global chromatin de-compaction, every element would need to be regulated by Suv39h, which has not been demonstrated. Together this suggests that at least some of the global chromatin de-compaction is likely due to changes in chromatin structure at genic regions.

To determine if this effect was due to clonal variation, the chromatin compaction state of an additional Suv39h double null clone (DN72) was investigated (**Figure 5.9**). DN72 also demonstrated a slower sedimentation rate (6.5% change in DNA fragment size at 9 kb) indicative global de-compaction of chromatin fibres albeit slightly lower than DN57 cells (7-9%). To determine if this was directly linked to Suv39h activity, exogenous human Suv39h1 was transfected via a pPyGAGASIZ cassette. This resulted in stable expression of human Suv39h1 with the Suv39h double null mESC background, although at lower levels than endogenous Suv39h1/2 in wild type cells (**Figure 5.10**). The expression of human Suv39h1 was subsequently sufficient to restore H3K9me3 deposition at chromocenters and HP1α recruitment (Figure **5.11**). Together this suggests that human Suv39h1 expression was sufficient to ablate the endogenous Suv39h double null phenotype.

When chromatin fibres from DN72R cells (expressing exogenous human Suv39h1) were compared to wild type chromatin, the original chromatin de-compaction phenotype was completely reversed. DN72R chromatin fibres were comparatively 4.4% smaller than WT41 suggesting a more compact chromatin fragment for a 9 kb DNA fragment size (**Figure 5.12**). This demonstrates for the first time a direct relationship between a histone modification deposition and chromatin fibre compaction. The increased compaction beyond wild type could be due to slightly differing functionality of human Suv39h1 compared to mouse Suv39h1. Alternatively, regulatory changes induced by Suv39h1/2 KO results are not completely reversed by human Suv39h1 expression and in combination with exogenous Suv39h1 expression contribute to chromatin compaction.

Given the growing body of evidence suggesting an RNA component to heterochromatin regulation (Arnoult, Van Beneden and Decottignies, 2012; Maison *et al.*, 2016; Shirai *et al.*, 2017), the levels and distribution of chromatin associated RNA was investigated (**Figures 5.13, 5.14**). Loss of Suv39h HMTs in DN72 clearly led to an increase in chromatin associated RNAs that was reversed with exogenous human Suv39h1 expression. The major question from this result is whether Suv39h/H3K9me3/HP1α recruitment mediates the RNA's chromatin association, or whether Suv39/H3K9me3/HP1 supresses the transcription of ncRNAs from the underlying DNA. This remains a pertinent question yet to be answered in understanding heterochromatin regulation. While Suv39h and HP1 proteins clearly interact with RNAs, the global chromatin de-compaction cannot be completely attributed to altered Suv39h-HP1 recruitment (Meehan, Kao and Pennings, 2003; Bulut-Karslioglu *et al.*, 2014; Maison *et al.*, 2016). Therefore the regulation of underlying ncRNAs by Suv39h H3K9me3 deposition would project changes in chromatin associated RNAs beyond regions bound by Suv39h-HP1 complexes. This would be more representative of the global chromatin de-compaction observed in these experiments.

5.5.2 Sucrose sedimentation and click-fixation

The validity of analysing unfixed chromatin fibres remains a debated question, particularly in relating the sedimentation properties of chromatin *in vitro* to an *in vivo* structure. Formaldhyde fixation is known to induce aggregate formation that can result in large biases in chromatin immunoprecipitation (ChIP) experiments (Baranello *et al.*, 2016). This aggregate formation prevents MNase catalytic activity and chromatin fibre release (**Figure 5.16, A**). Furthermore, in the same way as GFP can be artificially recruited by formaldhyde in ChIP experiments, the dynamic properties of the chromatin fibre could result in artificial formaldhyde induced chromatin compaction.

However, if the chromatin fibre is unfixed the process of micrococcal nuclease digestion will release the torsional stress in the fibre. Additionally the process of releasing chromatin fibres into solution could alter the chromatin state. Whether formaldhyde fixation or native methods are representative of the true physiological chromatin state *in vivo* remains debated and has led to the development of native ChIP and native conformation capture methods (i4C) (Dorbic and Wittig, 1986; Thorne, Myers and Hebbes, 2004; Brant *et al.*, 2016).

While formaldhyde fixation is possible after MNase treatment, the nuclei must be treated with SDS in order to extract the fixed chromatin fibres (**Figure 5.16, B**). This suggests that a degree of fibre flexibility in the chromatin fibre is required for chromatin release. However, the use of detergents to disrupt ionic bonding and denaturing proteins could alter

chromatin compaction to a greater extent than no fixation. Additionally, the smearing in SDS formaldehyde fixed fractions is indicative of interstrand crosslinks from a large chromatin fragment to a small fragment. This significantly disrupts the resolution of the experiment and induces an additional bias (**Figure 5.16, B**).

To try and circumvent the negative drawbacks of formaldhyde fixation and native chromatin fibre sucrose sedimentation, the use of copper assisted cycloaddition chemistry to covalently crosslink only DNA was investigated. By only creating DNA:DNA crosslinks this should maintain some fibre flexibility while preventing aggregation. Additionally this method will allow fixation before MNase digestion and therefore before chromatin RNAs are affected (Huebner *et al.*, 1981; Maison, Bailly, Peters, J.-P. Quivy, *et al.*, 2002).

Preliminary studies demonstrated that thymidine-alkyne tags could be incorporated into DNA at high density without inducing cell cycle arrest (**Figures 5.18, 5.21**). The discovery that EdC is deaminated before DNA incorporation demonstrates a bias in DNA incorporation (**Figures 5.18, D, 5.20**). At a 10 nm chromatin fibre scale, linker regions are enriched for adenine-thymidine nucleotides, suggesting that more alkyne tags will be between nucleosomes (Trifonov and Sussman, 1980; Cui and Zhurkin, 2009). This may affect the accessibility of the alkyne tag while affecting its ability to fix the chromatin conformation. Furthermore, at large scale chromatin structure, euchromatic regions are enriched for AT sequences compared to heterochromatin (Dekker, 2007). This suggests that the distribution of alkyne tags will be skewed to euchromatic regions. Therefore the use of EdC as a single agent or in combination with EdU will not increase coverage at heterochromatin domains when compared to euchromatin.

A high incorporation rate is therefore required to assure genome coverage with multiple alkyne tags per histone. A nucleosome has ~147 bp of DNA wrapped around it, of which 58.76% on average (SD: 7.85%) in mice would be A-T base pairs (Romiguier *et al.*, 2010). Therefore, each mouse nucleosome will have between 49 and 95 thymidine nucleotides across both DNA strands. With 20 μ M EdU treatment, EdU makes up 7% of all incorporated nucleotides, corresponding to 7-14 EdU molecules per nucleosome (**Figure 5.18, A**). As copper assisted cycloaddition results in a triazole mediated bond, one crosslink with each adjacent nucleosome should be sufficient to maintain the chromatin fibre structure.

Although nuclei are porous, allowing small molecules to enter by diffusion, cell membranes contain multiple efflux transporters to remove metals and toxins (Petris, 2004). These cellular processes limit the click reaction speed, requiring optimisation for fast and efficient reactions (**Figure 5.22**). Once optimised completion of cellular click reactions of incorporated EdU occurred within 5 hours (**Figures 5.25, 5.26**). This would allow between 1-3 click reactions per nucleosome per hour with a standard azide.

Further chemical studies have indicated that this reaction speed can be further enhanced from the addition of a picoyl group inside the azide group. Azide picoyl groups chelate with the first copper ion that attacks the alkyne group reducing the partial molar free energy needed 25 fold for the click reaction (Uttamapinant *et al.*, 2012). The can be further reduced by reversing the amide group on the opposite side of the picoyl group from the azide (**Figure 5.16, E**). This makes the amide electron donating and further increases the reaction speed 2-3 fold. The subsequent 50 fold reduction of reaction time via a picoyl-azide would allow reaction completion in 10-12

minutes in live cells. Although a bis-picoyl-PEG crosslinker was designed, this was not synthesised within the timeframe of this study.

Instead, a PEG linker (MW, 5 kDa) with two azide groups was used to crosslink DNA fragments (**Figure 5.16, D**). Using *in vitro* naked DNA, interstrand crosslinks were visible after 1 hour (**Figure 5.20**). Following these positive results the ability of a 1-hour click reaction to fix EdU containing chromatin fibres was investigated and analysed by sucrose sedimentation (**Figure 5.27**). The ionic conditions of the chromatin solution, has previously been shown to dramatically alter the chromatin compaction state with low NaCl concentrations associated with de-compaction (Thoma, *et al*, 1979). To determine if a 1-hour click reaction could fix chromatin structure in live cells, Click-fixed chromatin was analysed in physiological (80 mM) and low (1 mM) NaCl conditions (**Figure 5.27**). Unfortunately, in 1 mM NaCl click-fixed chromatin demonstrated significant de-compaction compared to 80 mM NaCl conditions. However, when compared to unfixed chromatin in these conditions, click-fixation did partially reduce chromatin de-compaction (**Figures 5.15, 5.27**) and suggests that a click-based approach could fix chromatin fibre structure. The lack of complete fixation could be due to not producing enough DNA click crosslinks within a 1-hour reaction. While a longer reaction time could increase the number of crosslinks, this might also induce a bias similar to the long fixation times in formaldhyde (Baranello *et al.*, 2016). Moreover, analysis in 1 mM NaCl treatment may be too excessive an alteration compared to physiological conditions. As DNA crosslinks would not prevent proteins dissociating from the chromatin fibre, the loss of linker histones or the production of heminucleosomes in 1 mM NaCl could be responsible for partial chromatin de-compaction.

Chapter 6: Discussion

6.1 Heterochromatin regulators

The cytological restriction of centromeric DNA during metaphase identifies the centromere as having a distinct chromatin structure. In some organisms centromeres remain cytologically compact throughout the cell cycle leading to their label as constitutively compact (or heterochromatic) DNA regions. This provides a good distinction from which to investigate chromatin structure and function, leading initial studies to focus on effectors of heterochromatin formation and maintenance (Muller, H, 1930). Using the position-effect variegation (PEV), determined by an eye pigment gene translocation to centromeric regions, gave a phenotypic output to identifying factors regulating heterochromatin formation and regulation.

Since the development of sequencing based 'omics' approaches, our understanding of euchromatin organisation has advanced significantly. However the repetitive nature of centromeric DNA sequences has prevented chromatin conformation and modification distributions to be resolved at these regions. Therefore identifying factors and regulators of heterochromatin structure remains an important question within the chromatin field.

Model systems, such as artificial chromosomes, have often been used to investigate heterochromatin structure (Grimes, Rhoades and Willard, 2002; Ohzeki *et al.*, 2002). However, measuring the stability of artificial chromosomes to identify centromeric components is difficult, and it has limitations for identifying heterochromatin components. This approach also lacks scalability, and is limited to essential components of faithful chromosome segregation rather than heterochromatin structure directly. The artificial heterochromatin system developed by the Larionov lab enables large scale screening of heterochromatin factors, while its artificial nature should limit cell type specific regulation. This artificial system uses a centromeric sequence from yeast chromosome 6 and a 10 kb array of human alpha satellite, and mimics the epigenetic profiles of constitutive and facultative heterochromatin resulting in transcriptional silencing (Figure **3.9**) (Ebersole *et al.*, 2005). A GFP reporter can then be used to provide a fast and efficient output of gene expression.

5'azacyctidine and trichostatin A, well characterised inhibitors of DNA methyltransferases and HDACs respectively, triggered GFP expression. This demonstrates that inhibition of canonical heterochromatin components results in GFP expression within this system and helps to validate it as a screening tool (**Figure 3.2**). Additionally many specific HDAC inhibitors gave GFP expression with this screen (**Table 3.1**).

The identification of kinase signalling pathways in modulating heterochromatin is not surprising given that cells utilise kinase signalling to adapt to their environments and alter transcription. As transcriptional changes require chromatin remodelling it is also not surprising that some kinase pathways are involved in heterochromatin maintenance. Indeed

aurora kinase has well characterised roles in regulating cohesin loading and proper chromatin compaction (Nishiyama *et al.*, 2010; Tedeschi *et al.*, 2013).

The surprising result from the work presented here was the identification of BET proteins in maintaining heterochromatic gene repression. Both pan-BET inhibitor bromosporine and selective inhibitor JQ1 de-repressed GFP expression and caused G1 cell cycle arrest demonstrating the effect is not compound specific (**Figure 3.4, 3.5**). BET proteins canonically function as transcriptional activators (Chapuy, McKeown and Lin, 2013) where they bind to acetylated histones and are therefore often associated with euchromatin (Najafova *et al.*, 2017). Additionally Wang *et al.*, (2012) demonstrated that full length Brd4 protein was required to maintain chromatin structure and prevent abnormal heterochromatinisation.

However some recent studies suggest that histone acetylation and BET proteins can also be associated with pericentric heterochromatin maintenance (Grézy *et al.*, 2016). This study demonstrated that when H3K9me3/Suv39h/HP1 heterochromatin association is disrupted, that TIP60 acetylation recruits BET proteins to maintain heterochromatin compaction.

Further studies have demonstrated specific recruitment of BET proteins to heterochromatin due to multiple stress responses (Floyd *et al.*, 2013). This study demonstrated that Brd4 can recruit condensin II preventing DNA damage response pathways, while Col *et al.*, (2017) demonstrated BET proteins were essential for pericentric transcription after heat shock. Together these studies support the idea that BET proteins can function at heterochromatin in certain situations.

The synthetic GFP cassette in the MEL cells is marked by H3K9me3 enrichment suggesting Suv39h/HP1 mediates its heterochromatinisation. This therefore implicates BET proteins function beyond abnormal heterochromatin organisation and stress responses.

When global histone modifications were analysed by protein arrays, H3K4 methylation was elevated (Figure **3.10**). This could be due to inhibition of BET proteins binding to acetylated lysines, which exposes histone acetylation to increased de-acetylation. H3K4 acetylation is associated with pericentric heterochromatin in yeast, and has an attributed function in recruiting the HP1 homologue Swi6 (Xhemalce and Kouzarides, 2010). If BET proteins bind to H3K4ac at pericentric regions this could provide a potential mechanism of action for heterochromatin maintenance.

Additionally BET inhibitors resulted in significant decreases in MAPK signalling, and compensatory up regulation of PI3K/Akt and JNK signalling (**Table 3.2**) (Chen and Sytkowski, 2001; Mirzoeva *et al.*, 2009). BET proteins have a key function in regulating c-Myc transcription, which is downstream of MAPK signalling. In turn, c-Myc is stabilised by MEK1 phosphorylation, but acts as a negative feedback loop for MAPK signalling by supressing ERBB-kinases (Tsai *et al.*, 2012; C. Sun *et al.*, 2014). This provides a mechanism for BET protein mediated activation of MAPK signalling pathways. As aberrant MAPK signalling is associated with driving EMT-like transitions in cancer, the role of BET inhibitors in MEK inhibition resistance was investigated.

6.2 The relationship between BET proteins and EMT driven drug resistance

Epithelial mesenchymal transitions (EMT) is a natural developmental process first observed in the heart (Markwald, Fitzharris and Smith, 1975). The process was initially described as the invasion of the cardiac matrix between E8.5 and E12, when cells morphologically change and aggregate into fibroblastic cushions. However this pathway is often hijacked by cancer cells to promote invasion and tumour metastasis (Yang *et al.*, 2004; S. H. Wang *et al.*, 2017).

The EMT phenotype is the loss of cellular adhesion and membrane polarisation via reduced levels of E-cadherin and claudin proteins. Additionally N-cadherin, fibronectin, and extracellular matrix proteases are up regulated. Snail or Twist regulates this phenotypic switch and is strongly associated with metastasis (Rosivatz *et al.*, 2002; Yang *et al.*, 2004). Cells that have undergone an EMT-like transition often require the hyper activation of the Ras/Raf/MEK/ERK signalling pathway (Oft *et al.*, 1996; Seton-Rogers *et al.*, 2004; Xie *et al.*, 2004). In addition, compensatory kinase pathways (Pi3K and Src) that are known to have crossover with the Ras/Raf pathway have also been implicated as drivers of EMT and metastasis (Bakin *et al.*, 2000; Fang *et al.*, 2017).

EMT-like transitions occur with a high frequency in cutaneous melanomas, leading to aggressive metastasis and poor patient prognosis (Dissanayake *et al.*, 2007; Fenouille *et al.*, 2012). As 45% of patients present with BRAF mutations and 20% present with NRAS mutations, MAPK inhibition has been explored as a therapeutic avenue (Hocker and Tsao, 2007; Flaherty *et al.*, 2012). Unfortunately, melanomas rapidly develop resistance and metastasise by hyper activating the MAPK pathway and only 20% present with new genetic abnormalities (Shi *et al.*, 2012; Long *et al.*, 2014). This suggests that acquired drug resistance occurs on a genome regulation level, rather than by aberrant genetic instability. Additional studies indicate that EMT-like status was completely independent of MAPK mutational status and is reversible (Hoek *et al.*, 2006; Fallahi‐Sichani *et al.*, 2017). This further suggests that MAPK acquired drug resistance linked EMT-like transitions may be epigenetically regulated.

BET inhibition and loss of artificial heterochromatin silencing in the α-MEL system (**Table 3.2**) resulted in hyper phosphorylation of MAPK signalling, in addition to up regulation of EMT biomarkers including JNK signalling, FAK1, and STAT signalling. This suggested that BET proteins might function during EMT.

An HCT116 cell line, developed by John Dawson, has n-Ras driven MAPK signalling that when exposed to MEK inhibitor trametinib, developed resistance with a mesenchymal phenotype (**Figure 4.1**). This provided a useful model to utilise epigenetic inhibitors to determine EMT-like pathway epigenetic components in relation to patient phenotype.

As one might expect, crossover kinase inhibitors (PLK/Akt) were more sensitive in resistant cells with hyper phosphorylation of MAPK signalling (**Figure 4.3**). Additionally identifying polycomb as functioning in acquired drug resistance is supported by recent evidence implicating PRC2 as a regulator of EMT and poor patient prognosis (Jene-Sanz *et al.*, 2013; Tiwari *et al.*, 2013; Cardenas *et al.*, 2016).

BET inhibition sensitivity increased further in mesenchymal-like cells and correlates with the kinase signalling response identified in α-MEL cells (**Figure 4.8**). The use of multiple BET inhibitors enabled off-target effects to be ruled out, and were used to investigate the role of specific BET proteins based on inhibitor selectivity. This demonstrated that selectivity toward Brd2 correlated with cell survival (**Figure 4.7**). This specificity towards Brd2 has recently been supported by studies suggesting that Brd2 and Brd4 function as opposite drivers of EMT and MET respectively. Andrieu and Denis, (2018) demonstrated that EMT-like transitions in triple negative breast cancer are induced by an up regulation of Brd2 expression, a process repressed by Brd4. This is also supported in non-disease cellular environments. Brd4 to Brd2 occupancy switching at enhancers, including Nodal, results in mesodermal differentiation of mES cells (Fernandez‐Alonso *et al.*, 2017). This would explain the antagonistic effect observed in low concentrations in combination with trametinib (**Figure 4.5**).

Furthermore, c-Myc, the downstream effector protein for Ras/Raf/MEK/ERK signalling is up regulated by acquired MAPK inhibitor resistance (Singleton *et al.*, 2017; Zawistowski *et al.*, 2017). BET proteins are known to have an essential function in regulating c-Myc expression, presenting another dependency of EMT-like acquired drug resistance on Brd2/4 (Lovén *et al.*,

2013). There is growing evidence that cells having gone through an EMT-like transition, can overcome the loss of EMT drivers such as Notch/TGF-β signalling via enhancer BET protein occupancy (Yashiro-Ohtani *et al.*, 2014). Together this evidence supports the data presented here that BET proteins, and specifically Brd2, have a key regulatory role in EMT-like transitions and resistance to MEK inhibition.

When BET protein levels were observed in endothelial like (HCT116) and mesenchymal like (TRAMR) cells, Brd2 transcription and nuclear protein levels were elevated in the trametinib resistant mesenchymal like cells. Additionally Brd2 protein and transcript levels were both reduced upon BET inhibition in TRAMR cells indicative of a specific function on TRAMR cells (**Figures 4.12, 4.13**). Intriguingly this correlated with HP1α and HP1γ protein levels. Given HP1 proteins key role in chromatin compaction, this suggests that BET proteins may function to modulate chromatin organisational changes in mesenchymal like cells. Comparison of multiple endothelial and mesenchymal cell types demonstrated that BET protein occupancy at HP1 promoters only occurred in mesenchymal cells and that bromodomain inhibition reduced Brd2 occupancy (**Figures 4.15, 4.16**) (W. Liu *et al.*, 2013; Asangani *et al.*, 2014; Knoechel *et al.*, 2014).

HP1 proteins and large scale conformation changes in chromatin organisation are associated with EMT (McDonald *et al.*, 2011). Maybe, this is not surprising given the stark and relatively stable phenotypes of endothelial and mesenchymal cells. TGF-β induced EMT causes initial repression of pericentric transcription mediated by Snail1 recruitment and HP1α release (Millanes-Romero *et al.*, 2013). This demonstrates the potential for MAPK signalling to regulate the large scale chromatin reorganisation during EMT.

Furthermore BRCA1 functions to supress EMT with mutations associated with poor patient prognosis (Bai *et al.*, 2014). Loss of BRCA1 elevates major satellite transcription in mice while it also associates with HP1γ to form facultative heterochromatin mediated silencing of interspersed retrotransposons (Zhu *et al.*, 2011; Filipponi *et al.*, 2013).

To determine BET protein distribution immunofluorescence across the nucleus was used in endothelial and mesenchymal like cells (Figure **4.10**). While no discernible distribution pattern was observed for Brd2 or Brd3, JQ1 treatment resulted in the formation of Brd4 foci that were associated with the nuclear periphery in mesenchymal like cells. This suggests a direct function for BET proteins at heterochromatin, supported by the recent study demonstrating TIP60 mediated BET protein recruitment to heterochromatin (Grézy *et al.*, 2016). Together these data support the current opinion that BET proteins have a function in EMT-like transitions, while also suggesting that this function may be important for heterochromatin regulation and nuclear organisation.

6.3 H3K9me3 and chromatin compaction

Our understanding of heterochromatin structure and regulation currently remains limited. A key model system for investigation of HP1 proteins role at pericentric heterochromatin, are mouse embryonic stem cells and their Suv39h1 and Suv39h2 double null sister cells (Peters *et al.*, 2001).

Unlike human cells mouse constitutive heterochromatin is readily visible by microscopy and DAPI staining (**Figures 1.4, 5.13**). Despite the classical studies identifying Suv39h methyltransferases and HP1 proteins as suppressors of variegation, the cytologically distinct aggregates of constitutive heterochromatin are not lost upon Suv39h/H3K9me3/HP1 loss from these domains (**Figures 5.3, 5.11**). These domains in Suv39h knockouts also lack DNA methylation, H4K20me3, and increased histone acetylation (Peters *et al.*, 2001). Given these large-scale changes to the heterochromatin epigenetic profile, the maintained presence of chromocenters, questions the relevance of histone modifications and their binding partners having a causal role in chromatin structure regulation. Indeed studies have directly demonstrated that loss of DNA methylation from heterochromatin had no effect on chromatin structure (Gilbert, Thomson, Boyle, Allan, Ramsahoye and Wendy A. Bickmore, 2007).

To determine if H3K9me3 and HP1 proteins had a functional structural role at heterochromatin, the chromatin compaction state of wild type (WT41) and Suv39h1 and Suv39h2 double null (DN57)) mouse ES cells was analysed (**Figures 5.5, 5.6**). It was demonstrated that there was a resolvable loss in chromatin compaction in DN57 cells. This chromatin de-compaction was not

however limited to pericentric heterochromatin and suggested a global effect on chromatin compaction. Although H3K9me3 and HP1 is also found at facultative heterochromatin and interspersed retrotransposons, de-compaction of these additional regions would still not account for the global change in chromatin compaction. This suggests that the effects of correct heterochromatin formation and H3K9me3/HP1 association extend beyond heterochromatin, effecting euchromatic regions. This affect was abrogated by the reestablishment of H3K9me3 by exogenous human Suv39h1 expression (**Figure 5.12**). This is the first evidence that alterations in histone modifications can affect chromatin structure.

There is a growing body of evidence for an RNA component in chromatin compaction (Maison, Bailly, Peters, J. P. Quivy, *et al.*, 2002; Arnoult, Van Beneden and Decottignies, 2012). Both Suv39h and HP1 protein families have RNA binding domains, but the exact function of RNA is hotly debated (Maison *et al.*, 2011; Johnson *et al.*, 2017; Shirai *et al.*, 2017; Velazquez Camacho *et al.*, 2017). Chromatin associated RNA in DN57 cells was analysed and preliminary results indicated that H3K9me3 loss correlated with a global elevation in chromatin associated RNA (**Figures 5.13, 5.14**).

As previously stated, transitions to a mesenchymal-like phenotype require elevated levels of pericentric transcription and chromatin reorganisation (Zhu *et al.*, 2011). The expression of heterochromatic repetitive elements is inversely correlated with H3K9me3 and HP1 association in a mesnchymal setting (Filipponi *et al.*, 2013). This suggests that while RNA functions in heterochromatin formation, transcription of heterochromatic elements requires its absence (Casanova *et al.*, 2013; Velazquez Camacho *et al.*, 2017). Loss of H3K9me3 from constitutive heterochromatin is therefore likely to

increase satellite transcription. These repeat transcripts are non-coding and have been observed up to 8 kb in length in mouse cells (Quivy *et al.*, 2004).

Chromatin associated RNA has long been identified as a major chromatin component *in vivo* (Holmes *et al.*, 1972; Berezney and Coffey, 1974). Recent work by Nozawa *et al.*, (2017) demonstrated that chromatin associated RNA interacts with scaffold attachment factor A (SAF-A) to de-compact chromatin. This mechanism, coupled with increased satellite transcripts in the absence of H3K9me3 presents a potential mechanism for global chromatin de-compaction beyond the Suv39h wild type mediated domains of H3K9me3.

6.4 Perspectives

Regulation of chromatin structure is a complex multifaceted system utilising many biochemical and spatial components. These include; the transcriptional status, radial nuclear distribution, histone modifications, RNA containing nuclear scaffolds, cohesin and condensin mediated TAD formation, and most recently phase separation based on hydrophillicity (Wiblin *et al.*, 2005; Larson *et al.*, 2017; Nozawa *et al.*, 2017; Rao *et al.*, 2017). The interplay between these components has yet to reveal a causal driver of large-scale chromatin regulation.

However one can think of chromatin fibre structure regulation as a similar process to protein folding. Multiple orders of protein folding are required, and the local environment and physical forces must be tightly regulated to ensure a correct structure. In this manner, recent work understanding chromatin organisation into phase separated states with different hydrophilic forces suggests that chromatin regulators can alter the chromatin local environment to affect its structure (Larson *et al.*, 2017). This is consistent with protein folding where hydrophilicity is the greatest force effecting folding across the sequence (Dyson, Wright and Scheraga, 2006) and in proteins this results in the aggregation of hydrophobic residues to form secondary and tertiary structures (Camilloni *et al.*, 2016).

As such it is important to re-evaluate chromatin structure regulatory processes within a similar context. Histone acetylation or phosphorylation states for instance alters histone hydrophilicity (Lindner *et al.*, 1996). Additionally the disordered hydrophobic C-terminal domain of linker

histone H1 is required for chromatin compaction (Allan *et al.*, 1986). This suggests that H1 proteins alter the hydophilicity of the chromatin supramolecule to facilitate compaction. In this same way, H3K9me3 recruited HP1 proteins have an essential unstructured hinge region, that interacts with RNA (Meehan, Kao and Pennings, 2003). The oligomierisation of HP1 into large arrays in the supramolecule are therefore likely to change the fibres hydrophilictiy facilitating conformational changes or sequestration into liquid droplets (Strom *et al.*, 2017).

The large RNA component of chromatin, suggests that it would also have a significant effect on the chromatin fibre supramolecules hydrophilicity. The base pairs of nucleic acids are naturally hydrophobic while the polar phosphate backbone is hydrophilic. In physiological conditions DNA generally forms B-form helices with charges distributed throughout. RNA, in contrast, forms A-form helices where the base pairs are more exposed. RNA secondary structures can therefore dramatically alter their hydrophilicity profile dependent on conformation (Suga *et al.*, 2012). This switching between hydrophobic and hydrophilic states could therefore be regulatory by sequestering chromatin into liquid phase states. Altered RNA conformation by methylation or protein binding may also affect the physical properties of the underlying complex or molecule, providing a mechanism of action for RNA mediated tethering or aggregation.

While the studies presented here demonstrate that histone modifications can directly alter chromatin fibre compaction, it is possibly indirect via altering non-coding RNA transcription. Pericentric non-coding RNA transcription has been presented as a driver of chromatin reorganisation in EMT/MET-like processes (Millanes-Romero *et al.*, 2013). This supports observations herein of

Brd4 foci formation at the nuclear periphery once global Brd2 levels were reduced.

This work suggests that a Brd2/Brd4 switch functions in altering chromatin organisation and is supported by recent publications (Cheung *et al.*, 2017; Fernandez‐Alonso *et al.*, 2017). It also suggests that Brd2 is a key regulator of EMT-like acquired drug resistance, but understanding mechanistically how Brd2 modulates this process would be the next step. These studies investigating the fundamental components of heterochromatin provide further evidence that RNA can modulate chromatin structure; the mechanism behind such regulation remains the elusive goal of the heterochromatin field.

Appendices

Appendix 1. α-MEL eGFP reactivation compound screen. eGFP expression after α-MEL cells were screened with each compound in turn for 48 hours, and fluorescence determine by flow cytometry. Table of initially screened compounds (n = 1) GFP fluorescence after treatment for 48 hours at 1 μM (unless stated otherwise).

Compound	Δ Mean GFP		Compound	Δ Mean GFP
(-)-Neplanocin A	0.81		*Au7*	-0.52
(5Z)-7-Oxozeaenol	0.53		*Au8*	-0.65
(BIX)	-1.09		*Au9*	-0.54
0572-0022	0.58		*Aurora*	4.10
2-PCPA	0.29		*BAY 11-7082*	1.07
2,4 DPD	0.34		*Benzo(a)pyrene*	16.82
2,4-Pyridinedicarboxylic Acid	0.33		*Bromosporin*	1.56
3-amino Benzamide	0.37		*Bromosporin (0.05uM)*	0.41
3-Deazaneplanocin A	0.36		*Bromosporin (0.1uM)*	0.25
3270-0102	0.45		*Bromosporin (0.2uM)*	0.58
3606-0139	0.35		*Bromosporin (0.5uM)*	1.14
3656-0028	0.42		*Bromosporin (1.5uM)*	2.22
4-ido-SAHA	0.36		*BSI-201*	0.53
8012-2210	0.37		*Capcecitabine*	0.90
AG 490	0.42		*Carmofur 1uM*	245.02
AG-014699	2.39		*CAY10398*	2.79
AGK2	0.30		*CAY10433*	3.74
Akt Inhibitor IV	0.22		*CAY10603*	13.73
Akt Inhibitor VIII, Isozyme-Selective, Akti-1/2	0.41		*CBHA*	0.36
Aldrin	20.18		*CCG-100602*	0.33
Anacardic Acid	0.27		*Chaetocin (100nM)*	0.42
Apicidin	0.34		*Chidamide*	0.43
Aspirin	-0.03		*CR8*	6.04
Aspirin (500uM)	2.07		*Cy1*	-0.55
Aspirin (5uM)	0.06		*Cy10*	-0.52
Au1	-0.63		*Cy11*	-0.56
Au10	-0.64		*Cy12*	-0.58
Au11	-0.63		*Cy13*	-0.60
Au12	-0.64		*Cy14*	-0.58
Au13	-0.59		*Cy15*	-0.60
Au14	-0.55		*Cy16*	-0.55
Au15	0.51		*Cy17*	0.09
Au16	-0.52		*Cy18*	-0.62
Au17	-0.65		*Cy19*	4.48
Au2	-0.64		*Cy2*	-0.60
Au3	-0.56		*Cy20*	-0.63
Au4	-0.68		*Cy21*	-0.58
Au5	0.38		*Cy22*	-0.62
Au6	-0.56		*Cy3*	-0.59

Compound	Δ Mean GFP		Compound	Δ Mean GFP
Cy4	-0.56		*Dg29*	-0.58
Cy5	0.52		*Dg3*	-0.52
Cy6	-0.52		*Dg30*	-0.51
Cy7	-0.51		*Dg31*	-0.61
Cy8	-0.51		*Dg32*	-0.68
Cy9	-0.56		*Dg33*	-0.69
Daminozide	0.36		*Dg34*	0.50
Decitabine	2.71		*Dg35*	-0.67
Dg1	-0.57		*Dg36*	-0.62
Dg10	0.15		*Dg37*	-0.53
Dg11	-0.58		*Dg38*	-0.60
Dg12	-0.59		*Dg4*	-0.60
Dg13	-0.58		*Dg5*	-0.05
Dg14	-0.60		*Dg6*	-0.66
Dg15	-0.59		*Dg7*	-0.55
Dg16 (10uM)	4.17		*Dg8*	-0.57
Dg16 (0.05uM)	1.62		*Dg9*	-0.63
Dg16 (0.1uM)	1.39		*Diloxanide Furoate*	17.52
Dg16 (1.5uM)	0.63		*DMOG*	0.36
Dg16 (0.5uM)	2.36		*EGFR*	7.24
Dg17 (5uM)	0.93		*EGFR (0.2uM)*	0.35
Dg17	-0.57		*Ellagic Acid*	0.38
Dg18	-0.57		*Emi1 (15um)*	3.17
Dg19 (10uM)	4.10		*Emi1 (10uM)*	2.27
Dg19 (0.05uM)	0.98		*Emi1*	0.57
Dg19 (0.1uM)	0.65		*ERK Inhibitor II*	0.35
Dg19 (0.5uM)	1.30		*Estradiol Acetate*	15.71
Dg19 (1uM)	2.83		*Et-18-OCH3*	0.37
Dg2 (5uM)	1.20		*EX-527*	0.33
Dg2	-0.58		*F-Amidine*	0.33
Dg20	-0.18		*Garcinol*	0.32
Dg21	-0.57		*Gemcitabine*	6.25
Dg22	-0.58		*GSK2801*	0.71
Dg23	-0.60		*GSK343*	-0.14
Dg24	-0.65		*Guanabenz acetate (1uM)*	58.97
Dg25	-0.07		*GW 843682X*	2.79
Dg26	-0.60		*HC Toxin*	-0.28
Dg27	-0.55		*Heptachlor (1uM)*	28.62
Dg28	-0.56		*Histone Acetyltransferase Inhibitor II*	0.51

Compound	Δ Mean GFP		Compound	Δ Mean GFP
HNHA	0.47		*Lp32*	0.43
IKK VII	1.96		*Lp4*	0.46
IL-1 Receptor-Associated-Kinase-1/4 Inhibitor	0.41		*Lp5*	0.37
IOX1	3.30		*Lp6*	0.00
isoliquiritigenin	0.17		*Lp7*	0.80
JC1	0.14		*Lp8*	1.67
JC2	0.19		*Lp9*	0.31
JGB1741	1.84		*LY 294002*	0.34
JNK II	0.30		*LY 303511*	0.53
JNK IX	8.05		*M 344*	0.81
JQ1 -/-	0.21		*MEK1/2 Inhibitor*	0.41
JQ1 +/-	11.13		*MG-132*	0.00
Larixol Acetate	17.75		*MI-2 (hydrochloride)*	0.31
Lomeguatrib	0.57		*MI-nc (hydrochloride)*	0.45
Lp1	0.44		*Mirin*	0.43
Lp10	0.36		*MK2a Inhibitor*	0.38
Lp11	0.17		*MNK1 Inhibitor*	0.36
Lp12	0.35		*MS-275*	16.37
Lp13	0.46		*N-Oxalylglycine*	11.74
Lp14	0.26		*NEMO Binding Domain Peptide, Cell-Permeable*	0.47
Lp15	0.63		*Neplanocin A*	-0.19
Lp16	0.21		*NF-kB SN50 cell-permeable inhibitor peptide*	0.51
Lp17	0.40		*Nicotinamide*	7.29
Lp18	0.58		*Norethindrone Acetate (1uM)*	39.69
Lp19	1.88		*Oxamflatin / CR8 0.1uM*	0.31
Lp2	0.54		*p212 - positive control*	3.84
Lp20	0.36		*p38 MAP Kinase V*	0.47
Lp21	0.00		*PCI 34051*	0.32
Lp22	0.38		*PD 153035*	0.49
Lp23	0.33		*PD 168393*	0.36
Lp24	0.50		*PD 98059*	0.36
Lp25	0.23		*PDK1/Akt/Flt Dual Pathway Inhibitor*	1.49
Lp26	0.68		*Phthalazinone pyrazole*	0.87
Lp27	1.25		*PI 3-Ka Inhibitor IV*	0.41
Lp28	0.73		*PI 3-Ka Inhibitor VIII*	0.00
Lp29	0.61		*PI 3-Ky Inhibitor*	0.39
Lp3	0.59		*PI 3-Ky Inhibitor II*	0.44
Lp30	0.34		*PI-103*	0.46
Lp31	0.43		*Piceatannol*	0.33

Compound	Δ Mean GFP		Compound	Δ Mean GFP
Pimelic Diphenylamide 106	0.49		*Splitomicin*	0.47
PKC	5.10		*Suramin (sodium salt)*	1.80
Polo	4.16		*Tenovin-1*	0.38
PP2	0.36		*Tenovin-6*	1.03
Raf Kinase Inhibitor IV	0.36		*TIRAP Inhibitor Peptide*	0.41
Rapamycin	0.40		*Tpl2 Kinase Inhibitor*	0.46
RG-108	0.34		*transreservatol*	1.72
Ro-31-8220	6.78		*TSA*	3.18
Ronnel (1uM)	50.83		*TSA (0.05uM)*	0.17
Roscovitine	0.66		*Tubastatin A*	2.44
S-Adenosylhomocysteine	0.38		*UNC0224*	5.28
S-HDAC-42	5.48		*UNC0321*	0.40
SAHA	0.75		*UNC0638*	0.31
Salermide	0.40		*UNC642*	1.30
SB 203580	0.34		*Valproic Acid (sodium salt)*	1.03
SB 939	0.34		*Wortmannin*	0.34
Scriptaid	0.45		*Zebularine*	-0.15
SGC0946	0.25		*ZM 336372*	0.32
SGC946	-1.25		*ZM447439*	0.26
Sinefungin	0.35			
Sirtinol	0.29			
Sodium Butyrate	0.29			
Sp1	0.45			
Sp10	0.90			
Sp11	1.29			
Sp12	0.63			
Sp13	0.81			
Sp14	0.67			
Sp15	5.35			
Sp16	-0.22			
Sp17	0.85			
Sp18	1.51			
Sp2	0.55			
Sp3	0.35			
Sp4	0.85			
Sp5	0.62			
Sp6	0.83			
Sp8	0.60			
Sp9	1.07			

Appendix 2. Significant kinase changes to BET inhibition in α-MEL cells. α-MEL cells were treated with I-BET151 or JQ1$^{+/-}$ 1 μM for 24 hours. Protein lysates were spotted onto arrays and changes in kinase signaling after JQ1 treatment when compared to DMSO controls. JQ1 and IBET151 treated α-MEL cells were treated as replicates and binned together before compared to DMSO controls. Bonferoni two-tail T-test analysis performed (*, $p < 0.05$) (**, $p < 0.01$).

Antibody	Δ from DMSO (%)	p-value (Bonfferoni)	
Aurora A/B/C P Thr288/Thr232/Thr198	6.44519	0.10506	
4E-BP1 P Thr37,Thr46	0.87368	0.64904	
cdc25c P Ser216	-9.11976	0.94855	
Chk2 P Thr68	11.88517	0.18978	
c-Jun N-term	17.69132	0.01145	*
c-Myc P Thr58,Ser62	-7.35673	0.39302	
E-Cadherin	-6.67194	0.91235	
MSK1 P Ser376	-30.26415	0.45308	
mTOR	-11.02459	0.14509	
mTOR P Ser2448	17.66879	0.39144	
NFkB p65 Ser536	-9.24335	0.16715	
PKC-zeta	4.34305	0.54305	
PKC-zeta/lambda P Thr410/403	60.84479	1.4041E-8	**
PLC-gamma1 P Tyr783	-9.89165	0.50011	
S6 Ribosomal Protein	78.53622	7.21852E-6	**
S6 Ribosomal protein p Ser240,Ser244	-8.22251	0.30155	
Smad2 P Ser465,Ser467	28.16944	0.86498	
Rap1	8.55371	0.01055	*
SHP2 P Tyr542	39.49585	0.226	
Rsk2 Pser 227	24.95864	0.29239	
HSP27 (HSPB1) P Ser78	6.6682	0.71094	
4E-BP1 P Ser65	-20.83569	0.42234	
Akt	-34.06083	0.39016	
Akt P Ser473	36.70238	0.80798	
Akt P Thr308	-12.04095	0.74826	
Caspase 3 cleaved	11.92449	0.06253	
cdc25A	9.44207	0.15076	
c-Myc	-17.4683	0.27919	
FAK1	38.03102	0.03026	*
FAK1 P Y397	19.6461	0.27548	
FLT3 P Tyr591 P Tyr591	8.64978	0.94429	
FRA1 (R20)	-36.14749	0.03756	*
CrkL P Tyr207	5.78553	0.82463	
IkB-alpha P Ser32	-21.707	0.61878	
JAK1	52.46253	0.22952	
M-CSF P Tyr723	12.72261	0.87217	
Met	-3.26008	0.83988	
p44/42 MAPK (ERK1/2)	19.71564	0.73101	
p44/42 MAPK (ERK1/2) P Thr202/ Thr185,Tyr204/Tyr187	-21.25869	0.01666	*
PARP	31.4968	0.9208	

Antibody	Δ from DMSO (%)	p-value (Bonfferoni)	
MNK1 (MKNK) P Thr197,Thr202	-39.27636	0.61036	
PLC-gamma1	-3.1172	0.16989	
Rb P Ser807,Ser811	-16.34957	0.30713	
Rb P Ser780	-27.31356	0.24622	
SAPK/JNK P Thr182,Tyr185	-36.06825	0.79981	
Smad1/5 P Ser463/Ser465	18.54171	0.49885	
Smad2/3 P Ser465/Ser423,Ser467/ Ser425	10.2274	0.1277	
Src	-13.18699	0.6444	
Src (family) P Tyr416	15.72738	0.32347	
Stat1 P Tyr701	0.62763	0.61232	
Tyk2 P Tyr1054,Tyr1055	2.40378	0.93809	
p38 MAPK PThr180,Tyr182	15.41003	0.19554	
SAPK/JNK P Thr183,Tyr185	34.97637	0.01578	*
Stat5 - P Tyr694	20.41217	0.14411	
CamKII P Thr286	-3.39871	0.29391	
c-Jun P Ser73	-4.13745	0.81072	
IkB-alpha	-26.71028	0.42434	
Met P Tyr1234	-64.97844	0.01494	*
mTOR P Ser2481	-35.38782	0.62712	
NFkB p105/p50	-18.58814	0.12048	
PKA	68.94439	6.83351E-6	**
PKA RII P Ser96	14.90733	0.06074	
PKC (pan) P Ser660 (beta-2)	11.15055	0.15356	
PKC substrate P (R/K)X(S*)(Hyd)(R/k)	-6.04377	0.85386	
PKC-alpha P Thr638	14.41444	0.09393	
Smad3 P Ser423,Ser425	-32.06197	0.2913	
GFAP	43.36762	0.97368	
JAK1 P Tyr1022,Thr1023	30.51295	0.46123	
Stat1 P Ser727	-2.50696	0.28895	
Stat5	-12.56719	0.00665	**
ATM/ATR Substrate P Ser/Thr	27.32039	0.08394	
beta-Tubulin	60.8556	0.08571	
BRCA1	-15.7777	0.6025	
PKC-gamma P Thr514	-37.18325	0.42836	
Stat6 P Tyr641	-53.17693	0.48437	
Zap70	3.22279	0.97344	
PDGFR P Tyr751	-58.16615	0.4269	
PDGFR P Tyr1021	-12.30663	0.6137	
MAPKAPK-2	91.92744	3.82085E-9	**
SAPK/JNK	30.08464	0.00565	*

Appendix 3. Kinase signaling changes in response to trametinib. Cells were treated with DMSO or 300 nM Trametinib for 24 hours before protein lysates were prepared and spotted onto arrays. List of all changes to kinase antibody fluorescence between either; **(1)** basal states of HCT116 and its trametinib resistant sister cells TRAMR, **(2)** HCT116 cells trametinib 300nM 24 hour treatment to DMSO controls, or **(3)** TRAMR cells trametinib 300 nM 24 hour treatment to DMSO controls.

Antibody	Basal Δ TRAMR	*p-value*	HCT116 Δ Trametinib	p-value	TRAMR Δ Trametinib	*p-value*
PKM2 XP(R)	1.09	0.874	1.51	0.468	0.98	0.965
SQSTM1	0.98	0.969	1.32	0.643	1.25	0.594
PLC-gamma1	1.16	0.782	0.85	0.832	0.93	0.874
Puma	1.17	0.777	0.97	0.961	0.87	0.784
VEGFR *P Tyr951*	0.88	0.834	1.33	0.632	1.23	0.632
Plk1 *P*	1.37	0.530	0.37	0.367	0.73	0.572
Calpastatin	1.46	0.433	1.48	0.492	1.01	0.977
ErbB-2/Her2/EGFR	0.63	0.527	1.72	0.305	1.53	0.258
FRA1 (R20)	0.93	0.904	1.06	0.937	1.11	0.816
cdc2	0.97	0.958	1.62	0.378	1.26	0.583
Bcl-2 *P Ser70*	1.25	0.666	0.86	0.844	0.76	0.614
Fox01 *P*	1.42	0.478	0.88	0.866	0.80	0.678
HDAC4/5/6/7 *P*	1.37	0.525	0.82	0.797	0.77	0.630
Ezrin/ERM *P*	0.97	0.960	1.62	0.372	1.19	0.684
ErbB-2/Her2/EGFR *P Tyr1248/Tyr1173*	0.97	0.958	3.79	<0.001	2.09	0.021
IGF-1R beta *P Tyr1162,Tyr1163*	0.82	0.761	1.79	0.261	1.22	0.648
SAPK/JNK	0.86	0.813	0.96	0.954	0.95	0.922
LKB1	0.92	0.897	1.13	0.849	1.04	0.931
GSK-3-alpha/beta *P Ser21/Ser9*	1.39	0.510	0.58	0.550	0.55	0.345
Stat6	0.94	0.925	1.88	0.210	1.35	0.457
MAPKAPK-2	1.07	0.901	0.91	0.900	0.93	0.889
Stat3	0.46	0.360	1.24	0.730	1.17	0.722
VEGFR *P Tyr1059*	0.52	0.414	1.37	0.595	1.56	0.237
XIAP	0.78	0.712	0.60	0.570	0.76	0.611
CamKII *P Thr286*	0.86	0.817	0.68	0.642	0.84	0.729
IkB-alpha	0.91	0.881	2.19	0.089	1.64	0.176
MEK1/2	0.85	0.793	1.12	0.864	0.96	0.937
MEK1/2 *P Ser217/221*	1.79	0.175	1.31	0.653	0.96	0.934
Met *P Tyr1234*	0.99	0.980	2.66	0.018	1.94	0.048
PKA RII P Ser96	1.05	0.930	0.87	0.853	0.95	0.921
PKC (pan) *P Ser660* (beta-2)	1.22	0.706	0.94	0.929	0.79	0.651
PKC substrate *P (R/K)X(S*)(Hyd)(R/k)*	1.23	0.689	0.82	0.800	0.96	0.931
Met *P Tyr1349*	0.97	0.964	2.36	0.052	1.69	0.146
ErbB-1/EGFR	1.22	0.709	1.03	0.968	0.86	0.761
EGFR *P Tyr1173*	0.97	0.964	1.73	0.293	1.36	0.441

Antibody	Basal Δ TRAMR	*p-value*	HCT116 Δ Trametinib	p-value	TRAMR Δ Trametinib	*p-value*
S6 Ribosomal protein *P Ser235,Ser236*	1.13	0.830	0.06	0.178	0.30	0.141
beta-actin	1.15	0.802	0.66	0.626	0.69	0.508
c-Jun *P Ser73*	1.34	0.558	1.67	0.340	0.85	0.753
Rb	0.98	0.979	0.13	0.216	0.35	0.172
beta-Catenin *P Ser33,Ser37,Thr41*	1.12	0.844	0.90	0.881	1.45	0.337
Tsc-2 (Tuberin)	0.94	0.914	1.42	0.549	1.23	0.622
Bax	1.11	0.848	0.75	0.716	0.86	0.763
Bcl-x	0.87	0.831	0.71	0.676	0.75	0.592
IRS-1	2.07	0.069	0.44	0.423	0.83	0.724
IRS-1 *P S636/639*	1.00	0.994	0.67	0.634	0.72	0.547
VEGFR *P Tyr1175*	1.04	0.948	0.24	0.276	0.48	0.273
Smad3 *P Ser423,Ser425*	1.08	0.891	0.56	0.531	1.12	0.795
NFkB *p105/p50*	1.08	0.890	1.75	0.284	1.36	0.440
PKA	0.95	0.930	1.20	0.771	1.18	0.701
PKC-alpha *P Thr638*	0.78	0.708	0.92	0.914	0.99	0.979
Raf1 (C-12)	1.02	0.979	0.93	0.917	1.01	0.990
p21 CIP/WAF1 *p Thr145*	0.99	0.984	0.96	0.953	1.27	0.569
mTOR *P Ser2481*	0.76	0.676	1.17	0.808	1.30	0.519
p70 S6 Kinase *P Thr421,Ser424*	1.29	0.618	0.44	0.419	0.28	0.128
EGFR *P Tyr1086*	0.42	0.326	2.36	0.051	1.92	0.052
GFAP	1.22	0.711	1.63	0.365	1.09	0.845
ATM/ATR Substrate *P Ser/Thr*	0.80	0.728	0.68	0.645	0.71	0.541
Stat5	1.02	0.971	1.17	0.810	1.06	0.891
Stat1 *P Ser727*	1.04	0.951	0.73	0.700	0.85	0.752
JAK1 *P Tyr1022,Thr1023*	1.06	0.919	1.56	0.421	1.36	0.448
beta-Tubulin	1.18	0.760	0.75	0.725	0.85	0.751
Prohibitin	0.69	0.597	0.76	0.729	0.78	0.639
p90 S6 kinase (Rsk1-3)	0.47	0.365	1.30	0.665	1.48	0.310
p53	0.79	0.724	0.71	0.680	0.95	0.914
Histone H2A.X *P Ser139*	0.92	0.887	1.37	0.601	1.25	0.602
Cyclin D1	1.07	0.910	0.51	0.481	0.61	0.412
CrkL	1.06	0.924	0.73	0.698	0.79	0.656
Ki-67 (Annexin II, p36)	0.24	0.196	-0.04	0.138	0.94	0.907

Antibody	Basal Δ TRAMR	*p-value*	HCT116 Δ Trametinib	p-value	TRAMR Δ Trametinib	*p-value*
Calmodulin	1.29	0.620	0.97	0.970	0.99	0.976
Stat1	0.67	0.575	1.00	0.994	1.01	0.988
HSP27 (HSPB1)	1.02	0.975	1.00	0.995	1.15	0.745
Stat3 *P Tyr705*	0.90	0.858	0.69	0.655	0.87	0.776
Ras	0.91	0.881	0.84	0.823	0.89	0.812
p21 CIP/WAF1	1.02	0.976	1.12	0.864	1.03	0.952
PKC-alpha	0.89	0.848	1.06	0.933	1.03	0.950
CamKII alpha (22B1) *P Thr286*	0.95	0.935	1.19	0.787	1.01	0.976
GAPDH	0.42	0.324	1.17	0.807	1.70	0.137
Ubiquitin (P4D1)	0.99	0.988	0.59	0.555	0.68	0.495
rabbit	0.75	0.665	0.89	0.876	1.73	0.125
Aurora A/B/C *P Thr288/ Thr232/Thr198*	1.15	0.801	0.61	0.578	0.81	0.689
Bad *P Ser136*	0.81	0.742	0.72	0.687	0.71	0.537
Bak	0.95	0.937	0.78	0.758	0.79	0.662
HSP27 (HSPB1) *P Ser78*	0.84	0.787	0.84	0.815	1.08	0.872
IKK alpha/beta *P Ser176/Ser177*	0.96	0.946	1.90	0.198	1.45	0.344
MSK1 *P Ser376*	1.16	0.786	0.97	0.971	0.82	0.704
PKC-zeta	1.05	0.929	0.98	0.981	1.00	0.996
PKC-zeta/lambda *P Thr410/403*	1.08	0.897	1.25	0.718	1.22	0.634
Bim	0.97	0.962	1.04	0.950	0.96	0.932
Rap1	0.95	0.934	1.30	0.664	1.14	0.766
ErbB-2/Her2/EGFR *P Tyr1248/Tyr1173*	1.03	0.955	1.99	0.156	1.28	0.551
mTOR *P Ser2448*	1.11	0.847	0.85	0.832	1.05	0.908
S6 Ribosomal Protein	0.93	0.900	1.30	0.667	1.15	0.747
NFkB p65 *P Ser536*	1.05	0.939	0.94	0.933	0.96	0.926
cdc25c *P Ser216*	0.80	0.733	0.60	0.566	0.90	0.838
Chk2 *P Thr68*	1.17	0.774	0.83	0.810	0.77	0.632
E-Cadherin	0.70	0.613	1.08	0.905	0.90	0.825
4E-BP1 *P Thr37,Thr46*	1.14	0.817	1.09	0.898	1.13	0.786
beta-Catenin *P Thr41,Ser45*	0.58	0.473	0.57	0.543	1.53	0.266
Survivin	0.83	0.769	0.76	0.732	0.85	0.759

Antibody	Basal Δ TRAMR	*p-value*	HCT116 Δ Trametinib	p-value	TRAMR Δ Trametinib	*p-value*
PTEN *P Ser380,Thr382,Thr383*	0.95	0.927	0.77	0.744	0.94	0.901
PLC-gamma1 *P Tyr783*	1.04	0.939	3.29	0.001	1.83	0.078
PDK-1 *P Ser241*	0.98	0.975	0.85	0.835	0.93	0.885
p90 S6 kinase (Rsk1-3) *P Thr359,Ser363*	1.53	0.362	0.56	0.526	0.33	0.155
p70 S6 Kinase	1.03	0.960	0.79	0.760	0.91	0.841
S6 Ribosomal protein *P Ser240,Ser244*	1.33	0.575	0.32	0.330	0.31	0.146
mTOR	0.96	0.941	1.20	0.774	1.14	0.768
c-Myc *P Thr58,Ser62*	0.99	0.988	1.03	0.968	0.91	0.846
AMPK alpha	1.05	0.936	1.01	0.987	1.00	0.999
c-Jun N-term	1.20	0.731	1.99	0.155	1.82	0.081
CDK1 (p34cdc2) *P Tyr15*	1.10	0.862	1.68	0.331	1.23	0.627
CREB	0.93	0.910	0.98	0.981	0.88	0.801
SHP2 *P Tyr542*	1.30	0.610	3.26	0.001	1.91	0.053
Smad2 *P Ser465,Ser467*	1.05	0.937	0.60	0.564	1.11	0.820
Tau	0.86	0.805	-0.02	0.146	0.41	0.213
Tau *Phospho/non Phos ser 305*	1.12	0.838	0.37	0.364	0.53	0.319
Rsk2 *P ser 227*	1.02	0.977	0.69	0.659	0.54	0.327
ATM	0.82	0.759	0.94	0.927	1.17	0.724
Stat6 *P Tyr641*	0.94	0.913	1.89	0.204	1.37	0.439
BRCA1	0.92	0.897	0.31	0.321	0.70	0.531
CDK2	0.92	0.885	0.60	0.563	0.77	0.629
Zap70	0.89	0.853	1.13	0.852	0.95	0.914
PDGFR *P Tyr1021*	0.78	0.712	1.54	0.438	1.49	0.302
PDGFR *P Tyr751*	0.85	0.803	1.91	0.193	1.46	0.331
TBK1/NAK	1.11	0.848	1.07	0.922	1.13	0.786
FAK1	0.90	0.861	0.64	0.609	0.95	0.920
FAK1 *P Y397*	0.80	0.728	2.35	0.054	1.48	0.306
Bad *P Ser112*	1.23	0.697	0.82	0.797	0.80	0.670
CrkL *P Tyr207*	1.55	0.346	1.44	0.531	0.31	0.143
FLT3 *P Tyr591 P Tyr591*	0.98	0.974	3.13	0.002	1.91	0.055
JAK1	0.93	0.903	1.31	0.660	1.52	0.275

Antibody	Basal Δ TRAMR	*p-value*	HCT116 Δ Trametinib	p-value	TRAMR Δ Trametinib	*p-value*
MNK1 (MKNK) *P Thr197,Thr202*	1.08	0.887	0.56	0.524	0.75	0.601
PARP	1.16	0.779	1.13	0.853	0.95	0.915
PI3 Kinase p110-alpha	0.96	0.940	0.65	0.613	0.76	0.617
GSK-3-beta	1.02	0.969	0.81	0.782	0.89	0.818
ErbB-3/Her3/EGFR	0.86	0.812	1.16	0.817	1.07	0.885
ErbB-3/Her3/EGFR *P Tyr1289*	1.03	0.964	1.23	0.747	1.07	0.882
Stat5 *P Tyr694*	1.12	0.832	2.21	0.084	1.49	0.301
Akt *P Thr308*	0.92	0.892	0.99	0.990	0.99	0.978
Met	0.87	0.826	1.05	0.945	0.93	0.876
IkB-alpha *P Ser32*	0.86	0.814	0.79	0.764	0.87	0.785
p44/42 MAPK (ERK1/2)	1.02	0.978	1.34	0.625	1.11	0.815
p44/42 MAPK (ERK1/2) *P Thr202/ Thr185,Tyr204/Tyr187*	2.43	0.015	0.65	0.616	-0.72	0.000
Src	1.04	0.948	1.01	0.990	0.92	0.869
Akt	0.82	0.764	1.02	0.981	1.09	0.848
Akt *P Ser473*	2.10	0.062	1.11	0.875	0.47	0.258
PARP cleaved Asp214	1.06	0.920	1.02	0.976	0.92	0.871
Chk1 *P Ser345*	0.99	0.981	0.78	0.754	1.01	0.975
c-Myc	1.05	0.932	0.63	0.599	0.59	0.389
M-CSF *P Tyr723*	0.91	0.876	0.96	0.958	0.93	0.884
4E-BP1 *P Ser65*	1.19	0.740	0.83	0.810	0.99	0.984
beta-Catenin	0.88	0.841	1.01	0.986	1.00	0.996
cdc25A	1.25	0.664	1.32	0.647	1.55	0.243
PTEN	0.91	0.882	1.35	0.613	1.14	0.762
Tyk2 *P Tyr1054,Tyr1055*	0.83	0.776	1.64	0.358	1.86	0.069
Tsc-2 (Tuberin) *P Thr1462*	0.86	0.809	0.99	0.985	0.97	0.957
p70 S6 Kinase *P Thr389*	1.04	0.949	0.79	0.764	0.84	0.728
SAPK/JNK *P Thr183,Tyr185*	1.06	0.913	2.66	0.018	1.66	0.161
p53 *P Ser15*	0.93	0.906	1.40	0.564	1.97	0.041
p38 MAPK *P Thr180,Tyr182*	1.11	0.847	1.21	0.760	1.05	0.910
p38 MAPK	1.00	0.995	0.98	0.982	0.94	0.907

Antibody	Basal Δ TRAMR	*p-value*	HCT116 Δ Trametinib	p-value	TRAMR Δ Trametinib	*p-value*
Raf *P Ser259*	1.05	0.934	1.08	0.905	1.13	0.783
PDK_1	0.94	0.922	0.91	0.896	1.02	0.967
IGF1R	0.93	0.903	0.90	0.890	1.10	0.832
Rb *P Ser807,Ser811*	0.91	0.877	0.18	0.242	0.49	0.279
Rb *P Ser780*	1.15	0.798	0.56	0.525	0.71	0.536
Raf *P Ser338*	0.99	0.984	0.94	0.933	0.91	0.849
MAPKAPK-2 *P Thr334*	1.07	0.899	0.83	0.805	0.93	0.888
Stat1 *P Tyr701*	1.02	0.975	2.16	0.096	1.50	0.289
Src (family) *P Tyr416*	1.16	0.788	1.58	0.407	1.13	0.776
Smad2/3 *P Ser465/ Ser423,Ser467/ Ser425*	1.16	0.788	1.02	0.973	0.93	0.886
Smad1/5 *P Ser463/ Ser465*	1.03	0.958	0.95	0.938	0.91	0.855
Cyclin D1 *P Thr286*	0.83	0.778	0.93	0.923	0.80	0.678
AMPK alpha *P Thr172*	1.00	0.997	1.39	0.572	1.08	0.873
Bcl_2	1.05	0.929	1.11	0.878	1.06	0.892
Bid	0.98	0.968	1.10	0.886	0.96	0.940
Bim *P Ser69*	0.99	0.987	0.96	0.952	0.90	0.834
Caspase 3	1.02	0.978	0.97	0.961	1.20	0.669
Caspase 3 cleaved	0.95	0.927	0.91	0.892	0.97	0.954
SHP2	1.06	0.915	1.23	0.742	1.10	0.833
GSK-3-beta *P Ser9*	1.37	0.533	0.74	0.710	0.67	0.489
GSK 3 B	1.09	0.875	0.71	0.678	0.82	0.696
Hexokinase	0.97	0.957	0.82	0.794	0.85	0.756
SHP2 *P Tyr580*	0.89	0.854	1.40	0.566	1.17	0.713
Calpain2	1.29	0.626	1.28	0.692	0.97	0.955
Tuberin *P S1387*	0.97	0.959	0.94	0.937	1.45	0.346

References

Aagaard, L. *et al.* (2000) 'Mitotic phosphorylation of SUV39H1, a novel component of active centromeres, coincides with transient accumulation at mammalian centromeres.', *Journal of cell science*, 113 (5), pp. 817–29.

Abe, H. *et al.* (2011) 'Discovery of a highly potent and selective MEK inhibitor : GSK1120212 (JTP-74057 DMSO Solvate)', *ACS Medicinal Chemistry Letters*, 1120212, pp. 320–324.

Adachi, Y., Luke, M. and Laemmli, U. K. (1991) 'Chromosome assembly in vitro: topoisomerase II is required for condensation.', *Cell*, 64(1), pp. 137–148.

Adams, R. R. *et al.* (2001) 'Essential roles of Drosophila inner centromere protein (INCENP) and aurora B in histone H3 phosphorylation, metaphase chromosome alignment, kinetochore disjunction, and chromosome segregation', *Journal of Cell Biology*, 153(4), pp. 865–879.

Ainsztein, A. M. *et al.* (1998) 'INCENP centromere and spindle targeting: Identification of essential conserved motifs and involvement of heterochromatin protein HP1', *Journal of Cell Biology*, 143(7), pp. 1763–1774.

Alabert, C. *et al.* (2014) 'Nascent chromatin capture proteomics determines chromatin dynamics during DNA replication and identifies unknown fork components', *Nature Cell Biology*, 16(3), pp. 181-191

Alarcon-vargas, D. and Ronai, Z. (2004) 'c-Jun-NH 2 Kinase (JNK) contributes to the regulation of c-Myc protein stability', *Journal of Biological Chemistry*, 279(6), pp. 5008–5016.
Alberts, B. *et al*. (1994) *Chromosomal DNA and its packaging - Molecular Biology of the Cell. 3rd edition. New York: Garland Science*.

Aldrup-MacDonald, M. E. and Sullivan, B. A. (2014) 'The past, present, and future of human centromere genomics', *Genes*, 5(1), pp. 33–50.

Alekseyenko, A. A. *et al.* (2015) 'The oncogenic BRD4-NUT chromatin regulator drives aberrant transcription within large topological domains', *Genes and Development*, 29(14), pp. 1507–1523.

Alipour, E. and Marko, J. F. (2012) 'Self-organization of domain structures by DNA-loop-extruding enzymes', *Nucleic Acids Research*, 40(22), pp. 11202–11212.

Allan, J. *et al.* (1980) 'The structure of histone H1 and its location in chromatin.', *Nature*, 288(5792), pp. 675–679.

Allan, J. *et al.* (1986) 'Roles of H1 domains in determining higher order chromatin structure and H1 location', *Journal of Molecular Biology*, 187(4), pp. 591–601.

Allan, J. *et al.* (2012) 'Micrococcal nuclease does not substantially bias nucleosome mapping', *Journal of Molecular Biology*, 417(3), pp. 152–164.

Alonso, A. *et al.* (2010) 'A paucity of heterochromatin at functional human neocentromeres', *Epigenetics & Chromatin*, 3(6), p. 1-12.

Alsarraj, J. *et al.* (2013) 'BRD4 Short Isoform Interacts with RRP1B , SIPA1 and Components of the LINC Complex at the Inner Face of the Nuclear Membrane', *PLoS ONE*, 8(11), pp. 1–17.

Andersson, K. *et al*. (1984) 'Packing of a Specific Gene into Higher OrderStructures following Repression of RNASynthesis', *Journal of Cell Biology*, 98(April), pp. 1296–1303.

Andersson, R. *et al.* (2014) 'An atlas of active enhancers across human cell types and tissues.', *Nature*, 507(7493), pp. 455–61.

Andrieu, G. P. and Denis, G. V (2018) 'BET Proteins Exhibit Transcriptional and Functional Opposition in the Epithelial-to-mesenchymal Transition', *Molecular Cancer Research*, 16(4), pp. 580-586.

Aramayo, R. J. *et al.* (2018) 'Cryo-EM structures of the human INO80 chromatin-remodeling complex', *Nature Structural and Molecular Biology*, 25(1), pp. 37–44.

Arnoult, N. *et al*. (2012) 'Telomere length regulates TERRA levels through increased trimethylation of telomeric H3K9 and HP1α', *Nature Structural and Molecular Biology*, 19(9), pp. 948–956.

Asangani, I. a *et al.* (2014) 'Therapeutic targeting of BET bromodomain proteins in castration-resistant prostate cancer', *Nature*, 510(7504), pp. 278–282.

Bai, F. *et al.* (2014) 'BRCA1 suppresses epithelial-to-mesenchymal transition and stem cell dedifferentiation during mammary and tumor development', *Cancer Research*, 74(21), pp. 6161–6172.

Bakin, A. V. *et al.* (2000) 'Phosphatidylinositol 3-kinase function is required for transforming growth factor β-mediated epithelial to mesenchymal transition and cell migration', *Journal of Biological Chemistry*, 275(47), pp. 36803–36810.

Bao, Y. and Shen, X. (2011) 'Chromatin Remodeling: INO80 and SWR1', *Cell,* 144(1), pp. 158-163.

Baranello, L. *et al.* (2016) 'ChIP bias as a function of cross-linking time', *Chromosome Research*, 24(2), pp. 175–181.
Barnhart-Dailey, M. C. *et al.* (2017) 'HJURP interaction with the condensin II complex during G1 promotes CENP-A deposition', *Molecular Biology of the Cell*, 28(1), pp. 54–64.

Basquin, D. *et al.* (2014) 'The Drosophila Su(var)3-7 gene is required for oogenesis and female fertility, genetically interacts with piwi and aubergine, but impacts only weakly transposon silencing', *PLoS ONE*, 9(5), pp. 3–7.

Baxter, J. and Diffley, J. F. X. (2008) 'Topoisomerase II inactivation prevents the completion of DNA replication in budding yeast', *Molecular Cell*, 30(6), pp. 790–802.

Bednar, J. *et al.* (2017) 'Structure and dynamics of a 197 bp nucleosome in complex with linker Histone H1', *Molecular Cell*, 66, pp. 384–397.

Benesch, S. *et al.* (2002) 'Phosphatidylinositol 4,5-Biphosphate (PIP2)-induced vesicle', *Journal of Biological Chemistry*, 277(40), pp. 37771–37776.

Benetti, R. *et al.* (2007) 'Suv4-20h deficiency results in telomere elongation and derepression of telomere recombination', *Journal of Cell Biology*, 178(6), pp. 925–936.

Berezney, R. and Coffey, D. (1974) 'Identification of a nuclear protein matrix', *Biochemical and biophysical research communications*, 60(4), pp. 1410–1417.

Berger, J. M. *et al.* (1996) 'Structure and mechanism of DNA topoisomerase II.', *Nature*, 379(6562), pp. 225–232.

Bergmann, J. H. *et al.* (2011) 'Epigenetic engineering shows H3K4me2 is required for HJURP targeting and CENP-A assembly on a synthetic human kinetochore.', *The EMBO Journal*, 30(2), pp. 328–340.

Bernard, P. *et al.* (2001) 'Requirement of Heterochromatin for Cohesion at Centromeres', *Science*, 294(5551), pp. 2539–2542.

Bickmore, W. A. and Van Steensel, B. (2013) 'Genome architecture: Domain organization of interphase chromosomes', *Cell*, 152(6), pp. 1270–1284.

Birgisdottir, V. *et al.* (2006) 'Epigenetic silencing and deletion of the BRCA1 gene in sporadic breast cancer', *Breast Cancer Research*, 8(4), pp. 2–11.

Blackburn, E. H. (2001) 'Switching and signaling at the telomere', *Cell*, 106(6), pp. 661–673.

Blackledge, N. P. *et al.* (2014) 'Variant PRC1 complex-dependent H2A ubiquitylation drives PRC2 recruitment and polycomb domain formation', *Cell*, 157(6), pp. 1445–1459.

Bloom, K. S. and Anderson, J. N. (1979) 'Conformation of ovalbumin and globin genes in chromatin during differential gene expression', *Journal of Biological Chemistry*, 254(20), pp. 10532–10539.

Blower, M. D. *et al*. (2002) 'Conserved organization of centromeric chromatin in flies and humans', *Developmental Cell*, 2(3), pp. 319–330.

Bodor, D. L. *et al.* (2014) 'The quantitative architecture of centromeric chromatin', *eLife*, 2014(3), pp. 1–26.

Boettiger, A. N. *et al.* (2016) 'Super-resolution imaging reveals distinct chromatin folding for different epigenetic states.', *Nature*, 529(7586), pp. 418–22.

Bonne, G. *et al.* (1999) 'Mutations in the gene encoding lamin A / C cause autosomal dominant Emery-Dreifuss muscular dystrophy', *Nature Genetics*, 21, pp. 285–288.

Boren, B. C. *et al.* (2008) 'Ruthenium-Catalyzed Azide− Alkyne Cycloaddition: Scope and Mechanism, *Journal of the American Chemical Society*, 130(28), pp. 8923–8930.

Borengasser, S. J. *et al.* (2013) 'Differentiation and alters genome-scale DNA methylation in male rat offspring', *Endocrinology*, 154(11), pp. 4113–4125.

Boros, J. *et al.* (2014) 'Polycomb repressive complex 2 and H3K27me3 cooperate with H3K9 methylation to maintain heterochromatin protein 1α at chromatin.', *Molecular and cellular biology*, 34(19), pp. 3662–74.

Bos, J. L. (1989) 'ras Oncogenes in Human Cancer : A Review'. *Cancer Research*, 49, pp. 4682-4689

Boyle, S. *et al.* (2001) 'The spatial organization of human chromosomes within the nuclei of normal and emerin-mutant cells', *Human Molecular Genetics* 10(3), pp. 211–220.

Boyle, S. *et al.* (2011) 'Fluorescence in situ hybridization with high-complexity repeat-free oligonucleotide probes generated by massively parallel synthesis', *Chromosome Research*, 19, pp. 901–909.

Bracken, A. P. *et al.* (2003) 'EZH2 is downstream of the pRB-E2F pathway, essential for proliferation and amplified in cancer', *EMBO*, 22(20), pp. 5323–5335.

Brakke, M. K. (1953) 'Zonal separations by density-gradient centrifugation', *Biochemistry and Biophysics*, 45(2), pp. 275–290.

Brant, L. *et al.* (2016) 'Exploiting native forces to capture chromosome conformation in mammalian cell nuclei', *Molecular Systems Biology*, 12(12), p. 891.

Braunstein, M. *et al.* (1996) 'Efficient transcriptional silencing in Saccharomyces cerevisiae requires a heterochromatin histone acetylation pattern.', *Molecular and cellular biology*, 16(8), pp. 4349–56.

Brien, G. L. *et al.* (2012) 'Polycomb PHF19 binds H3K36me3 and recruits PRC2 and demethylase NO66 to embryonic stem cell genes during differentiation', *Nature Structural Molecular Biology*, 19(12), pp. 1273–1281.

Britton, S. *et al.* (2014) 'DNA damage triggers SAF-A and RNA biogenesis factors exclusion from chromatin coupled to R-loops removal', *Nucleic Acids Research*, 42(14), pp. 9047–9062.

Brown, D. T. *et al*. (2006) 'Mapping the interaction surface of linker histone $H1^0$ with the nucleosome of native chromatin in vivo', *Nature Structural & Molecular Biology*, 13(3). pp. 250-255.

Brown, K. E. *et al.* (1999) 'Dynamic repositioning of genes in the nucleus of lymphocytes preparing for cell division', *Molecular Cell*, 3(2), pp. 207–217.

Brownlee, P. M. *et al.* (2014) 'BAF180 Promotes cohesion and prevents genome instability and aneuploidy', *Cell Reports*, 6(6), pp. 973–981.

Bulut-Karslioglu, A. *et al.* (2014) 'Suv39h-dependent H3K9me3 marks intact retrotransposons and silences LINE elements in mouse embryonic stem cells', *Molecular Cell*, 55(2), pp. 277–290.

Burman, B. *et al.* (2015) 'Histone modifications predispose genome regions to breakage and translocation', *Genes & Development*, 29, pp. 1393–1402.

Byeon, H. K. *et al.* (2017) 'Acquired resistance to BRAF inhibition induces epithelial-to- mesenchymal transition in BRAF (V600E) mutant thyroid cancer by c-Met-mediated AKT activation', *Oncotarget*, 8(1), pp. 596–609.

Cai, L. *et al.* (2013) 'An H3K36 methylation-engaging tudor motif of polycomb-like proteins mediates PRC2 complex targeting', *Molecular Cell*, 49(3), pp. 571–582.

Cai, X. P. *et al.* (2016) 'PLK1 promotes epithelial-mesenchymal transition and metastasis of gastric carcinoma cells', *American Journal of Translational Research*, 8(10), pp. 4172–4183.

Camilloni, C. *et al.* (2016) 'Towards a structural biology of the hydrophobic effect in protein folding', *Scientific Reports*, 6(July), pp. 1–9.

Cano, A. *et al.* (2000) 'The transcription factor Snail controls epithelial-mesenchymal transitions by repressing E-cadherin expression', *Nature Cell Biology*, 2(2), pp. 76–83.

Cante-Barrett, K. *et al.* (2016) 'MEK and PI3K-AKT inhibitors synergistically block activated IL7 receptor signaling in T-cell acute lymphoblastic leukemia', *Leukeamia*, 30(9), pp. 1832–1843.

Canzio, D. *et al.* (2011) 'Chromodomain-mediated oligomerization of HP1 suggests a nucleosome bridging mechanism for heterochromatin assembly', *Molecular Cell*, 41(1), pp. 67–81.

Capanni, C. *et al.* (2008) 'Prelamin A is involved in early steps of muscle differentiation', *Experimental Cell Research*, 314(20), pp. 3628–3637.

Caplan, A. *et al.* (1987) 'Perturbation of chromatin structure in the region of the adult beta-globin gene in chicken erythrocyte chromatin', *Journal of Molecular Biology*, 193(1), pp. 57–69.

Cardenas, H. *et al.* (2016) 'EZH2 inhibition promotes epithelial-to-mesenchymal transition in ovarian cancer cells', *Oncotarget*, 7(51), pp. 84453–84467.

Carpenter, A. J. and Porter, A. C. G. (2004) 'Construction, Characterization, and Complementation of a Conditional-Lethal DNA Topoisomerase II Mutant Human Cell Line', *Molecular Biology of the Cell*, 15, pp. 5700–5711.

Carracedo, A. and Pandolfi, P. P. (2008) 'The PTEN-PI3K pathway: Of feedbacks and cross-talks', *Oncogene*, 27(41), pp. 5527–5541.

Carretero, J. *et al.* (2010) 'Integrative genomic and proteomic analyses identify targets for Lkb1 deficient metastatic lung tumors', *Cancer Cell*, 17(6), pp. 547–559.

Carrozza, M. J. *et al.* (2005) 'Histone H3 methylation by Set2 directs deacetylation of coding regions by Rpd3S to suppress spurious intragenic transcription', *Cell*, 123(4), pp. 581–592.

Casanova, M. *et al.* (2013) 'Heterochromatin reorganization during early mouse development requires a single-stranded noncoding transcript', *Cell Reports*, 4(6), pp. 1156–1167.

Ceccacci, E. and Minucci, S. (2016) 'Inhibition of histone deacetylases in cancer therapy: lessons from leukaemia', *British Journal of Cancer*, 114(6), pp. 605–611.

Celeste, A. *et al.* (2003) 'H2A.X Haploinsufficiency Modifes Genomic Stability and Tumor Susceptibility', *Cell*, 114(3), pp. 371–383.

Cereghini, S. and Yaniv, M. (1984) 'Assembly of transfected DNA into chromatin: structural changes in the origin-promoter-enhancer region upon replication.', *The EMBO journal*, 3(6), pp. 1243–53.

Chadwick, B. P. and Willard, H. F. (2003) 'Chromatin of the Barr body: Histone and non-histone proteins associated with or excluded from the inactive X chromosome', *Human Molecular Genetics*, 12(17), pp. 2167–2178.

Chakravarthy, S. *et al.* (2005) 'Structural characterization of the histone variant macroH2A structural characterization of the histone variant macroH2A', *Molecular and cellular biology*, 25(17), pp. 7616–7624.

Chambers, I. *et al.* (2003) 'Functional expression cloning of Nanog, a pluripotency sustaining factor in embryonic stem cells', *Cell*, 113(5), pp. 643–655.

Chambeyron, S. and Bickmore, W. A. (2004) 'Chromatin decondensation and nuclear reorganization of the HoxB locus upon induction of transcription', *Genes & Development*, 18, pp. 1119–1130.

Chan, F. L. *et al.* (2012) 'Active transcription and essential role of RNA polymerase II at the centromere during mitosis', *PNAS*, 109(6), pp. 1979–1984.

Chan, G., *et al.* (2013) 'Erk1 and Erk2 are required for maintenance of hematopoietic stem cells and adult hematopoiesis':, *Blood*, 121(18), pp. 3594–3599.

Chang, C.-J. *et al.* (2008) 'Phosphorylation at Ser473 regulates heterochromatin protein 1 binding and corepressor function of TIF1beta/KAP1.', *BMC molecular biology*, 9, p. 61.

Chapuy, B., *et al.* (2013) 'Discovery and characterization of super-enhancer-associated dependencies in diffuse large B cell lymphoma', *Cancer Cell*, 24(6), pp. 777–790.

Charvin, G., *et al.* (2003) 'Single-molecule study of DNA unlinking by eukaryotic and prokaryotic type-II topoisomerases.', *PNAS*, 100(17), pp. 9820–9825.

Chaturvedi, C.-P. *et al.* (2009) 'Dual role for the methyltransferase G9a in the maintenance of beta-globin gene transcription in adult erythroid cells.', *PNAS*, 106(43), pp. 18303–18308.

Chen, C.-K. *et al.* (2016) 'Xist recruits the X chromosome to the nuclear lamina to enable chromosome-wide silencing', *Science*, 354(6311), pp. 468–473.
Chen, C. C. *et al.* (2015) 'Establishment of centromeric chromatin by the CENP-A assembly factor CAL1 requires FACT-mediated transcription', *Developmental Cell*, 34(1), pp. 73–84.

Chen, C. and Sytkowski, A. J. (2001) 'Erythropoietin activates two distinct signaling pathways required for the initiation and the elongation of c-myc', *Journal of Biological Chemistry*, 276(42), pp. 38518–38526.

Chen, P. *et al.* (2013) 'H3.3 actively marks enhancers and primes gene transcription via opening higher-ordered chromatin', *Genes and Development*, 27(19), pp. 2109–2124.

Chen, Z. Y. *et al.* (2004) 'Silencing of episomal transgene expression by plasmid bacterial DNA elements in vivo.', *Gene therapy*, 11(10), pp. 856–864.

Cheung, K. L. *et al.* (2017) 'Distinct roles of Brd2 and Brd4 in potentiating the transcriptional program for Th17 cell differentiation', *Molecular Cell*, 65(6), p. 1068–1080.

Cho, Y. *et al.* (2008) 'The role of transcriptional activator GATA-1 at human β-globin HS2', *Nucleic Acids Research*, 36(14), pp. 4521–4528.

Choudhary, C. *et al.* (2009) 'Lysine acetylation targets protein complexes and co-regulated major cellular functions', *Science*, 325(2009), pp. 834–840.

Chowdhury, D. *et al.* (2005) 'γ-H2AX dephosphorylation by protein phosphatase 2A facilitates DNA double-strand break repair', 20, pp. 801–809.

Ciosk, R. *et al.* (2000) 'Cohesin's binding to chromosomes depends on a separate complex consisting of Scc2 and Scc4 proteins.', *Molecular cell*, 5(2), pp. 243–54.

Clarke, L. (1998) 'Centromeres: Proteins, protein complexes, and repeated domains at centromeres of simple eukaryotes', *Current Opinion in Genetics and Development*, 8(2), pp. 212–218.

Clavadetscher, J. *et al.* (2016) 'Copper catalysis in living systems and *In Situ* drug synthesis', *Angewandte Chemie*, 55(50), pp. 15662–15666.

Clemson, C. M. *et al.* (1996) 'XIST RNA paints the inactive X chromosome at interphase: Evidence for a novel RNA involved in nuclear/chromosome structure', *Journal of Cell Biology*, 132(3), pp. 259–275.

Coelho, P. A., *et al.* (2003) 'Condensin-dependent localisation of topoisomerase II to an axial chromosomal structure is required for sister chromatid resolution during mitosis.', *Journal of cell science*, 116(23), pp. 4763–76.

Col, E. *et al.* (2017) 'Bromodomain factors of BET family are new essential actors of pericentric heterochromatin transcriptional activation in response to heat shock', *Scientific Reports*, 7(1), pp. 1–12.

Collins, K. and Miller, M. C. (2002) 'Telomerase recognizes its template by using an adjacent RNA motif.', *PNAS*, 99(10), pp. 6585–90.

Cook, D. N. *et al.* (1992) 'Dynamics of DNA supercoiling by transcription in Escherichia coli (DNA gyrase/topoisomerase I/topology/gene expression)', *Biochemistry*, 89(November), pp. 10603–10607.

Coppola, J. A. and Cole, M. D. (1986) 'Constitutive c-myc oncogene expression blocks mouse erythroleukaemia cell differentiation but not commitment.', *Nature*, 320(6064), pp. 760–3.
Corte, V. De, *et al.* (1997) 'Phosphatidylinositol 4 , 5-bisphosphate specifically stimulates PP60 C src catalyzed phosphorylation of gelsolin and related actin-binding proteins', *FEBS letters*, 401, pp. 191–196.

Coudé, M.-M. *et al.* (2015) 'BET inhibitor OTX015 targets BRD2 and BRD4 and decreases c-MYC in acute leukemia cells.', *Oncotarget*, 6(19), pp. 17698–712.

Coulthard, A. B. *et al.* (2010) 'Essential loci in centromeric heterochromatin of Drosophila melanogaster. I: The right arm of chromosome 2', *Genetics*, 185(2), pp. 479–495.

Cowieson, N. P. *et al.* (2000) 'Dimerisation of a chromo shadow domain and distinctions from the chromodomain as revealed by structural analysis', *Current Biology*, 10(9), pp. 517–525.

Craig, J. M. *et al.* (1997) 'Scaffold attachments within the human genome.', *Journal of Cell Science*, 110(2), pp. 2673–2682.

Crane-Robinson, C. (1999) 'How do linker histones mediate differential gene expression?', *BioEssays*, 21(5), pp. 367–371.

Cremer, T. *et al.* (1988) 'Detection of chromosome aberrations in metaphase and interphase tumor cells by in situ hybridization using chromosome-specific library probes', *Human Genetics*, 80, pp. 235–246.

Croft, J. A. *et al.* (1999) 'Differences in the localization and morphology of chromosomes in the human nucleus', 145(6), pp. 1119–1131.

Cui, F. and Zhurkin, V. B. (2009) 'Distinctive sequence patterns in metazoan and yeast nucleosomes: Implications for linker histone binding to AT-rich and methylated DNA', *Nucleic Acids Research*, 37(9), pp. 2818–2829.

Cunningham, L. (1959) 'Micrococcal Nuclease and Some Products of Its Action', *Annals of the New York Academy of Sciences*, 81(3), pp. 788–791.

D'Assoro, A. *et al.* (2014) 'The mitotic kinase Aurora-A promotes distant metastases by inducing epithelial-to-mesenchymal transition in ERα+ breast cancer cells', *Oncogene*, 33(5), pp. 599–610.

Dambacher, S. *et al.* (2012) 'CENP-C facilitates the recruitment of M18BP1 to centromeric chromatin.', *Nucleus*, 3(1), pp. 101–110.

Daneholt, B. *et al.* (1982) 'Visualization of active 75 S RNA genes in the Balbiani rings of Chironomus tentans', *European journal of cell biology*, 26(2), pp. 325–332.

Darlington, C. D. (1936) 'The External Mechanics of the Chromosomes I - The Scope of Enquiry', *Proc. R. Soc. B Biol. Sci*, (121), pp. 264–319.

Dawson, M. a. *et al.* (2011) 'Inhibition of BET recruitment to chromatin as an effective treatment for MLL-fusion leukaemia', *Nature*, 478, pp. 529–533.

Deardorff, M. A. *et al.* (2012) 'HDAC8 mutations in Cornelia de Lange syndrome affect the cohesin acetylation cycle.', *Nature*, 489(7415), pp. 313–7.

Dechassa, M. L. *et al.* (2012) 'Disparity in the DNA translocase domains of SWI / SNF and ISW2', 40(10), pp. 4412–4421.

Dekker, J. (2007) 'GC- and AT-rich chromatin domains differ in conformation and histone modification status and are differentially modulated by Rpd3p', *Genome Biology*, 8(6). pp. R116

Dekker, N. H. *et al.* (2002) 'The mechanism of type IA topoisomerases.', *PNAS*, 99(19), pp. 12126–31.

Deng, W. *et al.* (2012) 'Controlling long-range genomic interactions at a native locus by targeted tethering of a looping factor', *Cell*, 149(6), pp. 1233–1244.

Deng, W. *et al.* (2013) 'Controlling long range genomic interactions at a native locus by targeted tethering of a looping factor', *Cell*, 149(6), pp. 1233–1244.

Deng, W. *et al.* (2014) 'Reactivation of developmentally silenced globin genes by forced chromatin looping', *Cell*, 158(4), pp. 849–860.

Dernburg, A. F. *et al.* (1996) 'Perturbation of nuclear architecture by long-distance chromosome interactions', *Cell*, 85(5), pp. 745–759.

Deuring, R. *et al.* (2000) 'The ISWI Chromatin-remodeling protein is required for gene expression and the maintenance of higher order chromatin structure *In Vivo*', *Molecular Cell*, 5, pp. 355–365.

Dhalluin, C. *et al.* (1999) 'Structure and ligand of a histone acetyltransferase bromodomain', *Nature*, 399(6735), pp. 491–496.

Dileep, V. *et al.* (2015) 'Topologically-associating domains and their long-range contacts are established during early G1 coincident with the establishment of the replication timing program':, *Genome Research*, (25), pp. 1104–1113.

Dissanayake, S. K. *et al.* (2007) 'The Wnt5A/protein kinase C pathway mediates motility in melanoma cells via the inhibition of metastasis suppressors and initiation of an epithelial to mesenchymal transition', *Journal of Biological Chemistry*, 282(23), pp. 17259–17271.

Ditchfield, C. *et al.* (2003) 'Aurora B couples chromosome alignment with anaphase by targeting BubR1, Mad2, and Cenp-E to kinetochores', *Journal of Cell Biology*, 161(2), pp. 267–280.

Doheny, J. G., *et al.* (2008) 'Telomeric position effect - A third silencing mechanism in eukaryotes', *PLoS ONE*, 3(12), pp. 3–9.

Dong, C. *et al.* (2012) 'G9a interacts with Snail and is critical for Snail-mediated E-cadherin repression in', *Journal of Clinical Investigation*, 122(4), pp. 1469–1486.

Dorbic, T. and Wittig, B. (1986) 'Isolation of oligonucleosomes from active chromatin using HMG17-specific monoclonal antibodies', *Nucleic Acids Research*, 14(8), pp. 3363–3376.

Dovey, O. M. *et al.* (2013) 'Histone deacetylase (HDAC) 1 and 2 are essential for normal T cell development and genomic stability in mice', 121(8), pp. 1335–1345.

Downward, J. (2003) 'Targeting RAS signalling pathways in cancer therapy', *Nature Reviews, Cancer*, 3(January). pp 11-22

Drané, P. *et al.* (2010) 'The death-associated protein DAXX is a novel histone chaperone involved in the replication-independent deposition of H3.3', *Genes and Development*, 24(12), pp. 1253–1265.

Dreier, M. R., *et al.* (2011) 'Regulation of sororin by Cdk1-mediated phosphorylation.', *Journal of cell science*, 124(17), pp. 2976–87.

Dudek, S. M. *et al.* (2010) 'Abl tyrosine kinase phosphorylates nonmuscle Myosin light chain kinase to regulate endothelial barrier function.', *Molecular Biology of the cell*, 21(22), pp. 4042–4056.

Dunleavy, E. M., *et al.* (2011) 'H3.3 is deposited at centromeres in S phase as a placeholder for newly assembled CENP-A in G_1 phase.', *Nucleus*, 2(2), pp. 146–57.

Dunleavy, E. M., *et al.* (2013) 'Solo or doppio: how many CENP-As make a centromeric nucleosome?', *Nature Structural {&} Molecular Biology*, 20(6), pp. 648–650.

Dykhuizen, E. C. *et al.* (2013) 'mSWI/SNF (BAF) complexes facilitate decatentation of DNA by Topoisomerase IIα', *Nature*, 497(7451), pp. 624–627.

Dyson, H. J., *et al*. (2006) 'The role of hydrophobic interactions in initiation and propagation of protein folding.', *PNAS*, 103(35), pp. 13057–13061.

Earnshaw, W. *et al.* (1989) 'Visualization of centromere proteins CENP-B and CENP-C on a stable dicentric chromosome in cytological spreads', *Chromosoma*, 98(1), pp. 1–12.

Earnshaw, W. C. and Rothfield, N. (1985) 'Identification of a family of human centromere proteins using autoimmune sera from patients with scleroderma.', *Chromosoma*, 91(3–4), pp. 313–21.

Eberl, D. F, *et al.* (1993) 'The role of heterochromatin in the expression of a heterochromatic gene, the rolled Locus of Drosophila melanogaster', *Genetics*, (134), pp. 277–292.

Ebersole, T. *et al.* (2005) 'Rapid generation of long synthetic tandem repeats and its application for analysis in human artificial chromosome formation', *Nucleic Acids Research*, 33(15), pp. 1–8.

Ehrlich, M. *et al.* (2002) 'DNA methyltransferase 3B mutations linked to the ICF syndrome cause dysregulation of lymphogenesis genes.', *Human Molecular Genetics*, 10(25), pp. 2917–31.

Eissenberg, J. C. *et al.* (1990) 'Mutation in a heterochromatin-specific chromosomal protein is associated with suppression of position-effect variegation in Drosophila melanogaster.', *PNAS*, 87(24), pp. 9923–7.

Eissenberg, J. C. *et al.* (1992) 'The heterochromatin-associated protein HP-1 is an essential protein in Drosophila with dosage-dependent effects on position-effect variegation', *Genetics*, 131(2), pp. 345–352.

Ekwall, K. *et al.* (1997) 'Transient inhibition of histone deacetylation alters the structural and functional imprint at fission yeast centromeres', *Cell*, 91(7), pp. 1021–1032.

Ernst, T. *et al.* (2010) 'Inactivating mutations of the histone methyltransferase gene EZH2 in myeloid disorders', *Nature Genetics*, 42(8), pp. 722–726.

Eskeland, R. *et al.* (2010) 'Ring1B compacts chromatin structure and represses gene expression independent of histone ubiquitination', *Molecular Cell*, 38(3), pp. 452–464.

Eskeland, R., *et al.* (2007) 'HP1 Binding to Chromatin Methylated at H3K9 Is Enhanced by Auxiliary Factors, *Molecular and Cellular Biology*, 27(2), pp. 453–465.

Fachinetti, D. *et al.* (2015) 'DNA Sequence-Specific Binding of CENP-B enhances the fidelity of human centromere function', *Developmental Cell*, 33(3), pp. 314–327.

Falk, S. J. *et al.* (2015) 'CENP-C reshapes and stabilizes CENP-A nucleosomes at the', *Science*, 348(6235), pp. 699–704.

Fallahi‐Sichani, M. *et al.* (2017) 'Adaptive resistance of melanoma cells to RAF inhibition via reversible induction of a slowly dividing de‐differentiated state', *Molecular Systems Biology*, 13(1), p. 905.

Fan, Y. *et al.* (2005) 'Histone H1 depletion in mammals alters global chromatin structure but causes specific changes in gene regulation', *Cell*, 123(7), pp. 1199–1212.

Fang, D. *et al.* (2017) 'Epithelial-mesenchymal transition of ovarian cancer cells is sustained by Rac1 through simultaneous activation of MEK1/2 and Src signaling pathways', *Oncogene*, 36(11), pp. 1546–1558.

Feinberg, A. P., *et al.* (2006) 'The epigenetic progenitor origin of human cancer', *Nature Reviews Genetics*, 7(1), pp. 21–33.

Feinberg, A. P. and Vogelstein, B. (1983) 'Hypomethylation distinguishes genes of some human cancers from their normal counterparts.', *Nature*, 301(5895), pp. 89–92.

Feng, Y. *et al.* (2005) 'The Human ß-Globin Locus Control Region Can Silence as Well as Activate Gene Expression', *Molecular and Cellular Biology*, 25(10), pp. 3864–3874.

Fenouil, R. *et al.* (2012) 'CpG islands and GC content dictate nucleosome depletion in a transcription-independent manner at mammalian promoters', *Genome Research*, 22(12), pp. 2399–2408.

Fenouille, N. *et al.* (2012) 'The epithelial-mesenchymal transition (EMT) regulatory factor SLUG (SNAI2) is a downstream target of SPARC and AKT in promoting melanoma cell invasion', *PLoS ONE*, 7(7).

Ferguson, J. *et al.* (2017) 'Effect of SMURF2 targeting on susceptibility to MEK inhibitors in Melanoma', *Journal of the National Cancer Institute*, 105(1), pp. 33–46.

Fernandez-capetillo, O., *et al.* (2004) 'Phosphorylation of Histone H2B at DNA Double-Strand Breaks', *Journal of Experimental Medicine*, 199(12). pp. 1671-1677.

Fernandez‐Alonso, R. *et al.* (2017) 'Brd4‐Brd2 isoform switching coordinates pluripotent exit and Smad2‐dependent lineage specification', *EMBO reports*, 18(7), pp. 1108–1122.

Ferrarotto, R. *et al.* (2017) 'Epithelial-Mesenchymal Transition predicts Polo-Like Kinase 1 inhibitor-mediated apoptosis in non-small cell lung cancer', *Clinical Cancer Research*, 22(7), pp. 1674–1686.

Fey, E. G., *et al.* (1984) 'Epithelial cytoskeletal framework and nuclear matrix-intermediate filament scaffold: three-dimensional organization and protein composition', *Journal of Cell Biology*, 98(6), pp. 1973–1984.

Filippakopoulos, P. *et al.* (2010) 'Selective inhibition of BET bromodomains', *Nature*, 468(7327), pp. 1067–1073.

Filippakopoulos, P. *et al.* (2012) 'Histone recognition and large-scale structural analysis of the human bromodomain family', *Cell*, 149(1), pp. 214–231.

Filipponi, D. *et al.* (2013) 'Wip1 Controls Global Heterochromatin Silencing via ATM/BRCA1-Dependent DNA Methylation', *Cancer Cell*, 24(4), pp. 528–541.

Finn, E. H. *et al.* (2017) 'Heterogeneity and intrinsic variation in spatial genome organziation', *BioRxiv*.

Fischle, W. *et al.* (2003) 'Molecular basis for the discrimination of repressive methyl-lysine marks in histone H3 by polycomb and HP1 chromodomains', *Genes and Development*, 17(15), pp. 1870–1881.

Fishel, B. *et al.* (1988) 'Structural organization and functional analysis of centromeric DNA in the fission yeast Schizosaccharomyces pombe.', *Molecular Cellular Biology*, 8(2), pp. 754–63.

Fittler, F. and Zachau, H. G. (1979) 'Subunit structure of a-satellite DNA containing chromatin from African Green Monkey cells', *Nucleic Acids Research*, 7(1), pp. 1–13.

Flaherty, K. T. *et al.* (2012) 'Improved Survival with MEK Inhibition in BRAF-Mutated Melanoma', *The New England Journal of Medicine*, 367(2), pp. 107–114.

Flemming, W. (1878) 'Zur Kenntnis der Zelle in ihrer Teilung-Erscheinungen', *Schriften Naturwiss. Vereins Schl.-Holsk*, pp. 23–27.

Flemming, W. (1882) 'Zellsubstanz, kern und zelltheilung', *Vogel*.

Floyd, S. R. *et al.* (2013) 'The bromodomain protein Brd4 insulates chromatin from DNA damage signalling', *Nature*, 498(7453), pp. 246–250.

Folco, H. D. *et al.* (2008) 'Heterochromatin and RNAi are required to establish CENP-A chromatin at centromeres.', *Science*, 319(5859), pp. 94–7.

Follo, M. Y. *et al.* (2008) 'PI-PLCbeta-1 and activated Akt levels are linked to azacitidine responsiveness in high-risk myelodysplastic syndromes.', *Leukemia*, 22(1), pp. 198–200.

Follo, M. Y. *et al.* (2012) 'Activation of nuclear inositide signalling pathways during erythropoietin therapy in low-risk MDS patients.', *Leukemia*. Nature, 26(12), pp. 2474–82.

Follows, G. A. *et al.* (2012) 'Mapping and functional characterisation of a CTCF-dependent insulator element at the 3′ border of the murine Scl transcriptional domain', *PLoS ONE*, 7(3).

Forbes, S. A. *et al.* (2011) 'COSMIC: Mining complete cancer genomes in the catalogue of somatic mutations in cancer', *Nucleic Acids Research*, 39(1), pp. 945–950.

Friend, C. *et al.* (1971) 'Hemoglobin synthesis in murine virus-induced leukemic cells in vitro: stimulation of erythroid differentiation by dimethyl sulfoxide.', *PNAS*, 68(2), pp. 378–82.

Furuyama, S. and Biggins, S. (2007) 'Centromere identity is specified by a single centromeric nucleosome in budding yeast.', *PNAS*, 104(37), pp. 14706–14711.

Furuyama, T. and Henikoff, S. (2009) 'Centromeric nucleosomes induce positive DNA supercoils', *Cell*, 138(1), pp. 104–113.

Gall, J. (1966) 'Chromosome fibers studied by a spreading', *Chromosoma*, 233, pp. 221–233.

Gao, Z. *et al.* (2013) 'PCGF Homologs, CBX Proteins, and RYBP define functionally distinct PRC1 family complexes', *Molecular Cell*, 45(3), pp. 344–356.

García-Cao, M. *et al.* (2003) 'Epigenetic regulation of telomere length in mammalian cells by the Suv39h1 and Suv39h2 histone methyltransferases', *Nature Genetics*, 36(1), pp. 94–99.

Gerlich, D. *et al.* (2006) 'Condensin I stabilizes chromosomes mechanically through a dynamic interaction in live cells', *Current Biology*, 16(4), pp. 333–344.

Giaever, G. N. and Wang, J. C. (1988) 'Supercoiling of intracellular DNA can occur in eukaryotic cells', *Cell*, 55(5), pp. 849–856.

Gibcus, J. H. *et al.* (2018) 'A pathway for mitotic chromosome formation', *Science*, 359(652), pp. 6135-6147.

Gierlich, J. *et al.* (2006) 'Click chemistry as a reliable method for the high-density postsynthetic functionalization of alkyne-modified DNA', *Organic Letters*, 8(17), pp. 3639–3642.

Giet, R. and Glover, D. M. (2001) 'Drosophila aurora B kinase is required for histone H3 phosphorylation and condensin recruitment during chromosome condensation and to organize the central spindle during cytokinesis', *Journal of Cell Biology*, 152(4), pp. 669–681.

Gilbert, N. *et al.* (2003) 'Formation of facultative heterochromatin in the absence of HP1', *EMBO Journal*, 22(20), pp. 5540–5550.

Gilbert, N. *et al.* (2004) 'Chromatin architecture of the human genome: gene-rich domains are enriched in open chromatin fibers', *Cell*, 118(5), pp. 555–566.

Gilbert, N., T *et al.* (2007) 'DNA methylation affects nuclear organization, histone modifi cations, and linker histone binding but not chromatin compaction', *Journal of Cell Biology*, 177(3), pp. 401–411.

Gilbert, N. and Allan, J. (2001) 'Distinctive higher-order chromatin structure at mammalian centromeres', *PNAS*, 98(21), pp. 11949–11954.

Gilchrist, S. *et al.* (2004) 'Nuclear organization of centromeric domains is not perturbed by inhibition of histone deacetylases', *Chromosome Research*, 12, pp. 505–516.

Gilmartin, A. G. *et al.* (2011) 'GSK1120212 (JTP-74057) is an inhibitor of MEK activity and activation with favorable pharmacokinetic properties for sustained in vivo pathway inhibition', *Clinical Cancer Research*, 17(5), pp. 989–1000.

Giménez-Abián, J. F. *et al.* (1995) 'A postprophase topoisomerase II-dependent chromatid core separation step in the formation of metaphase chromosomes', *Journal of Cell Biology*, 131(1), pp. 7–17.

Glynn, E. F. *et al.* (2004) 'Genome-wide mapping of the cohesin complex in the yeast Saccharomyces cerevisiae', *PLoS Biology*, 2(9). pp. 1325-1339

Goldberg, A. D. *et al.* (2010) 'Distinct factors control histone variant H3.3 localization at specific genomic regions', *Cell*., 140(5), pp. 678–691.

Goldmark, J. P. *et al.* (2000) 'The Isw2 chromatin remodeling complex represses early meiotic genes upon recruitment by Ume6p', 103, pp. 423–433.

González-Melendi, P. *et al.* (2001) 'Single ribosomal transcription units are linear, compacted Christmas trees in plant nucleoli', *Plant Journal*, 27(3), pp. 223–233.

Gonzalez, J. *et al.* (2016) 'Unravelling Protein-DNA Interactions at Molecular Level: A DFT and NCI Study', *Journal of Chemical Theory and Computation*, 12(2), pp. 523–534.

Gonzalo, S. *et al.* (2006) 'DNA methyltransferases control telomere length and telomere recombination in mammalian cells', *Nat Cell Biol*, 8(4), pp. 416–424.

Goudarzi, A. *et al.* (2016) 'Dynamic Competing Histone H4 K5K8 Acetylation and Butyrylation Are Hallmarks of Highly Active Gene Article Dynamic Competing Histone H4 K5K8 Acetylation and Butyrylation Are Hallmarks of Highly Active Gene Promoters', *Molecular Cell*. The Authors, 62(2), pp. 169–180.

Goodarzi, A. A., *et al.* (2011) 'KAP-1 phosphorylation regulates CHD3 nucleosome remodeling during the DNA double-strand break response', *Nature Structural & Molecular Biology*, 18(7), pp. 831–839.

Gospodinov, A. *et al.* (2011) 'Mammalian Ino80 mediates double strand break repair through its role in DNA end strand resection', *Molecular Cellular Biology*, 31(23), pp. 4735-3745

Gottesfeld, J. M., *et al.* (1975) 'Structure of transcriptionally active chromatin', *PNAS*, 72(11), pp. 4404–4408.

Gottgens, B. *et al.* (1997) 'Transcription of the SCL gene in erythroid and CD34 positive primitive myeloid cells is controlled by a complex network of lineage-restricted chromatin-dependent and chromatin-independent regulatory elements', *Oncogene*, 15(20), pp. 2419–2428.

Göttgens, B. *et al.* (2001) 'Long-range comparison of human and mouse SCL Loci: Localized regions of sensitivity to restriction endonucleases correspond precisely with peaks of conserved noncoding sequences', *Genome Research*, 11(1), pp. 87–97.

Gramlich, P. M. E. *et al.* (2008) 'Click-click-click: Single to triple modification of DNA', *Angewandte Chemie*, 47(18), pp. 3442–3444.

Grau, D. J. *et al.* (2011) 'Compaction of chromatin by diverse polycomb group proteins requires localized regions of high charge', *Genes and Development*, 25(20), pp. 2210–2221.

Green, L. C. *et al.* (2012) 'Contrasting roles of condensin I and condensin II in mitotic chromosome formation', *Journal of Cell Science*, 125(6), pp. 1591–1604.

Greider, C. W. (1998) 'Telomerase activity, cell proliferation, and cancer', *PNAS*, 95(1), pp. 90–92.

Grézy, A. *et al.* (2016) 'Control of genetic stability by a new heterochromatin compaction pathway involving the Tip60 histone acetyltransferase.', *Molecular Biology of the Cell*, 27(4), pp. 599–607.

Griffith, J. D. *et al.* (1999) 'Mammalian telomeres end in a large duplex loop', *Cell*, 97(4), pp. 503–514.

Grigoryev, S. A. *et al.* (2009) 'Evidence for heteromorphic chromatin fibers from analysis of nucleosome interactions', *PNAS*, 106(32), pp. 13317–13322.

Grimes, B. R., *et al.* (2002) 'α-Satellite DNA and Vector Composition Influence Rates of Human Artificial Chromosome Formation', *Molecular Therapy*., 5(6), pp. 798–805.

Guerra, M. *et al.* (2010) 'Neocentrics and holokinetics (holocentrics): Chromosomes out of the centromeric rules', *Cytogenetic and Genome Research*, 129(1–3), pp. 82–96.

Guetg, C. *et al.* (2012) 'Inheritance of silent rDNA chromatin is mediated by PARP1 via noncoding RNA', *Molecular Cell*., 45(6), pp. 790–800.

Guillemette, B. *et al.* (2011) 'H3 lysine 4 is acetylated at active gene promoters and is regulated by H3 lysine 4 methylation', *PLoS Genetics*, 7(3). pp. e1001354.

Gupta, S. *et al.* (1996) 'Selective interaction of JNK protein kinase isoforms with transcription factors.', *The EMBO journal*, 15(11), pp. 2760–70.

Haack, H. *et al.* (2009) 'Diagnosis of NUT Midline Carcinoma Using a NUT-Specific Monoclonal Antibody', *American Journal of Surgery, The*, 33(7), pp. 984–991.

Haaf, T. *et al.* (1995) 'Presence and abundance of CENP-B box sequences in great ape subsets of primate-specific α-satellite DNA', *Journal of Molecular Evolution*, 41(4), pp. 487–491.

Haering, C. H. *et al.* (2002) 'Molecular architecture of SMC proteins and the yeast cohesin complex', *Molecular Cell*, 9(4), pp. 773–788.

Hahn, M. *et al.* (2013) 'Suv4-20h2 mediates chromatin compaction and is important for cohesion recruitment to heterochromatin', *Genes and Development*, 27(8), pp. 859–872.

Hahn, W. C. and Weinberg, R. A. (2002) 'Rules for making human cancer cells', *The New England journal of medicine*, 347(20), pp. 1593–1603.

Haldar, S. *et al.* (2011) 'Role of Swi6/HP1 self-association-mediated recruitment of Clr4/Suv39 in establishment and maintenance of heterochromatin in fission yeast', *Journal of Biological Chemistry*, 286(11), pp. 9308–9320.

Hall, L, L. *et al.* (2014) 'Stable CoT-1 repeat RNA is abundant and associated with euchromatic interphase chromosomes', *Cell*, 156(5), pp. 907–919.

Hall, I. M. *et al.* (2002) 'Establishment and maintenance of a heterochromatin domain.', *Science*, 297(5590), pp. 2232–2237.

Hande, M. P. *et al.* (2001) 'Extra-chromosomal telomeric DNA in cells from Atm(-/-) mice and patients with ataxia-telangiectasia.', *Human molecular genetics*, 10(5), pp. 519–528.

Harington, J. J. *et al.* (1997) 'Formation of de novo centromere and construction of first-generation human artificial chromosomes', *Nature Genetics*, 15, pp. 57–61.

Hashimoto, H. *et al.* (2010) 'Histone H1 null vertebrate cells exhibit altered nucleosome architecture', *Nucleic Acids Research*, 38(11), pp. 3533–3545.

Hawkins, R. D. *et al.* (2010) 'Distinct epigenomic landscapes of pluripotent and lineage-committed human cells', *Cell Stem Cell.*, 6(5), pp. 479–491.

Hayashi, T. *et al.* (2004) 'Mis16 and Mis18 are required for CENP-A loading and histone deacetylation at centromeres', *Cell*, 118(6), pp. 715–729.

Haynes, S. R. *et al.* (1992) 'The bromodomain: a conserved sequence found in human,Drosophilaand yeast proteins', *Nucleic Acids Research*, 20(10), p. 2603.

Hebbes, T. R., *et al.* (1988) 'A direct link between core histone acetylation and transcriptionally active chromatin', *The EMBO Journal*, 7(5), pp. 1395–1402.

Hennekes, H. *et al.* (1993) 'Phosphorylation on Protein Kinase C Sites Inhibits Nuclear Import of Lamin', *The Journal of Cell Biology*, 120(6), pp. 1293–1304.

Helbo, A. S. *et al.* (2017) 'Nucleosome positioning and NDR structure at RNA polymerase III promoters', *Scientific Reports.*, 7(February), pp. 1–11.

Heo, K. *et al.* (2008) 'FACT-mediated exchange of histone variant H2AX regulated by phosphorylation of H2AX and ADP-ribosylation of Spt16', *Molecular Cell, 30,* pp. 86–97.

Hietakangas, V. *et al.* (2001) 'Activation of the MKK4-JNK pathway during erythroid differentiation of K562 cells is inhibited by the heat shock factor 2-beta isoform.', *FEBS letters*, 505(1), pp. 168–72.

Himo, F. *et al.* (2005) 'Copper(I)-catalyzed synthesis of azoles. DFT study predicts unprecedented reactivity and intermediates', *Journal of the American Chemical Society*, 127(1), pp. 210–216.

Hirano, T., *et al.* (1997) 'Condensins, chromosome condensation protein complexes containing XCAP-C, XCAP-E and a Xenopus homolog of the Drosophila barren protein', *Cell*, 89(4), pp. 641–653.

Hirota, T. *et al.* (2004) 'Distinct functions of condensin I and II in mitotic chromosome assembly', *Journal of Cell Science*, 117(26), pp. 6435–6445.

Hirota, T. *et al.* (2005) 'Histone H3 serine 10 phosphorylation by Aurora B causes HP1 dissociation from heterochromatin', *Nature*, 438(7071), pp. 1176–1180.

Hockemeyer, D. *et al.* (2006) 'Recent expansion of the telomeric complex in rodents: Two distinct POT1 proteins protect mouse telomeres', *Cell*, 126(1), pp. 63–77.

Hocker, T. and Tsao, H. (2007) 'Ultraviolet radiation and melanoma : A systematic review and analysis of reported sequence variants', 28(February), pp. 578–588.

Hoek, K. S. *et al.* (2006) 'Metastatic potential of melanomas defined by specific gene expression profiles with no BRAF signature', *Pigment Cell Research*, 19(4), pp. 290–302.

Hofmann, A., *et al.* (2009) 'The winged-helix transcription factor JUMU is a haplo-suppressor/triplo- enhancer of PEV in various tissues but exhibits reverse PEV effects in the brain of Drosophila melanogaster', *Chromosome Research*, 17(3), pp. 347–358.

Hofmann, T. *et al.* (1999) 'Direct activation of human TRPC6 and TRPC3 channels by diacylglycerol.', *Nature*, 397(6716), pp. 259–63.

Holde, K. E. van (1989) 'A Chromatin Retrospective', *Cell*, 59, pp. 243–244.

Holmes, S. D. *et al.* (1972) 'Chromosomal RNA: Its properties', *Science*, 177, pp. 72–74.

Hoppe-Seyler, F. (1871) 'Ueber die chemische Zusammensetzung des Eiters', *Med.-Chem. Unters., 4 (1871), pp. 486–501,*.

Hori, T. *et al.* (2013) 'The CCAN recruits CENP-A to the centromere and forms the structural core for kinetochore assembly', *Journal of Cell Biology*, 200(1), pp. 45–60.

Horita, D. A. *et al.* (2001) 'Solution structure, domain features, and structural implications of mutants of the chromo domain from the fission yeast histone methyltransferase Clr4', *Journal of Molecular Biology*, 307(3), pp. 861–870.

Hou, F. and Zou, H. (2005) 'Two human orthologues of Eco1/Ctf7 acetyltransferases are both required for proper sister-chromatid cohesion', *Molecular Biology of the Cell*, 16(8), pp. 3908–3918.

Houlard, M. *et al.* (2015) 'Condensin confers the longitudinal rigidity of chromosomes.', *Nature Cell Biology*, 17(6), pp. 771–781.
Hsu, S. C. *et al.* (2017) 'The BET protein BRD2 cooperates with CTCF to enforce transcriptional and architectural boundaries', *Molecular Cell*., 66(1), p. 102–116.e7.

Houzelstein, D. *et al.* (2002) 'Growth and Early Postimplantation Defects in Mice Deficient for the Bromodomain-Containing Protein Brd4 †', *Molecular and cellular biology*, 22(11), pp. 3794–3802.

Hu, B. *et al.* (2011) 'ATP hydrolysis is required for relocating cohesin from sites occupied by its Scc2/4 loading complex', *Current Biology*, 21(1), pp. 12–24.

Hua, K. T. *et al.* (2014) 'The H3K9 methyltransferase G9a is a marker of aggressive ovarian cancer that promotes peritoneal metastasis', *Molecular Cancer*, 13(1), pp. 1–13.

Huang, B. *et al.* (2009) 'Brd4 coactivates transcriptional activation of NF- B via specific binding to acetylated RelA', *Molecular and Cellular Biology*, 29(5), pp. 1375–1387.

Huang, H.-T. *et al.* (2013) 'A network of epigenetic regulators guides developmental haematopoiesis in vivo.', *Nature Cell Biology*. Nature, 15(12), pp. 1516–25.

Huang, J. *et al.* (2015) 'Predicting chromatin organization using histone marks', *Genome Biology*., 16(1), p. 162.

Hudson, D. F. *et al.* (1998) 'Centromere protein B null mice are mitotically and meiotically normal but have lower body and testis weights', *Journal of Cell Biology*, 141(2), pp. 309–319.

Hudson, D. F. *et al.* (2003) 'Condensin is required for nonhistone protein assembly and structural integrity of vertebrate mitotic chromosomes', *Developmental Cell*, 5(2), pp. 323–336.
Huebner, K. *et al.* (1981) 'Deoxyribonuclease I sensitivity of plasmid genomes in teratocarcinoma-derived stem and differentiated cells.', *PNAS*, 78(8), pp. 5071–5.

Hughes, C. S., *et al.* (2010) 'Matrigel: a complex protein mixture required for optimal growth of cell culture.', *Proteomics*, 10(9), pp. 1886–1890.

Hughes, R. M. *et al.* (2007) 'Recognition of trimethyllysine by a chromodomain is not driven by the hydrophobic effect', *PNAS*, 104(27), pp. 11184–11188.

Huppert, J. L. and Balasubramanian, S. (2007) 'G-quadruplexes in promoters throughout the human genome', *Nucleic Acids Research*, 35(2), pp. 406–413.

Hur, S. *et al.* (2010) 'Roles of human INO80 chromatin remodeling enzyme in DNA replication and chromosome segregation suppress genome instability', pp. 2283–2296.

Hussain, S. *et al.* (2010) 'Single-base resolution mapping of H1–nucleosome interactions and 3D organization of the nucleosome', *PNAS*, pp. 1–6.

Huyen, Y. *et al.* (2004) 'Methylated lysine 79 of histone H3 targets 53BP1 to DNA double-strand breaks', *Nature*, 432(7015), pp. 406–411.

Ingham, P. W. (1983) 'Differential expression of bithorax complex genes in the absence of the extra sex combs and trithorax genes', *Nature*, 306(5943), pp. 591–593.

Itzen, F. *et al.* (2014) 'Brd4 activates P-TEFb for RNA polymerase II CTD phosphorylation', *Nucleic Acids Research*, 42(12), pp. 7577–7590.

Iwasaki, H. and Takahagi, M. (1991) 'Escherichia coli RuvC protein is an endonuclease that resolves the Holliday structure', *EMBO Journal*, 10(13), pp. 4381–4389.

Izzo, A. *et al.* (2013) 'The genomic landscape of the somatic linker histone subtypes H1.1 to H1.5 in human cells', *Cell Reports*, 3(6), pp. 2142–2154.

Jabs, E. W. *et al.* (1991) 'Studies of mitotic and centromeric abnormalities in roberts syndrome: Implications for a defect in the mitotic mechanism', *Chromosoma*, 100(4), pp. 251–261.

Jacobs, S. A. and Khorasanizadeh, S. (2002) 'Structure of HP1 chromodomain bound to a lysine 9-methylated histone H3 tail', *Science*, 295(5562), pp. 2080–2083.

Jakobsen, K. R. *et al.* (2016) 'The role of epithelial to mesenchymal transition in resistance to epidermal growth factor receptor tyrosine kinase inhibitors in non-small cell lung cancer', *Trans. Lung Cancer Research*, 5(1), pp. 172–182.

James, T. C. and Elgin, S. C. (1986) 'Identification of a nonhistone chromosomal protein associated with heterochromatin in *Drosophila melanogaster* and its gene.', *Molecular and Cellular Biology*, 6(11), pp. 3862–3872.

Jansen, L. E. T. *et al.* (2007) 'Propagation of centromeric chromatin requires exit from mitosis', *Journal of Cell Biology*, 176(6), pp. 795–805.

Javaid, S. *et al.* (2013) 'Dynamic chromatin modification sustains epithelial- mesenchymal transition following inducible expression of Snail1', *Cell Reports*, 5(6), pp. 1679–1689.

Jeanpierre, M. *et al.* (1993) 'An embryonic-like methylation pattern of classical satellite DNA is observed in ICF syndrome', *Human Molecular Genetics*, 2(6), pp. 731–735.

Jene-Sanz, A. *et al.* (2013) 'Expression of polycomb targets predicts breast cancer prognosis', *Molecular and Cellular Biology*, 33(19), pp. 3951–3961.

Jeppesen, P. *et al.* (1992) 'Antibodies to defined histone epitopes reveal variations in chromatin conformation and underacetylation of centric heterochromatin in human metaphase chromosomes', *Chromosoma*, 101(5–6), pp. 322–332.

Jeppesen, P. and Turner, B. M. (1993) 'The inactive X chromosome in female mammals is distinguished by a lack of histone H4 acetylation, a cytogenetic marker for gene expression', *Cell*, 74(2), pp. 281–289.

Jiang, H. *et al.* (2014) 'Monitoring dynamic glycosylation in vivo using supersensitive click chemistry', *Bioconjugate Chemistry*, 25(4), pp. 698–706.

Jih, G. *et al.* (2017) 'Unique roles for histone H3K9me states in RNAi and heritable silencing of transcription', *Nature*., 547(7664), pp. 463–467.

Jin, C. *et al.* (2011) 'H3.3/H2A.Z double variant-containing nucleosomes mark 'nucleosome free regions' of active promoters and other regulatory regions in the human genome.', *Nature Genetics*, 41(8), pp. 941-945

John, B. and Miklos, G. G. L. M. (1979) 'Functional aspects of satellite DNA and heterochromatin', *International Review of Cytology*, 58, pp. 1–114.

Johnson, K. D., *et al.* (2002) 'Requirements for utilization of CREB binding protein by hypersensitive site two of the beta-globin locus control region.', *Nucleic acids research*, 30(7), pp. 1522–30.

Johnson, W. L. *et al.* (2017) 'RNA-dependent stabilization of SUV39H1 at constitutive heterochromatin', *eLife*, 6, pp. 1–32.

Kakarougkas, A. *et al.* (2014) 'Requirement for PBAF in transcriptional repression and repair at DNA breaks in actively transcribed regions of chromatin', pp. 723–732.

Kalitsis, P. and Choo, K. H. A. (2012) 'The evolutionary life cycle of the resilient centromere', *Chromosoma*, 121(4), pp. 327–340.

Kamakaka, R. T. and Thomas, J. O. (1990) 'Chromatin structure of transcriptionally competent and repressed genes.', *The EMBO journal*, 9(12), pp. 3997–4006.

Kaneko, S. *et al.* (2013) 'PRC2 binds active promoters and contacts nascent RNAs in embryonic stem cells', *Nature Structural and Molecular Biology*., 20(11), pp. 1258–1264.

Karlseder, J. *et al.* (2004) 'The telomeric protein TRF2 binds the ATM kinase and Can inhibit the ATM-dependent DNA damage response', *PLoS Biology*, 2(8).

Kasai, F. *et al.* (2003) 'Chromosome homology between chicken (Gallus domesticus) and the red-legged partridge (Alectoris rufa); evidence of the occurrence of a neocentromere during evolution', *Cytogenetic and Genome Research*, 102(1–4), pp. 326–330.

Kassis, J. and Brown, J. (2012) 'Polycomb group response elements in Drosophila and vertebrates', *Advances in genetics*, (81), pp. 83–118.

Katagiri, K. *et al.* (2002) 'Rap1 functions as a key regulator of T-Cell and antigen-presenting cell interactions and modulates T-Cell responses', *Molecular and Cellular Biology*, 22(4), pp. 1001–1015.

Kazazian, H. H. *et al.* (1988) 'Haemophilia A resulting from de novo insertion of L1 sequences represents a novel mechanism for mutation in man.', *Nature*, 332(6160), pp. 164–166.

Kehle, J. *et al.* (1998) 'dMi-2 , a hunchback-interacting protein that functions in polycomb repression', *Science*, 282(December), pp. 1897–1901.

Keller, C. *et al.* (2012) 'HP1/Swi6 mediates the recognition and destruction of heterochromatic RNA transcripts', *Molecular Cell*, 47(2), pp. 215–227.

Keller, C. *et al.* (2013) 'Noncoding RNAs prevent spreading of a repressive histone mark', *Nature Structural and Molecular Biology*, 20(8), pp. 994–1000.

Keohane, A. M. *et al.* (1996) 'X-inactivation and histone H4 acetylation in embryonic stem cells', *Developmental Biology*, 630(333), pp. 618–630.

Kilic, F., *et al.*. (1999) 'Subcellular localization and partial puri ¢ cation of prelamin A endoprotease : an enzyme which catalyzes the conversion of farnesylated prelamin A to mature lamin A', *FEBS Letters*, 450, pp. 61–65.

Kim, I. S. *et al.* (2012) 'Roles of Mis18α in epigenetic regulation of centromeric chromatin and CENP-A loading', *Molecular Cell*., 46(3), pp. 260–273.

Kim, J. H. *et al.* (2009) 'Human gamma-satellite DNA maintains open chromatin structure and protects a transgene from epigenetic silencing', *Genome Research*, 19(4), pp. 533–544.

Kim, Y. and Clark, D. J. (2002) 'SWI/SNF-dependent long-range remodeling of yeast HIS3 chromatin.', *PNAS*, 99(24), pp. 15381–6.

Kim, S. C. *et al.* (2006) 'Substrate and Functional Diversity of Lysine Acetylation Revealed by a Proteomics Survey', *Molecular Cell*, 23(4), pp. 607–618.

Kimura, T. *et al.* (1983) 'Selective unfolding of erythroid chromatin in the region of the active beta-globin gene.', *Nature*, 306(5944), pp. 709–12.

King, I. F. *et al.* (2013) 'Topoisomerases facilitate transcription of long genes linked to autism', *Nature*, 501(7465), pp. 58–62.

Kipling, D. *et al.* (1995) 'CENP-B binds a novel centromeric sequence in the asian mouse Mus caroli.', *Molecular and cellular biology*, 15(8), pp. 4009–20.

Kit, S. (1961) 'Equilibrium sedimentation in density gradients of DNA preparations from animal tissues', *Journal of Molecular Biology*., 3(6), pp. 711-716

Kit, S. (1962) 'Species differences in animal deoxyribonucleic acids as revealed by equilibrium sedimentation in density gradients', *Nature*, 193(4812), pp. 274–275.

Kitai, H. *et al.* (2017) 'Key roles of EMT for adaptive resistance to MEK inhibitor in KRAS mutant lung cancer', *Cancer Discovery*., 8(3), pp. 172–176.

Kitajima, T. S. *et al.* (2006) 'Shugoshin collaborates with protein phosphatase 2A to protect cohesin.', *Nature*, 441(7089), pp. 46–52.

Klose, R. J. *et al.* (2006) 'The transcriptional repressor JHDM3A demethylates trimethyl histone H3 lysine 9 and lysine 36.', *Nature*, 442(7100), pp. 312–316.

Knoechel, B. *et al.* (2014) 'An epigenetic mechanism of resistance to targeted therapy in T cell acute lymphoblastic leukemia.', *Nature genetics*, 46(4), pp. 364–70.

Koch, B. *et al.* (2008) 'The Suv39h-HP1 histone methylation pathway is dispensable for enrichment and protection of cohesin at centromeres in mammalian cells', *Chromosoma*, 117(2), pp. 199–210.

Komissarov, A. S. *et al.* (2011) 'Tandemly repeated DNA families in the mouse genome', *BMC Genomics*, 12(1), p. 531.

Konev, A. Y. *et al.* (2007) 'CHD1 Motor Protein Is Required for deposition of histone variant H3.3 in chromatin *in vivo*', *Science*, 317 pp. 1087-1090.

Korb, E. *et al.* (2015) 'BET protein Brd4 activates transcription in neurons and BET inhibitor Jq1 blocks memory in mice', *Nature Neuroscience*, 18(10), pp. 1464–1473.

Koster, D. a *et al.* (2005) 'Friction and torque govern the relaxation of DNA supercoils by eukaryotic topoisomerase IB.', *Nature*, 434, pp. 671–674.

Kotkow, K. J. and Orkin, S. H. (1995) 'Dependence of globin gene expression in mouse erythroleukemia cells on the NF-E2 heterodimer.', *Molecular and Cellular Biology*, 15(8), pp. 4640–4647.

Kozako, T. *et al.* (2014) 'Anticancer agents targeted to sirtuins', *Molecules*, 19(12), pp. 20295–20313.
Krishnakumar, R. *et al.* (2008) 'Reciprocal binding of PARP-1 and histone H1 at promoters specifies transcriptional outcomes', *Science*, 319(5864), pp. 819–821.

Krivega, I. *et al.* (2015) 'Inhibition of G9a methyltransferase stimulates fetal hemoglobin production by facilitating LCR/γ-globin looping', *Blood*, 126(5), pp. 665–672.

Kruhlak, M. J. *et al.* (2006) 'Changes in chromatin structure and mobility in living cells at sites of DNA double-strand breaks', *Journal of Cell Biology*, 172(6), pp. 823–834.

Kumar, R. *et al.* (2007) 'Template-directed oligonucleotide strand ligation, covalent intramolecular DNA circularization and catenation using click chemistry', *Journal of the American Chemical Society*, 129(21), pp. 6859–6864.

Kung, J. T. Y., *et al.* (2013) 'Long noncoding RNAs: Past, present, and future', *Genetics*, 193(3), pp. 651–669.

Kurimchak, A. M. *et al.* (2016) 'Resistance to BET bromodomain inhibitors is mediated by kinome reprogramming in ovarian cancer', *Cell Reports*, 16(5), pp. 1273–1286.

Kusch, T. *et al.* (2004) 'Acetylation by Tip60 Is required for selective histone variant exchange at DNA lesions', *Science*, 306(December), pp. 2084–2088.

Kuzmichev, A. *et al.* (2002) 'Histone methyltransferase activity associated with a human multiprotein complex containing the Enhancer of Zeste protein', *Genes & Development*, 16, pp. 2893–2905.

Kyoo Jang, M. *et al.* (2005) 'The bromodomain protein Brd4 is a positive regulatory component of P-TEFb and stimulates RNA polymerase II-dependent transcription', *Molecular Cell*, 19(4), pp. 523–534.

Lachman, H. and Skoultchi, A. I. (1984) 'Expression of c-myc changes during differentiation of mouse erythroleukaemia cells', *Nature*, 310, pp. 592–594.

Lachner, M. *et al.* (2001) 'Methylation of histone H3 lysine 9 creates a binding site for HP1 proteins.', *Nature*, 410(6824), pp. 116–20.

De Lange, T. (2005) 'Shelterin: The protein complex that shapes and safeguards human telomeres', *Genes and Development*, 19(18), pp. 2100–2110.

Lansing, T. J. *et al.* (2007) 'In vitro biological activity of a novel small-molecule inhibitor of polo-like kinase 1', *Molecular Cancer Therapeutics*, 6(2), pp. 450–459.

Larson, A. G. *et al.* (2017) 'Liquid droplet formation by HP1α suggests a role for phase separation in heterochromatin.', *Nature*., 547(7662), pp. 236–240.

Lamonica, J. M. *et al.* (2011) 'Bromodomain protein Brd3 associates with acetylated GATA1 to promote its chromatin occupancy at erythroid target genes', *PNAS*, 108(22), pp. 159–168.

Lattanzi, G. *et al.* (2007) 'Pre-Lamin A processing is linked to heterochromatin organization', *Journal of Cell Biology*, 102, pp. 1149–1159.

Laybourn, P. J. and Kadonaga, J. T. (1991) 'Role of nucleosomal cores and histone H1 in regulation of transcription by RNA Polymerase II', *Science*, 254, pp. 238–245.

Lechner, J. and Carbon, J. (1991) 'A 240 kd multisubunit protein complex, CBF3, is a major component of the budding yeast centromere', *Cell*, 64(4), pp. 717–725.

Lee, J. *et al.* (2015) AKT phosphorylates H3-threonine 45 to facilitate termination of gene transcription in response to DNA damage', *Nucleic Acid Research*, 43(9), pp. 4505–4516.

Lee, M. G. *et al.* (2005) 'An essential role for CoREST in nucleosomal histone 3 lysine 4 demethylation', *Nature*, 437(September), pp. 432–435.

Lee, T.-L. *et al.* (2010) 'JNK-mediated turnover and stabilization of the transcription factor p45/NF-E2 during differentiation of murine erythroleukemia cells.', *PNAS*, 107(1), pp. 52–57.

Lehmann, L. *et al.* (2012) 'Polycomb repressive complex 1 (PRC1) disassembles RNA polymerase II preinitiation complexes', *Journal of Biological Chemistry*, 287(43), pp. 35784–35794.

Lehnertz, B. *et al.* (2003) 'Suv39h-mediated histone H3 lysine 9 methylation directs DNA methylation to major satellite repeats at pericentric heterochromatin', *Current biology*, 13(2), pp. 1192–1200.

Lemay, J.-F. *et al.* (2014) 'The RNA exosome promotes transcription termination of backtracked RNA polymerase II', *Nature Structural & Molecular Biology*, 21(10), pp. 919–926.

Lessard, S. *et al.* (2015) 'Comparison of DNA methylation profiles in human fetal and adult red blood cell progenitors', *Genome Medicine*, 7(1), p. 1-12.

Levine, S. S. *et al.* (2002) 'The core of the polycomb repressive complex is compositionally and functionally conserved in flies and humans', *Molecular Cell Biology*, 22(17), pp. 6070–6078.

Li, K. *et al.* (2010) 'Fluorogenic "click" reaction for labeling and detection of DNA in proliferating cells', *BioTechniques*, 49(1), pp. 525–527.

Li, L. *et al.* (2016) 'Inhibition of EZH2 via activation of SAPK / JNK and reduction of p65 and DNMT1 as a novel mechanism in inhibition of human lung cancer cells by polyphyllin I', *Journal of Experimental & Clinical Cancer Research*., (111), pp. 1–13.

Lin, Y. C. *et al.* (2012) 'Global changes in the nuclear positioning of genes and intra- and interdomain genomic interactions that orchestrate B cell fate', *Nature Immunology*, 13(12), pp. 1196–1204.

Lindner, H. *et al.* (1996) 'Separation of acetylated core histones by hydrophilic-interaction liquid chromatography', *Journal of Chromatography*, 743(1), pp. 137–144.

Lito, P. *et al.* (2012) 'Relief of profound feedback inhibition of mitogenic signaling by RAF inhibitors attenuates their activity in BRAFV600E melanomas', *Cancer Cell*., 22(5), pp. 668–682.

Liu, F. *et al.* (2013) 'Discovery of an *in vivo* chemical probe of the lysine methyltransferases G9a and GLP', *Journal of Medicinal Chemistry*, 56(21), pp. 8931–8942.

Liu, H. *et al.* (2015) 'Mitotic transcription installs Sgo1 at centromeres to coordinate chromosome segregation', *Molecular Cell*., 59(3), pp. 426–436.

Liu, J. *et al.* (2009) 'Transcriptional dysregulation in NIPBL and cohesin mutant human cells.', *PLoS biology*, 7(5), p. e1000119.

Liu, L. F. and Wang, J. C. (1987) 'Supercoiling of the DNA template during transcription.', *PNAS*, 84(20), pp. 7024–7027.

Liu, S. *et al.* (2014) 'Targeting STAT5 in hematologic malignancies through inhibition of the bromodomain and extra-terminal (BET) bromodomain protein BRD2', *Molecular Cancer Therapy*, 13(May), pp. 1194–1206.

Liu, W. *et al.* (2013) 'Brd4 and JMJD6-associated anti-pause enhancers in regulation of transcriptional pause release', *Cell*, 155(7), pp. 1581–1595.

Locke, D. P. *et al.* (2011) 'Comparative and demographic analysis of orang-utan genomes.', *Nature*, 469(7331), pp. 529–33.

Loening, U. E. (1969) 'The determination of the molecular weight of ribonucleic acid by polyacrylamide-gel electrophresis. The effects of changes in conformation.', *The Biochemical journal*, 113, pp. 131–138.

Long, G. V *et al.* (2014) 'Increased MAPK reactivation in early resistance to dabrafenib/trametinib combination therapy of BRAF-mutant metastatic melanoma', *Nature Communications*., 5, pp. 1–9.

Loughery, J. *et al.* (2017) 'Critical role for p53-serine 15 phosphorylation in stimulating transactivation at p53-responsive promoters', *Nucleic Acids Research*, 42(12), pp. 7666–7680.

Lovén, J. *et al.* (2013) 'Selective Inhibition of Tumor Oncogenes by Disruption of Super- Enhancers', *Cell*, 153(2), pp. 320–334.

Lu, B. Y. *et al.* (2000) 'Heterochromatin protein 1 is required for the normal expression of two heterochromatin genes in Drosophila.', *Genetics*, 155(2), pp. 699–708.

Luijsterburg, M. S. *et al.* (2009) 'Heterochromatin protein 1 is recruited to various types of DNA damage', *Journal of Cell Biology*, 185(4), pp. 577–586.

Luk, E. *et al.* (2007) 'Chz1, a nuclear chaperone for histone H2AZ', *Molecular Cell*, 25(3), pp. 357–368.

Lundblad, V. and Blackburn, E. H. (1993) 'An alternative pathway for yeast telomere maintenance rescues est1-senescence', *Cell*, 73(2), pp. 347–360.

Lupiáñez, D. G. *et al.* (2015) 'Disruptions of topological chromatin domains cause pathogenic rewiring of gene-enhancer interactions', *Cell*, 161(5), pp. 1012–1025.

Chan, L. F. and Wong, L. H. (2012) 'Transcription in the maintenance of centromere chromatin identity', *Nucleic Acids Research*, 40(22), pp. 11178–11188.

Lyons, D. B. *et al.* (2014) 'Heterochromatin-mediated gene silencing facilitates the diversification of olfactory neurons', *Cell Reports*, 9(3), pp. 884–892.

Ma, N. *et al.* (2011) 'The nuclear scaffold protein SAF-A is required for kinetochore-microtubule attachment and contributes to the targeting of Aurora-A to mitotic spindles', *Journal of Cell Science*, 124(3), pp. 394–404.

Ma, Y. *et al.* (2017) 'The MAPK pathway regulates intrinsic resistance to BET inhibitors in colorectal cancer', *Clinical Cancer Research*, 23(8), pp. 2027–2037.

Mackay, A. M. *et al.* (1998) 'A dominant mutant of inner centromere protein (INCENP), a chromosomal protein, disrupts prometaphase congression and cytokinesis', *Journal of Cell Biology*, 140(5), pp. 991–1002.

Mahajan, M. C. and Weissman, S. M. (2002) 'DNA-dependent adenosine triphosphatase (helicaselike transcription factor) activates beta-globin transcription in K562 cells.', *Blood*, 99(1), pp. 348–356.

Maison, C., *et al.* (2002) 'Higher-order structure in pericentric heterochromatin involves a distinct pattern of histone modification and an RNA component', *Nature Genetics*, 30(3), pp. 329–334.

Maison, C. *et al.* (2011) 'SUMOylation promotes de novo targeting of HP1α to pericentric heterochromatin.', *Nature genetics*, 43(3), pp. 220–227.

Maison, C. *et al.* (2012) 'The SUMO protease SENP7 is a critical component to ensure HP1 enrichment at pericentric heterochromatin', *Nature Structural & Molecular Biology*, 19(4), pp. 458–460.

Maison, C. *et al.* (2016) 'The methyltransferase Suv39h1 links the SUMO pathway to HP1α marking at pericentric heterochromatin', *Nature Communications*, 7, pp. 1–9.

Makarov, V. L. *et al.* (1993) 'Nucleosomal organization of telomere-specific chromatin in rat', *Cell*, 73(4), pp. 775–787.

Malik, H. S. and Henikoff, S. (2009) 'Major evolutionary transitions in centromere complexity', *Cell*, 138(6), pp. 1067–1082.

Manzo, M. *et al.* (2017) 'Isoform‐specific localization of DNMT3A regulates DNA methylation fidelity at bivalent CpG islands', *The EMBO Journal*, 36(23), p. e201797038.

Maresca, T. J., *et al.* (2005) 'Histone H1 is essential for mitotic chromosome architecture and segregation in Xenopus laevis egg extracts', *Journal of Cell Biology*, 169(6), pp. 859–869.

Markwald, R. R., *et al.* (1975) 'Structural analysis of endocardial cytodifferentiation', *Developmental Biology*, 42(1), pp. 160–180.

Marshall, O. J., *et al.* (2008) 'Three-dimensional localization of CENP-A suggests a complex higher order structure of centromeric chromatin', *Journal of Cell Biology*, 183(7), pp. 1193–1202.

Martens, J. H. A. *et al.* (2005) 'The profile of repeat-associated histone lysine methylation states in the mouse epigenome.', *The EMBO journal*, 24(4), pp. 800–12.

Martin, C. *et al.* (2009) 'Lamin B1 maintains the functional plasticity of nucleoli'. *Journal of Cell Science*, 122, pp. 1551-1562

Martin, C. and Zhang, Y. (2005) 'The diverse functions of histone lysine methylation', *Nature Reviews Molecular Cell Biology*, 6(11), pp. 838–849.

Mattioli, E. *et al.* (2007) 'Drugs affecting prelamin A processing : Effects on heterochromatin organization', *Experimental Cell Research*, 14. pp. 453-462.

Mayer, C. *et al.* (2006) 'Intergenic transcripts regulate the epigenetic state of rRNA genes', *Molecular Cell.*, 22(3), pp. 351–361.

McCall, K. and Bender, W. (1996) 'Probes of chromatin accessibility in the Drosophila bithorax complex respond differently to polycomb-mediated repression.', *The EMBO journal*, 15(3), pp. 569–580.

Mcclintock, B. (1951) 'Chromosome organization and genic expression', *Cold Spring Harbor Symposia on Quantitative Biology*, (16), pp. 13–47.

McDonald, O. G. *et al.* (2011) 'Genome-scale epigenetic reprogramming during epithelial-to-mesenchymal transition', *Nature Structural and Molecular Biology*, 18(8), pp. 867–874.

McHugh, C. A. *et al.* (2015) 'The Xist lncRNA interacts directly with SHARP to silence transcription through HDAC3', *Nature*, 521(7551), pp. 232–236.

Meehan, R. R., *et al.* (2003) 'HP1 binding to native chromatin in vitro is determined by the hinge region and not by the chromodomain', *EMBO Journal*, 22(12), pp. 3164–3174.

Meluh, P. B. and Koshland, D. (1995) 'Evidence that the MIF2 gene of *Saccharomyces cerevisiae* encodes a centromere protein with homology to the mammalian centromere protein CENP-C.', *Molecular Biology of the Cell*, 6(7), pp. 793–807.

Mendiburoa, M. J. *et al.* (2011) 'Drosophila CENH3 is sufficient for centromere formation', *Science*, 334, pp. 686–690.

Meppelink, A. *et al.* (2015) 'Shugoshin-1 balances Aurora B kinase activity via PP2A to promote chromosome bi-orientation', *Cell Reports*, 11(4), pp. 508–515.

Messmer, S., *et al.* (1992) 'Analysis of the functional role of the Polycomb chrom domain in Drosophila melanogaster.', *Genes and Development*, 6, pp. 1241–1254.

Meyne, J., *et al.* (1989) 'Conservation of the human telomere sequence (TTAGGG)n among vertebrates.', *PNAS*, 86(18), pp. 7049–53.

Mika, S. and Rost, B. (2005) 'NMPdb: Database of nuclear matrix proteins', *Nucleic Acids Research*, 33(DATABASE ISS.), pp. 160–163.

Mikkelsen, T. S. *et al.* (2007) 'Genome-wide maps of chromatin state in pluripotent and lineage-committed cells.', *Nature*, 448(7153), pp. 553–560.

Millanes-Romero, A. *et al.* (2013) 'Regulation of heterochromatin transcription by snail1/LOXL2 during epithelial-to-mesenchymal transition', *Molecular Cell*, 52(5), pp. 746–757.

Min, J. *et al.* (2002) 'Structure of the SET domain histone lysine methyltransferase Clr4', *Nature Structural Biology*, 9(11), pp. 828–832.

Minc, E., *et al.* (2000) 'HP1gamma associates with euchromatin and heterochromatin in mammalian nuclei and chromosomes.', *Cytogenetics and cell genetics*, 90(3–4), pp. 279–284.

Mirguet, O. *et al.* (2013) 'Discovery of epigenetic regulator i-bet762: Lead optimization to afford a clinical candidate inhibitor of the bet bromodomains', *Journal of Medicinal Chemistry*, 56(19), pp. 7501–7515.

Mirzoeva, O. K. *et al.* (2009) 'Basal subtype and MAPK/ERK kinase (MEK)-phosphoinositide 3-kinase feedback signaling determine susceptibility of breast cancer cells to MEK inhibition', *Cancer Research*, 69(2), pp. 565–572.

Mizuguchi, G. *et al.* (1997) 'Role of Nucleosome Remodeling Factor NURF in Transcriptional Activation of Chromatin', *Molecular Cell,* 1, pp. 141–150.

Moen, P. T. and Johnson, C. V (2003) 'Repositioning of muscle-specific genes relative to the periphery of SC-35 domains during skeletal myogenesis'. *Molecular Biology of the Cell,* 15, pp. 197-206

Mohrmann, L. and Verrijzer, C. P. (2005) 'Composition and functional specificity of SWI2 / SNF2 class chromatin remodeling complexes', *Biochemica et Physica Acta,* 1681, pp. 59–73.

Moitreyee, C. K., *et al.* (1998) 'Potential role of NF-kB and RXR beta like proteins in interferon induced HLA class I and beta globin gene transcription in K562 erythroleukaemia cells', *Molecular and Cellular Biochemistry*, 178(1–2), pp. 103–112.

Molete, J. M. *et al.* (2002) 'Functional and binding studies of HS3.2 of the beta-globin locus control region', *Gene*, 283, pp. 185–197.

Montagut, C. *et al.* (2008) 'Elevated CRAF as a potential mechanism of acquired resistance to BRAF inhibition in melanoma', *Cancer Research*, 68(12), pp. 4853–4861.

Montefalcone, G. *et al.* (1999) 'Centromere repositioning', *Genome Research*, 9(12), pp. 1184–1188.

Moree, B. *et al.* (2011) 'CENP-C recruits M18BP1 to centromeres to promote CENP-A chromatin assembly', *Journal of Cell Biology*, 194(6), pp. 855–871.

Morettini, S. *et al.* (2011) 'The chromodomains of CHD1 are critical for enzymatic activity but less important for chromatin localization', *Nucleice Acids Research,* 39(8), pp. 3103–3115.

Mousavi, K. *et al.* (2013) 'eRNAs promote transcription by establishing chromatin accessibility at defined genomic loci', *Molecular Cell*., 51(5), pp. 606–617.

Mueller, K. L. *et al.* (2008) 'Met and c-Src cooperate to compensate for loss of epidermal growth factor receptor kinase activity in breast cancer cells', *Cancer Research*, 68(9), pp. 1–19.

Muller, H, J. (1930) 'Types of visible variations induced by X-rays in Drosophila.', *Journal of Genetics,* 22(3), pp. 1–2.

Muller, H, J. (1938) 'The remaking of chromosomes', *The Collecting Net.*, 116(13), pp. 180–195.

Müller, W. G. *et al.* (2004) 'Generic features of tertiary chromatin structure as detected in natural chromosomes.', *Molecular and cellular biology*, 24(21), pp. 9359–70.

Murayama, Y. and Uhlmann, F. (2014) 'Biochemical reconstitution of topological DNA binding by the cohesin ring.', *Nature*, 505(7483), pp. 367–71.

Muro, Y. *et al.* (1992) 'Centromere protein B assembles human centromeric α-satellite DNA at the 17-bp sequence, CENP-B box', *Journal of Cell Biology*, 116(3), pp. 585–596.

Murphy, T. D. and Karpen, G. H. (1995) 'Localization of centromere function in a drosophila minichromosome', *Cell*, 82(4), pp. 599–609.

Myung, K. *et al.* (2004) 'Regulation of telomere length and suppression of genomic instability in human somatic cells by Ku86', *Molecular Cell Biology*, 24(11), pp. 5050–5059.

Najafova, Z. *et al.* (2017) 'BRD4 localization to lineage-specific enhancers is associated with a distinct transcription factor repertoire', *Nucleic Acids Research*, 45(1), pp. 127–141.

Nakamura, Y. *et al.* (2007) 'Crystal structure of the human BRD2 bromodomain: Insights into dimerization and recognition of acetylated histone H4', *Journal of Biological Chemistry*, 282(6), pp. 4193–4201.

Nakano, M. *et al.* (2008) 'Inactivation of a human kinetochore by specific targeting of chromatin modifiers', *Developmental Cell*., 14(4), pp. 507–522.

Nakayama, J., *et al.* (2000) 'A chromodomain protein, Swi6, performs imprinting functions in fission yeast during mitosis and meiosis', *Cell*, 101(3), pp. 307–317.

Naumova, N. *et al.* (2013) 'Organization of the mitotic chromosome.', *Science*, 342(6161), pp. 948–53.

Neef, A. B. and Luedtke, N. W. (2011) 'Dynamic metabolic labeling of DNA *in vivo* with arabinosyl nucleosides', *PNAS*, 108(51), pp. 20404–20409.

Neganova, I. *et al.* (2016) 'JNK / SAPK signaling is essential for efficient reprogramming of human fibroblasts to induced pluripotent stem cells', *Stem Cells*, 34, pp. 1198–1212.

Neumann, H. *et al.* (2009) 'Resource a method for genetically installing site-specific acetylation in recombinant histones defines the effects of H3 K56 acetylation', *Molecular Cell*., 36(1), pp. 153–163.

Nickerson, J. A. *et al.* (1997) 'The nuclear matrix revealed by eluting chromatin from a cross-linked nucleus', *PNAS*, 94(9), pp. 4446–4450.

Nicodeme, E. *et al.* (2010) 'Suppression of inflammation by a synthetic histone mimic', *Nature*, 468(7327), pp. 1119–1123.

Nielsen, A. L. *et al.* (2001) 'Heterochromatin formation in mammalian cells: Interaction between histones and HP1 Proteins', *Molecular Cell*, 7(4), pp. 729–739.

Nielsen, P. R. *et al.* (2002) 'Structure of the HP1 chromodomain bound to histone H3 methylated at lysine 9', *Nature*, 416(6876), pp. 103–107.

Nishiyama, T. *et al.* (2010) 'Sororin mediates sister chromatid cohesion by antagonizing Wapl', *Cell*., 143(5), pp. 737–749.

Niwa, H., *et al.* (2016) 'Quantitative expression of OCT3/4 defines differentiation, dedifferentiation or self-renewal of ES cells.', *Nature Genetetics*, 24(July), pp. 2–6.

Nogami, A. *et al.* (2015) 'FLT3-ITD confers resistance to the PI3K/Akt pathway inhibitors by protecting the mTOR/4EBP1/Mcl-1 pathway through STAT5 activation in acute myeloid leukemia', *Oncotarget*, 6(11). pp. 9189-9205

Noll, H. (1967) 'Characterization of macromolecules by constant velocity sedimentation', *Nature*, 215, pp. 360–361.
Nonaka, N. *et al.* (2002) 'Recruitment of cohesin to heterochromatic regions by Swi6/HP1 in fission yeast.', *Nature Cell Biology*, 4(1), pp. 89–93.

Nora, E. P. *et al.* (2012) 'Spatial partitioning of the regulatory landscape of the X-inactivation centre', *Nature*, 485(7398), pp. 381–385.

Nozawa, R. *et al.* (2017) 'SAF-A regulates interphase chromosome structure through oligomerisation with chromatin- associated RNAs', *Cell*., 169(7), p. 1214–1227.

Obri, A. *et al.* (2014) 'ANP32E is a histone chaperone that removes H2A.Z from chromatin', *Nature*., 505(7485), pp. 648–653.

Oca, R. M. *et al.* (2011) 'Barrier-to-Autointegration factor influences specific histone modifications', *Nucleus*, 2(6), pp. 1–11.

Oft, M. *et al.* (1996) 'TGF-beta and Ha-Ras collaborate in modulating the phenotypic plasticity and mvaslveness of epithelial tumor cells', *Genes & Development*, 10, pp. 2462–2477.

Ogawa, H. *et al.* (2002) 'A complex with chromatin modifiers that occupies E2F- and Myc-responsive genes in G0 Cells', *Science*, 296(May), pp. 1132–1137.

Ohtsuki, A. *et al.* (1989) 'Two human myeloma cell lines, amylase-producing KMS-12-PE and amylase-non-producing KMS-12-BM, were established from a patient, having the same chromosome marker, t(11;14)(q13;q32)', *British Journal of Haemotology*, 73(2), pp. 199–204.

Ohzeki, J. *et al.* (2012) 'Breaking the HAC Barrier: Histone H3K9 acetyl/methyl balance regulates CENP-A assembly', *The EMBO Journal*., 31(10), pp. 2391–2402.

Ohzeki, J. I. *et al.* (2002) 'CENP-B box is required for de novo centromere chromatin assembly on human alphoid DNA', *Journal of Cell Biology*, 159(5), pp. 765–775.

Ono, T. *et al.* (2003) 'Differential contributions of condensin I and condensin II to mitotic chromosome architecture in vertebrate cells', *Cell*, 115(1), pp. 109–121.

Ono, T. *et al.* (2004) 'Spatial and temporal regulation of condensins I and II in mitotic chromosome assembly in human cells', *Molecular Biology of the Cell*, 15, pp. 3296–3308.

Ono, T., *et al.* (2013) 'Condensin II initiates sister chromatid resolution during S phase', *Journal of Cell Biology*, 200(4), pp. 429–441.

Opresko, P. L. *et al.* (2002) 'Telomere-binding protein TRF2 binds to and stimulates the Werner and Bloom syndrome helicases', *Journal of Biological Chemistry*, 277(43), pp. 41110–41119.

Ottaviani, A. *et al.* (2009) 'The D4Z4 macrosatellite repeat acts as a CTCF and A-type lamins-dependent insulator in facio-scapulo- humeral dystrophy', 5(2).

Ottaviani, A., *et al.* (2008) 'Telomeric position effect: From the yeast paradigm to human pathologies?', *Biochimie*, 90(1), pp. 93–107.

Ou, H. D. *et al.* (2017) 'ChromEMT: Visualizing 3D chromatin structure and compaction in interphase and mitotic cells', *Science*, 357(6349). pp. eaag0025

Page, S. L. *et al.* (1995) 'Further evidence that CENP-C is a necessary component of active centromeres: Studies of a dic(X; 15) with simultaneous immunofluorescence and fish', *Human Molecular Genetics*, 4(2), pp. 289–294.

Panchenko, T. *et al.* (2011) 'Replacement of histone H3 with CENP-A directs global nucleosome array condensation and loosening of nucleosome superhelical termini', *PNAS*, 108(40), pp. 16588–16593.

Papamichos-chronakis, M. *et al.* (2012) 'Global regulation of H2A.Z localization by the INO80 chromatin remodeling enzyme is essential for genome integrity', *Cell*, 144(2), pp. 200–213.

Parada, L. A., *et al.* (2004) 'Tissue-specific spatial organization of genomes', *Genome biology*, 5, pp. R44, 1–9.

Parelho, V. *et al.* (2008) 'Cohesins functionally associate with CTCF on mammalian chromosome arms', *Cell*, 132(3), pp. 422–433.

Paro, R. and Hogness, D. S. (1991) 'The polycomb protein shares a homologous domain with a heterochromatin-associated protein of Drosophila.', *PNAS*, 88(1), pp. 263–267.

Pasini, D. *et al.* (2010) 'JARID2 regulates binding of the Polycomb repressive complex 2 to target genes in ES cells.', *Nature*., 464(7286), pp. 306–310.

Pefanis, E. *et al.* (2015) 'RNA exosome-regulated long non-coding RNA transcription controls super-enhancer activity', *Cell*., 161(4), pp. 774–789.

Pehrson, J. R. and Fried, V. A (1992) 'MacroH2A, a core histone containing a large nonhistone region.', *Science*, 257(5075), pp. 1398–1400.

Penny, G. D. *et al.* (1996) 'Requirement for Xist in X chromosome inactivation', *Nature*, 379, pp. 131–137.

Pérez-Balderas, F. *et al.* (2003) 'Multivalent neoglycoconjugates by regiospecific cycloaddition of alkynes and azides using organic-soluble copper catalysts', *Organic Letters*, 5(11), pp. 1951–1954.

Peric-hupkes, D. *et al.* (2010) 'Molecular maps of the reorganization of genome-nuclear lamina interactions during differentiation', *Molecular Cell, 38,* pp. 603–613.

Perpelescu, M. *et al.* (2009) 'Active establishment of centromeric cenp-a chromatin by rsf complex', *Journal of Cell Biology*, 185(3), pp. 397–407.

Peters, J, M. *et al.* (1998) 'Localization of the gene for familial partial lipodystrophy (Dunnigan variety) to chromosome 1q21-22', *Nature genetics*, 18, pp. 292-295.

Peters, A. H. F. M. *et al.* (2001) 'Loss of the Suv39h histone methyltransferases impairs mammalian heterochromatin and genome stability', *Cell*, 107(3), pp. 323–337.

Peters, A. H. F. M. *et al.* (2003) 'Partitioning and plasticity of repressive histone methylation states in mammalian chromatin', *Molecular Cell*, 12(6), pp. 1577–1589.

Petris, M. J. (2004) 'The SLC31 (Ctr) copper transporter family', *European Journal of Physiology*, 447(5), pp. 752–755.

Petryk, N. *et al.* (2016) 'Replication landscape of the human genome', *Nature Communications*, 7, pp. 1–13.

Picaud, S. *et al.* (2013) 'RVX-208, an inhibitor of BET transcriptional regulators with selectivity for the second bromodomain.', *PNAS*, 110(49), pp. 19754–9.

Picaud, S. *et al.* (2016) 'Promiscuous targeting of bromodomains by bromosporine identifies BET proteins as master regulators of primary transcription response in leukemia.', *Science Advances*, 2(10), p. e1600760.

Piras, F. M. *et al.* (2010) 'Uncoupling of satellite DNA and centromeric function in the genus Equus', *PLoS Genetics*, 6(2). pp. e1000845

Pluta, A. F. *et al.* (1995) 'Centromere - Hub of chromosomal activities', *Science*, 270(5242), pp. 1591–1594.

Pope, B. D. *et al.* (2014) 'Topologically associating domains are stable units of replication-timing regulation', *Nature*, 515(7527), pp. 402–405.

Pope, L. H. *et al.* (2005) 'Single chromatin fiber stretching reveals physically distinct populations of disassembly events', *Biophysical Journal*, 88(5), pp. 3572–3583.

Porter, E. G. and Dykhuizen, E. C. (2017) 'Individual bromodomains of polybromo-1 contribute to chromatin association and tumor suppression in clear cell renal carcinoma', *Journal of Biological Chemistry*, 292(7), pp. 2601–2610.

Portoso, M. *et al.* (2017) 'PRC2 is dispensable for *HOTAIR* ‐mediated transcriptional repression', *The EMBO Journal*, 36(8), pp. 981–994.

Prasanth, K. V. *et al.* (2010) 'Nuclear organization and dynamics of 7SK RNA in regulating gene expression', *Molecular Biology of the Cell*, 21(2), pp. 4184–4196.

Probst, A. V. and Almouzni, G. (2011) 'Heterochromatin establishment in the context of genome-wide epigenetic reprogramming', *Trends in Genetics*, 27(5), pp. 177–185.

Pruss, D. *et al.* (1996) 'An asymmetric model for the nucleosome: A binding site for linker histones inside the DNA Gyres', *Science*, 274(October), pp. 614–618.

Purgato, S. *et al.* (2015) 'Centromere sliding on a mammalian chromosome', *Chromosoma*, 124(2), pp. 277–287.

Qin, J. *et al.* (2012) 'The polycomb group protein L3mbtl2 assembles an atypical PRC1-family complex that is essential in pluripotent stem cells and early development', *Cell Stem Cell*., 11(3), pp. 319–332.

Qin, P. *et al.* (2017) 'Live cell imaging of low- and non-repetitive chromosome loci using CRISPR-Cas9', *Nature Communications*. 8, pp. 14725.

Quénet, D. and Dalal, Y. (2014) 'A long non-coding RNA is required for targeting centromeric protein A to the human centromere', *eLife*, 3, p. e03254.

Quivy, J.-P. *et al.* (2004) 'A CAF-1 dependent pool of HP1 during heterochromatin duplication.', *The EMBO journal*, 23(17), pp. 3516–26.

Rabl, C. (1885) 'Ueber Zelltheilung', *Morpholog. Jahrbuch*, 10, pp. 214–330.

De Raedt, T. *et al.* (2014) 'PRC2 loss amplifies Ras-driven transcription and confers sensitivity to BRD4-based therapies', *Nature.*, 514(7521), pp. 247–251.

Rao, S. S. P. *et al.* (2014) 'A 3D map of the human genome at kilobase resolution reveals principles of chromatin looping', *Cell.*, 159(7), pp. 1665–1680.

Rao, S. S. P. *et al.* (2017) 'Cohesin Loss Eliminates All Loop Domains', *Cell.*, 171(2), p. 305–320.

Ravelli, A. C. J. *et al.* (1998) 'Glucose tolerance in adults after prenatal exposure to famine', *The Lancet*, 351, pp. 173–177.

Rea, S. *et al.* (2000) 'Regulation of chromatin structure by site-specific histone H3 methyltransferases.', *Nature*, 406(6796), pp. 593–599.

Reddington, J. P. *et al.* (2013) 'Redistribution of H3K27me3 upon DNA hypomethylation results in de-repression of polycomb target genes', *Genome Biology.*, 14(3), p. R25.

Renčiuk, D. *et al.* (2017) 'G-quadruplex formation in the Oct4 promoter positively regulates Oct4 expression', *Biochimica et Biophysica Acta - Gene Regulatory Mechanisms*, 1860(2), pp. 175–183.

Reuter, G. *et al.* (1990) 'Dependence of position-effect variegation in Drosophila on dose of a gene encoding an unusual zinc-finger protein', *Nature*, pp. 219–223.

Ribeiro-Mason, K. *et al.* (2012) 'Nuclear dynamics of histone H3 trimethylated on lysine 9 and/or phosphorylated on serine 10 in mouse cloned embryos as new markers of reprogramming?', *Cellular reprogramming*, 14(4), pp. 283–94.

Ribeiro, S. A. *et al.* (2010) 'A super-resolution map of the vertebrate kinetochore.', *PNAS*, 107(23), pp. 10484–10489.

Ricci, M. A. *et al.* (2015) 'Chromatin fibers are formed by heterogeneous groups of nucleosomes *in vivo*', *Cell.*, 160, pp. 1145–1158.

Riddle, N. C. *et al.* (2008) 'An investigation of heterochromatin domains on the fourth chromosome of Drosophila melanogaster', *Genetics*, 178(3), pp. 1177–1191.

Rinn, J, L. *et al.* (2007) 'Functional demarcation of active and silent chromatin domains in human HOX loci by non-coding RNAs', *Cell*, 129(7), pp. 1311–1323.

Roca, J. and Wang, J. C. (1992) 'The capture of a DNA double helix by an ATP-dependent protein clamp: A key step in DNA transport by type II DNA topoisomerases', *Cell*, 71(5), pp. 833–840.

Rocchi, M. *et al.* (2012) 'Centromere repositioning in mammals.', *Heredity*, 108(1), pp. 59–67.

Roe, J. S. *et al.* (2015) 'BET bromodomain inhibition suppresses the function of hematopoietic transcription factors in acute myeloid leukemia', *Molecular Cell.*, 58(6), pp. 1028–1039.

Rogakou, E. P. *et al.* (1998) 'DNA double-stranded breaks induce histone H2AX phosphorylation on serine 139', *Biological Chemistry*, 273(10), pp. 5858–5868.

Romeo, K. *et al.* (2015) 'The SENP7 SUMO-protease presents a module of two HP1 interaction motifs that locks HP1 protein at pericentric heterochromatin', *Cell Reports*, 10(5), pp. 771–782.

Romig, H. *et al.* (1992) 'Characterization of SAF-A, a novel nuclear DNA binding protein from HeLa cells with high affinity for nuclear matrix/scaffold attachment DNA elements.', *The EMBO journal*, 11(9), pp. 3431–3440.

Romiguier, J. *et al.* (2010) 'Contrasting GC-content dynamics across 33 mammalian genomes: Relationship with life-history traits and chromosome sizes', *Genome Research*, 20(8), pp. 1001–1009.

Rousseaux, S. *et al.* (2009) 'Cooperative binding of two acetylation marks on a histone tail by a single bromodomain', *Nature*, 461(October), pp. 664–669.

Rosivatz, E. *et al.* (2002) 'Differential expression of the epithelial-mesenchymal transition regulators Snail, SIP1, and twist in gastric cancer', *American Journal of Pathology*, 161(5), pp. 1881–1891.

Ruthenburg, A. J. *et al.* (2011) 'Recognition of a Mononucleosomal Histone Modification Pattern by BPTF via Multivalent Interactions', *Cell*. Elsevier Inc., 145(5), pp. 692–706.

Rylski, M. *et al.* (2003) 'GATA-1-mediated proliferation arrest during erythroid maturation.', *Molecular and cellular biology*, 23(14), pp. 5031–42.

Sabari, B. R. *et al.* (2015) 'Intracellular Crotonyl-CoA Stimulates Transcription Article Intracellular Crotonyl-CoA Stimulates Transcription through p300-Catalyzed Histone Crotonylation', *Molecular Cell*. Elsevier Inc., 58(2), pp. 203–215.

Sabatelli, P. *et al.* (2001) 'Nucleur alterations in autosomal-dominant emery-dreifuss muscular dystrophy', *Muscle & Nerve*, 24(6), pp. 826–829.

Sadaie, M. *et al.* (2008) 'Balance between distinct HP1 family proteins controls heterochromatin assembly in fission yeast', *Molecular and Cellular Biology*, 28(23), pp. 6973–6988.

Sadoni, N. *et al.* (1999) 'Nuclear Organization of Mammalian Genomes : Polar Chromosome', *Journal of Cell Biology*, 146(6), pp. 1211-1226.

Saffery, R. *et al.* (2000) 'Human centromeres and neocentromeres show identical distribution patterns of >20 functionally important kinetochore-associated proteins.', *Human molecular genetics*, 9(2), pp. 175–185.

Sandell, L. L. and Zakian, V. A. (1993) 'Loss of a yeast telomere: Arrest, recovery, and chromosome loss', *Cell*, 75(4), pp. 729–739.

de Santa, F. *et al.* (2010) 'A large fraction of extragenic RNA Pol II transcription sites overlap enhancers', *PLoS Biology*, 8(5). pp. e1000384

Santanach, A. *et al.* (2017) 'The polycomb group protein CBX6 is an essential regulator of embryonic stem cell identity', *Nature Communications*, 8(1), pp. 1–11.

Schalch, T. *et al.* (2009) 'High-affinity binding of Chp1 chromodomain to K9 methylated histone H3 is required to establish centromeric heterochromatin', *Molecular Cell*., 34(1), pp. 36–46.

Schermelleh, L. *et al.* (2008) 'Subdiffraction multicolor imaging of the nuclear periphery with 3D structured illumination microscopy', *Science*, 320(5881), pp. 1332–1336.

Schmiesing, J. *et al.* (2000) 'A human condensin complex containing hCAP-C-hCAP-E and CNAP1, a homolog of Xenopus XCAP-D2, colocalizes with phosphorylated histone H3 during the early stage of mitotic chromosome condensation.', *Molecular and cellular biology*, 20(18), pp. 6996–7006.

Schoeftner, S. and Blasco, M. A. (2008) 'Developmentally regulated transcription of mammalian telomeres by DNA-dependent RNA polymerase II', *Nature Cell Biology*, 10(2), pp. 228–236.

Schones, D. E. *et al.* (2008) 'Dynamic regulation of nucleosome positioning in the human genome', *Cell*, 132(5), pp. 887–898.

Schönwasser, D. C. *et al.* (1998) 'Activation of the mitogen-activated protein kinase/extracellular signal-regulated kinase pathway by conventional, novel, and atypical protein kinase C isotypes.', *Molecular and Cellular Biology*, 18(2), pp. 790–8.

Schotta, G. *et al.* (2004) 'A silencing pathway to induce H3-K9 and H4-K20 trimethylation at constitutive heterochromatin', *Genes and Development*, 18(11), pp. 1251–1262.

Schramek, D. *et al.* (2011) 'The stress kinase MKK7 couples oncogenic stress to p53 stability and tumor suppression', *Nature genetics*., 43(3), pp. 212–219.

Schueler, M. G. *et al.* (2001) 'Genomic and genetic defnition of a functional human centromere', *Science*, 294(October), pp. 109–115.

Schwarzer, W. *et al.* (2017) 'Two independent modes of chromatin organization revealed by cohesin removal', *Nature*., 551(7678), pp. 51–56.

Sekulic, N. *et al.* (2010) 'The structure of (CENP-A-H4)(2) reveals physical features that mark centromeres', *Nature*., 467(7313), pp. 347–351.

Serrano, Á., *et al.* (2009) 'Heterochromatin protein 1 (HP1) proteins do not drive pericentromeric cohesin enrichment in human cells', *PLoS ONE*, 4(4). pp. e5118

Seton-Rogers, S. E. *et al.* (2004) 'Cooperation of the ErbB2 receptor and transforming growth factor beta in induction of migration and invasion in mammary epithelial cells.', *PNAS*, 101(5), pp. 1257–1262.

Sewry, C. A. *et al.* (2001) 'Skeletal muscle pathology in autosomal dominant Emery-Dreifuss muscular dystrophy with lamin A/C mutations', *Neuropathology & Applied Neurobiology, 27,* pp. 281–290.

Shachar, S. *et al.* (2015) 'Identification of gene positioning factors using high-throughput imaging mapping', *Cell*., 162(4), pp. 911–923.

Shang, E. *et al.* (2007) 'The first bromodomain of Brdt , a testis-specific member of the BET sub-family of double-bromodomain-containing proteins , is essential for male germ cell differentiation', *Development*, 134, pp. 3507–3515.

Shang, E. *et al.* (2009) 'The double bromodomain-containing gene Brd2 is essential for embryonic development in mouse', *Developmental dynamics*, 238(4), pp. 908–917.

Shang, W. H. *et al.* (2010) 'Chickens possess centromeres with both extended tandem repeats and short non-tandem-repetitive sequences', *Genome Research*, 20(9), pp. 1219–1228.

Shao, Z. *et al.* (1999) 'Stabilization of chromatin structure by PRC1, a polycomb complex', *Cell*, 98(1), pp. 37–46.

Sharma, G. G. *et al.* (2003) 'Human heterochromatin protein 1 isoforms HP1(Hsalpha) and HP1(Hsbeta) interfere with hTERT-telomere interactions and correlate with changes in cell growth and response to ionizing radiation.', *Molecular and cellular biology*, 23(22), pp. 8363–8376.

Shaytan, A. K., *et al.* (2015) 'Nucleosome adaptability conferred by sequence and structural variations in histone H2A-H2B dimers', *Current Opinion in Structural Biology*., 32, pp. 48–57.

Shearstone, J. R. *et al.* (2016) 'Chemical inhibition of histone deacetylases 1 and 2 induces fetal hemoglobin through activation of GATA2', *PLoS ONE*, 11(4), pp. 1–27.

Shelby, R. D., *et al.* (2000) 'Chromatin assembly at kinetochores is uncoupled from DNA replication', *Journal of Cell Biology*, 151(5), pp. 1113–1118.

Shen, W. *et al.* (2007) 'Solution structure of human Brg1 bromodomain and its specific binding to acetylated histone tails', *Biochemistry*, 46(8), pp. 2100–2110.

Shen, X. *et al.* (2000) 'A chromatin remodelling complex involved in transcription and DNA processing', *Nature,* 406, pp. 541–544.

Shen, X. and Gorovsky, M. a (1996) 'Linker histone H1 regulates specific gene expression but not global transcription *in vivo*', *Cell*, 86(3), pp. 475–83.

Shi, H. *et al.* (2012) 'Melanoma whole-exome sequencing identifies V600EB-RAF amplification-mediated acquired B-RAF inhibitor resistance', *Nature Communications*., 3, pp. 724–728.

Shi, J., *et al.* (2015) 'Twist-BRD4 Complex: Potential Drug Target for Basal-like Breast Cancer', *Current Pharm Des*, 21(10), pp. 1256–1261.

Shi, Y. *et al.* (2004) 'Histone demethylation mediated by the nuclear amine oxidase homolog LSD1', *Cell*, 119(7), pp. 941–953.

Shimura, M. *et al.* (2011) 'Epigenetic displacement of HP1 from heterochromatin by HIV-1 Vpr causes premature sister chromatid separation', *Journal of Cell Biology*, 194(5), pp. 721–735.

Shin, J. A. *et al.* (2005) 'SUMO modification is involved in the maintenance of heterochromatin stability in fission yeast', *Molecular Cell*, 19(6), pp. 817–828.

Shintomi, K. and Hirano, T. (2011) 'The relative ratio of condensin I to II determines chromosome shapes', *Genes & development*, 25, pp. 1464–1469.

Shirai, A. *et al.* (2017) 'Impact of nucleic acid and methylated H3K9 binding activities of Suv39h1 on its heterochromatin assembly', *eLife*, 6. pp. e25317

Siatecka, M., Xue, L. and Bieker, J. J. (2007) 'Sumoylation of EKLF promotes transcriptional repression and is involved in inhibition of megakaryopoiesis', *Molecular and Cellular Biology*, 27(24), pp. 8547–8560.

Sigova, A. A., *et al.* (2015) 'Transcription factor trapping by RNA in gene regulatory elements', *Science*, 350(6263), pp. 978–982.

Singh, P. B. *et al.* (1991) 'A sequence motif found in a Drosophila heterochromatin protein is conserved in animals and plants', *Nucleic Acids Research*, 19(4), p. 789.

Singleton, K. R. *et al.* (2017) 'Melanoma therapeutic strategies that select against resistance by exploiting MYC-driven evolutionary convergence', *Cell Reports*., 21(10), pp. 2796–2812.

Sinha, A., *et al.* (2005) 'Bromodomain analysis of Brd2-dependent transcriptional activation of cyclin A.', *The Biochemical journal*, 387(Pt 1), pp. 257–69.

Skoko, D. *et al.* (2006) 'Mechanism of chromosome compaction and looping by the E. coli nucleoid protein Fis', *Journal of Molecular Biology*, 364(4), pp. 777–798.

Smeets, D. *et al.* (2014) 'Three-dimensional super-resolution microscopy of the inactive X chromosome territory reveals a collapse of its active nuclear compartment harboring distinct Xist RNA foci', *Epigenetics & Chromatin*, 7(8), pp. 1-27.

Smith, R. D. and Yus, J. (1984) 'Alterations in globin gene chromatin conformation during murine erythroleukemia cell differentiation', *Journal of Biochemical Chemistry*, 259(7). pp. 4609-4615.

Solovei, I. *et al.* (2011) 'LBR and Lamin A/C sequentially tether peripheral heterochromatin and inversely regulate differentiation', *Cell*., 152(3), pp. 584–598.

Son, J. *et al.* (2013) 'Nucleosome-binding activities within JARID2 and EZH1 regulate the function of PRC2 on chromatin', *Genes and Development*, 27(24), pp. 2663–2677.

Song, F. *et al.* (2014) 'Cryo-EM study of the chromatin fiber tetranucleosomal units', *Science*, 344, pp. 376–381.

Southern, E. M. (1975) 'Detection of specific sequences among DNA fragments separated by gel electrophoresis', *Journal of Molecular Biology*, 98(3), pp. 503–517.

Soutoglou, E. and Misteli, T. (2010) 'Activation of the cellular DNA damage response in the absence of DNA lesions', *Science*, 320, pp. 1507-1510.

Spence, J. M. *et al.* (2007) 'Depletion of topoisomerase IIalpha leads to shortening of the metaphase interkinetochore distance and abnormal persistence of PICH-coated anaphase threads.', *Journal of cell science*, 120(22), pp. 3952–64.

Sperling, L. and Tardieu, A. (1976) 'The mass per unit length of chromatin by low-agnle X-ray scattering', *FEBS Letters*, 64(1), pp. 89–91.

Stansel, R. M., *et al.* (2001) 'T-loop assembly in vitro involves binding of TRF2 near the 3' telomeric overhang', *EMBO Journal*, 20(19), pp. 5532–5540.

Steensel, B. Van (2011) 'Chromatin : constructing the big picture', *The EMBO Journal*., 30(10), pp. 1885–1895.

Strohner, R. *et al.* (2001) 'NoRC - A novel member of mammalian ISWI-containing chromatin remodeling machines', *EMBO Journal*, 20(17), pp. 4892–4900.

Strom, A. R. *et al.* (2017) 'Phase separation drives heterochromatin domain formation', *Nature*., 547(7662), pp. 241–245.

Suga, K. *et al.* (2012) 'Hydrophobic properties of tRNA with varied conformations evaluated by an aqueous two-phase system', *International Journal of Biological Sciences*, 8(8), pp. 1188–1196.

Sullivan, B. A. and Karpen, G. H. (2004) 'Centromeric chromatin exhibits a histone modification pattern that is distinct from both euchromatin and heterochromatin.', *Nature Structural & Molecular Biology*, 11(11), pp. 1076–83.

Sun, C. *et al.* (2014) 'Intrinsic resistance to MEK inhibition in kras mutant lung and colon cancer through transcriptional induction of ERBB3', *Cell Reports*., 7(1), pp. 86–93.

Sun, W. *et al.* (2014) 'High expression of polo-like kinase 1 is associated with early development of hepatocellular carcinoma', *International Journal of Genomics*, 2014(312130), pp. 1-9.

Sunwoo, H., *et al.* (2015) 'The Xist RNA-PRC2 complex at 20-nm resolution reveals a low Xist stoichiometry and suggests a hit-and-run mechanism in mouse cells', *PNAS*, 112(31), pp. E4216–E4225.

Suto, R. K. *et al.* (2000) 'Crystal structure of a nucleosome core particle containing the variant histone H2A.Z.', *Nature Structural Biology*, 7(12), pp. 1121–1124.

Suzuki, H. *et al.* (2004) 'Epigenetic inactivation of SFRP genes allows constitutive WNT signaling in colorectal cancer', *Nature Genetics*, 36(4), pp. 417–422.

Suzuki, M., *et al.* (2006) 'Plasmid DNA sequences present in conventional herpes simplex virus amplicon vectors cause rapid transgene silencing by forming inactive chromatin.', *Journal of Virology*, 80(7), pp. 3293–300.

Tachiwana, H. *et al.* (2011) 'Crystal structure of the human centromeric nucleosome containing CENP-A.', *Nature*., 476(7359), pp. 232–235.

Tachiwana, H. *et al.* (2015) 'HJURP involvement in de novo CenH3CENP-A and CENP-C recruitment', *Cell Reports*, 11(1), pp. 22–32.

Taddei, A. *et al.* (1999) 'Duplication and maintainance of heterochromatin domains', *Journal of Cell Biology*., 147(6), pp. 1153–1166.

Taddei, A. *et al.* (2001) 'Reversible disruption of pericentric heterochromatin and centromere function by inhibiting deacetylases.', *Nature Cell Biology*, 3(1), pp. 114–120.

Tagami, H. *et al.* (2004) 'Histone H3.1 and H3.3 complexes mediate nucleosome assembly pathways dependent or independent of DNA synthesis', *Cell*, 116(1), pp. 51–61.

Takami, Y. and Nakayama, T. (1997) 'A single copy of linker H1 genes is enough for proliferation of the DT40 chicken B cell line, and linker H1 variants participate in regulation of gene expression', *Genes*, 2(11), pp. 711–723.

Talbert, P. B. and Henikoff, S. (2017) 'Histone variants on the move: Substrates for chromatin dynamics', *Nature Reviews Molecular Cell Biology*., 18(2), pp. 115–126.

Tan, M. *et al.* (2011) 'Resource Identification of 67 Histone Marks and Histone Lysine Crotonylation as a New Type of Histone Modification', *Cell*. Elsevier Inc., 146(6), pp. 1016–1028.

Taneja, B. *et al.* (2007) 'Topoisomerase V relaxes supercoiled DNA by a constrained swiveling mechanism', *PNAS*, 104(37), pp. 14670–14675.

Taniguchi, K. *et al.* (2009) 'Sprouty4 deficiency potentiates Ras-independent angiogenic signals and tumor growth', *Cancer Science*, 100(9), pp. 1648–1654.

Tarsounas, M. *et al.* (2004) 'Telomere maintenance requires the RAD51D recombination/repair protein', *Cell*, 117(3), pp. 337–347.

Tavares, L. *et al.* (2012) 'RYBP-PRC1 complexes mediate H2A ubiquitylation at polycomb target sites independently of PRC2 and H3K27me3', *Cell*, 148(4), pp. 664–678.

Tazi, J. and Bird, A. (1990) 'Alternative chromatin structure at CpG islands', *Cell*, 60(6), pp. 909–920.

Tedeschi, A. *et al.* (2013) 'Wapl is an essential regulator of chromatin structure and chromosome segregation.', *Nature*, 501(7468), pp. 564–8.

Therizols, P. *et al.* (2014) 'Chromatin decondensation is sufficient to alter nuclear organization in embryonic stem cells.', *Science*, 346(6214), pp. 1238–42.

Thoma, F., *et al*. (1979) 'Involvement of histone H1 in the organization of the nucleosome and of thesalt-dependent superstructures of chromatin', *Journal Cell Biology*, 83, pp. 403–427.

Thomas, J. O. (1984) 'The higher order structure of chromatin and histone H1.', *Journal of Cell Science.*, 1, pp. 1–20.

Thorne, A. W., *et al*. (2004) Native chromatin immunoprecipitation. *Methods in Molecular Biology: Epigenetics Protocols,* 287, pp. 21-44

Ting, D. T. *et al.* (2011) 'Aberrant overexpression of satellite repeats in pancreatic and other epithelial cancers', *Science*, 331(6017), pp. 593–596.

Tiwari, N. *et al.* (2013) 'Sox4 is a master regulator of epithelial-mesenchymal transition by controlling Ezh2 expression and epigenetic reprogramming', *Cancer Cell*, 23(6), pp. 768–783.

Tiwari, V. K. *et al.* (2012) 'A chromatin-modifying function of JNK during stem cell differentiation.', *Nature genetics*., 44(1), pp. 94–100.

Tóth, A. *et al.* (1999) 'Yeast cohesin complex requires a conserved protein, Eco1p(Ctf7), to establish cohesion between sister chromatids during DNA replication', *Genes and Development*, 13(3), pp. 320–333.

Trievel, R. C. *et al.* (2002) 'Structure and catalytic mechanism of a SET domain protein methyltransferase', *Cell*, 111(1), pp. 91–103.

Trifonov, E. N. and Sussman, J. L. (1980) 'The pitch of chromatin DNA is reflected in its nucleotide sequence.', *PNAS*, 77(7), pp. 3816–3820.

Tsai, W. *et al.* (2010) 'TRIM24 links a non-canonical histone signature to breast cancer', *Nature*. Nature Publishing Group, 468(7326), pp. 927–932.

Tsai, W.-B. *et al.* (2012) 'Activation of Ras/PI3K/ERK pathway induces c-Myc stabilization to upregulate argininosuccinate synthetase, leading to arginine deiminase resistance in melanoma cells', *Cancer Research*, 72(10), pp. 2622–2633.

Tschiersch, B. *et al.* (1994) 'The protein encoded by the Drosophila position-effect variegation suppressor gene Su(var)3-9 combines domains of antagonistic regulators of homeotic gene complexes', *The EMBO journal*, 13(16), pp. 3822–3831.

Tsukada, Y. *et al.* (2006) 'Histone demethylation by a family of JmjC domain-containing proteins', *Nature*, 439, pp. 811–816.

Tsukamoto, T. *et al.* (2000) 'Visualization of gene activity in living cells.', *Nature Cell Biology*, 2(12), pp. 871–878.

Tuduri, S. *et al.* (2009) 'Topoisomerase I suppresses genomic instability by preventing interference between replication and transcription', *Nature Cell Biology*., 11(11), pp. 1315–1324.

Tumbar, T., *et al*. (1999) 'Large-scale chromatin unfolding and remodeling induced by VP16 acidic activation domain', *Journal of Cell Biology*, 145(7), pp. 1341–1354.

Turner, B. M., *et al*. (1992) 'Histone H4 isoforms acetylated at specific lysine residues define individual chromosomes and chromatin domains in Drosophila polytene nuclei.', *Cell*, 69, pp. 375–384.

Tyler-Smith, C. *et al.* (1999) 'Transmission of a fully functional human neocentromere through three generations.', *Am. Journal of Human Genetics*, 64(5), pp. 1440–4.

Uemura, T. *et al.* (1987) 'DNA topoisomerase II is required for condensation and separation of mitotic chromosomes in S. pombe', *Cell*, 50(6), pp. 917–925.

Uhlmann, F., *et al.* (1999) 'Sister-chromatid separation at anaphase onset is promoted by cleavage of the cohesin subunit Scc1.', *Nature*, 400(6739), pp. 37–42.

Ui, A., *et al.* (2015) 'Transcriptional elongation factor ENL phosphorylated by ATM recruits polycomb and switches off transcription for DSB repair', *Molecular Cell*., 58(3), pp. 468–482.

Usatyuk, P. V *et al.* (2014) 'Role of c-Met/phosphatidylinositol 3-Kinase (PI3k)/Akt signaling in hepatocyte growth factor (HGF)-mediated lamellipodia formation, reactive oxygen species (ROS) generation, and motility of lung endothelial cells', *Journal of Biological Chemistry*, 289(19), pp. 13476–13491.

Uttamapinant, C. *et al.* (2012) 'Fast, cell-compatible click chemistry with copper-chelating azides for biomolecular labeling', *Angewandte Chemie*, 51(24), pp. 5852–5856.

Vader, G. *et al.* (2011) 'Protection of repetitive DNA borders from self-induced meiotic instability.', *Nature*., 477(7362), pp. 115–9.

Vagnarelli, P. *et al.* (2006) 'Condensin and Repo-Man/PP1 co-operate in the regulation of chromosome architecture during mitosis', *Cell*, 8(10), pp. 1133–1142.

Vakoc, C. R. *et al.* (2005) 'Histone H3 lysine 9 methylation and HP1γ are associated with transcription elongation through mammalian chromatin', *Molecular Cell*, 19(3), pp. 381–391.

Valouev, A. *et al.* (2011) 'Determinants of nucleosome organization in primary human cells.', *Nature*., 474(7352), pp. 516–20.

Van Holde, K. E. (1989). 'Chromatin. Series in molecular biology. *Springer-Verlag*, 530.

Vaquero, A. *et al.* (2004) 'Human SirT1 interacts with histone H1 and promotes formation of facultative heterochromatin', *Molecular Cell*, 16(1), pp. 93–105.

Velazquez Camacho, O. *et al.* (2017) 'Major satellite repeat RNA stabilize heterochromatin retention of Suv39h enzymes by RNA-nucleosome association and RNA:DNA hybrid formation', *eLife*, 6, pp. 1–29.

Ventura, M. *et al.* (2007) 'Evolutionary formation of new centromeres in macaque.', *Science*, 316(5822), pp. 243–246.

Vergani, E. *et al.* (2011) 'Identification of MET and SRC activation in melanoma cell lines showing primary resistance to PLX4032', *Neoplasia*, 13(12), pp. 1132–1142.

Di Veroli, G. Y. *et al.* (2016) 'Combenefit: An interactive platform for the analysis and visualization of drug combinations', *Bioinformatics*, 32(18), pp. 2866–2868.

Viejo-borbolla, A. *et al.* (2005) 'Brd2/RING3 interacts with a chromatin-binding domain in the Kaposi's sarcoma-sssociated herpesvirus latency-associated nuclear antigen 1 (LANA-1) that is required for multiple functions of LANA-1', *Journal of Virology*, 1(21), pp. 13618–13629.

Vissel, B. and Choo, K. H. (1989) 'Mouse major (γ) satellite DNA is highly conserved and organized into extremely long tandem arrays: Implications for recombination between nonhomologous chromosomes', *Genomics*, 5(3), pp. 407–414.

Voigt, P. *et al.* (2012) 'Asymmetrically modified nucleosomes', *Cell*., 151(1), pp. 181–193.

Voullaire, L. E. *et al.* (1993) 'A functional marker centromere with no detectable alpha-satellite, satellite III, or CENP-B protein: activation of a latent centromere?', *American Journal of Human Genetics*, 52(6), pp. 1153–63.

Walker, E. *et al.* (2010) 'Polycomb-like 2 associates with PRC2 and regulates transcriptional networks during mouse embryonic stem cell self-renewal and differentiation', *Cell*, 6(2), pp. 153–166.

Wan, X. B. *et al.* (2008) 'Inhibition of aurora-A suppresses epithelial-mesenchymal transition and invasion by downregulating MAPK in nasopharyngeal carcinoma cells', *Carcinogenesis*, 29(10), pp. 1930–1937.

Wang, H. *et al.* (2004) 'Role of histone H2A ubiquitination in polycomb silencing', *Nature*, 431, pp. 873–878.

Wang, R. *et al.* (2012a) 'Bromodomain protein Brd4 associated with acetylated chromatin is important for maintenance of higher-order chromatin structure', *Journal of Biological Chemistry*, 287(14), pp. 10738–10752.

Wang, S. H. *et al.* (2017) 'Tumour cell-derived WNT5B modulates in vitro lymphangiogenesis via induction of partial endothelial-mesenchymal transition of lymphatic endothelial cells', *Oncogene*., 36(11), pp. 1503–1515.

Wang, X. *et al.* (2017) 'Molecular analysis of PRC2 recruitment to DNA in chromatin and its inhibition by RNA', *Nature Structural & Molecular Biology*, 24(12), pp. 1028–1038.

Wang, Z. *et al.* (2008) 'Combinatorial patterns of histone acetylations and methylations in the human genome', *Nature Genetics*, 40(7), pp. 897–903.

Waterston, R. H. *et al.* (2002) 'Initial sequencing and comparative analysis of the mouse genome', *Nature*, 420(6915), pp. 520–562.

Wee, S. *et al.* (2009) 'PI3K pathway activation mediates resistance to MEK inhibitors in KRAS mutant cancers', *Cancer Research*, 69(10), pp. 4286–4294.

Wei, Y. *et al.* (1999) 'Phosphorylation of histone H3 is required for proper chromosome condensation and segregation.', *Cell*, 97, pp. 99–109.

Weiss, M., *et al*. (1951) 'Elevated serum amylase associated with bronchogenic carcinoma; report of case', *Am. Journal of Clinical Pathology*, 21(11), pp. 1057-1–61.

Wen, B. *et al.* (2009) 'Large histone H3 lysine 9 dimethylated chromatin blocks distinguish differentiated from embryonic stem cells', *Nature Genetics*, 41(2), pp. 246–250.

Whelan, G. *et al.* (2012) 'Cohesin acetyltransferase Esco2 is a cell viability factor and is required for cohesion in pericentric heterochromatin.', *The EMBO journal*., 31(1), pp. 71–82.

Whetstine, J. R. *et al.* (2006) 'Reversal of histone lysine trimethylation by the JMJD2 family of histone demethylases', *Cell*, 125(3), pp. 467–481.

Wiblin, A. E. *et al.* (2005) 'Distinctive nuclear organisation of centromeres and regions involved in pluripotency in human embryonic stem cells'., *Journal of Cell Science*, 118, pp. 3861-3868.

Wijchers, P. J. *et al.* (2016) 'Cause and consequence of tethering a SubTAD to different nuclear compartments', *Molecular Cell*., 61(3), pp. 461–473.

Williams, B. C. *et al.* (1998) 'Neocentromere activity of structurally acentric mini-chromosomes in Drosophila', *Nature Genetics*, 18(3), pp. 231–236.

Williamson, I. *et al.* (2014) 'Spatial genome organization: Contrasting views from chromosome conformation capture and fluorescence in situ hybridization', *Genes and Development*, 28(24), pp. 2778–2791.

Wilson, W. *et al.* (1986) 'Intercalators as probes of DNA conformation: Propidium binding to alternating and non-alternating polymers containing guanine', *Chemico-biological Interactions*, 58(C), pp. 41–56.

Wirbelauer, C. *et al*. (2005) 'Variant histone H3.3 is deposited at sites of nucleosomal displacement throughout transribed genes while active histone modifications show a promoter proximal bias', *Genes & Development*, 4, pp. 1761–1766.

Wong, A. K. C. and Rattner, J. B. (1988) 'Sequence organization and cytological localization of the minor satellite of mouse', *Nucleic Acids Research*, 16(24), pp. 11645–11661.

Wright, W. E. *et al.* (1997) 'Normal human chromosomes have long G-rich telomeric overhangs at one end', *Genes and Development*, 11(21), pp. 2801–2809.

Wu, H. A. *et al.* (2013) 'Mitogen-activated protein kinase signaling mediates phosphorylation of polycomb ortholog cbx7', *Journal of Biological Chemistry*, 288(51), pp. 36398–36408.

Wu, S. Y. and Chiang, C. M. (2007) 'The double bromodomain-containing chromatin adaptor Brd4 and transcriptional regulation', *Journal of Biological Chemistry*, 282(18), pp. 13141–13145.

Xhemalce, B. and Kouzarides, T. (2010) 'A chromodomain switch mediated by histone H3 Lys 4 acetylation regulates heterochromatin assembly', *Genes & Development*, 24(7), pp. 647–652.

Xi, Q. *et al.* (2011) 'A Poised Chromatin Platform for TGF- b Access to Master Regulators', *Cell*, 147, pp. 1511–1524.

Xiao, H. *et al.* (2001) 'Dual functions of largest NURF subunit NURF301 in nucleosome sliding and TF interactions', *Molecular Cell,* 8, pp. 531–543.

Xiao, R. *et al.* (2012) 'Nuclear matrix factor hnRNP U/SAF-A exerts a global control of alternative splicing by regulating U2 snRNP maturation', *Molecular Cell*, 45(5), pp. 656–668.

Xie, L. *et al.* (2004) 'Activation of the Erk pathway is required for TGF-β1-induced EMT in vitro', *Neoplasia*., 6(5), pp. 603–610.

Xiong, B., *et al*. (2010) 'Hos1 is a lysine deacetylase for the Smc3 subunit of cohesin', *Current Biology*., 20(18), pp. 1660–1665.

Yamagishi, Y. *et al.* (2008) 'Heterochromatin links to centromeric protection by recruiting shugoshin.', *Nature*, 455(7210), pp. 251–255.

Yamane, K. *et al.* (2006) 'JHDM2A, JmjC-Containing H3K9 demethylase, facilitates transcription activation by androgen receptor',*Cell*, 125(3), pp. 483–495.

Yang, D. D. *et al.* (1997) 'Absence of excitotoxicity-induced apoptosis in the hippocampus of mice lacking the Jnk3 gene.', *Nature*, 389(6653), pp. 865–70.

Yang, H. *et al.* (2008) 'Preferential dimethylation of histone H4 lysine 20 by Suv4-20', *Journal of Biological Chemistry*, 283(18), pp. 12085–12092.

Yang, J. *et al.* (2004) 'Twist, a master regulator of morphogenesis, plays an essential role in tumor metastasis', *Cell*, 117(7), pp. 927–939.

Yang, Z. *et al.* (2005) 'Recruitment of P-TEFb for Stimulation of Transcriptional Elongation by the Bromodomain Protein Brd4', *Molecular Cell*, 19, pp. 535–545.

Yao, J. *et al.* (2013) 'Plasticity and epigenetic inheritance of centromere-specific histone H3 (CENP-A)-containing nucleosome positioning in the fission yeast', *Journal of Biological Chemistry*, 288(26), pp. 19184–19196.

Yashiro-Ohtani, Y. *et al.* (2014) 'Long-range enhancer activity determines *Myc* sensitivity to Notch inhibitors in leukemia', *PNAS*, 111(46), pp. E4946–E4953.

Ye, J. *et al.* (2005) 'Histone H4 lysine 91 acetylation: A core domain modification associated with chromatin assembly', *Molecular Cell*, 18(1), pp. 123–130.

Yeh, E. *et al.* (2008) 'Pericentric chromatin is organized into an intramolecular loop in mitosis', *Current Biology*, 18(2), pp. 81–90.

Yeong, F. M. *et al.* (2003) 'Identification of a subunit of a novel Kleisin-β/SMC complex as a potential substrate of protein phosphatase 2A', *Current Biology*, 13(23), pp. 2058–2064.

Yisraeli, J. *et al.* (1988) 'Effect of in vitro DNA methylation on beta-globin gene expression.', *PNAS*, 85(13), pp. 4638–4642.

You, J. *et al.* (2004) 'Interaction of the bovine papillomavirus E2 protein with Brd4 tethers the viral DNA to host mitotic chromosomes', *Cell*, 117(3), pp. 349–360.

You, S. H. *et al.* (2013) 'Nuclear receptor co-repressors are required for the histone-deacetylase activity of HDAC3 in vivo', *Nature Structural and Molecular Biology*., 20(2), pp. 182–187.

Yuan, G. *et al.* (2005) 'Genome-Scale Identification of Nucleosome Positions in S . Cerevisiae', *Science*, 309, pp. 626–631.

Yuen, K. C., *et al*. (2017) 'Condensin II is anchored by TFIIIC and H3K4me3 in the mammalian genome and supports the expression of active dense gene clusters', *Science Advances*, 3(6), p. e1700191.

Zawistowski, J. S. *et al.* (2017) 'Enhancer remodeling during adaptive bypass to MEK inhibition is attenuated by pharmacologic targeting of the P-TEFb complex', *Cancer Discovery*, 7(3), pp. 302–21.

Zeng, W. *et al.* (2009) 'Specific loss of histone H3 lysine 9 trimethylation and HP1γ/cohesin binding at D4Z4 repeats is associated with facioscapulohumeral dystrophy (FSHD)', *PLoS Genetics*, 5(7). pp. e1000559

Zhang, M. *et al.* (2014) 'Somatic mutations of SUZ12 in malignant peripheral nerve sheath tumors', *Nature Genetics*., 46(11), pp. 1170–1172.

Zhang, S. *et al.* (2013) 'High mobility group protein N5 (HMGN5) and Lamina associated polypeptide 2α (LAP2α) interact and reciprocally affect their genome-wide chromatin', *Journal of Biological Chemistry*, 288(25), pp. 18104–18109.

Zhang, W. *et al.* (2012) 'Bromodomain-containing protein 4 (BRD4) regulates RNA polymerase II serine 2 phosphorylation in human CD4+ T cells', *Journal of Biological Chemistry*, 287(51), pp. 43137–43155.

Zhang, X.-Y., *et al* (1983) 'Eight different highly specific nucleosome phases on a-satellite DNA in the african green monkey', *Nucleic Acids Research*, 11(13), pp. 4287–4306.

Zhang, X. G. *et al.* (2012) 'PLK1 gene suppresses cell invasion of undifferentiated thyroid carcinoma through the inhibition of CD44v6, MMP-2 and MMP-9', *Experimental and Therapeutic Medicine*, 4(6), pp. 1005–1009.

Zhang, Y. *et al.* (1998) 'The dermatomyositis-specific autoantigen Mi2 is a component of a complex containing histone deacetylase and nucleosome remodeling activities', *Cell.*, 95, pp. 279–289.

Zhang, Y. *et al.* (2012) 'Chromosomal translocations are guided by the spatial organization of the genome', *Cell.*, 148(5), pp. 908–921.

Zhao, D. *et al.* (2014) 'Impact of acetylation on tumor metabolism', *Molecular & Cellular Oncology*, 1(3), p. e963452.

Zhao, H. *et al.* (2006) 'Enhancer blocking by chicken β-globin 5′-HS4: Role of enhancer strength and insulator nucleosome depletion', *Journal of Biological Chemistry*, 281(41), pp. 30573–30580.

Zhao, R. *et al.* (2011) 'Gene bookmarking accelerates the kinetics of post-mitotic transcriptional re-activation', *Nature Cell Biology*, 13(11), pp. 1295–1304.

Zhou, B. *et al.* (2016) 'A small number of residues can determine if linker histones are bound on or off dyad in the chromatosome', *Journal of Molecular Biology*., 428(20), pp. 3948–3959.

Zhu, Q. *et al.* (2011) 'BRCA1 tumour suppression occurs via heterochromatin-mediated silencing', *Nature*., 477(7363), pp. 179–184.

Zhu, X. D. *et al.* (2003) 'ERCC1/XPF removes the 3' overhang from uncapped telomeres and represses formation of telomeric DNA-containing double minute chromosomes', *Molecular Cell*, 12(6), pp. 1489–1498.